SCHEDULE

NF: Neal Fairley
ST: Sven Tougaard
MB: Mark C. Biesinger
ES: Emily Smith
DF: Delphine Flahaut
VF: Vincent Fernandez

SUNDAY	
17:00 – 19:00	
NF, MR,VF,CD,ST,ES+....	Registration workshop Installation data, programs, videos

MONDAY		
	Beginners	Experts
08:30 - 08:40	Welcome information VF	
08:40 - 10:10	Theory XPS (DF+ES)	New Features in CasaXPS 2.3.21 (NF)
10:10 - 10:30	Coffee	
10:30 - 12:30	XPS principle (DF+ES)	Understanding How Spectra are Acquired (VF)
12:45 - 14:15	Lunch	
14:30 - 15:30	Practical session (DF+ES) wide scans	Quantification and Instruments(NF+VF)
15:30 - 15:50	Coffee	
15:50 - 16:50	Practical session (DF+ES) narrow scans	Quantification *exercises* (NF+VF)
17:00 - 18:30	Poster session	
18:30 -	Welcome Reception	

TUESDAY		
	Beginners	Experts
08:30 - 10:10	Theory XPS (DF+ES)	CasaXPS Peak Fitting and Lineshapes (NF)
10:10 - 10:30	Coffee	
10:30 - 12:30	Practical session (DF+ES)	Instruments and lineshapes (NF+ VF)
12:45 - 14:15	Lunch	
14:30 - 15:30	Chemistry analysis theory XPS (MB)	Creating lineshapes from data (NF+VF)
15:30 - 15:50	Coffee	
15:50 - 17:20	Fit (MB)	Advanced spectroscopy analysis exercises (NF+VF)
17:20 - 18:20	XPS companies New developments + NAP XPS	

WEDNESDAY	
08:30 - 10:10	Theory behind the **Quases-Tougaard software** package(ST)
10:10 - 10:30	Coffee
10:30 - 12:30	**Practical application of the software (ST)**
12:45 - 13:15	Pic-nic
13:45 - 17:30	Island of Batz including garden visit with guide
17:30 - 18:20	Sample preparations (DM,MB,MG,ES,DF,VF,CC,MR)
	Free evening

THURSDAY		
	Beginners	Experts
08:30 - 10:10	Chemistry analysis theory XPS (MB)	
10:10 - 10:30	Coffee	
10:30 - 12:30	Exercise oxide (MB)	
12:45 - 14:15	Lunch	
14:30 - 15:30	Theory XPS (DF+ES+NF)	Theory behind the **Quases-Tougaard software** package(ST)
15:30 - 15:50	Coffee	
15:50 - 18:30	Practical session (DF+ES+NF)	Practical application of the software **Tougaard** (ST)
19:00	Gala Dinner	

FRIDAY		
	Beginners	Experts
08:30 - 10:10	Practical session and Questions (DF,ES)	Brainstorming on difficult cases (NF)
10:10 - 10:30	Coffee	
10:30 - 12:20	Practical session and Questions (DF,ES)	Brainstorming on difficult cases (NF)
12:20 - 12:30	Closure	
12:45 - 14:15	Lunch	

NO WARRANTY

Casa Software Ltd. does its best to ensure the accuracy and reliability of the Software and Related Documentation. Nevertheless, the Software and Related Documentation may contain errors that may affect its performance to a greater or lesser degree. Therefore no representation is made nor warranty given that the Software and Related Documentation will be suitable for any particular purpose, or that data or results produced by the Software and Related Documentation will be suitable for use under any specific conditions, or that the Software and Related Documentation will not contain errors. Casa Software Ltd. shall not in any way be liable for any loss consequential, either directly or indirectly, upon the existence of errors in the Software and Related Documentation. The Software and Related Documentation, including instructions for its use, is provided "AS IS" without warranty of any kind. Casa Software Ltd. further disclaims all implied warranties including without limitation any implied warranties of merchantability or fitness for a particular purpose. CasaXPS should not be relied on for solving a problem whose incorrect solution could result in injury to a person or loss of property. The entire risk arising out of the use or performance of the Software and Related Documentation remains with the Recipient. In no event shall Casa Software Ltd. be liable for any damages whatsoever, including without limitation, damages for loss of business profit, business interruption, loss of business information or other pecuniary loss, arising out of the use or inability to use the Software or written material, even if Casa Software Ltd. has been advised of the possibility of such damages.

Acknowledgements

As part of a sequence of Roscoff CNRS Thematic School on data processing, a set of videos and corresponding data files were prepared. These videos and data formed the basis for workshop sessions where students individually investigated data treatment presented during preceding lecture sessions. The Roscoff 2019 Cookbook is designed to, in some sense, replace the lecture sessions in which the context for and an introduction to data analysis was performed. Thus the Roscoff 2019 Cookbook provides a means for individuals to benefit from these videos and accompanying data without these lectures in the comfort of their own studying environment.

The authors would like to thank the organising committee (Vincent Fernandez, Mireille Richard-Plouet and Catherine Deudon), attendees and instructors (Emily Smith, Delphine Flahaut, Mark Biesinger, Sven Tougaard, Neal Fairley and Vincent Fernandez) at the CNRS Thematic School, as well as those offering data used within this book, as collectively their contributions have provided the guidance and motivation for producing The Roscoff 2019 Cookbook.

This work incorporates data from the Victorian node of the Australian National Fabrication Facility (ANFF), a company established under the National Collaborative Research Infrastructure Strategy to provide nano and microfabrication facilities for researchers in Australia, through the La Trobe University Centre for Materials and Surface Science. Data are reproduced under a Creative Commons licence (CC BY-NC 4.0 International).

Artwork for the Roscoff 2019 poster was designed by Aurelie Girard.

Table of Contents

Basics of Quantification by XPS

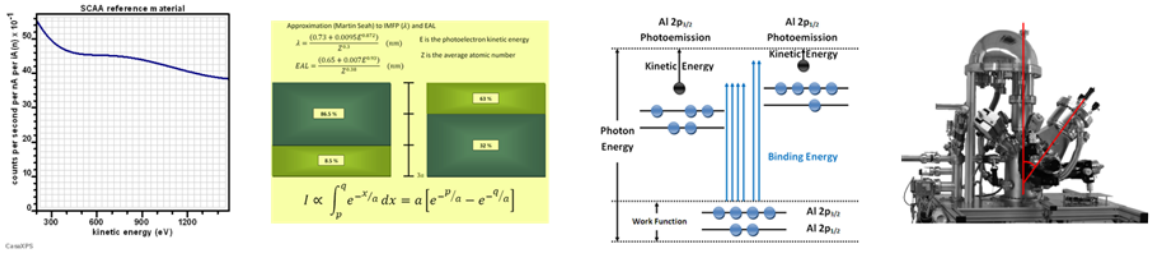

$$S_k = transmission \times escape\ depth \times cross\ section \times angular\ distribution\ correction$$

Percentage atomic concentration B_i for an element is computed from n peak areas $\{A_k : k = 1, n\}$ with corresponding total sensitivity factors $\{S_k : k = 1, n\}$ using the formula

$$B_i = 100 \times \frac{\frac{A_i}{S_i}}{\sum_{j=1}^{n} \frac{A_j}{S_j}}$$

An element library is a file containing information necessary when computing B_i and take different forms depending on instrument and philosophy followed by a particular instrument manufacturer.

Element Library and Relative Sensitivity Factors

The element library in CasaXPS is an ASCII file containing information relating to the identification of photoemission peaks and for use when quantification is performed based on computed photoemission signal after an inelastic scattered background signal is removed. The essential information within the element library for both these purposes is:

1. Element and photoelectron assignment for the emitted electron from a ground state electron configuration (e.g. Na 1s or Cu $2p_{1/2}$).
2. Approximate energy for photoemission corresponding to each photoemission process and each element in the periodic table.
3. Relative Sensitivity Factors (RSFs) for each photoemission process and each element.

The first two allow identification while the third is the means by which quantification is performed.

Characterising photoemission by these three entities is an over simplification for both identification of photoemission peaks within an XPS spectrum and for calculating amount of substance by XPS. Photoemission peaks described by an idealised symmetric bell shaped peak at a fixed energy with area proportional to sample composition is only possible for a small number of materials. Chemical state and complex interactions in final state electron configuration result in photoemission spectral shapes that do not follow a simple peak model, and signal can be spread over many electron volts. Nevertheless, these element library essentials are the starting points from which sample analysis by XPS begins and as such an element library based on these three sets of information is a required part of quantification by XPS. It is, however, important to understand how these values are compiled for a given instrument and the limitations of such information for different materials when analysed by XPS.

Relative sensitivity factor is the name given to a scaling factor used to convert peak area into an amount of substance. Historically the term RSF has at least two meanings, namely, empirical RSF or theoretical RSF.

Photoelectrons from a bulk solid state material are scattered by inelastic interactions with the sample material and so photoemission from a bulk material alters the relative intensity for photoemission peaks as a function of the scattering rate, which in turn varies as a function of kinetic energy for photoelectrons. These influences are referred to as escape depth corrections. Relative intensities for measured photoemission peaks will include the influence of inelastic scattering.

Empirical RSFs are the basis for element libraries used by the more established instrument manufacturers. By way of example, a paper by Wagner et al reported a set of sensitivity factors that were determined from a set of standard material using specific XPS instruments. Measured relative peak intensity RSFs represent empirical scaling factors that necessarily include instrumental factors commonly referred to as transmission characteristics, instrument geometry relating to intensity dependency on sampling direction with respect to the x-ray source direction and also escape depth differences for the materials used to calculate sensitivity factors. These empirical factors are therefore specific to both instrument and material composition. One essential consideration for empirical RSFs is the material used as a standard must be homogeneous in both area and depth (for a depth significantly greater than the sampling depth by XPS). Empirical RSFs therefore tend to be obtained for bulk materials.

It is possible to process empirical RSFs to remove transmission and angular distribution contributions to empirical RSFs resulting in RSFs that can be used for different instruments. The use of such RSFs for a range of instruments relies on a good knowledge of the transmission function for instruments making use of these processed empirical RSFs. An example of processed empirical RSFs is Ulvac PHI sensitivity factors that represent magic angle RSFs which can be applied, with appropriate corrections, to other PHI instruments with angles of 45^{o} and 90^{o} (two common arrangements for the angle between the direction for x-rays and sampling direction for photoemission on Ulvac PHI instruments).

The alternative to empirical RSFs is theoretical RSFs in the form of photoionisation cross-sections calculated for specific photon energies. Scofield reported theoretical photoionisation cross-sections for photon energies corresponding to x-ray energies for anode materials aluminium (1486.6 eV) and magnesium (1253.6 eV). These theoretical cross-sections are effectively relative sensitivity for photoemission intensities from an infinitely thin layer of a given element measured using polarized x-rays at the, so called, magic angle to the direction of the analyser. These Theoretical RSFs can therefore be considered a more fundamental entity and are related to empirical RSFs by adjusting these theoretical RSFs for angular distribution, escape depth and instrumental response.

Escape Depth Correction

The discussion that follows assumes the measurement is performed with an instrument with a flat transmission response to kinetic energy for photoemission intensity.

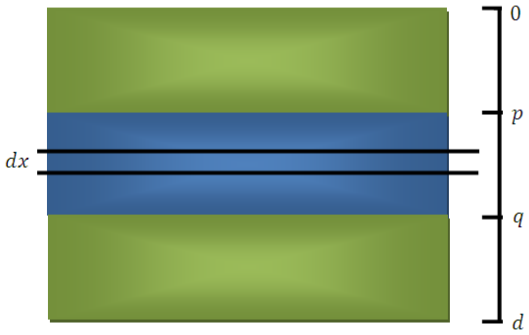

The intensity emitted at the surface I from a layer of material between the depths of p and q is proportional to the integral:

[1] $$I \propto \int_p^q \exp\left(-\frac{x}{\lambda\left(E_{Z_{nl}}\right)}\right)dx = \lambda\left(E_{Z_{nl}}\right)\left[\exp\left(-\frac{p}{\lambda\left(E_{Z_{nl}}\right)}\right) - \exp\left(-\frac{q}{\lambda\left(E_{Z_{nl}}\right)}\right)\right]$$

An element library containing Scofield cross-section $S_{Z_{nl}}$ (atomic number Z, principal quantum number n and orbital angular momentum quantum number l) represents a set of sensitivity factors assuming photoemission occurs at the precise interface between a material and the vacuum assuming photons arrive at the surface with the magic angle with respect to the direction for which electrons are recorded by the analyser. The measured photoemission intensity $I_{Z_{nl}}$ forming the basis for a measure of the amount of substance assuming a lamina associated with an element with atomic number Z must be scaled using Scofield cross-section $S_{Z_{nl}}$, namely, $\frac{I_{Z_{nl}}}{S_{Z_{nl}}}$, however if rather than a lamina the material is of thickness d, then the bulk equivalent amount of substance intensity $I^B_{Z_{nl}}$ is obtained as follows,

[2] $$I^B_{Z_{nl}} = \frac{I_{Z_{nl}}}{S_{Z_{nl}} \times \lambda\left(E_{Z_{nl}}\right) \times \left(1 - \exp\left[-\frac{d}{\lambda\left(E_{Z_{nl}}\right)}\right]\right)}$$

The expression $\lambda\left(E_{Z_{nl}}\right) \times \left(1 - \exp\left[-\frac{d}{\lambda\left(E_{Z_{nl}}\right)}\right]\right)$ derives from the escape depth correction assuming an exponential decay dependent on the effective attenuation length $\lambda\left(E_{Z_{nl}}\right)$ due to inelastic scattering of electrons within the sample prior to electrons emerging into the vacuum. If the material is of thickness d is greater than $3 \times \lambda\left(E_{Z_{nl}}\right)$ for all photoemission electron energies $E_{Z_{nl}}$, then $\exp\left[-\frac{d}{\lambda\left(E_{Z_{nl}}\right)}\right] \approx 0$ therefore the corrected intensity used in an atomic concentration calculation that accounts for escape depth is given by:

[3] $$I^B_{Z_{nl}} = \frac{I_{Z_{nl}}}{S_{Z_{nl}} \times \lambda\left(E_{Z_{nl}}\right)}$$

Escape depth has a profound influence on quantification by XPS for sample of a heterogeneous nature. The consequence of inhomogeneous depth distributions with very simple layer structure is illustrated by two scenarios for two materials measured using emission electrons with similar kinetic energy. Carbon and ruthenium measured using C 1s and Ru 3d emission peaks are two such materials.

Ru 3d and C 1s are emitted with the same kinetic energy. Assuming the same effective attenuation length $\lambda(E_{Z_{nl}})$ for both materials (which is not necessarily true), applying the exponential attenuation model then the following statements are true:

a) 95% of signal originates from $3\lambda(E_{Z_{nl}})$ depth.
b) 63% of signal originates from $\lambda(E_{Z_{nl}})$ depth.
c) 86.5% of signal originates from $2\lambda(E_{Z_{nl}})$ depth.
d) Only 8.5% of the signal originates from between $2\lambda(E_{Z_{nl}})$ and $3\lambda(E_{Z_{nl}})$ depths.

The following two depth distributions for carbon and ruthenium would result in very different atomic concentration values obtained by XPS.

Scenario 1: A layer of carbon of thickness $\lambda(E_{Z_{nl}})$ nm on top of a layer of ruthenium of depth $2\lambda(E_{Z_{nl}})$ nm measured using Al anode x-rays.

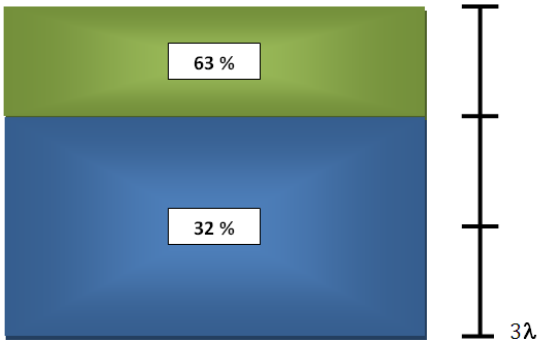

Given a model with ratio Ru:C = 2:1, XPS RSF corrected intensity ratio 32:63 approximately 1:2. Thus the ratio is the exact opposite of the true value for the amount of Ru to C.

Scenario 2: A layer of carbon of thickness $\lambda(E_{Z_{nl}})$ nm below a layer of ruthenium of depth $2\lambda(E_{Z_{nl}})$ nm measured using Al anode x-rays.

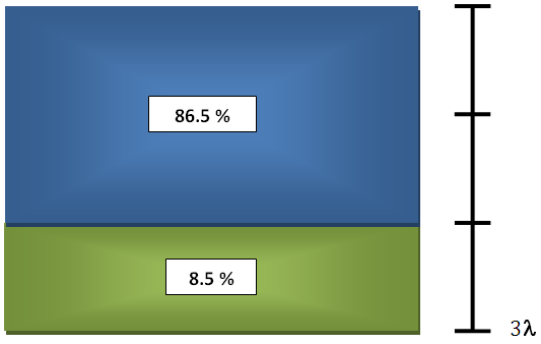

Given a model with Ru:C in the ratio 2:1 within the first $3\lambda(E_{Z_{nl}})$ nm, measured by XPS the RSF corrected intensity ratio would be 86.5:8.5 approximately 10:1.

The surface sensitivity of XPS provides remarkable information about the top 10 nm of material, but unless a sample is prepared to be homogeneous in depth and without contamination, the atomic concentration reported by XPS is not a representation of the sample composition in terms of proportions of elements.

Angular Distribution Correction

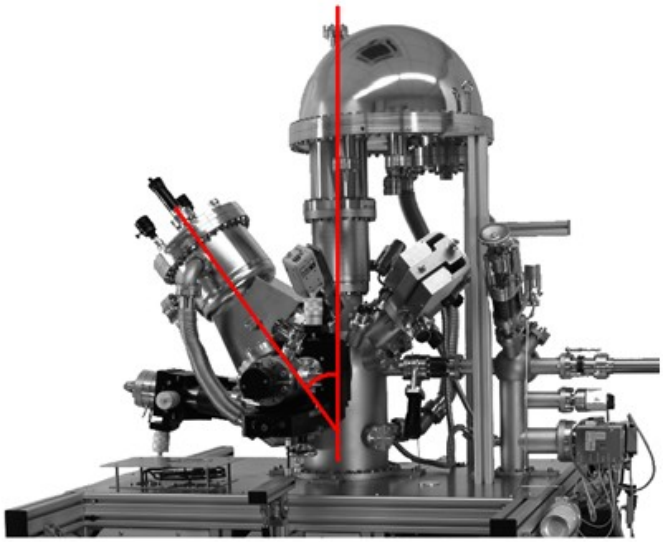

Scofield cross-sections do not account for angular distribution variation in intensity as a consequence of instruments detecting electrons in a specific direction relative to the photon source. Angular distribution correction to RSFs based on a given instrument geometry are applied resulting in total sensitivity values appropriate for a given x-ray source and the angle between the x-ray source and the direction defined by the electron energy analyser. Total sensitivity factors are corrected for angular distribution using the factor $1 - \frac{\beta}{4}(3\cos^2\theta - 1)$. Where θ is the angle between an x-ray source and the axis defined by the transfer lens system for an electron analyser angle and the value for β is computed for the element in question. Variation in intensity as a consequence of an instrument with $3\cos^2\theta - 1 \neq 0$ is performed at the time RSFs are extracted from the element library. Corrections due to angular distribution are applied to RSF values relative to s-orbital electron configurations which all respond identically in terms of direction, so RSFs are modified due to angular distribution correction for p, d and f photoemission lines only. These corrections appear as adjustments to element library RSFs when extracted from the element library and entered into quantification regions or component peaks RSF fields.

Instrumental Transmission Correction

The number of electrons recorded by an instrument at a specific kinetic energy for the detected electrons deviate from the number of electrons emitted from the sample. The ratio of electrons leaving the sample to the number of electrons recorded at the detector varies as a function of the kinetic energy for the emitted electrons. To adjust for these variations in collection efficiency an instrument transmission function is measured. A transmission function is prepared for each operating mode for a given instrument. Differences in operating mode may include specific settings for the pass energy, electron optical lens modes, aperture settings and detector settings.

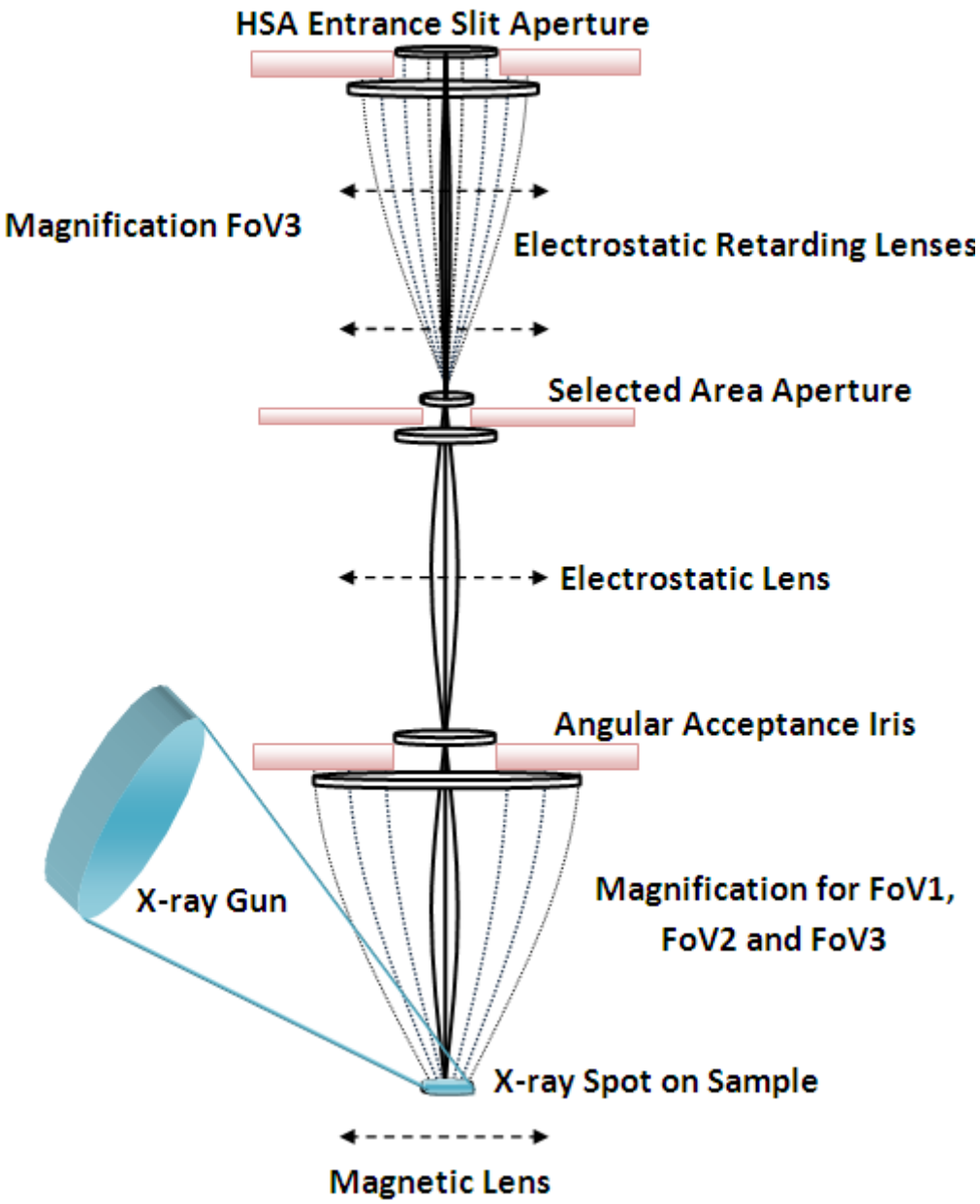

XPS Peak Fitting, Lineshapes and Quantification

Chemical state by XPS relies on accurate determination of binding energy, peak area and peak shape for photoemission signal. Electrons emitted from atoms in a specific chemical state are expected to appear with kinetic energy characteristic of the chemical state for that atom, while intensity measured by peak area allows stoichiometry for atoms to be assessed. Peak shape plays an important role for materials where multiplet splitting results in complex shapes in photoemission signal representing signatures for atoms in different oxidation states. While complex spectra are common with XPS, even complex spectral forms generate by XPS are attributed sequences of underlying peak shapes characterised by modified Lorentzian component peaks. It is therefore worth being a study of fitting XPS data with curves by considering the basics of fitting Lorentzian-like lineshapes to some of the more basic spectral shapes encountered in XPS data.

The starting point for almost all single peak lineshapes is based on the Cauchy probability density function which is referred to in XPS as a Lorentzian centre at the origin with height and FWHM equal to unity.

$$Lorentzian: l(x) = \frac{1}{1 + 4x^2}$$

There are many examples of XPS photoemission peaks that clearly contain a strong Lorentzian contribution. However, by virtue of measuring a photoemission peak, the instrument used to make such a measurement alters the recorded photoemission lineshape from that of the underlying photoemission shape. By considering the path of electrons emitted from the sample and before arriving at the detector it is possible to support the concept of a convolution as the mathematical tool used to modify a Lorentzian to model measured peak shapes (Figure 1). Approximating the interaction of these electrons with the instrument by a Gaussian through a convolution integral with a Lorentzian, a Voigt function (Figure 2) replaces a pure Lorentzian as the basis for a mathematic lineshape and once again there are many examples of photoemission peaks for which a Voigt function provides a very good fit to data.

The importance of lineshape to XPS is rooted in nonlinear least squares optimisation used to fit lineshapes to experimental data. The least squares criterion for selecting the best set of parameters used to specify a set of component peaks with respect to a given set of data works remarkably well provided the exact shapes for photoemission peaks are known precisely. However, if component peak within a model use lineshapes different from the exact photoemission lineshapes, then optimisation without constraints performs less well and can result in non-physical outcomes.

Not only is it important from a mathematical perspective to use lineshapes that closely model the actual photoemission signal, but it is also important to have reliable and understandable quantification that offers input when assessing stoichiometry and therefore relative numbers of expected component peaks when modelling chemical state signal. In the absence of such information as number of and shape for component peaks, parameter constraints are required to achieve satisfactory outcomes when modelling data with individual component peaks. Introducing of number of peaks presupposes chemical knowledge with respect to the sample and user intervention

via constraints to guide fitting of peaks to data also assumes prior sample knowledge. In an ideal experiment data would guide interpretation of spectra rather than bias introduced by user expectation.

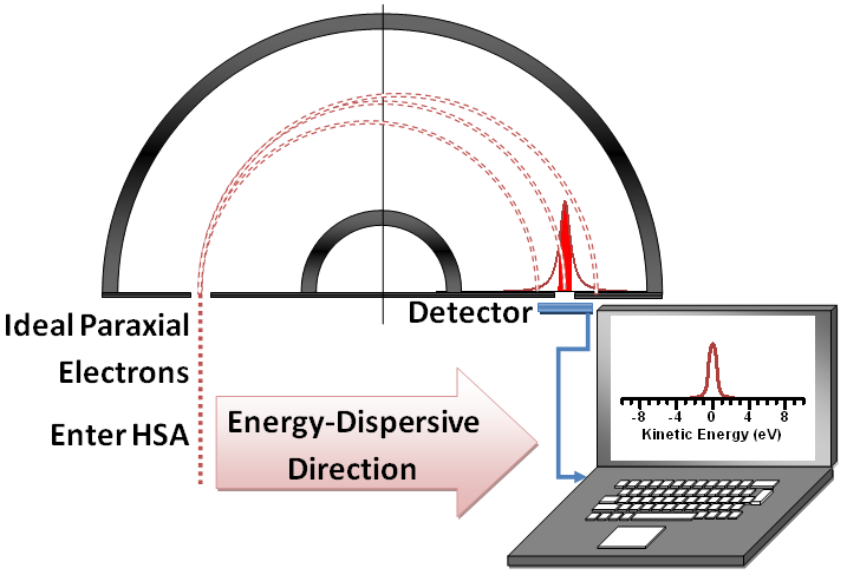

Figure 1: LA lineshape is a mathematical form that models the interaction of an input signal to an HSA with signal sampled through an exit slit leading to an electron detector. The larger the Gaussian parameter w the wider the exit slit and the closer the lineshapes resembles a Gaussian shape.

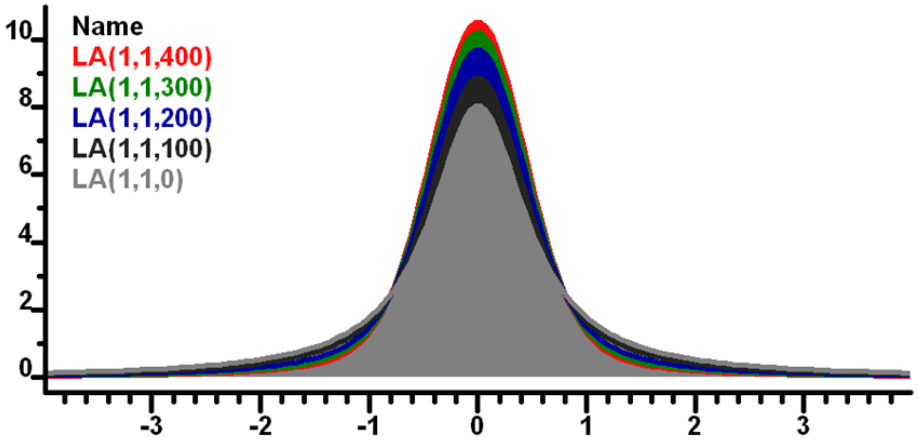

Figure 2: Voigt lineshapes formed by a convolution integral between a Lorentzian and a Gaussian. The LA(1,1,n) lineshape is a Lorentzian convoluted with a Gaussian of width controlled by the parameter n. The larger the value of n the greater becomes the Gaussian contribution to the Voigt lineshape.

Basics of Peak Fitting

Peak models are constructed from component peaks and a background approximation. A component peak is defined in terms of a lineshape and three optimisation parameters representing a component position, full width at half maximum (FWHM) and area. Using a simple case of a single photoemission peak from $AlPO_4$ in the form of Al 2s (Figure 3), a single component peak represents the entire peak model. A lineshape defined by the expression LA(1,193) is selected to obtain the best physically meaningful fit of a peak to data where the three optimisation parameters are

adjusted to achieve the best fit to data, in a least squares sense, given the lineshape and background approximation.

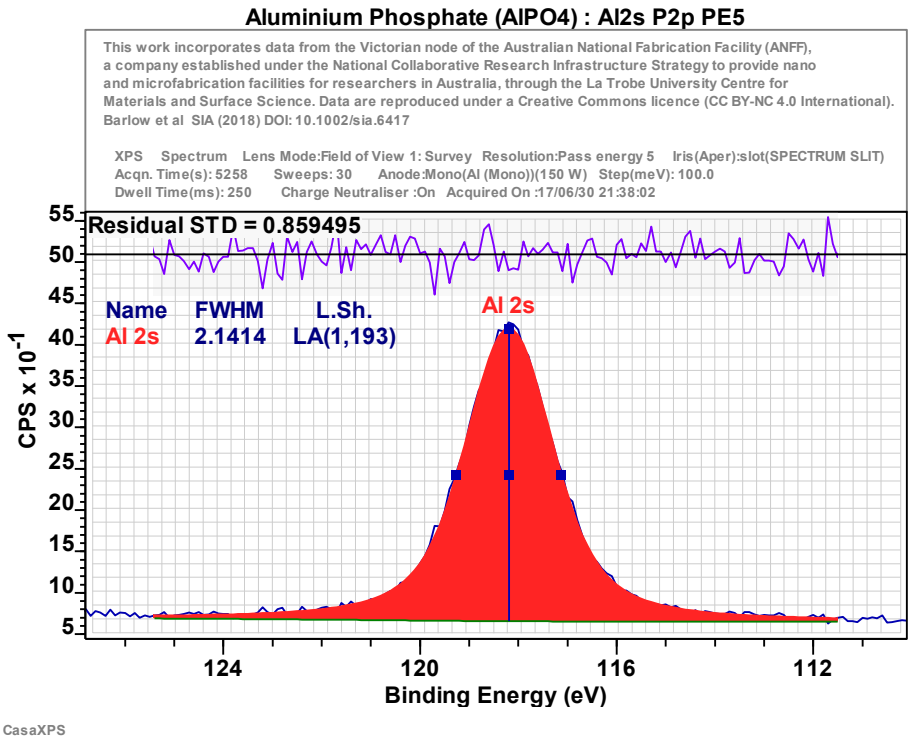

Figure 3: Example of fitting a Voigt lineshape plus a two parameter Tougaard universal cross-section background to Al 2s photoemission signal measured from aluminium phosphate.

Al 2s is a broad single peak with no overlapping peaks. The peak sits on a relatively flat background of inelastically scattered electrons from other processes allowing a model based on an LA (Voigt) lineshape which is a mathematically generated model that can be adjusted to match these real data. Features to observe from this example are:

1. The residual standard deviation is a measure for the goodness of fit encapsulated in a single value while the residual plot represents data from which the residual standard deviation is computed. The residual standard deviation for a well formed peak model fitted to pulse counted data should be close to unity while the normalised, with respect to standard deviation, residual plot should have the appearance of uniform random differences from a mean of zero.

2. The residual standard deviation in Figure 3 is less than unity because, while these are pulse counted data, the spectrum is formed by summing multiple data streams, the computation of which involves interpolation which if performed correctly effectively smooth data resulting in a figure of merit below the expected value of unity.

3. The lineshape is defined as LA (1, 193) representing a Voigt convolution integral between a Lorentzian and a Gaussian. The Lorentzian nature of Al 2s owes much to the lifetime broadening for these s-orbital states and a much less important contribution to the observed shape from instrumental factors.

4. Aluminium phosphate is an insulator and is such that few inelastic scattering events occur close to the Al peak resulting in energy loss for Al 2s photoemission the consequence of which is a flat background beneath the broad Al 2s peak.

5. The number of underlying peaks is known for such a simple peak model. For samples of less well known origin selecting the number of component peaks when modelling data is more of a problem.

6. There is little ambiguity within the optimisation parameters and identifying initial values used during optimisation is trivial in this case.

7. The relationship between lineshape and background is relatively easily understood compared to peak models involving multiple component peaks.

8. Optimisation of position, FWHM and area is achieved where both figure of merits, namely, χ^2 and root mean square yield almost identical results.

These points explain the successful fitting of a mathematically defined lineshape and a calculated background to an Al 2s peak. The background is in some sense equivalent to the selection of lineshapes as the background shape is computed from a mathematically specified inelastic scattering cross-section which is integrated with data to generate the background with little variation beneath the Al 2s peak.

The lesson taken from this simple example is that for a well formed peak model optimisation yields excellent results.

We now consider the next step-up in complexity for fitting of peaks to data, namely a spectral feature corresponding to two related photoemission processes.

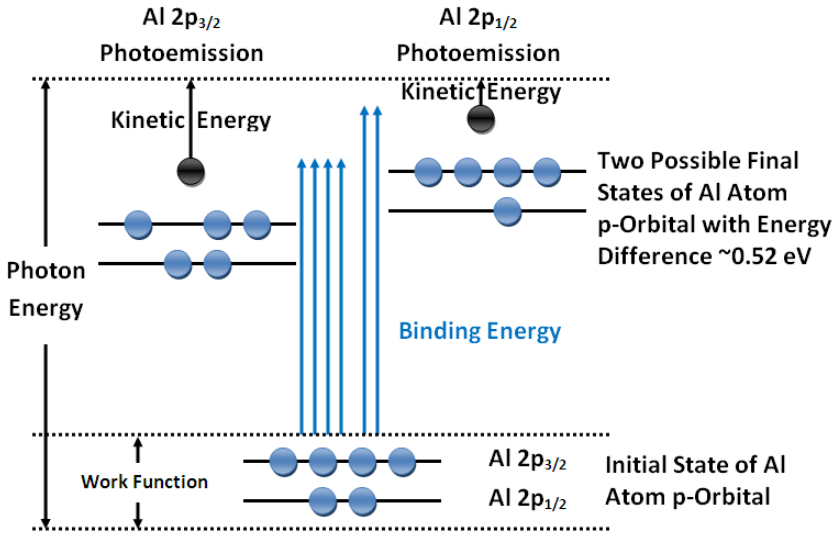

Figure 4: Mechanism by which p-orbital photoionisation results in a pair of photoemission peaks. The initial ground state is excited by photons via two possibilities specified by the j quantum number for an electron in an atom, where the resulting final states with a missing electron are offset in energy. The number of electrons corresponding to the j quantum number is 2j+1 and so the relative intensity, in a statistical sense, for these two peaks should be in the ratio 2:1.

In simple terms, XPS peaks appear as either singlet or doublet peaks. Al 2s is an example of a singlet peak where the initial and final states for the atom and the resulting ion are unique, hence for Al in a single chemical state only one peak is observed. Al 2p is an example of a doublet pair of peaks where a mechanism illustrated in Figure 4 shows the origin for labelling these doublet peaks Al $2p_{3/2}$ and Al $2p_{1/2}$ and the logic in terms of electronic configurations and energy levels for the existence of these two physically related doublet peaks corresponding to Al in a single chemical state. For the case of doublet peaks it is anticipated these peaks appear in a well defined intensity ratio, FWHM ratio and binding energy offset. In terms of constructing a peak model for Al 2p the physics underlying doublet peaks provides a clear connection between fitting parameters and such relationships can be used to define two component peaks in terms of three fitting parameters rather than six parameters required for two independent components within a peak model. Figure 5 is an Al 2p doublet measured from the same aluminium phosphate as the Al 2s spectrum in Figure 3.

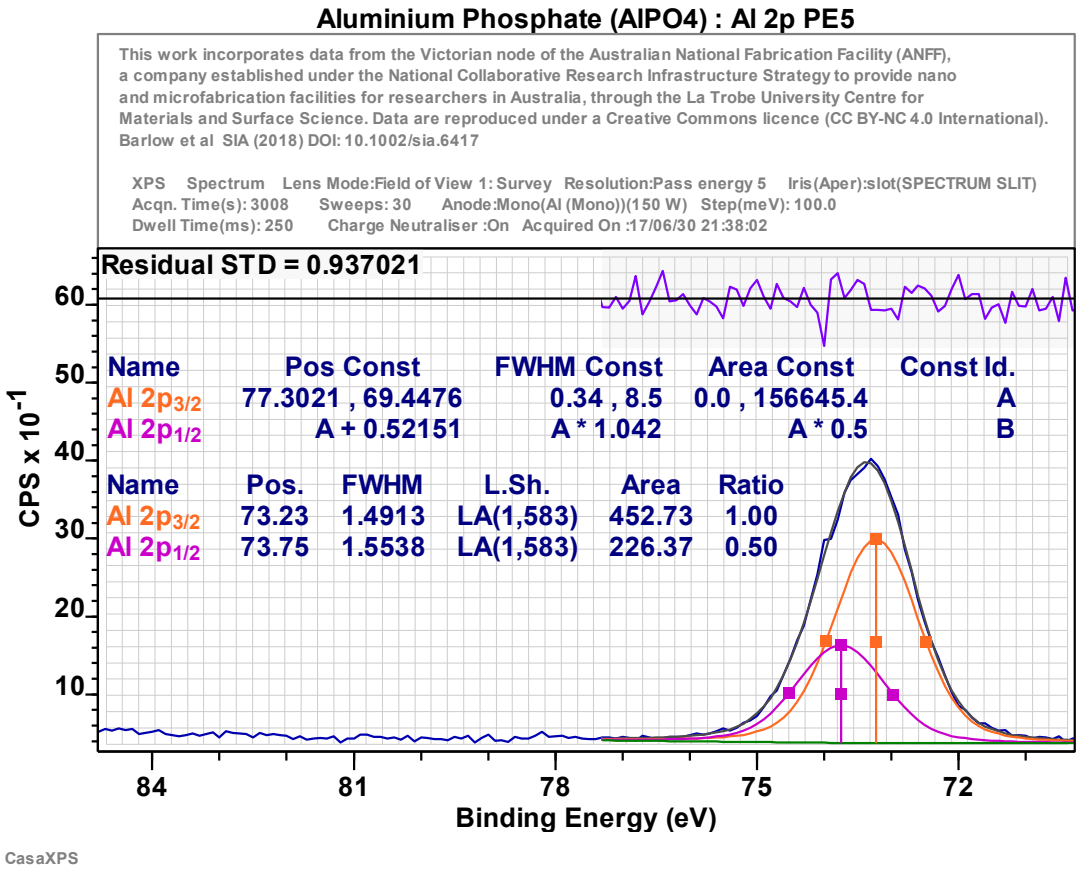

Figure 5: Al 2p measured from aluminium phosphate fitted using two component peaks. The constraints table indicates these two components are defined such that the area ratio is consistent with a pair of p-orbital peaks which should appear with intensity ratio of 2:1.

Points to observe about the peak model in Figure 5:

1. On first inspection this particular Al 2p spectrum appears to be a single peak and indeed it is possible to obtain a fit to these data by making use of a single peak. Nevertheless, Al 2p is a doublet and should be fitted using two components as shown in Figure 5.

2. The Al 2p doublet in Figure 5 represents an example of where two highly correlated peaks combine to form a spectral feature. Without prior knowledge about the nature of these peaks it would be very difficult to establish the intensities for these two peaks simply by guessing a lineshape and allowing optimisation to determine these component peaks that best fit the spectrum in Figure 5.

3. The lineshape for p-orbital Al photoemission is not the same as s-orbital Al photoemission. The component tables in Figure 5 indicate the lineshape for these Al 2p peaks are narrower than Al 2s and have a greater Gaussian contribution to the lineshape compared to the lineshape in Figure 3 used to model Al 2s.

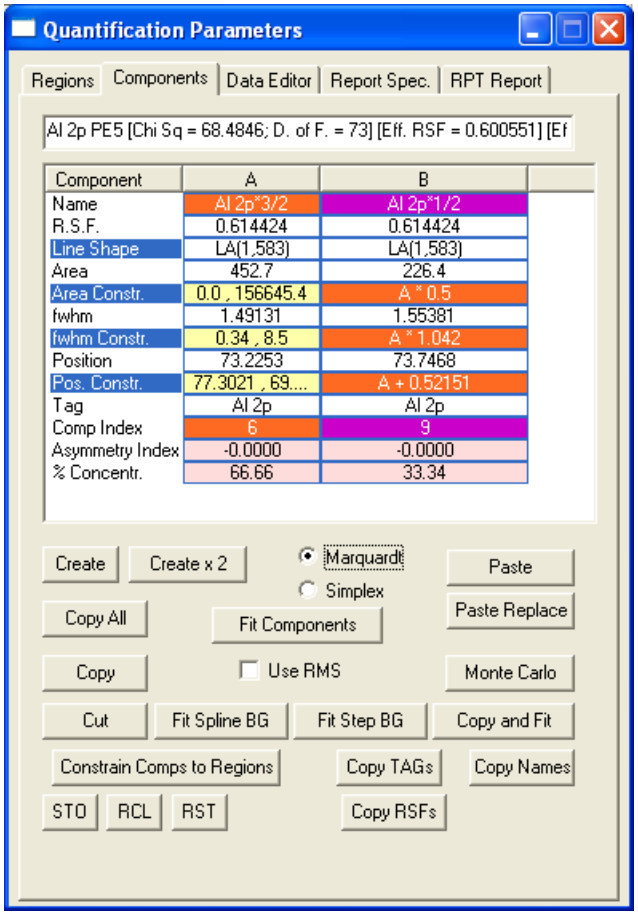

Figure 6: Quantification Parameters dialog window with Components property page top most. The two columns shown in the table correspond to two component peaks specified to reflect the nature of Al 2p doublet and illustrating how parameter constraints are defined between two components in a peak model. These component peaks and constraints correspond to the Al 2p peak model in Figure 5.

4. Parameter constraints are defined in terms of components in the order these components appear on the Quantification Parameters dialog window, Components property page of CasaXPS (Figure 6). The order for components is indicated by the heading labels to columns of component parameters and these headings are alphabetic characters starting with the character A. Thus Al $2p_{3/2}$ appears in the first column labelled A and Al $2p_{1/2}$ appears in column B. A constraint between the area parameter for these two components is entered in the constraints field in column B and specified as A*0.5 (Figure 6).

5. While two components are used to model the Al 2p spectrum, linking all three fitting parameters between these two components effectively reduces these two components to a new lineshape constructed using the sum of these two components in Figure 5. The concept of linking many components via optimisation parameters is applied to problems of significant complexity such as various iron oxides. Different oxidation states can be defined using many components but the number of optimisation parameters is small for each ensemble of components. Different oxidation states are described using different relationships between sets of components and separating oxidation states is reduced to fitting ensembles of component peaks all optimised as a unit by virtue of linked parameter constraints.

Applications of Fitting Peaks to Data

Charge Correction and Chemical State: Cellulose

Cellulose is a polymer containing carbon and oxygen in specific proportions (Figure 7). Hydrogen is also part of cellulose but XPS based on core level electrons does not offer information about hydrogen so an analysis of cellulose by XPS must focus on carbon and oxygen data only. However, hydrogen features in the XPS analysis by indirect means. These indirect means are differences in chemical state due to hydrogen implied by binding energy positions for component peaks within these carbon and oxygen spectra. C 1s and O 1s spectra fitted with component peaks are shown in Figure 8 and Figure 9. These spectra are plotted using a binding energy scale determined by the charge compensation state for the sample at the time of acquisition and as such do not offer an obvious connection between component peak position and chemical state for atoms within the cellulose polymer. Once a peak model is prepare for C 1s, energy calibration based on these carbon component peaks provides the means by which the binding energy for related carbon and oxygen components provide insight in to the state of the sample when measured and composition thereof.

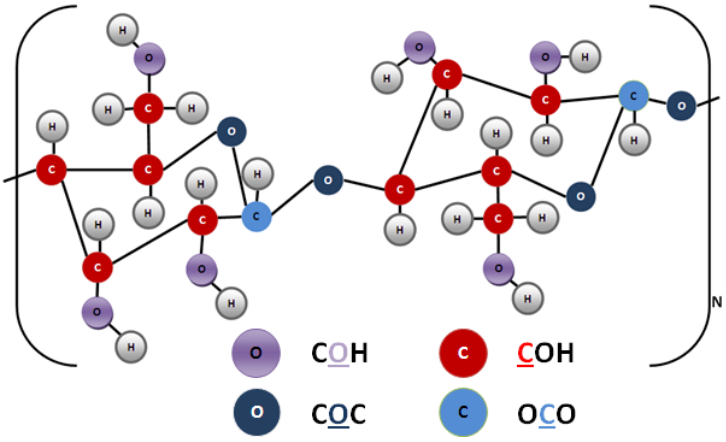

Figure 7 Cellulose polymer $C_6H_{10}O_5$

Observations about these peak models include:

1. Lineshapes for these C 1s and O 1s components are slightly asymmetric. Physics dictates that electrons ejected within the sample entering the vacuum chamber cannot gain energy unless energy is input at some point between the sample and the detectors. Any interaction with the instrument typically does not input energy so the most likely consequence for energy is that energy is lost rather than gained. Further, HSA and electron trajectories also

interact to provide other means for electrons of a given energy arriving at the detector in ways that move signal to lower energy, hence even for perfectly symmetrically shaped photoemission signal the recorded spectra tend to show evidence of asymmetry towards lower kinetic energy to the peak maximum. The exception to this rule is for samples suffering from poor charge compensation leading to a range of potentials at the sample surface that potentially accelerate and decelerate electron with respect to the most likely energy for a component peak. This caveat to the rule would imply analysis by modelling data with components is of limited value so the assumption when constructing peak models is that charge compensation is adequately performed.

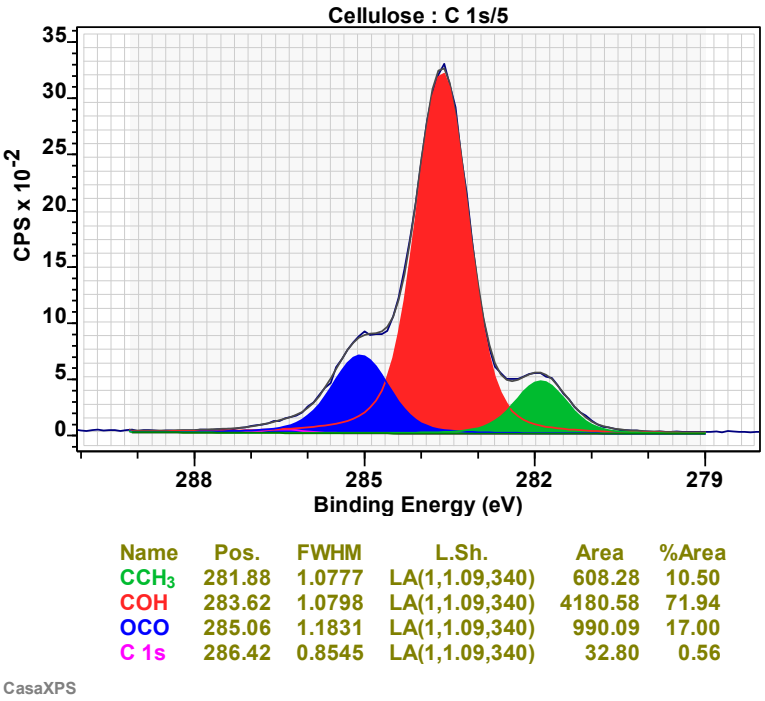

Figure 8: C 1s spectrum measured from cellulose. Data are presented using the charge compensated steady state for the measurement, that is, the binding energy scale is yet to be calibrated.

2. Construction for the peak models for C 1s and O 1s from cellulose was an iterative process coupled with comparison with spectra from a recognised database. Despite measuring these spectra from samples believed to be cellulose the existence of a low binding energy peak in Figure 8 is not consistent with the expected chemical environments for carbon. Figure 7 would suggest there should be two component peaks only, namely CO and OCO. We must therefore consider the possibility that these data are from a number of possible sources such as a contaminated sample, contamination is occurring during the period over which the sample is measured, cellulose degrades under x-rays or the sample may not have been pure cellulose in the first place.

3. Since C 1s appears to include three significant component peaks an analysis based on charge correction using different component peaks as the reference offers a means to investigate the possibilities for interpreting these spectra in Figure 8 and Figure 9. One scenario is to assume the lower binding energy peak corresponds to adventitious carbon and assign the right-most component a binding energy of 285.0 eV, after which other peaks within the C 1s

and O 1s spectra can be assessed by comparing binding energies to values reported in the literature for cellulose. Another possibility is to assume the central most intense component in Figure 8 is characteristic of CO and therefore charge correct components using the binding energy reported by Beamson and Briggs for the same component, for example, shifting all components by aligning the CO component with binding energy 286.73 eV.

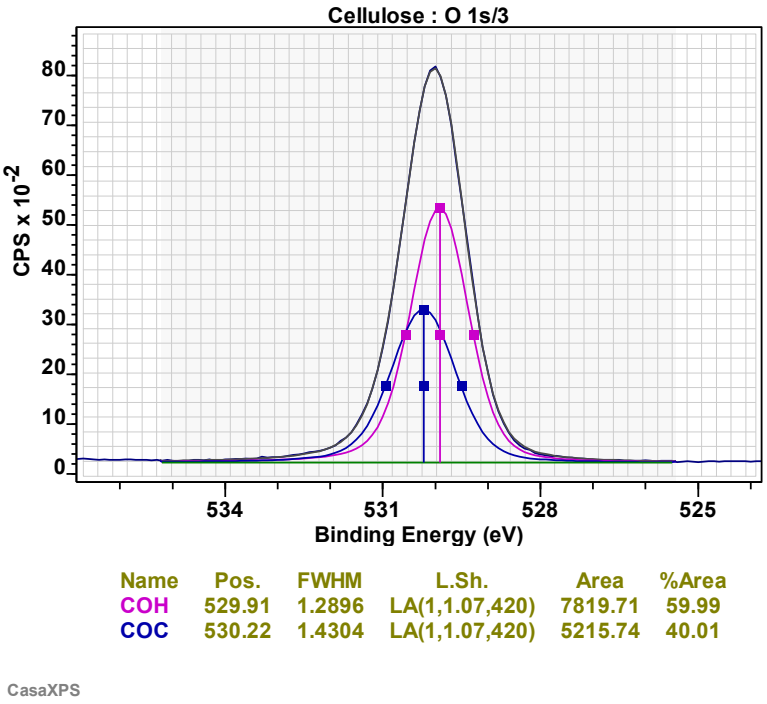

Figure 9: O 1s spectrum measured from cellulose. These O 1s components represent a challenge for optimisation and without the use of constraints the fit shown here would not be possible.

4. Cellulose as depicted in Figure 7 when measured using C 1s should yield two components in the proportion of 5:1 offset in energy due to chemical shifts due to CO and OCO. Similarly, O 1s components should appear as two components with intensity in the ratio 3:2 corresponding to COH and COC.

5. The chemical shift for O 1s photoemission between COH and COC chemical states is far less than for the corresponding C 1s peaks and is an example of highly correlated photoemission components where in the absence of parameter constraints a peak model fails to yield meaningful intensities and binding energies due to lack of perfectly defined lineshapes and background shape coupled with noise within data.

6. The ratio of 5:1 between C 1s cellulose peaks aids the construction of a peak model. A ratio of 3:2 with an energy offset of about 0.3 eV for O 1s components presents far more of a challenge to optimisation when fitting O 1s from cellulose.

7. Given an unexpected peak in the C 1s spectrum, these peak models in Figure 8 and Figure 9 are simplifications of the true model. One would expect other peaks to exist at low levels for both C 1s and O 1s. As a consequence uncertainty in binding energy assignments should be seen as possible and allowed for when comparisons are made to the literature.

8. Figure 10 shows the same cellulose C 1s and O 1s spectra after calibration based on the lowest binding energy component is assigned the binding energy 285 eV. Note that the CO component binding energy is almost exactly the energy report by Beamson and Briggs, namely binding energy 286.73 eV.

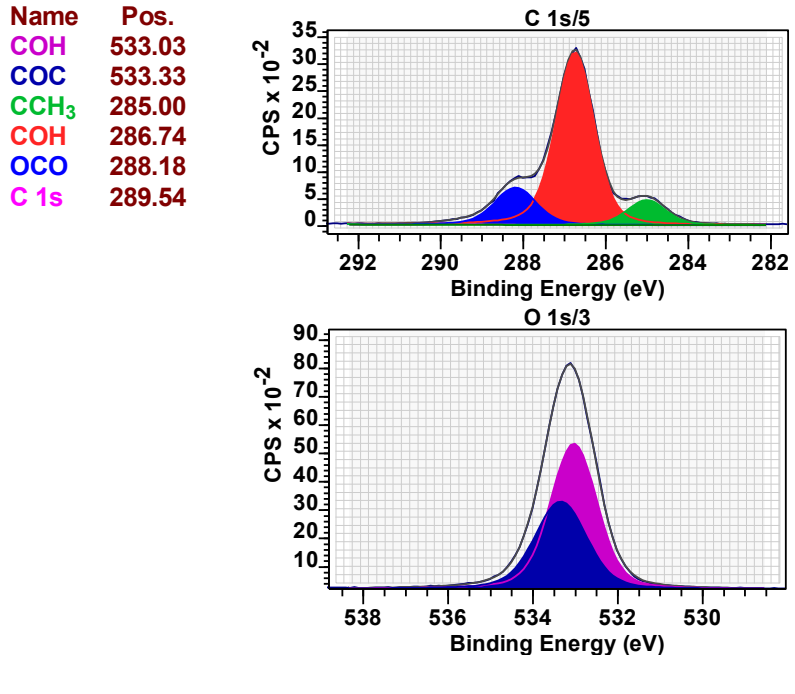

Figure 10: Cellulose C 1s and O 1s spectra after calibration based on lowest binding energy C 1s component assigned binding energy 285 eV.

Binding Energy and Kinetic Energy in XPS

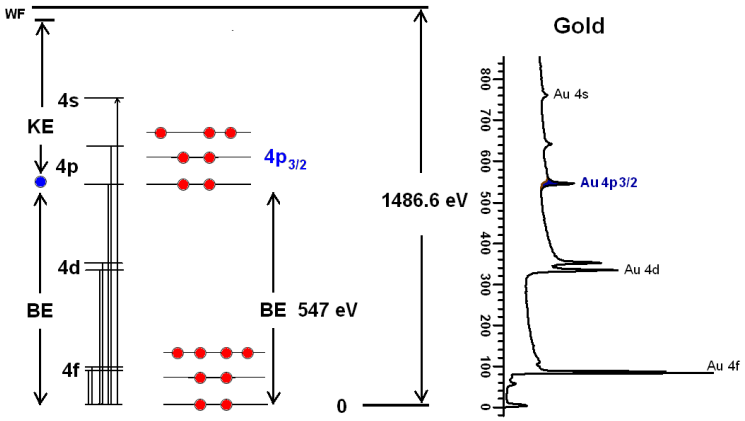

Figure 11: Energy diagram illustrating the relationship between the binding energy assigned to photoemission from $4p_{3/2}$ core level electrons in clean gold, recorded kinetic energy for photoelectrons, work function (WF) and excitation photon energy due to an aluminium anode X-ray gun.

XPS measures the kinetic energy E_{ke} for the photoelectrons (Figure 11). In the case of electrons emitted from bound states of atoms in an ideal conducting sample, the kinetic energy, the binding energy E_{be} and the photon energy $h\nu$ for an instrument with work function ϕ is given by

$$E_{ke} = h\nu - E_{be} - \phi$$

Energy from the perspective of XPS instrumentation is kinetic energy and for photoemission peaks the energy for these peaks, from the perspective of the instrument, changes with photon energy. Binding energy is a measure of potential energy with respect to an electron configuration within an atom from which photoemission occurs.

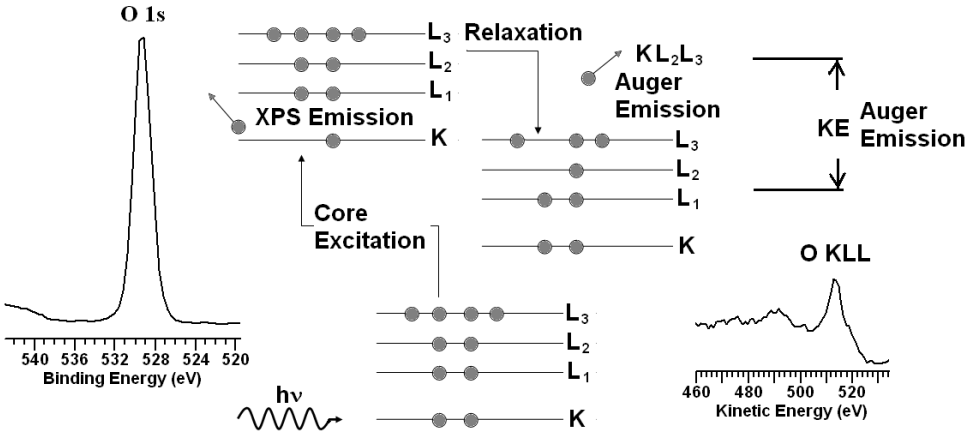

Figure 12: Energy diagram illustrating the relationship between photoionisation of an atom by a photon resulting in signal assigned to core level O 1s electrons and Auger signal due to emission of electrons as the excited state relaxes to a more stable excited state.

For the case of Auger emission (Figure 12), the relationship between the excitation source energy and the kinetic energy for the emitted electron is lost. Auger emission due to photoionisation generates electron emission with kinetic energy determined not by the photon energy, but by the difference between two bound electron states of the ion resulting from photoemission. Following the convention in XPS to use positive values for binding energy, kinetic energy for Auger photoemission measured by an XPS instrument is

$$E_{ke} = -(E_{be}[Initial] - E_{be}[Final]) - \phi$$

Both $E_{be}[Initial]$ and $E_{be}[Final]$ are binding energy values corresponding to ions created by photoionisation and are therefore absolute energies characteristic of these ions independently of the ionizing radiation energy.

Binding energy implies a clear relationship between the energy assigned to a photoemission peak and the chemical state from which signal derives. While the relationship between measured kinetic energy and binding energy is well defined for truly conducting materials connected to ground, for many samples the kinetic energy for photoelectrons depends on the actual potential between the sample and the detection system.

Without *charge compensation*, the act of returning charged particle to the sample surface to compensate for photoemission of electrons, a sample would become positively charged. For conducting samples that permit the free movement of electrons to all parts of a sample, charge compensation is a simple matter of electrically connecting the sample to ground. In the case of insulating samples charge compensation takes the form of actively returning charge to the sample via a cloud of low energy electrons and/or ions (Figure 13). If charge compensation is not performed electrons emitted by photons would be attracted by a constantly changing potential between the

surface and the analyser and therefore a photoemission peak would move in energy to lower kinetic energy as a function of measurement time (Figure 14). The act of charge compensation stabilises the potential at the sample and so kinetic energy for photoemission peaks is stable with time. Given stability of peaks in terms of kinetic energy, the energy scale can be calibrated to provide binding energy for peaks representing values of significance to identifying chemical state. The act of calibrating the energy scale in software is often referred to as *charge correction*.

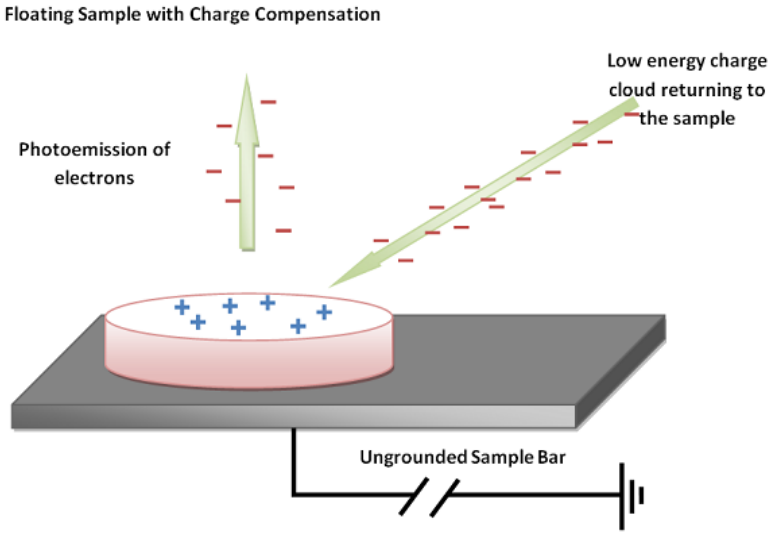

Figure 13: Insulating sample illustrating how photoemission results in positive charge on the sample that attracts low energy electrons from a charge compensation mechanism that prevents a continuous build-up of positive charge at the sample surface.

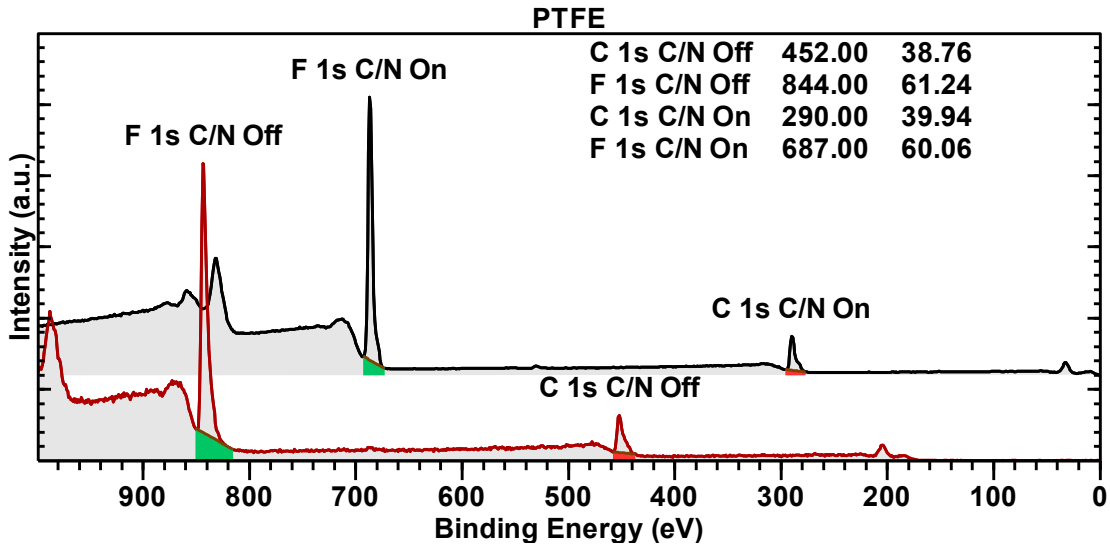

Figure 14: PTFE is an insulating material and when measured without the active use of charge neutralisation the sample potential increased with measurement time. These two spectra are measured from the same PTFE sample with (C/N On) and without (C/N Off) charge neutralisation. Note how the photoemission peaks for F 1s and C 1s are recorded at lower kinetic energies than is the case when charge compensation is enabled which is a consequence of a build-up of positive charge at the sample surface.

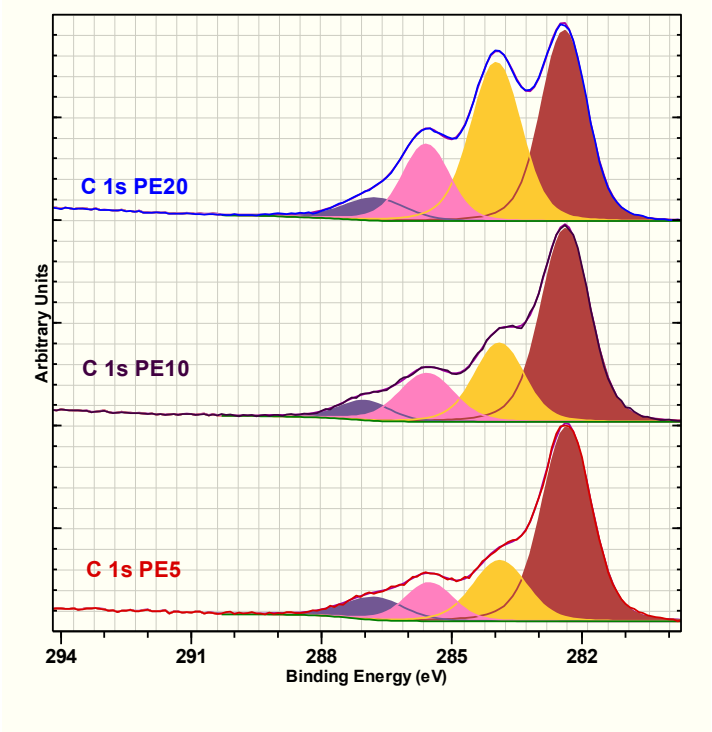

Figure 15: Alginic acid sodium salt C 1s measured over time using three different pass energy settings. Note how the initial PE20 C 1s spectral shape is significantly different from the one recorded using PE5. The evolution in C 1s component peaks is similarly matched by an evolution of O 1s suggesting the relative intensities for these component peaks are dependent on the sequence of measurements rather than the as received sample composition.

This work incorporates data from the Victorian node of the Australian National Fabrication Facility (ANFF), a company established under the National Collaborative Research Infrastructure Strategy to provide nano and microfabrication facilities for researchers in Australia, through the La Trobe University Centre for Materials and Surface Science. Data are reproduced under a Creative Commons licence (CC BY-NC 4.0 International).

Basic Approach to Fitting Data with Peaks: Alginic Acid Sodium Salt

In this section an apparently simple case for peak fitting is considered in detail.

A peak model is defined in terms of component peaks and a background algorithm. These component peaks are in turn specified using lineshapes and fitting-parameters to permit a component peak to vary in position, FWHM and area. Sets of component peaks are summed then added to a background shape to form an approximation to a data envelope.

The primary objective when fitting data with peaks is to assign component peaks to photoemission processes characteristic of elemental and/or chemical information. Optimisation algorithms help to fit peaks to data, but without significant input from physics and chemistry optimisation based on a single value figure-of-merit will not yield comprehensive scientifically meaningful results. Physical and chemical information is added to a peak model through the selection for lineshapes, the number of component peaks within a peak model and parameter constraints offering the means by which known relationships are imposed on otherwise independent component peaks.

The example used to discuss fitting data with peaks is based on data downloaded from the La Trobe XPS database (Barlow et al). These data are therefore typical of results obtained by XPS performed without access to or control of the experimental state during a sample analysis. These data are necessarily made available with limited sample and analysis information, meaning, the sample is

specified as alginic acid sodium salt but sample state, sample preparation and sample measurement are not under the control of the person wishing to understand this material by XPS. The real power of XPS lies in iteration and feedback which is especially the case whenever peak fitting is involved. That is, initial measurements after analysis provide insight stimulating later experiments focused on optimising information gathered by XPS.

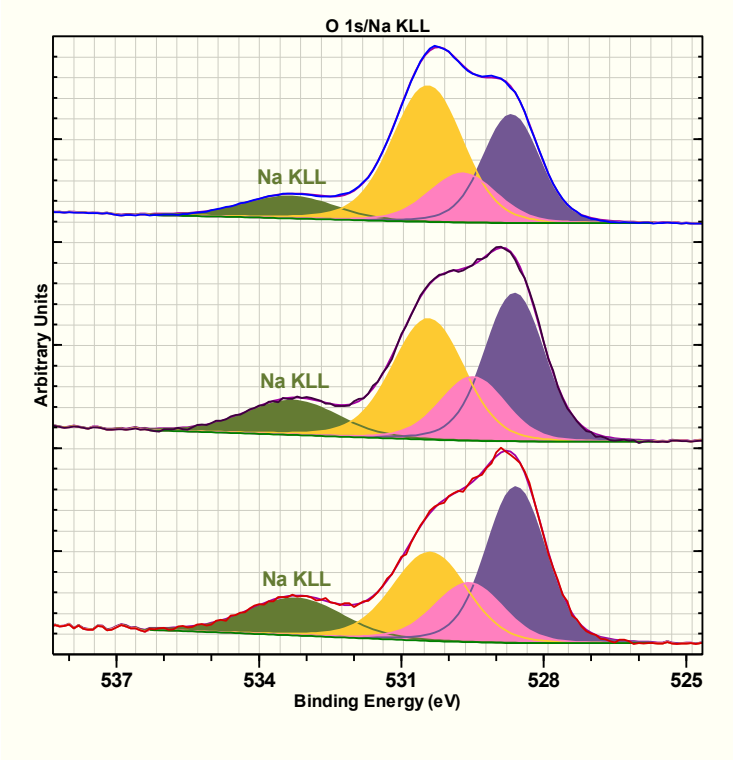

Figure 16: Alginic acid sodium salt O 1s spectra corresponding to C 1s spectra in Figure 15.

There is no easy prescription for constructing a peak model when simply supplied with a single spectrum such as the ones displayed in Figure 15. Happily, these C 1s spectra are accompanied by survey and relevant narrow scan spectra to supplement these C 1s spectra. The C 1s spectra in Figure 15 would be amongst some of the easiest for which a peak model could be constructed, but nevertheless, apart from providing an example of how some materials alter during measurement the model offered in Figure 15 is open to criticism for simply fitting obvious peaks within these data. In favour of fitting four peaks to these data in Figure 15 is that the model demonstrates how components attenuate relative to one another over a sequence of measurements, and represents qualitative information about the sample gained by virtue of repetition. Without additional information about the sample, measurement and more systematic repetitions of identical experiments it is difficult to construct a truly meaningful model for these data. The model ignores possible contamination issues. Contamination typically involves carbon and oxygen, so the peak model in Figure 15 is only presenting a partial story for these data as no explicit peaks target possible adventitious carbon. One should also be aware that chamber history and cleanliness is a potential source for evolution of C 1s spectra. Nevertheless, when coupled with O 1s spectra, XPS supports the existence of carbon bonded to oxygen and that the material loses carbon bonded to oxygen as a consequence of these measurements. The means by which this hypothesis is deduced is a similar simple peak model for O 1s in Figure 16 (allowing for Na KLL interference) similarly suggests changes in relative intensities in O 1s that correlate with C 1s attenuation. Thus even a limited peak model is

capable of extracting evidence about a sample even if a full understanding for a material is not necessarily possible.

At this point it is worth noting that any conclusions from the experiment resulting in data shown in Figure 15 and Figure 16 require verification by repeating these measurements on equivalent samples to confirm the observed changes are represented of the sample only.

Despite acknowledging the limited nature of the peak model in Figure 15, even for this basic peak model there is value in describing how such a peak model might be justified.

The mechanics of creating these peak models in Figure 15 and Figure 16 include considering the use of other data such as sodium chloride data (also within the La Trobe database) to confirm the Na KLL contribution to data nominally assigned as O 1s. Basic information about alginic acid sodium salt ($NaC_6H_7O_6$) correlated with elemental quantification from survey spectra provides context for these C 1s spectra. In particular based on survey data, within the volume of material sampled by XPS the amount of carbon compared to oxygen suggest an excess of carbon over oxygen. It is also worth looking at other similar materials in an attempt to gain understanding for what might be possible within these data. For example a similar material is cellulose. Consulting Beamson and Briggs XPS of Polymers Database suggests two C 1s peaks for a similar arrangement of carbon and oxygen in the absence of sodium ions and double bonds. Ethyl cellulose also within Beamson and Briggs offers a variation on cellulose where OCH_2CH_3 arrangements of carbon and oxygen introduce a third C 1s peak at binding energy 285 eV. So, based on this limited literature search it is feasible that at least four carbon peaks are offset in energy relating to C-O, O-C-O, O-C=O and then some other factor responsible for a low binding energy peak.

Once the number of peaks is established, the next step is to consider possible parameter constraints and how these can be used to enhance information gathered from a peak model.

Owing to the evolution of these C 1s data envelopes (Figure 15) between measurements the relative intensities for component intensity and therefore area parameters are not considered significant with respect to this particular sample chemistry. The implication for this statement is area parameter constraints linking the relative area for peaks are not appropriate in this instance. Application of area constraints to component peaks is an example of input of chemical knowledge when constructing a peaks model. However, since these C 1s peaks evolve with time it is not possible to provide chemical input in terms of peak area to help guide optimisation towards a scientifically meaningful result. For other samples, area constraints are used but should be recognised as potentially introducing user bias into the model.

Area parameter constraints are particularly useful for doublet peaks originating from the same electron configuration initial state where the final state electronic configuration is split between two possible outcomes. Physics for the photoionisation of electrons dictates these double peaks appear offset in energy, representing the difference in energy between the final states and in a defined ratio in terms of peak area. Scofield cross-sections were calculated for photons with energies corresponding to x-ray gun anodes made of aluminium and magnesium and these cross-sections include relative intensity for both peaks in a doublet pair. Thus the ratio for these peaks can be readily fixed by making use of Scofield cross-sections to estimate the relative area imposed by area constraints within a peak model.

Peak width represents another important constraint for peak models. The set of C 1s component peaks in Figure 15 when fitted to these different spectra measured using different pass energy should result in better resolved peaks. However peak width for a photoemission line can be due to factors other than the underlying lineshape (vibrational broadening for example) or the underlying lineshape is much broader than the instrumental broadening in which case reducing the pass energy does not necessarily lead to improved energy resolution, but in theory reducing the pass energy does improve the purity of energy information and therefore lineshape. Obtaining the best possible energy resolution (subject to signal-to-noise limitations) helps to establish lineshapes. These C 1s spectra are broader than can be explained by instrument broadening, so component widths are more related to sample. Monitoring component width is important in the sense that an element of consistency might be expected for a set of C 1s peaks. Abnormally narrow or wide peaks are an indication optimisation is resulting in a minimum for the figure-of-merit but failing to model physically meaningful signal. As a general rule, application of appropriate FWHM constraints guides optimisation to superior outcomes than models without any limits applied to component widths.

In the case of these C 1s components in Figure 15 (pass energy 20 and pass energy 5) there is a concern the smallest component has a FWHM noticeably wider than the other components. Some variation might be justified for these peaks, but a low intensity relatively broad component might indicate the component is of limited physical significance. In the case of alginic acid sodium salt the peak in question could be assigned to O=C-O signal so this could be important information aimed at characterising the sample by XPS.

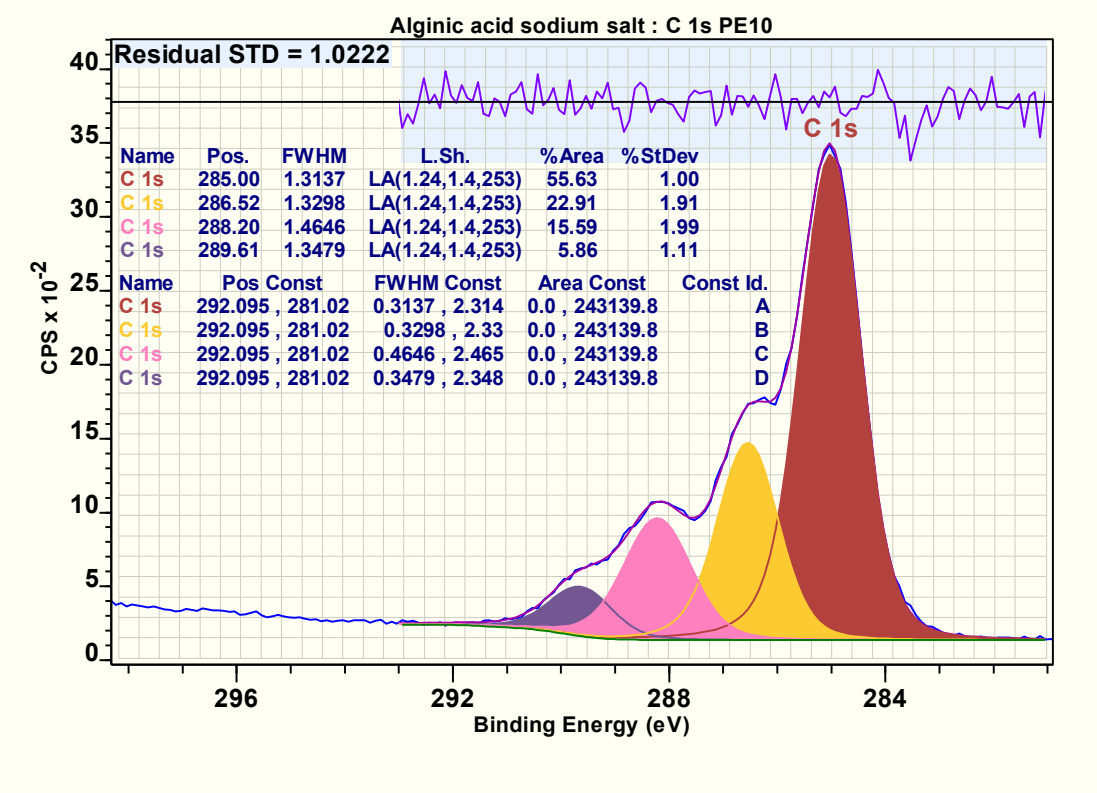

Figure 17: Pass energy 10 C 1s spectra shown in Figure 15 displaying component tables displaying Monte Carlo error estimates for the peak model subject to effectively no constraints applied to optimisation parameters used to fit these data. A comparison to the constrained model in Figure 18 illustrates how introduction of two constraints aimed at FHWM relationships significantly improves the ability of a peak model to measure intensity using component peaks.

Component binding energy is a strong indicator for possible peak assignment. FWHM and position tend to interact where the better defined FWHM the more significance can be attributed to component position. Relative component positions are the principal source for chemical state information. Beamson and Briggs when reporting results for cellulose assign binding energy of 286.73 eV to C-O bonds and 288.06 eV to O-C-O bonds. The peak model in Figure 15 after energy calibration assuming the low binding energy component is located at 285.0 eV yield binding energy for the remaining three components of 286.5 eV, 288.2 eV and 289.6 eV. These binding energy values, although not conclusive, would be consistent with C-O, O-C-O and O-C=O, respectively for these three component peaks. Position constraints represent a direct intervention to values of significance to a sample and for the most part these positions represent information we hope to extract from a peak model. For this reason it is more often the use of FWHM constraints and the indirect constraints imposed by lineshape selection that allows position information to translate into chemical state output from a peak model.

Assuming the lower binding energy peak is shifted to 285 eV is an assumption that results in the assignments for these other C 1s components. It is not entirely clear from these data this assignment is true. Doubt regarding the origin for the peak used to calibrate the binding energy scale implies uncertainty in the binding energy calibration, but experience of cellulose spectra lend support to the possibility of such a peak of similarly unknown origins. While calibration based on a peak at 285 eV is expedient for this discussion, it should be noted O-C=O can result in C-CH_3 C1s intensity shifted to higher binding energy so the peak used to calibrate the binding energy scale could easily be formed from two peaks offset in energy by about 0.5 eV and of different proportions in intensity.

The single biggest factor in calculating these component positions is the use of specific lineshapes and the C 1s data offering peak like structures that can be identified by eye. By way of contrast, apart from the component peak representing Na KLL, the O 1s peak model is without merit other than to illustrate at least one component peak resembles the attenuation seen in C 1s data. Fitting O 1s spectra, such as data in Figure 16, with multiple overlapping component peaks without sample knowledge based on optimisation alone is far less reliable than the information gathered from these C 1s spectra in Figure 15.

Stability with respect to optimisation for a peak model is another important consideration. Stability for a peak model with respect to a single spectrum only is less informative than if a peak model exhibits stability when applied to a number of equivalent measurements. In the absence of equivalent spectra the next best approach is to test a peak model using Monte Carlo methods to simulate a set of equivalent spectra and estimate uncertainties in outcome for a peak model fitted to these simulated data.

In terms of peak model stability, both peak models in Figure 15 and 16 make no use of optimisation-parameter constraints but rather rely on lineshape specification to return an optimised solution for the peak model to these data. While the resulting solution is stable with respect to these specific measurements, the value of FWHM parameter constraints is illustrated by considering how stable these four component peaks are in terms of peak area with respect to the level of signal to noise expected for these spectra. Figure 17 includes the four component peak model used in Figure 15 tested for stability with respect to noise using Monte Carlo error analysis. The component tables plotted in Figure 17 show the error calculated for the %Area for the case where fitting parameters

are allowed to adjust within intervals. These same data are fitted using a modified peak model where the same relative FWHM are maintained via optimisation parameter constraints shown in Figure 18. Monte Carlo error analysis indicates the model in Figure 18 is noticeably more reliable at measuring %Area than the model in Figure 17 and these improvements are achieved by linking FWHM constraints only.

A note of caution: if the goal is to understand chemical state information in spectra, adding parameter constraints will improve stability of a peak model with respect to noise, however with each new constraint the output from optimisation converges on the solution defined every more closely by these constraints until the usefulness of fitting peaks to data is lost. If the goal is to measure intensity and a peak model is well formed, then a rigid peak model heavily constrained will tend to return more consistent intensities for data with similar chemistry and experimental conditions when measured. Somewhere in the middle of these two extremes is the domain for most applications of constraints when fitting peaks to data.

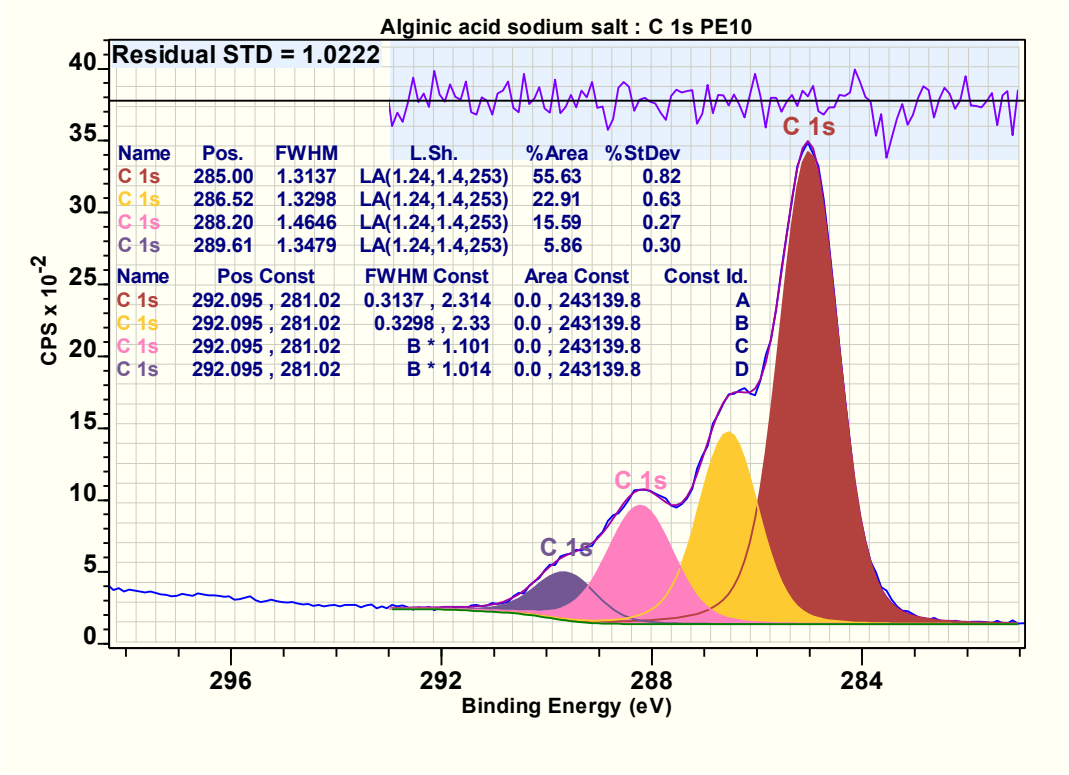

Figure 18: Pass energy 10 C 1s spectra shown in Figure 15 displaying component tables displaying Monte Carlo error estimates for the peak model subject to constraints applied to FWHM optimisation parameters used to fit these data. A comparison to the unconstrained model in Figure 17 illustrates how introduction of two constraints aimed at FHWM relationships significantly improves the ability of a peak model to measure intensity using component peaks.

Complex Peak Structure in XPS: Copper

The examples up to this point make use of the concept that to each chemical state within a peak model there is a component peak that identifies said chemical state. While for many samples the one-chemical-state one-synthetic-component approach is adequate, there are many examples where this model is of limited use. To illustrate this point, examples of copper oxide follow that exhibit both simple and complex structure.

For an isolated copper atom the electron configuration can be viewed as

$$1s^2 2s^2 2p^6 3s^2 3p^6 3d^{10} 4s = [\mathrm{Ar}] 3d^{10} 4s$$

When in solid state, the XPS of copper results in spectroscopic features depending how compounds make use of valence electrons $3d^{10}4s$ with both significant and insignificant differences in core level photoemission peaks depending on oxidation state. Only by comparing valence band and Auger spectra is it possible to distinguish between metallic copper and Cu_2O (Cu^{1+}). Photoemission from Cu 2p and Cu 3p for these Cu^0 and Cu^{1+} are highly correlated in terms of binding energy and peak shape, whereas there is a dramatic change to these photoemission peaks for copper in a 2+ oxidation state. These Cu^{2+} spectra demonstrate how photoemission peaks do not necessarily conform to the concept of well defined peaks that can easily be approximated by a single component within a peak model representing a chemical state for said material. Rather than one-to-one correspondence between component peaks and chemical states, copper provides examples of where XPS yields spectral signatures for chemical state spread over many eV. Separation of chemical state signal based on these types of data envelopes remains a goal for XPS, but assigning binding energy to specific features with these extended structures is not as important as the intrinsic shape that conveys the identity of oxidation state. Figure 20 displays Cu 2p doublet peaks that 1) spread over an energy interval of more than 30 eV and 2) illustrates the changes possible for spectra where incomplete electron shells results in complex structures not easily open to interpretation by individual components within a peak model.

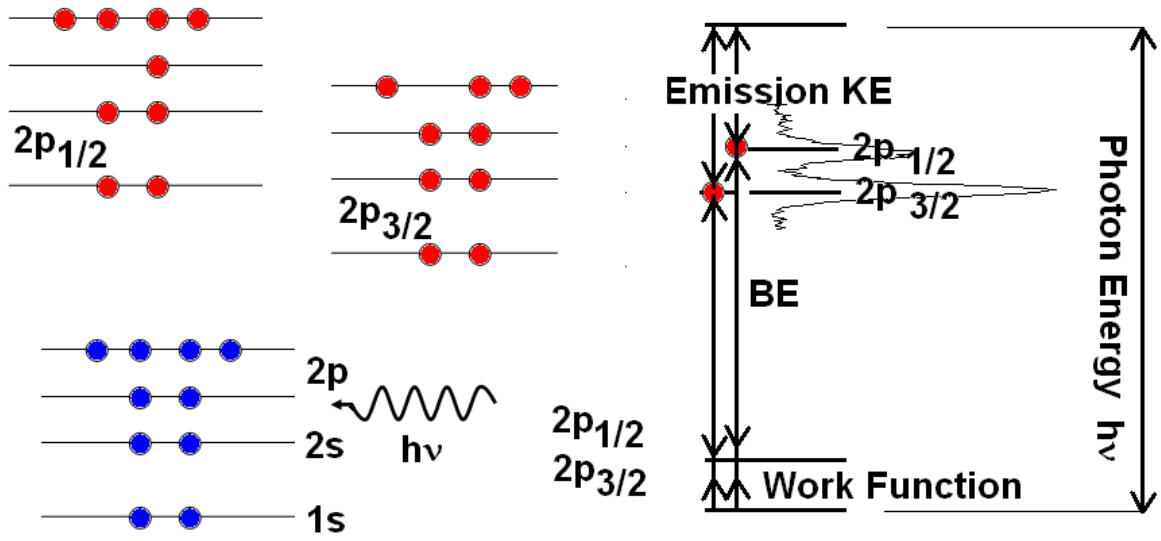

Figure 19: Photoemission of a 2p core electron results in two peaks due to unpaired electrons in two possible final states for the ion. In the case of Cu 2p photoemission these two doublet peaks appear at energies separated by about 20 eV. Depending on bonding of copper to other elements, additional splitting of energy levels is possible and these contribute to the complexity for Cu 2p doublets observed for Cu^{2+} compounds.

The concept of characteristic peak formations becomes more important for heavier elements. Cerium oxide represents a further example of where multiplet splitting creates shapes characteristic of Ce^{4+} and Ce^{3+}. These and many other cases emphasis the need to consider lineshapes as more than simply individual mathematical defined shapes capable of contributing to fitting of data, but rather as complex shapes extended over wide energy intervals which can be used within a peak model to replace complex component arrangements.

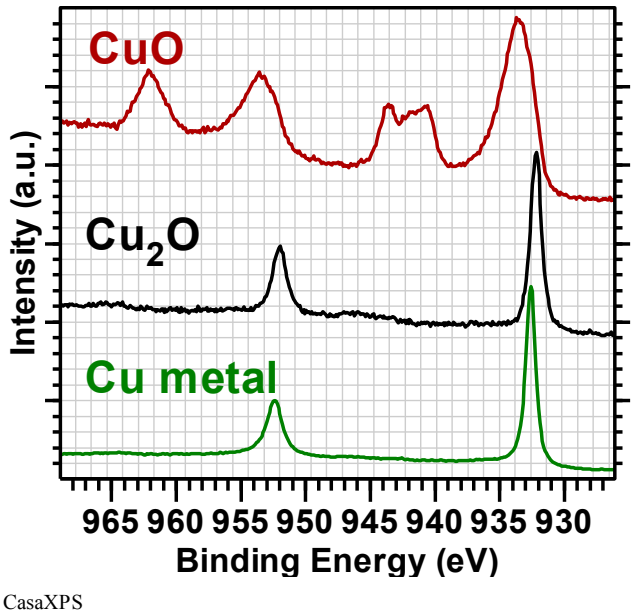

Figure 20: Copper metal and oxide spectra illustrating a similarity between Cu 2p for Cu^0 and Cu^{1+} (Cu_2O) while Cu^{2+} (CuO) takes a form dictated to by multiplet splitting for a material where both d and s orbitals contribute to the oxide formation. Binding energy for Cu^{1+} and Cu^{2+} are not well defined as both where measured using charge compensation.

We now return to the concept of individual component peaks associated with specific chemical state.

Asymmetry in Measured Photoemission Peaks

Measured photoemission peaks, particularly from metallic materials, exhibit asymmetric profiles. These profiles are a result of a number of factors. Nevertheless the objectives for modelling such data remains the same, namely, identification of signal for use in quantification calculations and assigning binding energy to component peaks as a means of separating chemical state information in spectra. In this section the origins of asymmetry in XPS peaks is discussed and asymmetric lineshapes are investigated.

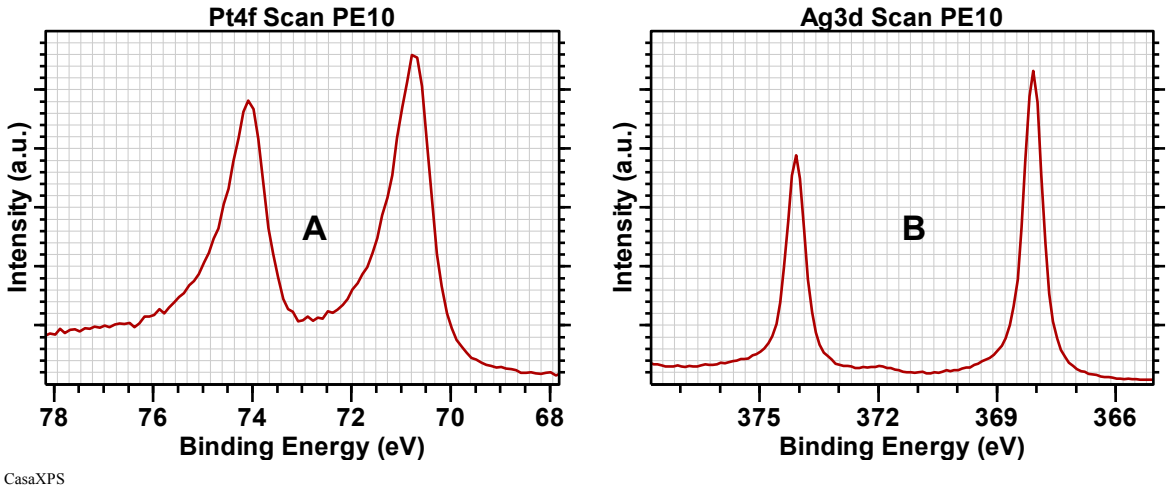

Figure 21: Sputtered platinum and silver foil measured using a Thermo K-Alpha XPS instrument under identical operating conditions.

Metallic photoemission peaks are a particular challenge for XPS as these are apparently well formed peaks but are accompanied by a rise in background and often suggest asymmetry should be part of a peak-model. Platinum is shown twice, once measured using a Thermo K-Alpha (Figure 21) and once using a Kratos Axis Nova (Figure 22). The reason these Pt 4f doublet peaks are shown is to demonstrate both instruments yield similarly asymmetric shapes but it should be noted there will be an element of instrumental factors in these data hence lineshapes from the same material measured using two different instruments will not necessarily be identical. It should also be noted these 4f doublets in Figure 22 vary in asymmetry and shape despite being measured using identical instrument settings. Lineshapes from one material do not translate into a lineshape for other similar photoemission signal from different materials.

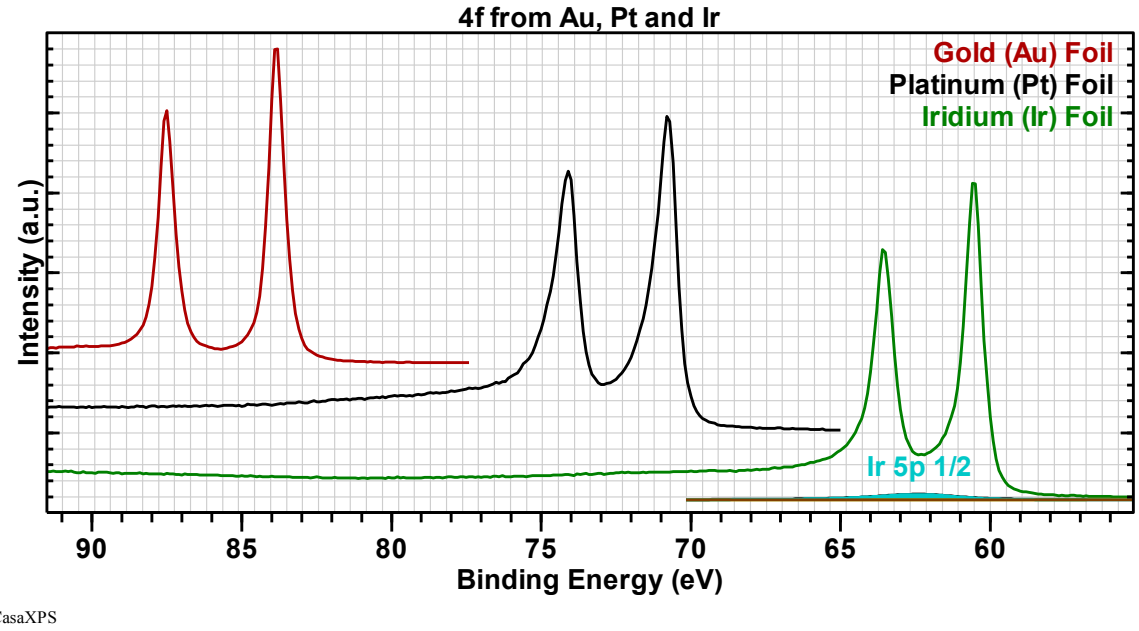

Figure 22: 4f doublet photoemission peaks from the La Trobe database. These data measured using a Kratos Axis Nova using pass energy 5 FoV1 slot/slot aperture illustrate how asymmetry is a feature of metallic samples and the apparent asymmetry changes for different metals. It should also be noted that Ir 4f overlaps with Ir $5p_{1/2}$.

There are several points regarding metallic peaks worth noting:

1. The background of inelastic scattered photoemission signal is much more of a challenge for metallic samples than for insulators. Energy loss events for signal from metallic photoemission peaks occur at energies characteristic of the zero-loss signal. This implies background and zero-loss signal are highly correlated and therefore difficult to separate.
2. A rising background signal is one potential source for asymmetry in metallic photoemission peaks.
3. Energy loss events include inelastic scattering where electrons moving through the solid state to the vacuum lose energy en route, shake-up events where excitation of bound states occurs as part of the photoionisation event leading to nominally zero-loss signal appearing at lower kinetic energy than the primary peak and shake-off which represents the equivalent to shake-up but where the excitation is from bound states to the continuum.
4. Elastic scattering altering apparent angles of emission and subsequent inelastic scattering may also contribute to photoemission peak distortion.

5. Instrumental artefacts play a role in peak shapes, where these influences progressively become more important as underlying peak widths decrease. That is, narrow photoemission peaks tend to show more distortion from instrumental factors than broad peaks.

Despite these influences as noted above, the splitting of energy levels resulting from unpaired electrons in both initial and final states for atoms within a solid create shapes within spectra difficult to model using individual component peaks to reconstruct spectra from synthetic lineshapes. Therefore asymmetric lineshapes are included more as tools for use when appropriate but not as a solution to all asymmetric forms seen within photoemission spectra.

Doublet Peaks and Inelastic Backgrounds in XPS

Doublet Peaks and Quantum Numbers

Electrons within an atom are assigned quantum numbers as a means of ordering electrons in terms of the contribution from individual electrons to a specific energy level for a given electron configuration for an atom. When a photon excites an atom by ejecting an electron, the label assigned to the photoemission peak within a spectrum is the set of quantum numbers for the emitted electron within the atom before photoionisation. For most elements and most photoemission lines three quantum numbers are sufficient when describing photoemission spectra. This statement breaks down for larger elements but even in these cases photoemission peaks can be classified loosely by means of three quantum numbers.

A photon of a given energy sufficient to remove an electron from an atom results in an ion plus a so called photoelectron. The energy imparted to the photoelectron from the photon depends on from which element and which bound state of the atom the electron is ejected. If the energy for electrons within the atom and the energy for the remaining electrons within the ion are both unique then a single photoemission peak may be expected. If either the initial electron configuration for the atom or the final electron configuration for the ion are split by spin-orbital interaction then more than one photoemission peak is possible.

The origin for doublet peaks in XPS is due to multiplicity in electronic energy levels, a concept that relates to total angular momentum for electrons within an atom. For certain combinations of electrons, total angular momentum results in energy levels with several configurations of electrons attaining identical energy, while other electron configurations result in multiple energy levels. If an energy level for an atom can be achieved for a range of angular momentum (orbital, magnetic moment and spin) then such an energy level is said to be degenerate and some form of perturbation is required to make observable these range of electronic configurations. If an atom undergoes ionization of an electron then the resulting ion with unpaired spin for electrons represents such a perturbation and potentially splits the set of electrons into two states with energy separation observable by XPS. These peaks in XPS are referred to as spin-orbit split doublet peaks.

One way to describe the state for electrons within an atom is to list electrons using the principal and orbital angular momentum quantum numbers n and l expressing the number of equivalent electrons or occupation number $2(2l+1)$ for an energy using a superscript. So for example, argon in a ground state would be written as follows.

$$1s^2 2s^2 2p^6 3s^2 3p^6$$

Argon in the ground state is formed from eighteen electrons assigned individual quantum numbers that can be listed as eighteen different states within the argon atom but as an ensemble these eighteen electrons always appear to an external observer as a single energy level. Each subshell of electrons is full meaning for each spin-up there is a spin-down for electrons with the same principal and orbital quantum numbers. Such a configuration of electrons is a singlet state, making reference to the actual number of observable energy levels for these electrons in an atom, namely one observable energy level.

After photoemission a hole is created within an electron configuration and as a result of unpaired electrons in terms of spin within a subshell there is a need to introduce a new quantum number j representing the coupling of orbital and spin for electrons. In the case of photoemission of an electron from argon with 2p state the resulting configuration (only using j where necessary for unpaired spin state) could be written as follows.

$$1s^2 2s^2 2p_{1/2}^2 2p_{3/2}^3 3s^2 3p^6$$

or

$$1s^2 2s^2 2p_{1/2}^1 2p_{3/2}^4 3s^2 3p^6$$

The missing electron alters the distribution of electrons in two possible ways resulting in two possible energy levels for the ion. The subscript to $2p$ electrons is the j quantum number formed from the sum of the orbital angular momentum quantum number l and the spin, namely $\pm\frac{1}{2}$. Thus for $2p$ electrons two possible values for the subscript are $1-\frac{1}{2}$ and $1+\frac{1}{2}$. These two j quantum numbers indicate different energy levels in the final state ion and when combined with a singlet for the initial state for the atom results in two photoemission peaks in spectra from argon due to emission of $2p$ subshell electrons.

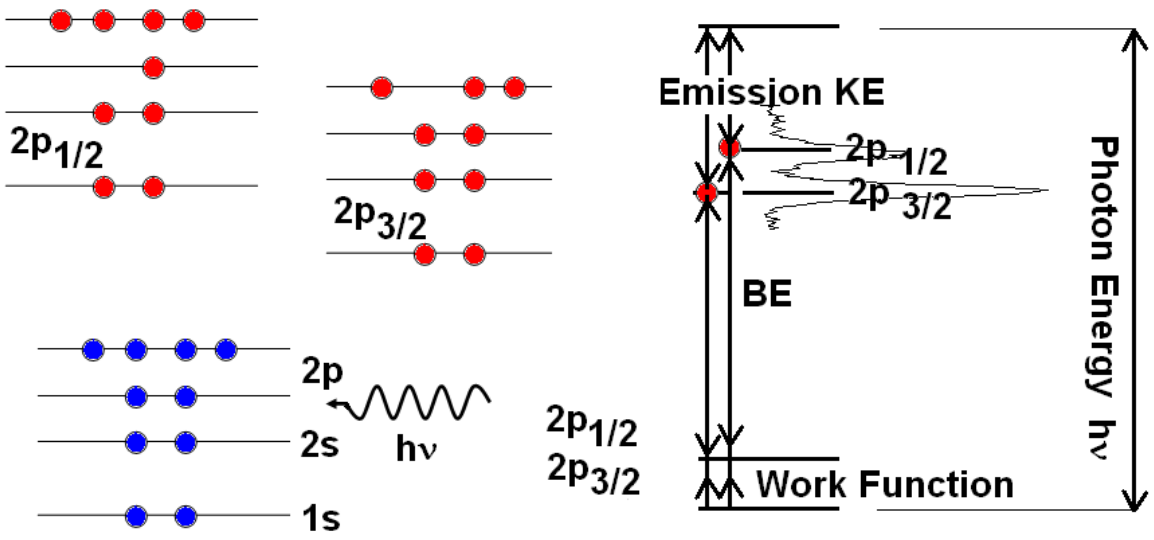

The relative intensity for doublet peaks is related to the assignment of electrons to a j quantum number. For example, a subshell with orbital angular momentum quantum number $l=1$ (p-orbital) includes six electrons forming a closed subshell but these six electrons can be separated in to $j=3/2$ and $j=1/2$ states. The j quantum number is useful because the number of electrons in the closed subshell with a given orbital angular momentum ground state for the atom is obtained via the use of j via the expression $(2j_1+1)+(2j_2+1)$ and for XPS a ratio formed from this expression for two j quantum numbers for electrons with the same orbital quantum number l provides the relative intensity for photoemission for these two spin-orbit split energy levels of the ion $(2j_1+1):(2j_2+1)$. Specifically, for p-orbitals in an atom these occur in the ratio $2\frac{3}{2}+1:2\frac{1}{2}+1$ or $4:2$, so when ionised by the emission of a p-orbital, assuming emission of all electrons from the same

subshell is equally likely, the final state ion is created with distinct energies in the ratio 2:1. It should be noted that the probability for excitation of electrons with different j quantum numbers from the same subshell is not necessarily equal and the computed ratio for doublet peaks, in the form of Scofield cross-sections, for p-orbitals in different elements is not exactly in the ratio 2:1.

XPS is typically performed on solid state material and while introducing new challenges compared to isolated atoms the same terminology for photoelectrons from solid state is used. For example the ground state for titanium in TiO_2 can be considered to have an argon configuration of $1s^2 2s^2 2p^6 3s^2 3p^6$ to which is added four electrons outside of the inner argon core, namely, $3d^2 4s^2$. These outer electrons are responsible for chemical bonds. In solid state the complexity increases to the point only core level electrons can be considered discrete in energy, nevertheless, non-core level electrons ionised by X-rays contribute to spectra as broad features close to the zero binding energy.

Background Signal

The influence of all electrons in solid state to photoemission spectra goes beyond photoemission peaks. In particular outer electrons and bonds formed by titanium with other elements have an influence on core-level spectra creating structure and shapes within XPS background intensity at or close to photoemission lines. These outer electrons form various chemical arrangements that alter energy loss processes for electrons moving through solid state resulting in background signal to core-level peaks that changes with chemical state. Outer electrons also alter the shape for core-level peaks due to fine structure within energy levels which are easily observed in metal oxides such as CuO or Fe oxides. There are situations where photoemission peaks appear to be classically formed from two components added to simple background signal, but even for these relatively simple cases closer inspection reveals structure important to understanding of chemical state and also elemental quantification by XPS. TiO_2 is a case in point where at first sight a basic two components doublet might be assumed but careful inspection suggests background and photoemission shape requires explanation beyond this simple model.

Doublet peaks pose a problem for algorithms typically used to remove background signal. Two peaks offset in energy often results in the background from the lower binding energy peak interfering with photoemission signal from the higher binding energy peak. This issue is the case for Ti 2p spectra from TiO_2 where two Ti 2p photoemission peaks are associated with a rising background signal which includes peak like structure within the background. It is therefore important to consider the implications of background signal when attempting to isolate Ti 2p photoemission signal.

When discussing background intensity it is worth pointing out that photoionisation occurs within the sample at depths greater than photoelectrons can escape the surface without losing energy. Only photoelectrons within a thin layer (less than 10 nm for Al K_α X-rays) at the interface between the sample and vacuum emerge with initial energy unaltered and it is for this reason XPS is considered a surface analysis technique.

The origin of background signal to photoemission peaks for solid state samples is the inelastic scattering of electrons emitted from both the photoemission line of interest and also photoemission of all electrons with kinetic energy greater than the energy for the photoemission peak of interest. Photoelectrons move to the interface between the sample and vacuum with a kinetic energy

characteristic of the photon energy for X-rays and the core level energy for an atom. Inelastic scattering of these electrons occurs with a probability that increases with increasing depth from within the sample an atom emitting the electron is located. The term inelastically scattered electrons means these electrons interact with electrons within atoms causing electron excitation within atoms and a corresponding energy loss for photoelectrons with respect to the initial energy at time of photoemission. These inelastically scattered electrons appear as background to electrons that escaped to the vacuum without losing energy.

Inelastic scattered background signal can vary in shape dramatically depending on the type of material analysed. Before turning to TiO_2 it is worth considering background shapes observed for other materials. The range and shapes for inelastic scattered signal can be surprising. Magnesium, aluminium or silicon without oxidation display sequences of narrow peaks associated with scattering by delocalised electrons for these elements referred to as plasmon loss peaks.

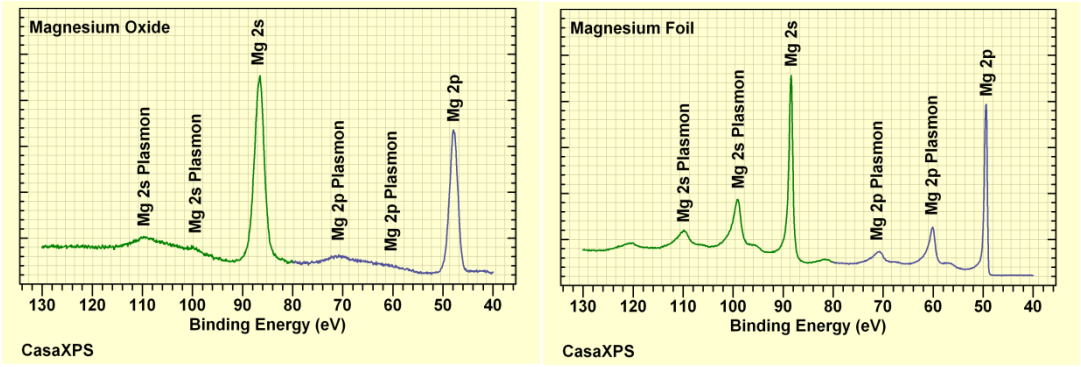

The shape and nature of plasmon peaks depends on oxidation state for an element. Magnesium oxide (MgO Mg^{2+}) plasmon peaks are broad compared to plasmon loss peaks observed for metallic magnesium foil. These magnesium examples also illustrate how background changes near to the energy for a photoemission peak also depend on material properties. Insulators where outer electrons are localised tend to exhibit flat backgrounds close to photoemission peaks whereas metallic or semiconductor materials are accompanied by a noticeable step in background at or near to the energy for a photoemission peak. These background characteristics are present for most materials but are not necessarily as obvious as is the case for magnesium.

When constructing a peak model it is worth considering band gap information. The band gap for TiO_2 is approximately 3 eV and measured Ti 2p doublet component peaks are separated by about 5.75 eV. As a consequence changes in background should occur within the energy interval corresponding to Ti 2p doublet photoemission signal. It could also be argued the background (due to the influence of the photoemission peak itself) beneath a photoemission for a material with a band gap should result in a flat background for intervals equivalent to the band gap. In essence, the background to TiO_2 should include shapes of significance to a peak model.

Common background types will now be considered in the context of Ti 2p from TiO_2.

Shirley Background

While it is common practice to remove inelastic scattered background using the approach describe as a Shirley background, the background shape represents a step in signal centred on peak maxima and does not include the option to offset the onset of inelastic scattering. There is therefore some

doubt as to whether a Shirley background is appropriate for materials such as TiO_2. One merit of Shirley backgrounds is that for isolated peaks the algorithm computes a background that is systematic. A disadvantage for the Shirley background occurs when complex peak structures are involved over extended energy intervals with rising count rates, an example of which is Ce 3d, at which point the systematic nature of a Shirley background breaks down.

Assuming the Shirley background is already known for a specific spectrum and given by $S(E)$, then each point within an energy interval follows the relationship in terms of area above background as shown below. Essentially for any energy E within the interval $[E_1, E_2]$ the Shirley background is computed from the photoemission peak area within the interval partitioned into the area to the left and right of a given energy. The obvious problem is for a photoemission peak initially the area for the photoemission peak is unknown and therefore a Shirley background is computed by means of an iterative scheme where the initial guess for the background might be a constant background. The iterative scheme is as follows.

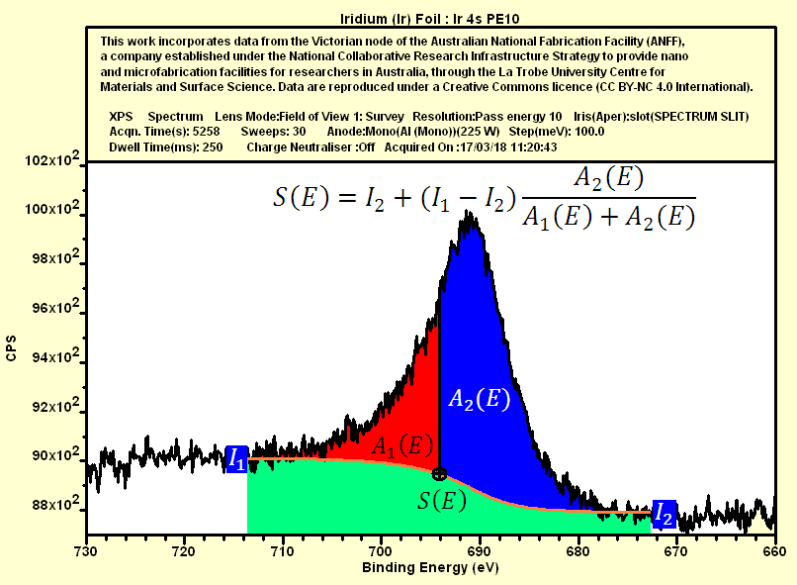

Given a spectrum $J(E)$ and an interval $[E_1, E_2]$. Define background signal such that: $B_{Sh}(E_1) = I_1$, $B_{Sh}(E_2) = I_2$ then the Shirley background is calculated by iteration using the formula

$$B_{Sh_{n+1}}(E) = I_2 + \frac{(I_1 - I_2)}{\int_{E_1}^{E_2} J(x) - B_{Sh_n}(x)\,dx} \int_E^{E_2} J(x) - B_{Sh_n}(x)\,dx$$

Note that the zero loss photoemission peak shape is given by $J(x) - B_{Sh_\infty}(x)$. Thus, given a component peak shape, it is possible to directly compute the curve corresponding to a Shirley background. If signal above inelastic scatter background is Lorentzian then without iteration the background equivalent to a Shirley background is given by:

$$B_L(E) = I_2 + \frac{(I_1 - I_2)}{\int_{-\infty}^{\infty} \frac{1}{1+x^2}\,dx} \int_E^{\infty} \frac{1}{1+x^2}\,dx = I_2 + \frac{(I_1 - I_2)}{\pi}\left(\frac{\pi}{2} - \tan^{-1} E\right)$$

U 4 Tougaard Background

An alternative approach to the Shirley background is computing background signal based on the Tougaard method.

The background is computed from the measured spectrum $J(E)$ generated by the photoemission peak plus inelastic scattering signal due to the photoemission peak using the integral:

$$T(E) = \int_E^\infty F(E' - E)J(E')dE'$$

The integral is formed with additional information in the form of the Tougaard Universal Cross-Section that provides a means of modifying background signal in response to material properties of a sample. These material properties are input via a cross-section defined as follows.

$$F(x) = U(x{:}\,B, C, D, T_0) = \begin{cases} \dfrac{Bx}{(C - x^2)^2 + Dx^2} & x > T_0 \\ 0 & x \leq T_0 \end{cases}$$

One advantage of the Tougaard approach is the use of T_0 to delay the onset of background signal. The more powerful aspect of the Tougaard approach is the cross-section, when available, provides informed guidance for shapes within background signal. The following example illustrates how U 4 Tougaard calculations for elemental silicon representing bulk and surface plasmon shapes can be combined to estimate a complex background shape not available to the Shirley approach.

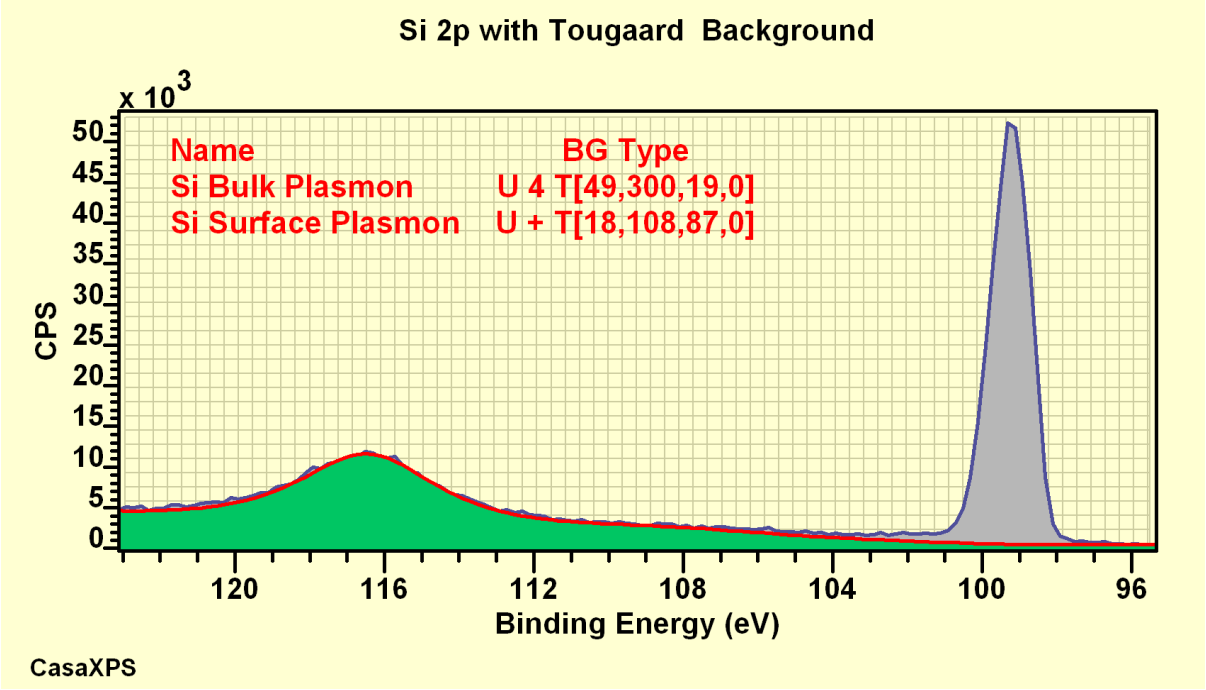

Applying Shirley and Tougaard backgrounds to Ti 2p photoemission from TiO_2 yields differences in background but peak area for these Ti 2p peaks can be made to be comparable. It is therefore not obvious from quantification results one approach has merit over the other, but physical properties of materials may be overlooked if the basic approach of Shirley is simply adopted. It is clear Ti 2p from TiO_2 includes shapes for which a Shirley background cannot provide a solution. These same data modelled using U 4 Tougaard cross-sections suggest TiO_2 background is formed from two

components analogous to the surface and bulk plasmon behaviour visible in elemental silicon spectra. A Tougaard approach demonstrates the need for these plasmon loss features and also allows the positioning and strength of these loss features to be assessed. By contrast the Shirley background generates a step the position of which is entirely dictated to by the photoemission peak regardless of material properties for the sample.

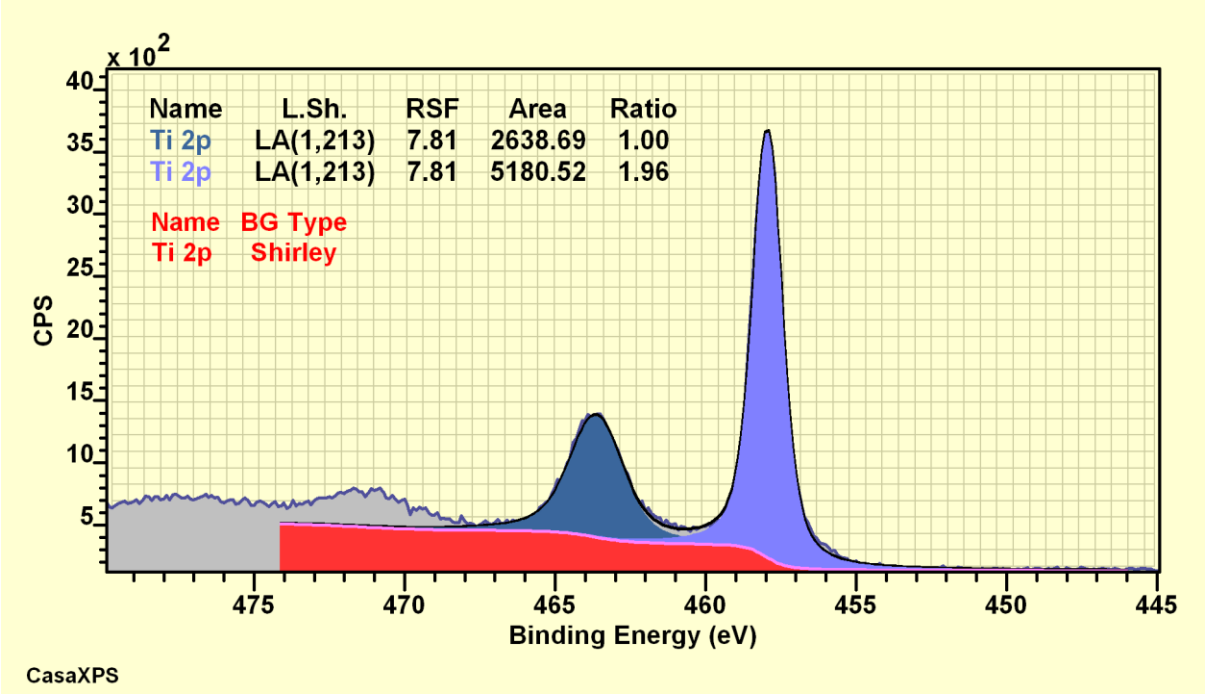

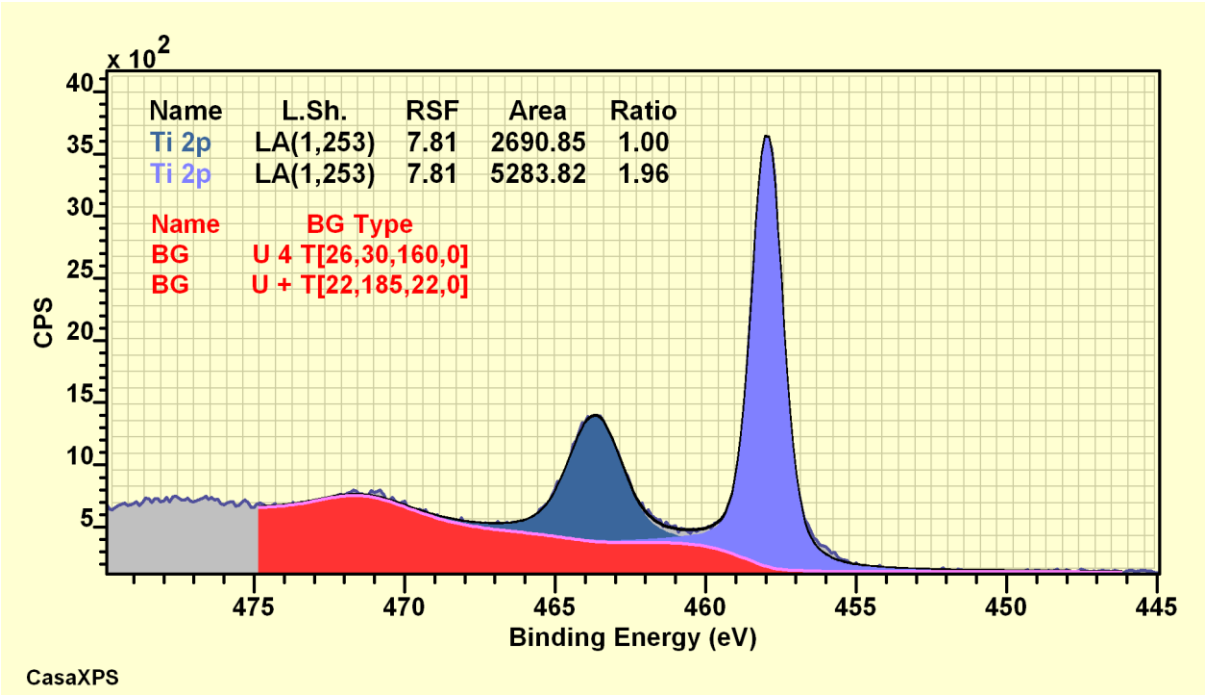

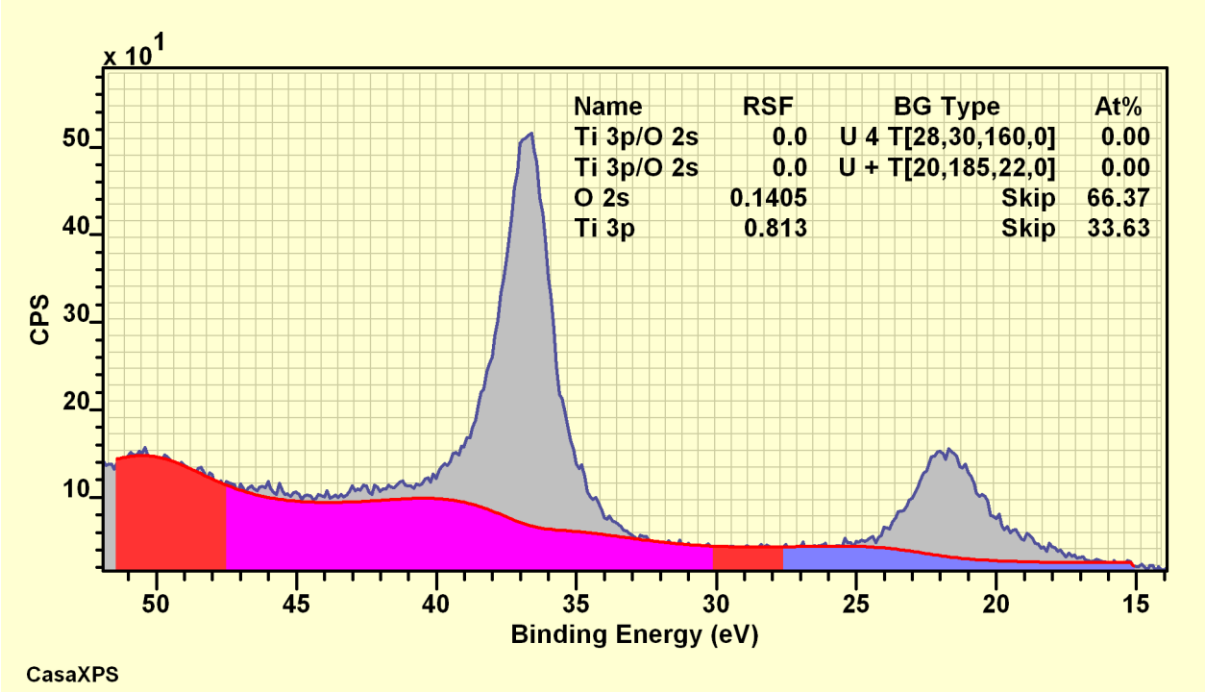

Simplicity of application owes much to the continued use of Shirley backgrounds in XPS but a wealth of sample information is gained by considering how Tougaard backgrounds might be created for a given sample. Any analysis for which the desire exceeds basic elemental-composition should consider the use of a Tougaard background. When constructing a peak model, the potential for including spurious components and deformed lineshapes as a consequence of the simple approach of Shirley coupled with additional understanding gained by considering background shapes suggests Tougaard backgrounds should feature more in XPS studies.

CasaXPS Overview

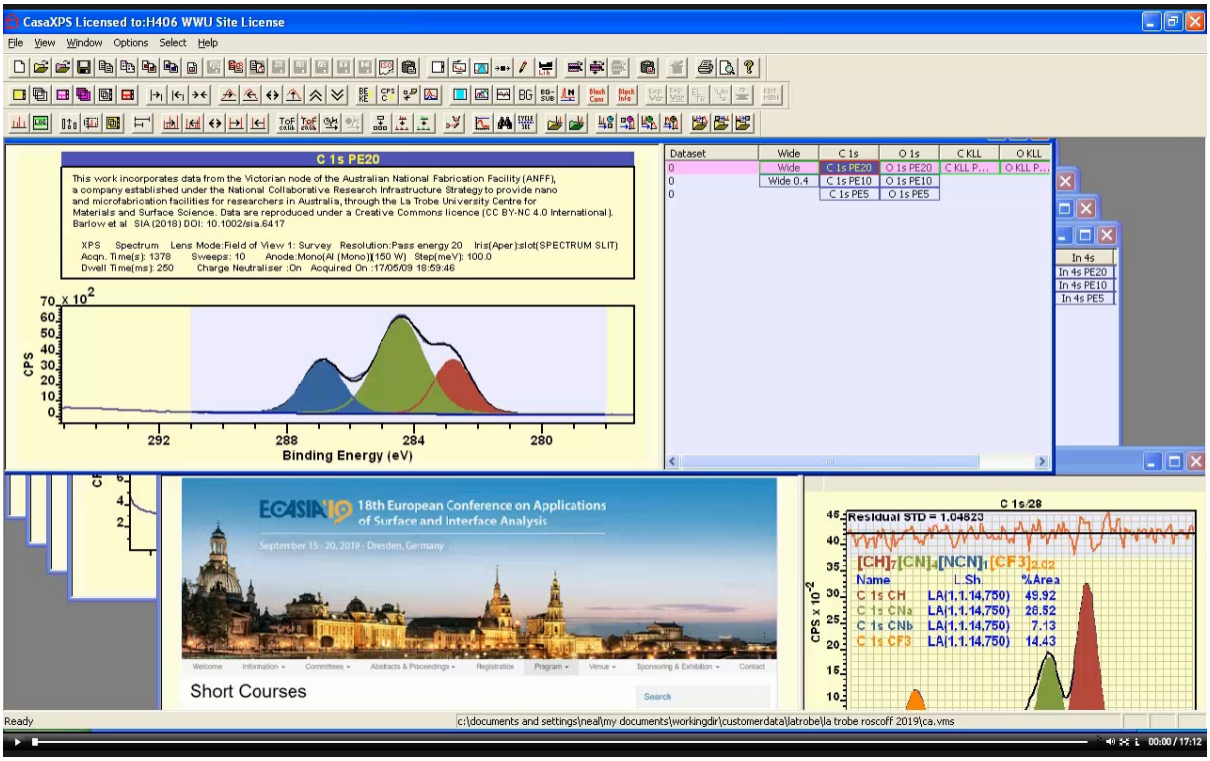

CasaXPS is a multiple document interface. This means the main CasaXPS window manages lists of open VAMAS files as a parent window for separate child windows which in turn manage data in VAMAS (ISO14976) format.

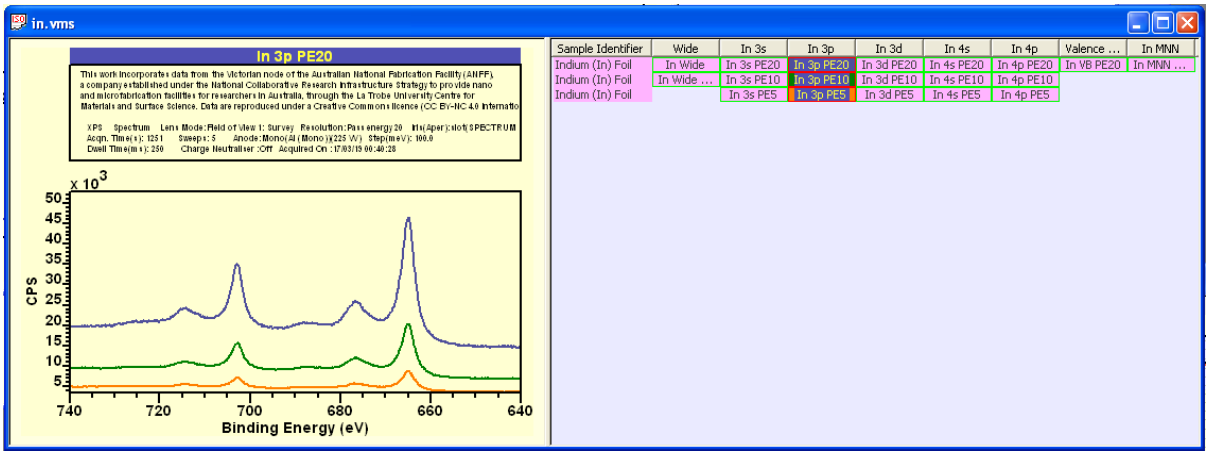

Within CasaXPS these child windows are referred to as Experiment Windows since each child window represents a view into a VAMAS file contain one or more spectra or images. Experiment windows are divided into two panes. The right hand pane of an experiment window displays an array of rectangles displaying the VAMAS block identifier string for each measurement saved as a VAMAS block of data within a VAMAS file. Data are displayed in the left hand pane in display tiles.

Display tiles are arranged within a sequence of display pages. Each display page is tiled with one or more display tiles. Each display tile can display one or more spectra or images.

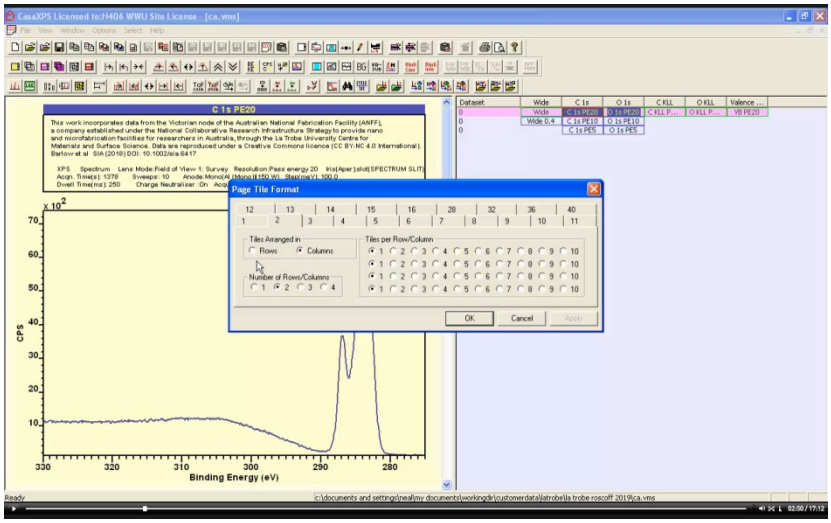

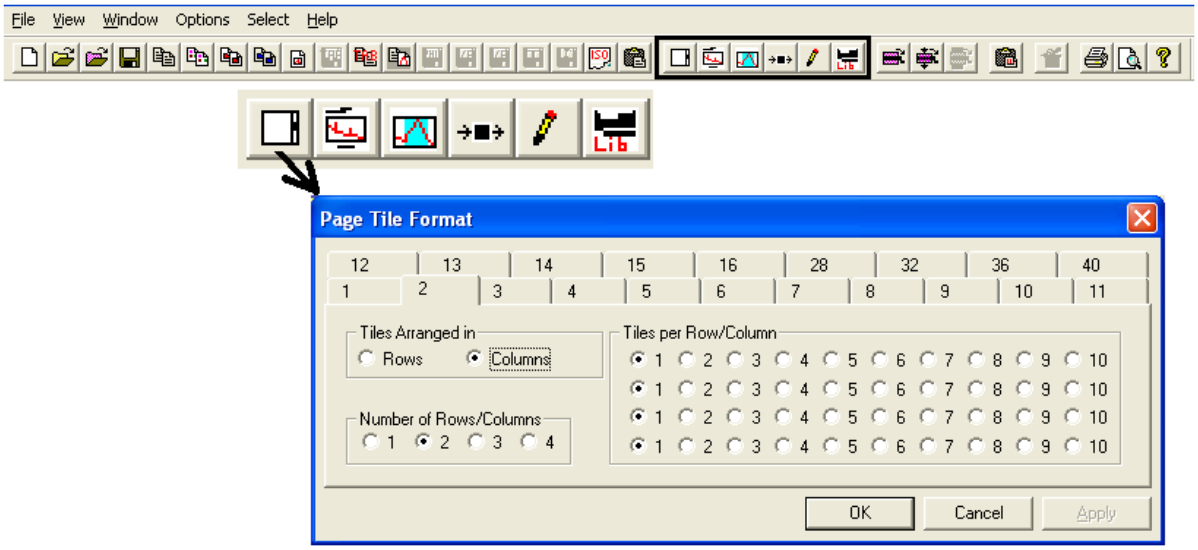

Two display tiles per display page arranged in columns allows two VAMAS blocks to be displayed next to each other.

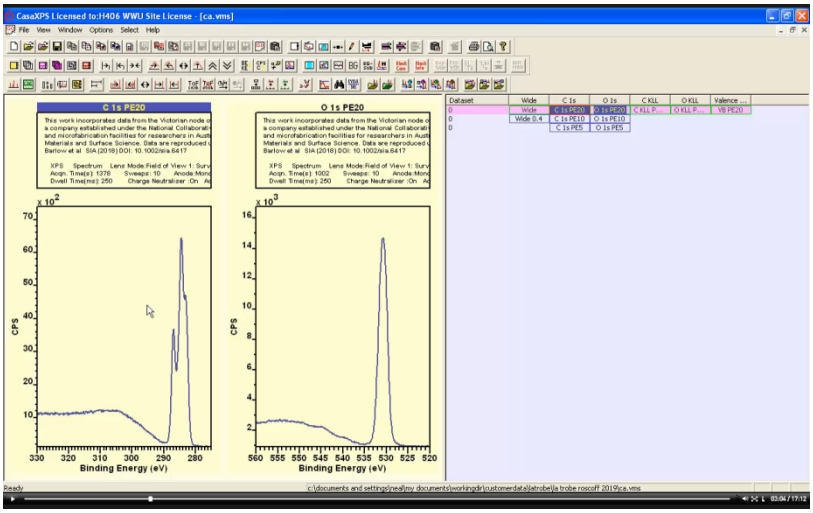

The number of display tiles per display page is adjusted using the Page Tile Format dialog window available from the Options menu or via a top toolbar button.

The left hand pane can display more than one display page. If more than one display page is displayed then a scrollbar is added to the left hand pane and left-clicking the mouse within the background to the scrollbar steps up and down through a list of display pages.

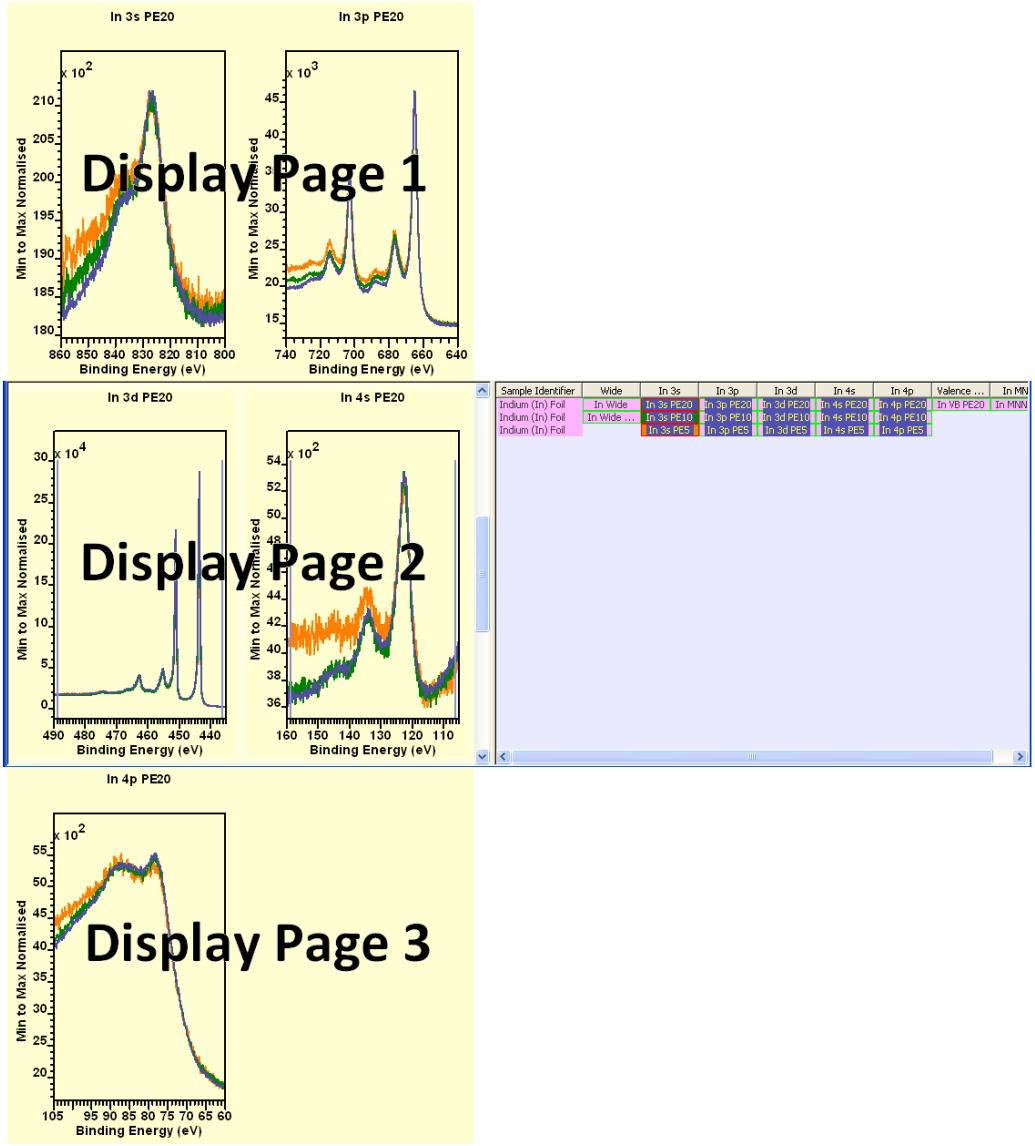

Display pages are added to the left hand pane by making a selection of VAMAS blocks using the right hand pane before pressing a display toolbar button.

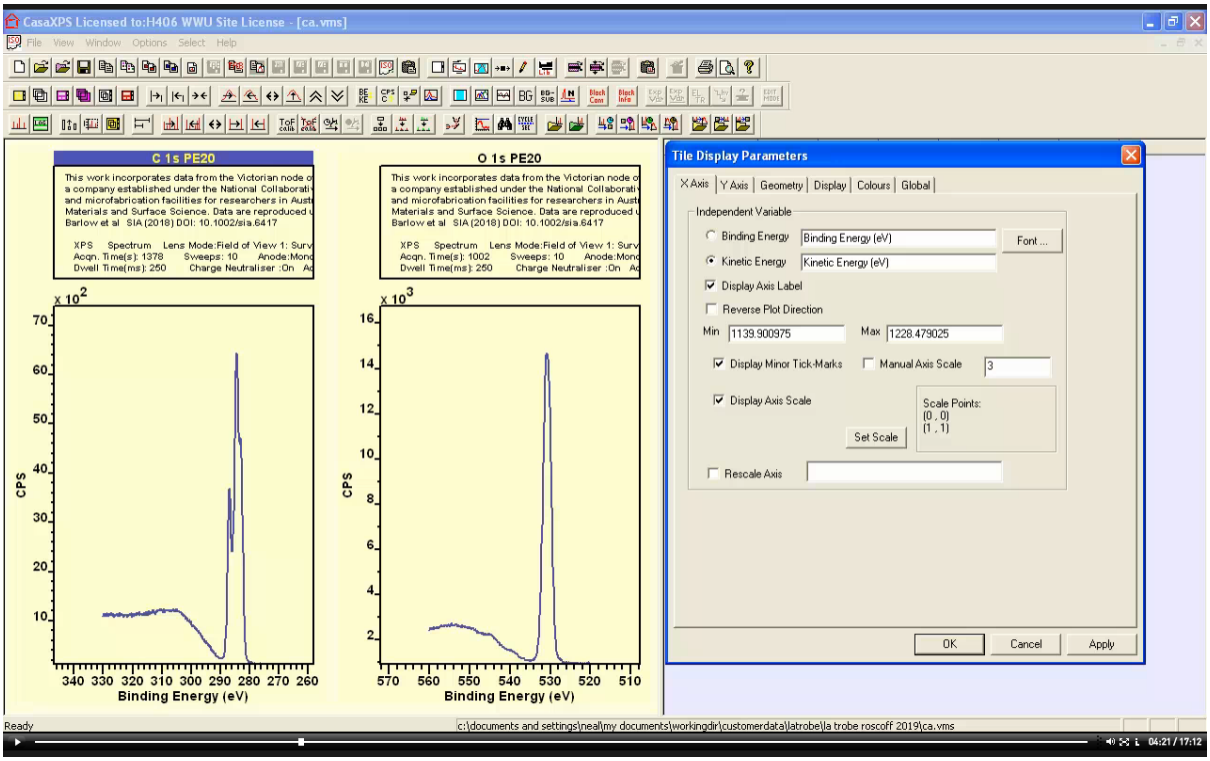

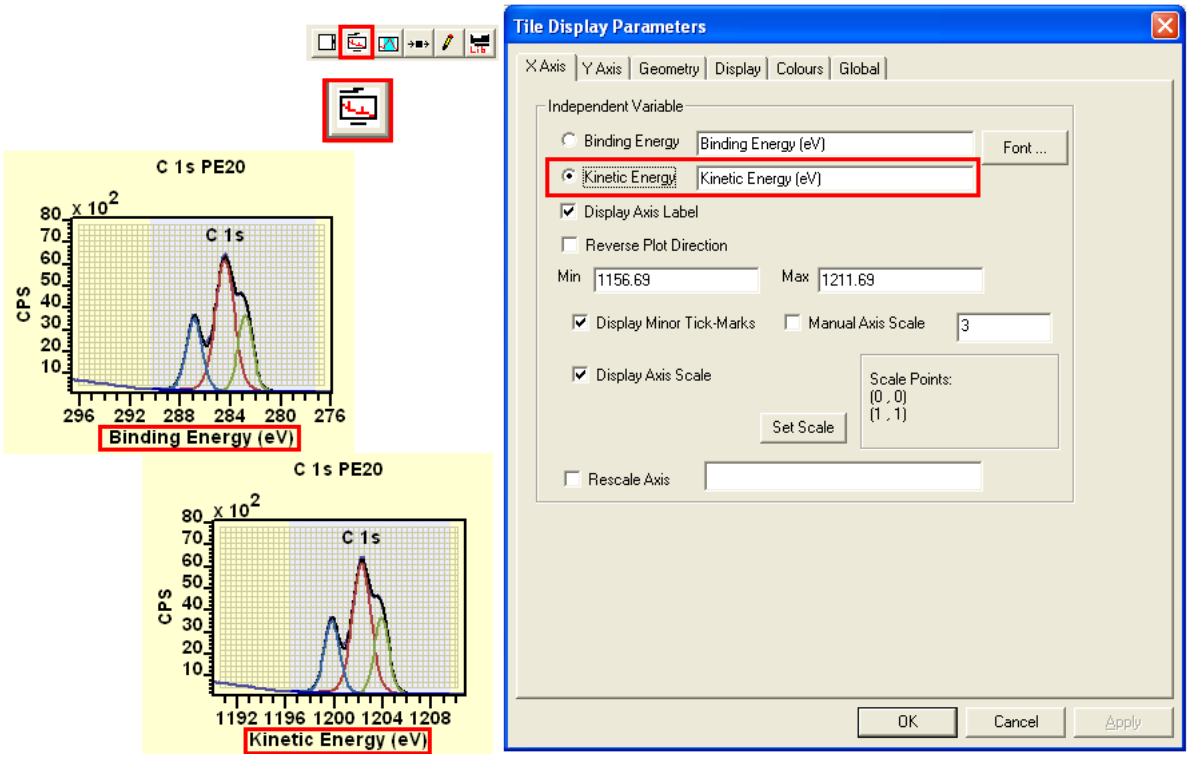

Tile Display Parameters dialog window includes a set of property pages with display options for data displayed in a display tile. Fonts, labels, colours, line widths, display ranges for kinetic or binding energy and counts per second or counts per bin are changed using settings on these property pages. Many display settings can be switched between using toolbar buttons on the second toolbar of CasaXPS.

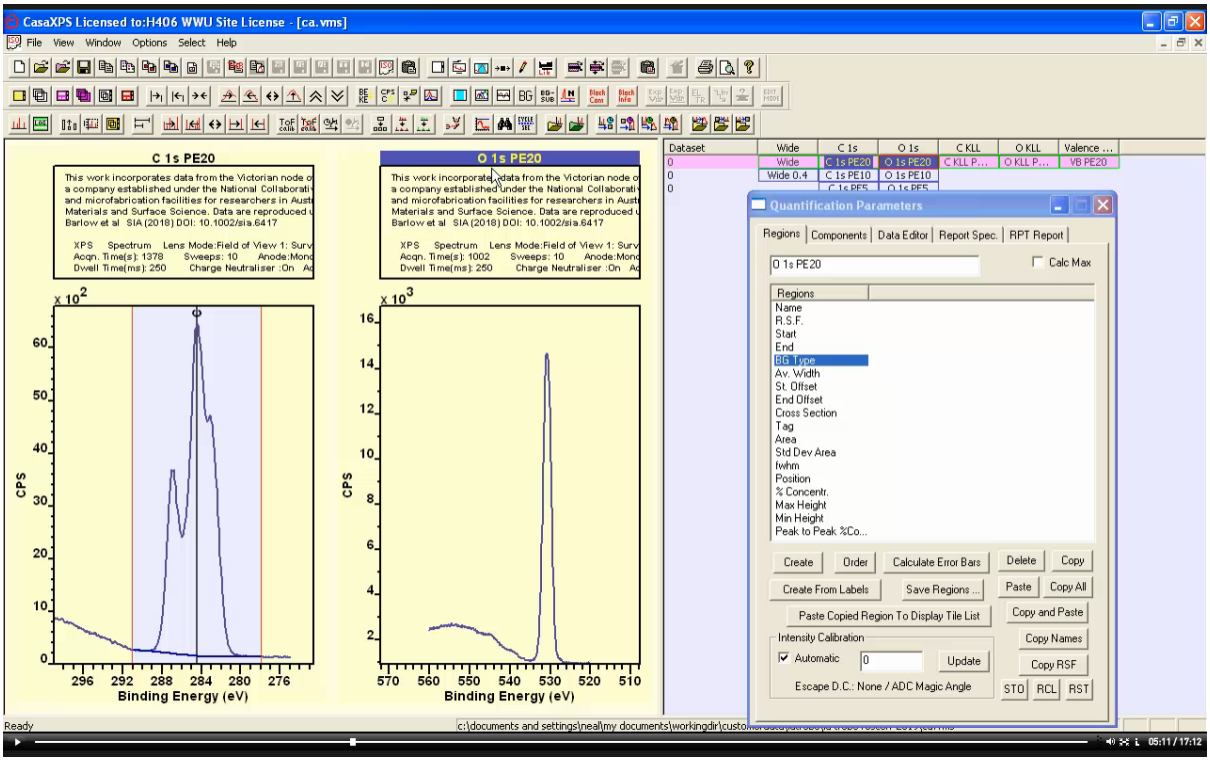

The active display tile is the tile with a highlighted title. The Quantifications Parameters dialog window, Regions property page displays the VAMAS block identifier string for the VAMAS block displayed in the active display tile. A peak model is created for spectra within a VAMAS block using the tables for parameters displayed on the Regions and Components property pages. Regions define the background and components representing distinct signal in a peak model are added to the active VAMAS block through the Regions and Components property pages.

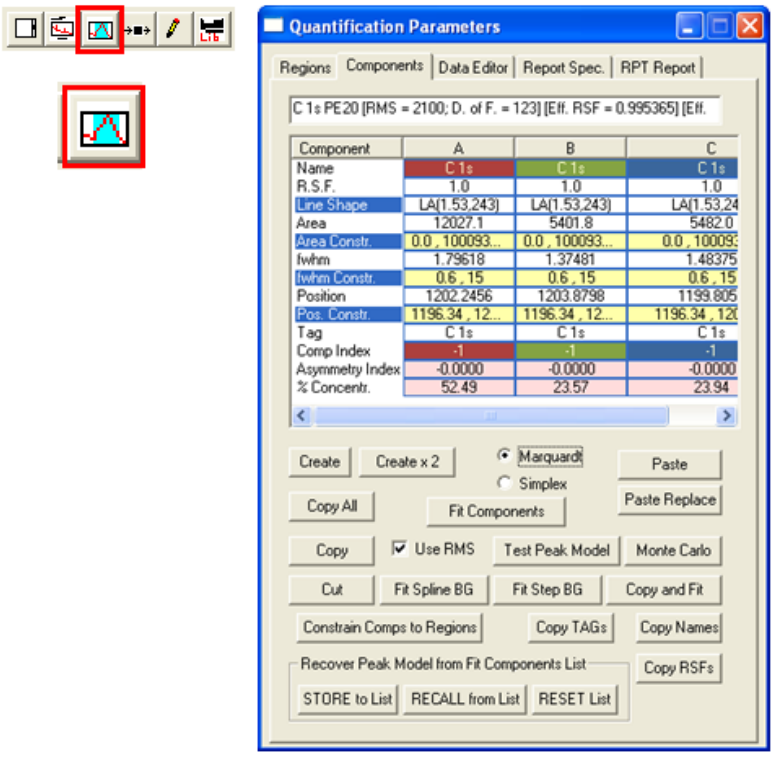

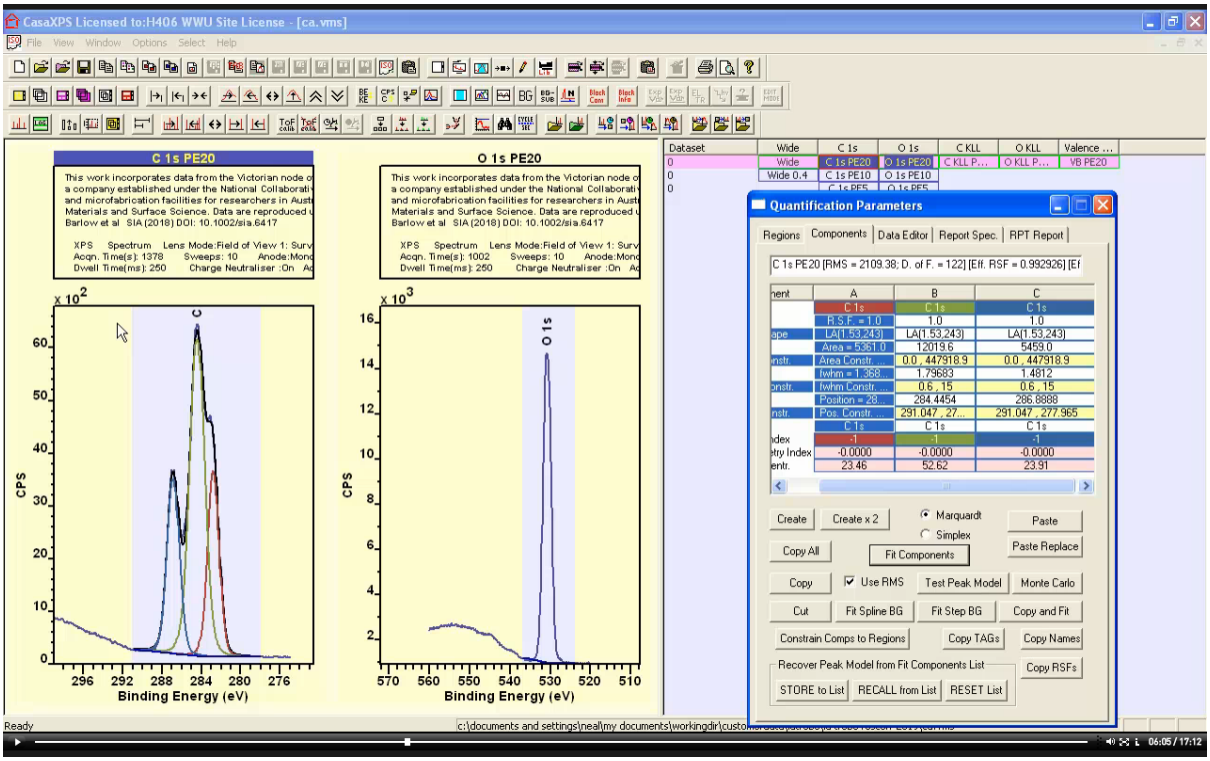

Both Regions and Components property pages include a text field in which a string is display that indicates the VAMAS block identifier for the active VAMAS block as defined by the title for the set of display tiles. Placing the mouse over a display tile then pressing the left-mouse button selects the indicated display tile as the active tile. The active VAMAS block within the active tile is the source for the string entered on the Quantification Parameters dialog window Regions and Components property pages.

Peak models defined on the Quantification Parameters dialog window can be fitted to the active VAMAS block via the Components property page.

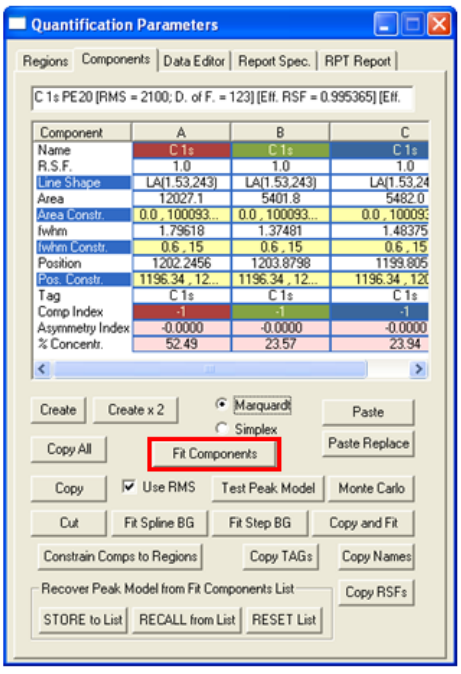

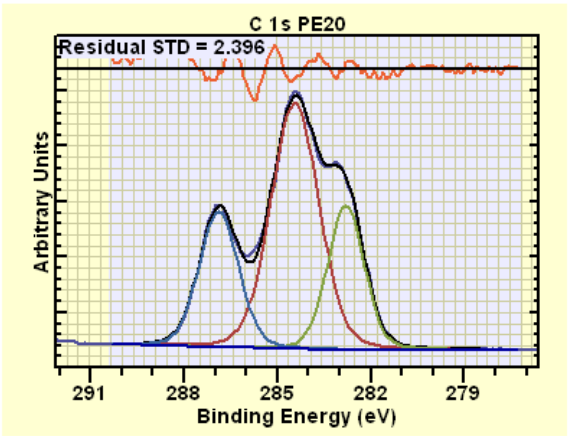

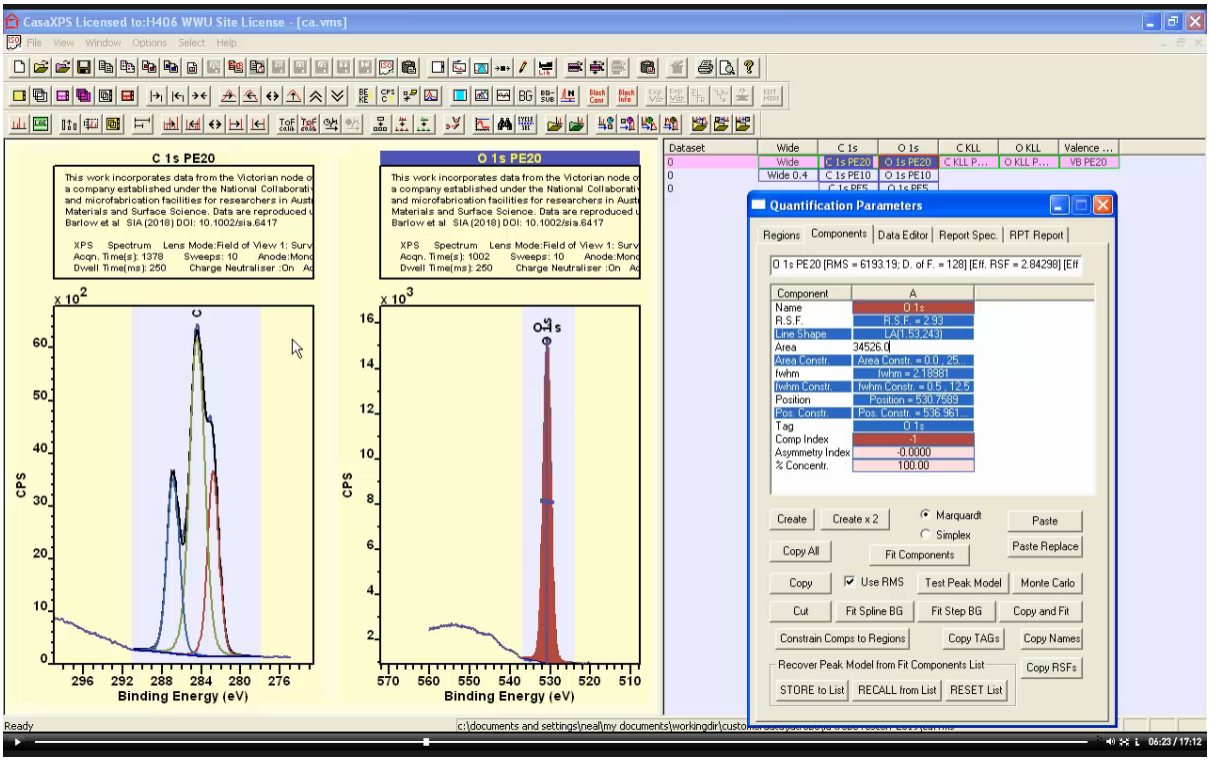

Component parameters defined on the Quantification Parameters Components property page include a component name, relative sensitivity factor, initial fitting parameters (area, fwhm and position), constraints for fitting parameters, a TAG string and a component index value.

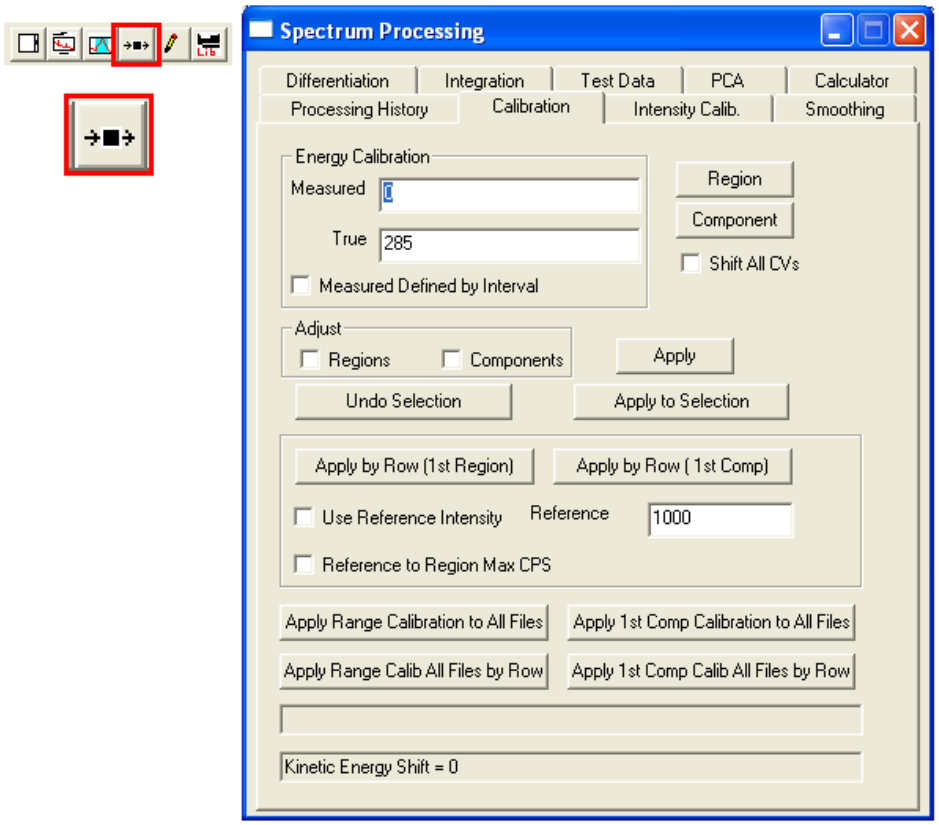

Spectrum Processing dialog window is invoked from the toolbar or the Options menu.

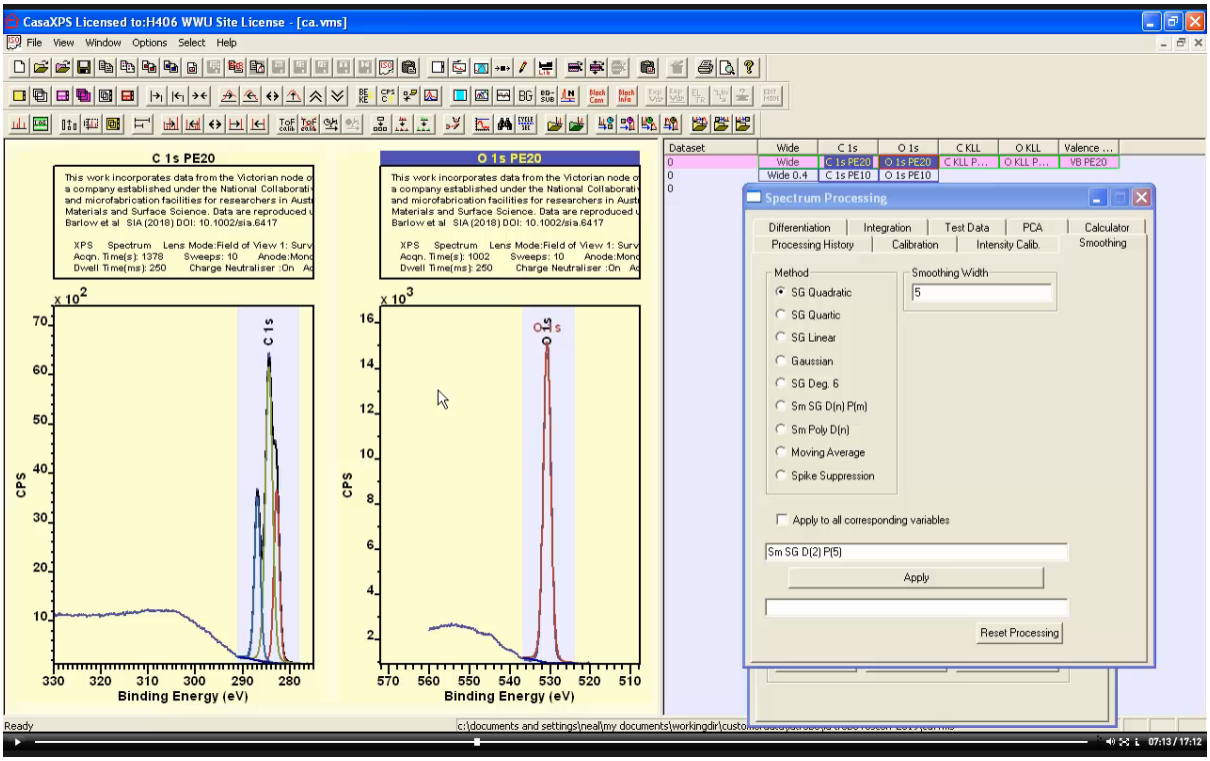

Spectrum processing dialog window offers a similar logic to the Quantification Parameters dialog window, namely, spectrum processing options are offered via a set of property pages where each property page acts on data within the active display tile. There are a few exceptions to this rule but the vast majority of spectrum processing options act on the active VAMAS block displayed in the active display tile.

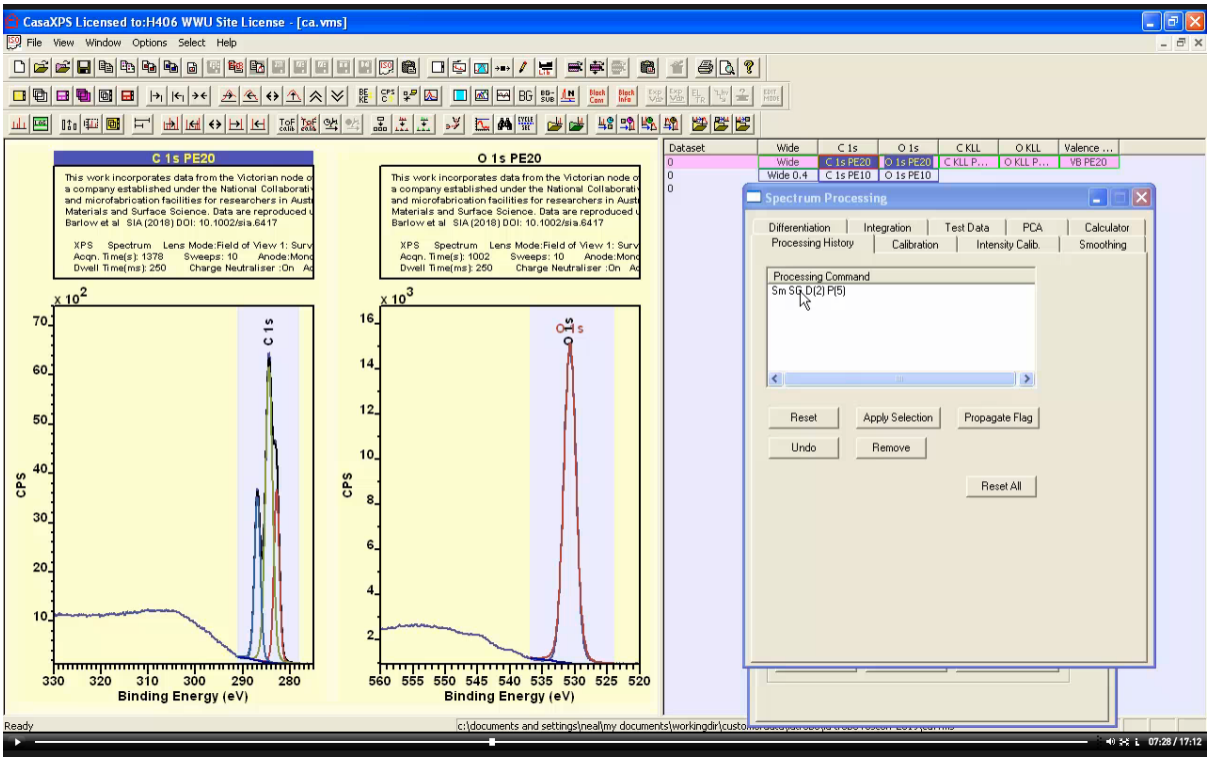

After a spectrum processing action has been applied to a VAMAS block a processing command string is added to the processing history for the VAMAS block and a list of processing commands for the active VAMAS block is displayed in a list on the Spectrum Processing History property page.

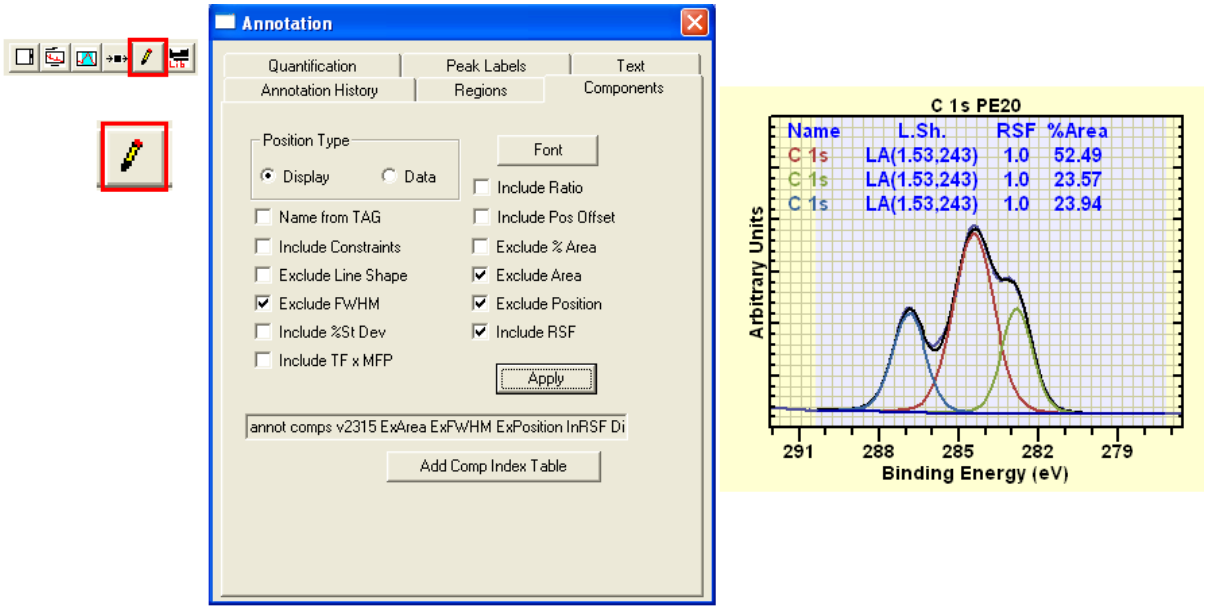

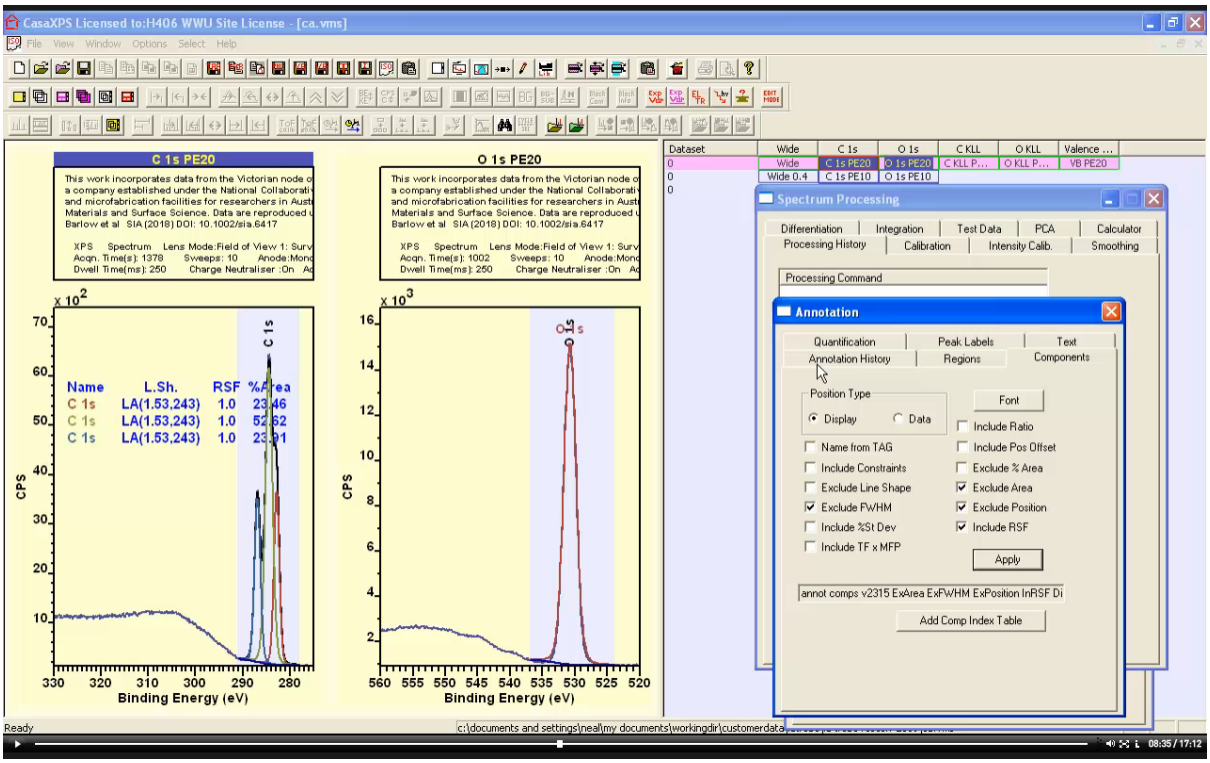

Annotation is added to the active VAMAS block using an analogous dialog window to Spectrum Processing where in the case of annotation the property pages are used to specify text in the form of tables, peak labels and general text.

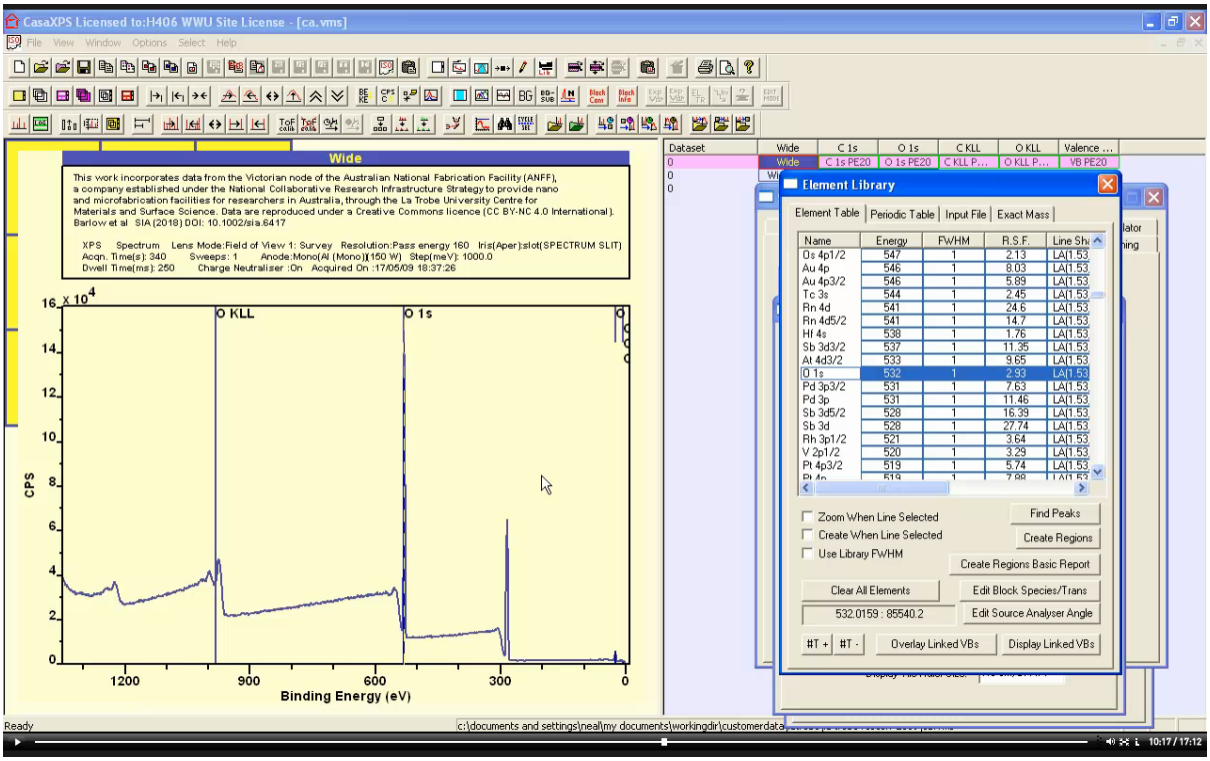

Element library comprising a list of photoemission lines assigned nominal binding energies for elements and transitions are displayed on the Element Library dialog window via the Element Table property page. These entries within the element library are used to identify elements associated with peaks within a photoemission spectrum and are also used to guide the creation of regions on a survey spectrum to permit the appropriate relative sensitivity factors to be entered for regions or components when created.

The element library displays a list of entries appropriate for data displayed in the active display tile. In particular the transitions display in the Element Table property page table correspond to library entries where the excitation source strings (for example “Al” for an aluminium anode x-ray gun) matches the element /transition field within the VAMAS block for the spectrum displayed in the active display tile.

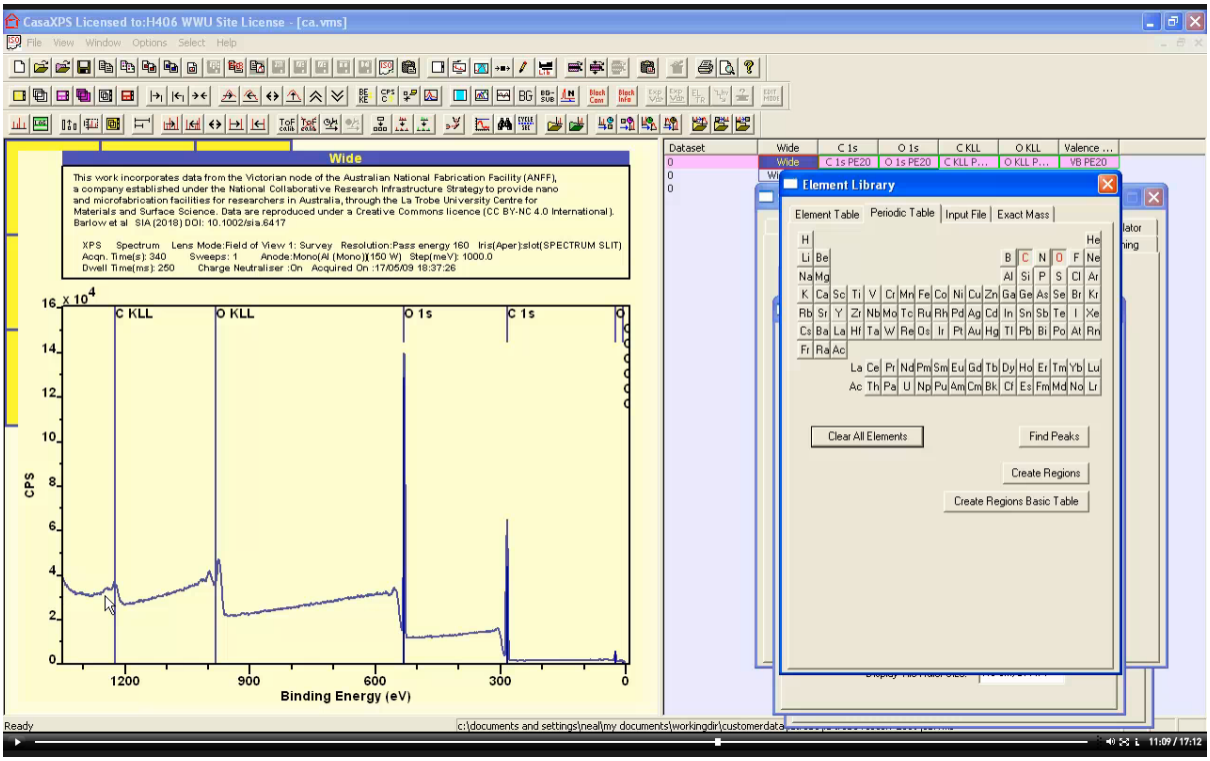

Markers are placed on the active display tile indicating transitions associated with a selected element in either the Element Table or chosen via buttons on the Periodic Table property page. Other property pages on the Element Library dialog window allow the loading and merging of new files containing lists of element/transitions.

The Exact Mass property page is designed for browsing ToF SIMS or general mass spectra.

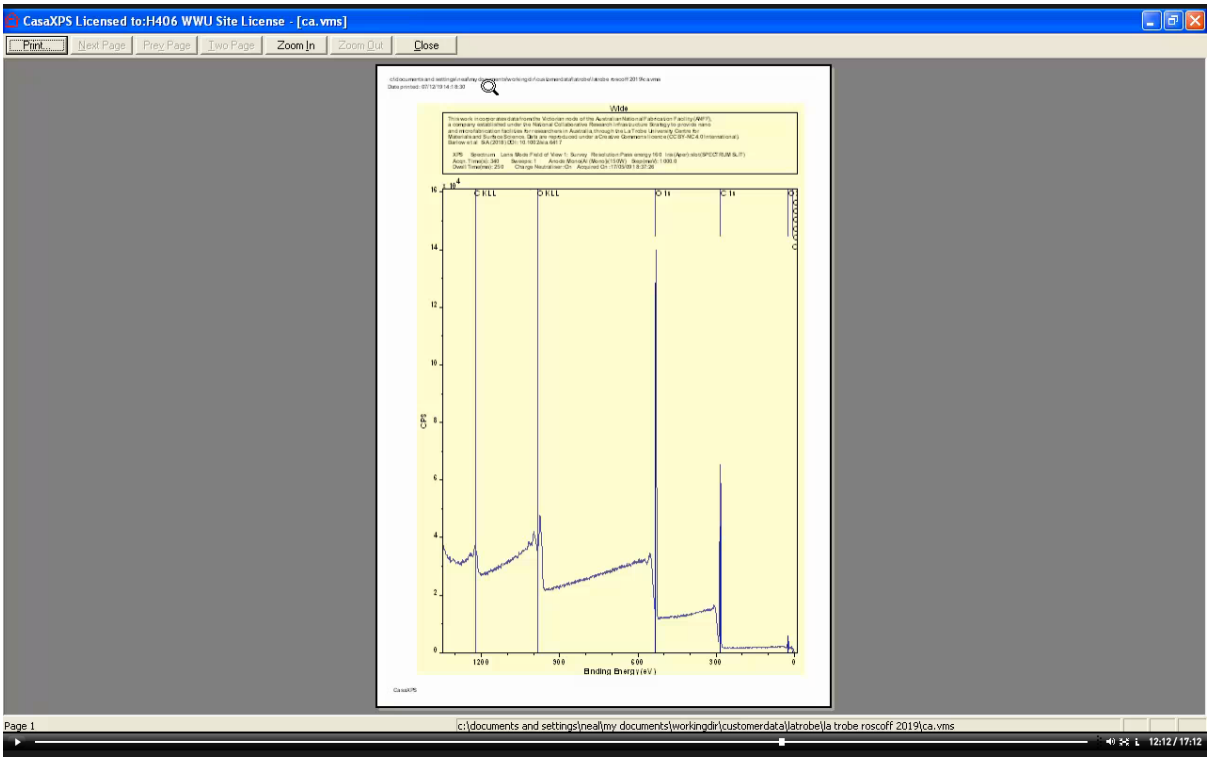

Toolbar buttons are also available to permit the printing of data. When the print toolbar button is selected the set of display pages of tiles is printed. The print preview button allows a preview of the pages and the appearance of these pages before actually being queued for printing to paper.

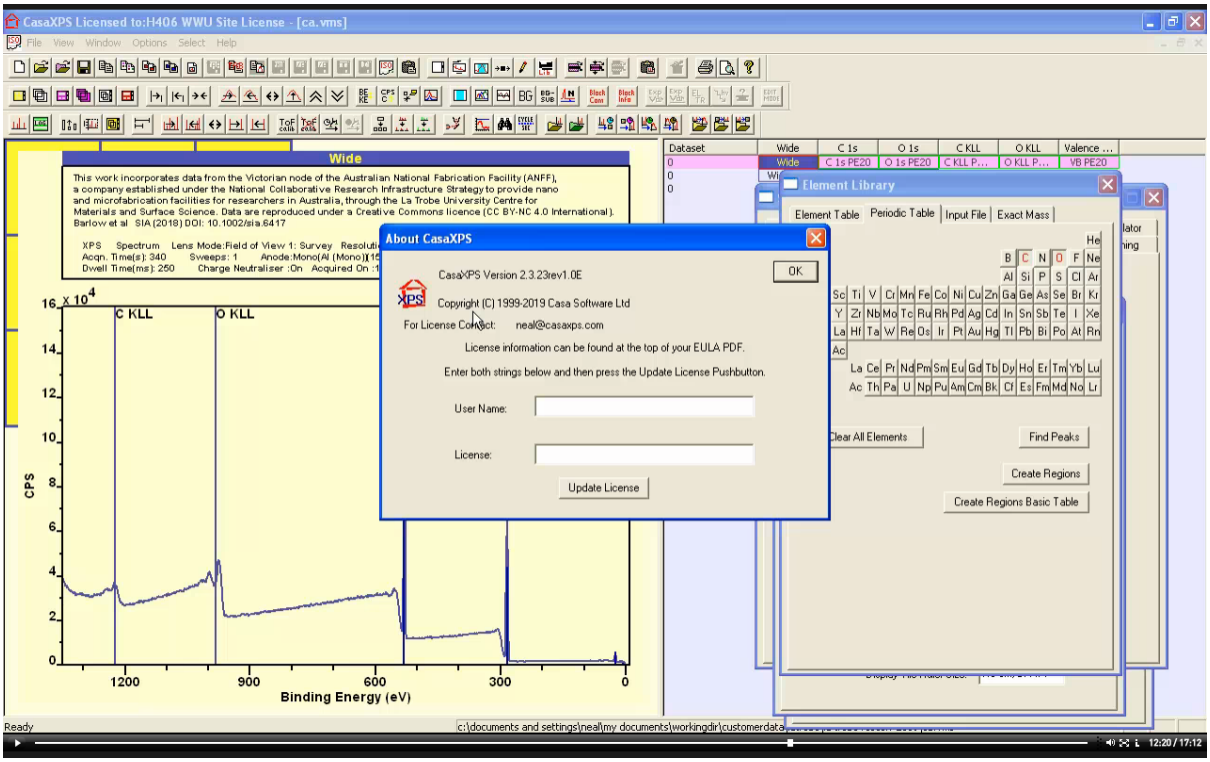

Version information for CasaXPS is available on the About Dialog of CasaXPS. The About Dialog window is invoked via the toolbar button or using the Help menu. License information that enables full functionality of CasaXPS is entered on the About Dialog of CasaXPS.

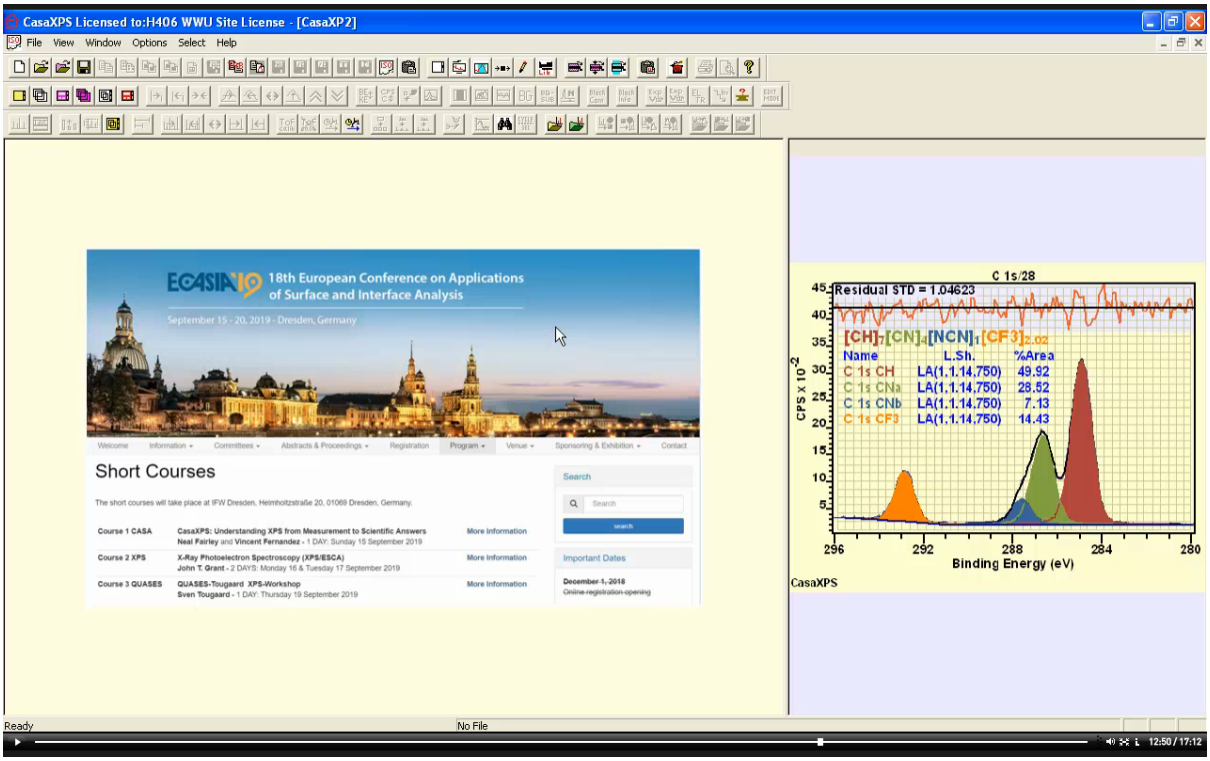

An empty experiment window, in the sense that no VAMAS data are associated with the window, displays bitmap images placed in the CasaXPS.DEF directory. The right hand pane shows an image in a file called CasaXPS.DEF\Message.bmp while the left hand pane displays a list of bitmaps in a directory called CasaXPS.DEF\SlideShow. The keyboard PageUp and PageDown buttons allow the viewing of bitmap files in alphabetical order to be displayed in the left hand pane.

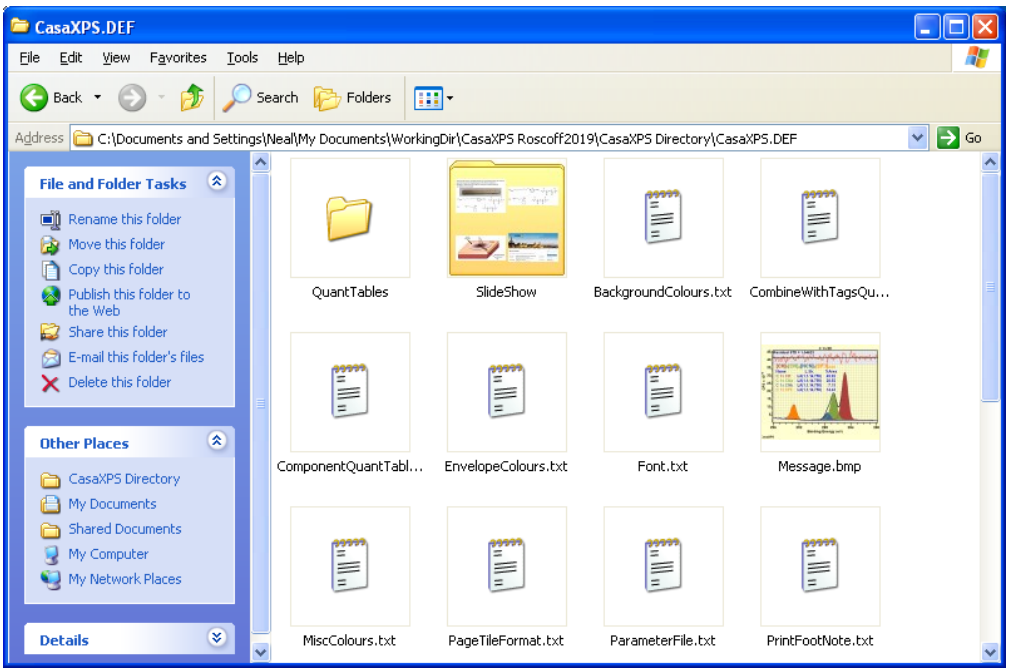

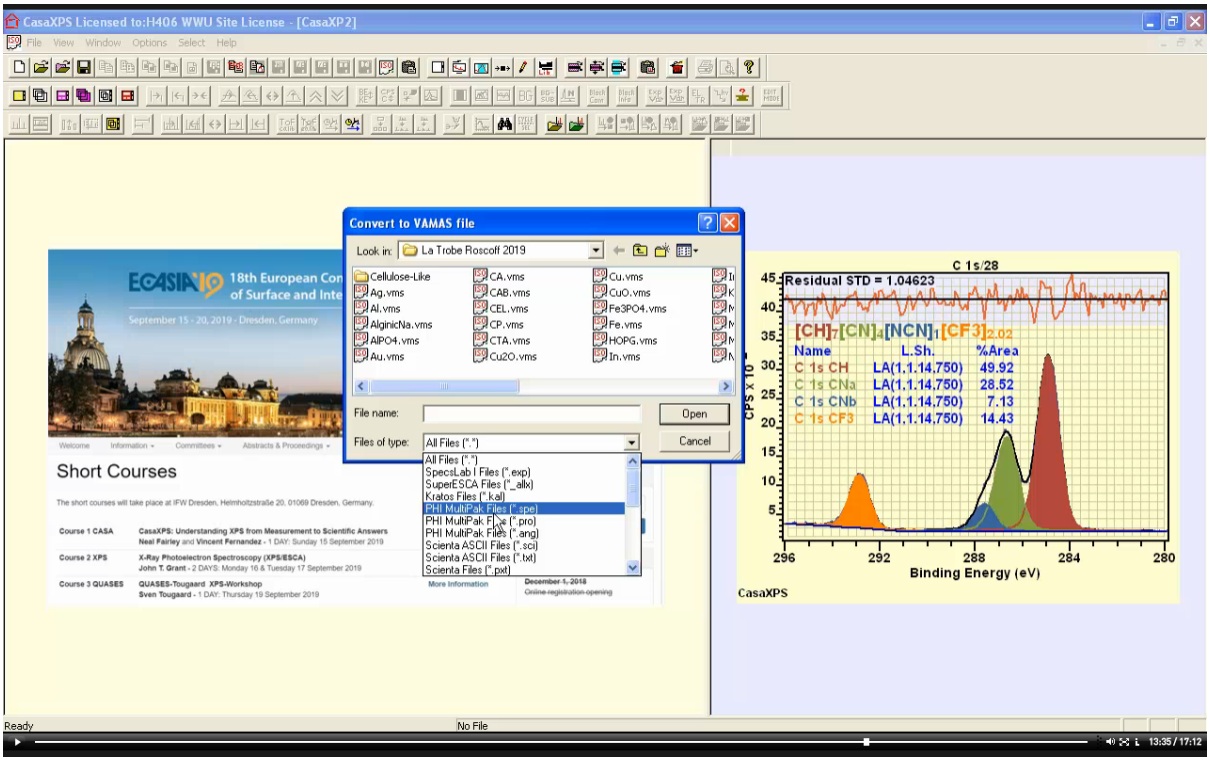

Data not already in VAMAS format must be converted to VAMAS format. The Convert toolbar button invoked the Convert to VAMAS file dialog window that allows the selection of a file in a range of formats known to CasaXPS that can be converted to VAMAS format. The selected file is read by CasaXPS and, if possible, converted data in VAMAS format is written back to the same directory as the original data file.

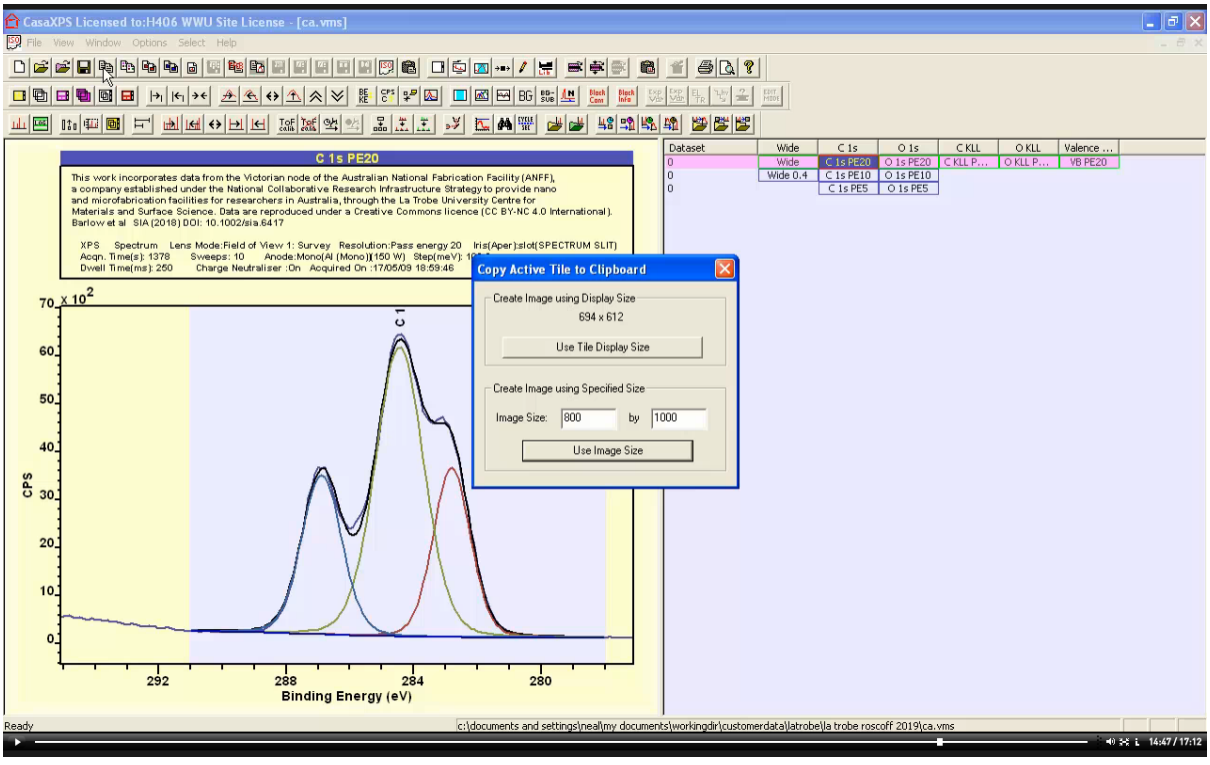

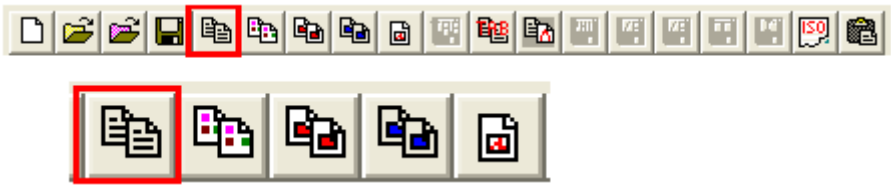

Once data are prepared in a form suitable for export, graphical data in the form of an enhanced meta file (EMF vector drawing instructions interpreted by Microsoft software) or as a bitmap can be copied through the clipboard and pasted into another software package such as Word, Excel, PowerPoint or MSPaint.

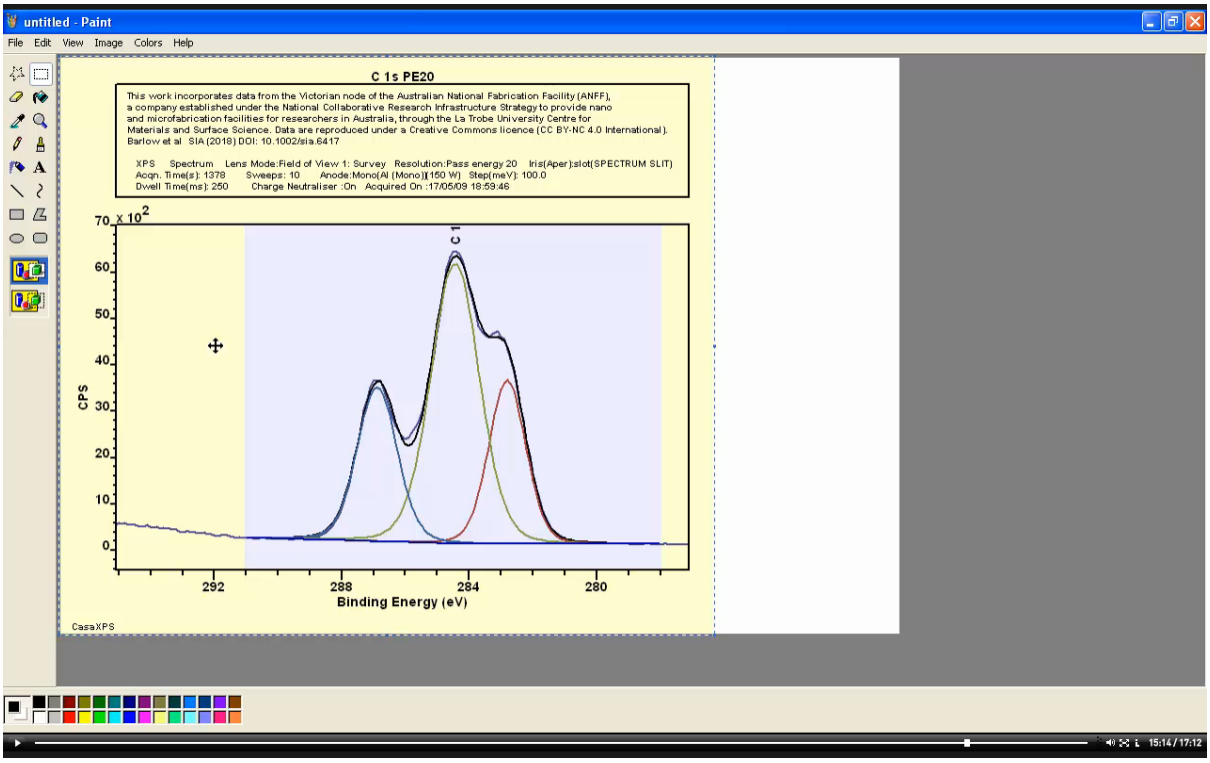

A bitmap of the active display tile is placed on the clipboard using the Copy toolbar button. The bitmap can be transferred into MS Paint, for example, using the Paste option.

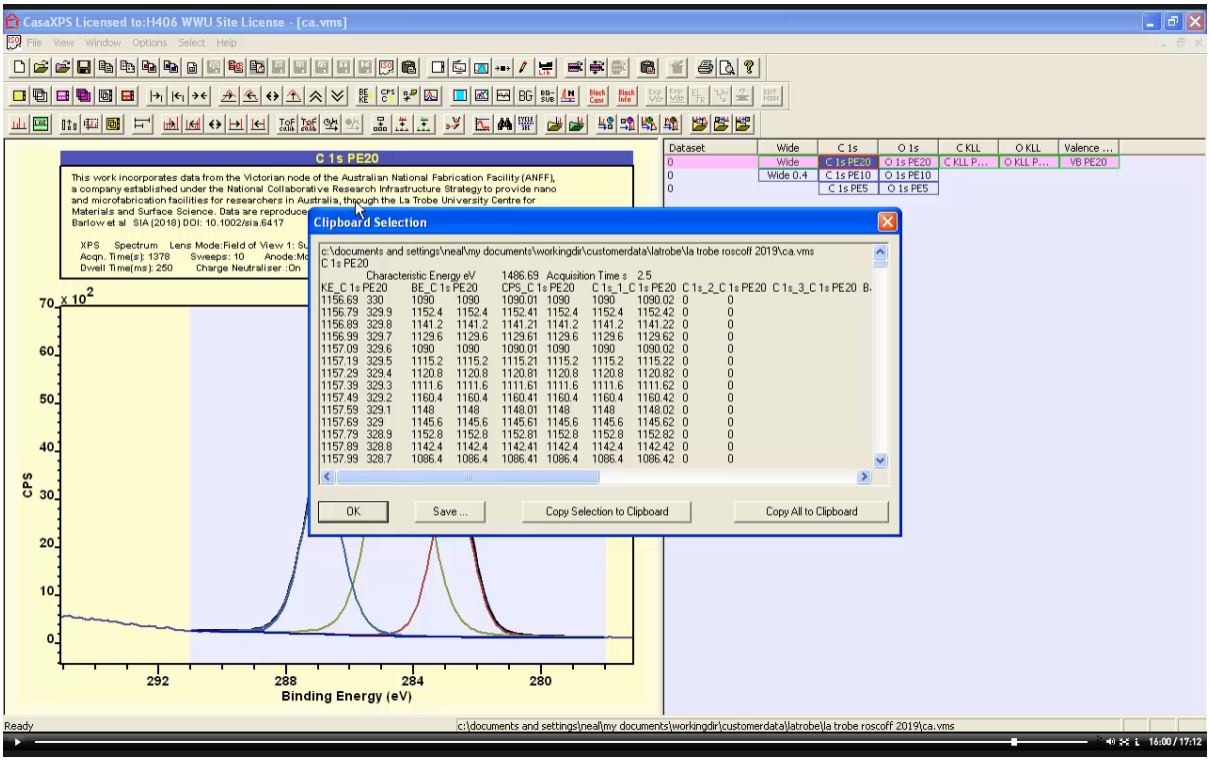

Data fitted with component peaks are exported via toolbar buttons through the clipboard or via TAB spaced ASCII format file. ASCII data for spectra, components, backgrounds etc are presented is a format to permit the plotting of these data in other software.

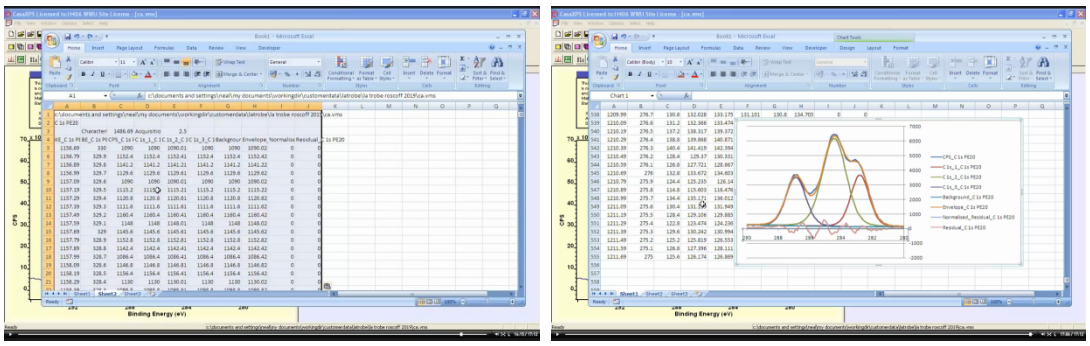

Data from a peak model placed on the clipboard can be pasted into Excel.

Quantification of Homogenous Samples

The following statement is intended to summarise the essence of quantification by XPS.

An atomic concentration computed from a XPS spectrum involves isolating emission peaks, one per element (XPS data in general include multiple emission peaks for each element), then performing a sequence of corrections to these spectral intensities leading to values (normalised peak intensities) representative of the amount of substance sampled by an XPS measurement.

Relative Sensitivity Factors

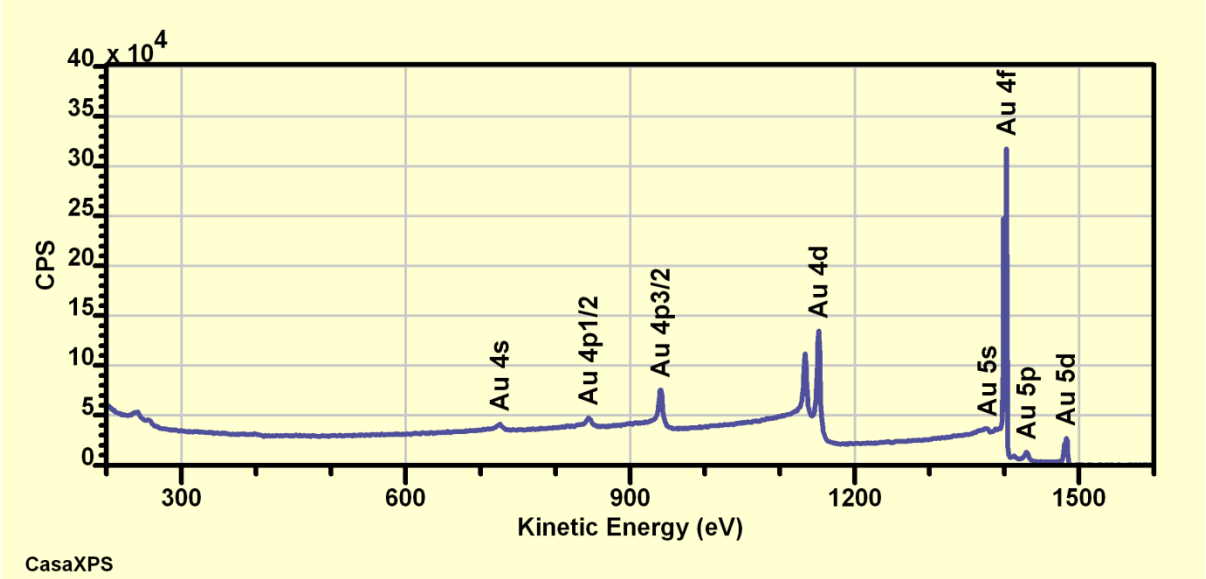

Essentially, the probability of a scattering of a photon by an atom leaving the final electronic configuration with a hole in a specific core electronic shell is dependent on which core level is altered in the final state. The relative intensities for these photoemission peaks depends on these probabilities for the final state configuration and therefore the number of electrons detected are not uniformly distributed between the set of photoemission peaks in an XPS spectrum from a given element, but appear as a sequence of emission peaks with varying intensity.

The purpose of Relative Sensitivity Factors (RSF) is to correct peak intensities to account for differences resulting from the photoemission process.

Theoretical RSF, referred to as Scofield cross-sections, are used to correct for peak intensity differences due to the photoemission process.

Transition probabilities calculated using Hartree-Slater approximations are tabulated by Scofield for photons of energy corresponding to Al and Mg x-ray sources. Scofield cross-sections do not account for angular distribution variation in the effective cross-section as a consequence of instruments detecting electrons in a specific direction relative to the photon source. Angular distribution correction to these Scofield cross-sections based on a given instrument geometry are applied resulting in RSF values appropriate for a given x-ray source and the angle between the x-ray source and the direction defined by the electron energy analyser.

Scofield cross-sections are corrected for angular distribution using the factor $1 - \frac{\beta}{4}(3\cos^2\theta - 1)$ relative to s-orbital electron configurations. The β value is computed for the element for which the Scofield cross-section is defined, and θ is the x-ray source to electron analyser angle. For data from a Kratos Axis Ultra the angle between the x-ray source and the direction of the electron analyser is assumed to be 60°. For an Ulvac PHI VersaProbe the angle θ is 45°. Magic angle instruments do not require angular distribution correction since the angle θ is chosen such that $3\cos^2\theta - 1 = 0$.

Instrumental Transmission Correction

The number of electrons recorded by an instrument at a specific kinetic energy for the detected electrons deviate from the number of electrons emitted from the sample. The ratio of electrons leaving the sample to the number of electrons recorded at the detector varies as a function of the kinetic energy for the emitted electrons. To adjust for these variations in collection efficiency an instrument transmission function is measured.

Data in these examples are corrected for transmission using the National Physical Laboratory (NPL) transmission correction software. A transmission function is prepared for each operating mode for a given instrument. Differences in operating mode may include specific settings for the pass energy, electron optical lens modes, aperture settings and detector settings.

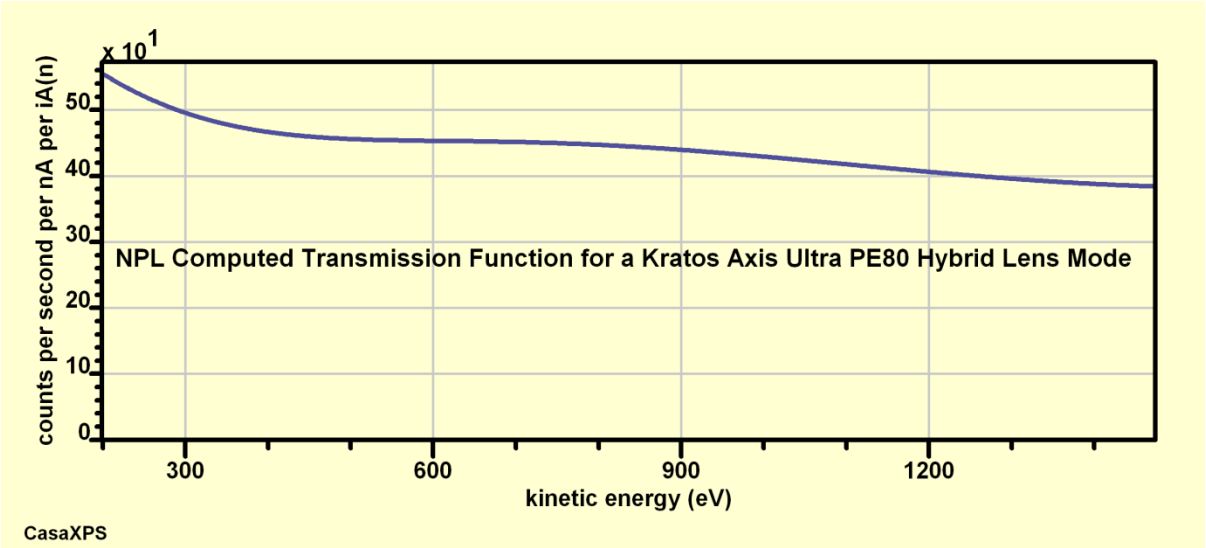

Escape Depth Correction

Inelastic scattering of electrons within solid state materials as measured by XPS results in the characteristic background to photoemission peaks obvious in survey spectra. The production of inelastic scattered electrons is modelled by an exponential decay in zero loss photoemission recorded. Intensity for electrons emerging from a layer within the surface is obtained by integrating the signal over the interval $[p, q]$ using the exponential attenuation model $e^{-x/a}$ for the reduction in intensity at the surface due to photoemission at a depth x beneath the surface. The value for a determines the sampling depth for photoemission from a specific material at a specific energy for a photoelectron.

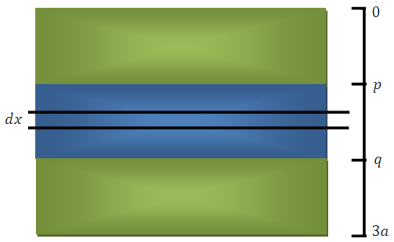

The intensity emitted at the surface I from a layer of material between the depths of p and q is proportional to the integral:

$$I \propto \int_p^q e^{-x/a}\,dx = a\left[e^{-p/a} - e^{-q/a}\right]$$

For $p = 0$ and $q = 3a$ then 95% of photoemission signal without energy loss is accounted for from the surface layer, hence the sampling depth for XPS is often referred to a three times the effective attenuation length. When considering the upper energies for Al anode x-ray emission the value for a is between 3 and 4 nm, hence a common rule of thumb is that for Al x-rays the maximum sampling depth is in the region of 10 nm.

The value a for photoemission from solid state materials varies as a function of kinetic energy of the electrons detected. Even for a sample of uniform depth distribution such as gold, silver or copper, the number of electrons recorded for an emission peak reduces as the energy of the electrons decreases simply because the volume of material from which an electron can emerge without inelastic scattering reduces.

For a given analysis area, the volume of material sampled for a given kinetic energy for the emitted electrons can be modelled using the Inelastic Mean Free Path (IMFP) λ or Effective Attenuation Length (EAL). Martin Seah publish universal equation approximations to IMPF (λ) and EAL

$$\lambda = \frac{(0.73 + 0.0095E^{0.872})}{Z^{0.3}} \quad (nm)$$

$$EAL = \frac{(0.65 + 0.007E^{0.93})}{Z^{0.38}} \quad (nm)$$

where E is the photoelectron kinetic energy and Z is the average atomic number provide a means of correcting for escape depth dependence on kinetic energy.

XPS data only offers the possibility for reporting the amount of substance when properly corrected emission peaks are used in the atomic concentration formula applied to truly homogeneous samples.

Quantification by XPS Illustrate using Fused Silica

Relative Sensitivity Factor
Scofield Cross-Sections

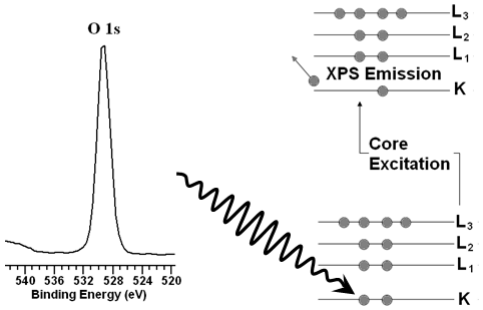

Instrument Geometry

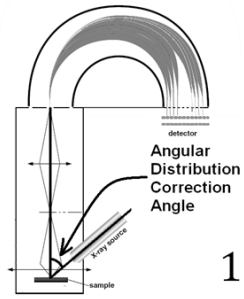

For Magic Angle Instruments Angular Distribution Correction is Not Required

$$1 - \frac{\beta}{4}(3\cos^2\theta - 1)$$

Approximation (Martin Seah) to IMFP (λ) and EAL

$$\lambda = \frac{(0.73 + 0.0095E^{0.872})}{Z^{0.3}} \quad (nm)$$

$$EAL = \frac{(0.65 + 0.007E^{0.93})}{Z^{0.38}} \quad (nm)$$

E is the photoelectron kinetic energy

Z is the average atomic number

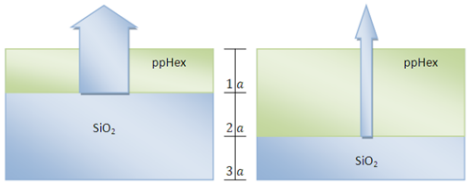

$$I \propto \int_p^q e^{-x/a}\,dx = a\left[e^{-p/a} - e^{-q/a}\right]$$

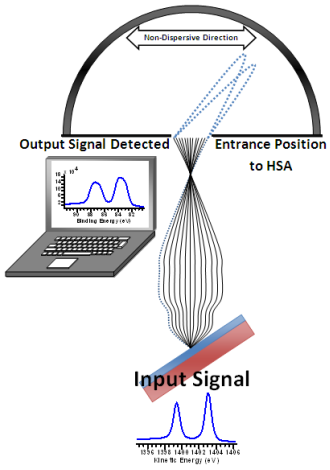

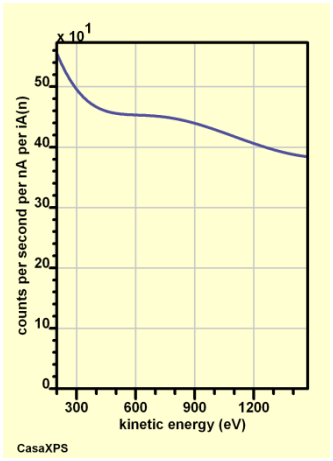

The basic tools used to assess sample chemistry are quantification regions defined for isolated photoemission peaks. In the case of fused silica photoemission peaks corresponding to Si 2p, O 1s and C 1s are isolated from any interfering photoemission peaks. As a consequence quantification regions can be used to define appropriate approximations to inelastic scattered background signal, intervals over which signal above the inelastic scatter background is integrated to yield raw counts per second eV (CPSeV) for each peak. These raw CPSeV are then scaled using relative sensitivity factors in the form of Scofield cross-sections, which are adjusted for angular distribution based on an angle of 60^o between the axis of the analysers lens column and the Al anode X-ray source. Escape depth correction is performed using the EAL approximation to allow for differences between the sampling depths for O 1s and Si 2p signal. Finally instrument response to kinetic energy is corrected by making use of a transmission function computed for these data using the NPL transmission correction procedure.

In principle, the computed transmission function effectively allows recorded data to appear as if it were measured from an instrument created with ideal flat transmission response to electron photoemission energy. Only when a precise transmission correction is available is the use of Scofield cross-sections appropriate. Another way of looking at this statement is, in principle, any instrument for which relative sensitivity factors are other than Scofield cross-sections does not have an absolute and true transmission function available.

Fused Silica Video

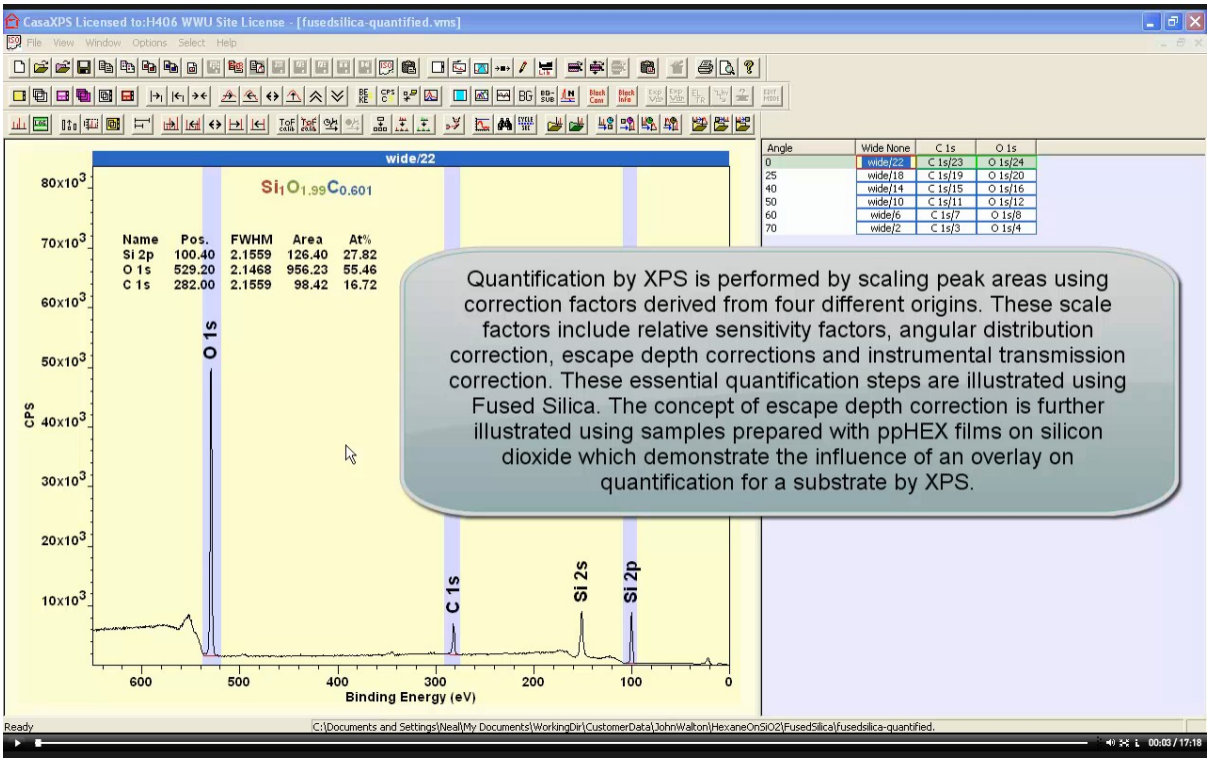

Quantification steps used to transform raw survey spectra into stoichiometric relationships between silicon and oxygen are explain for a sample expected to be fused silica.

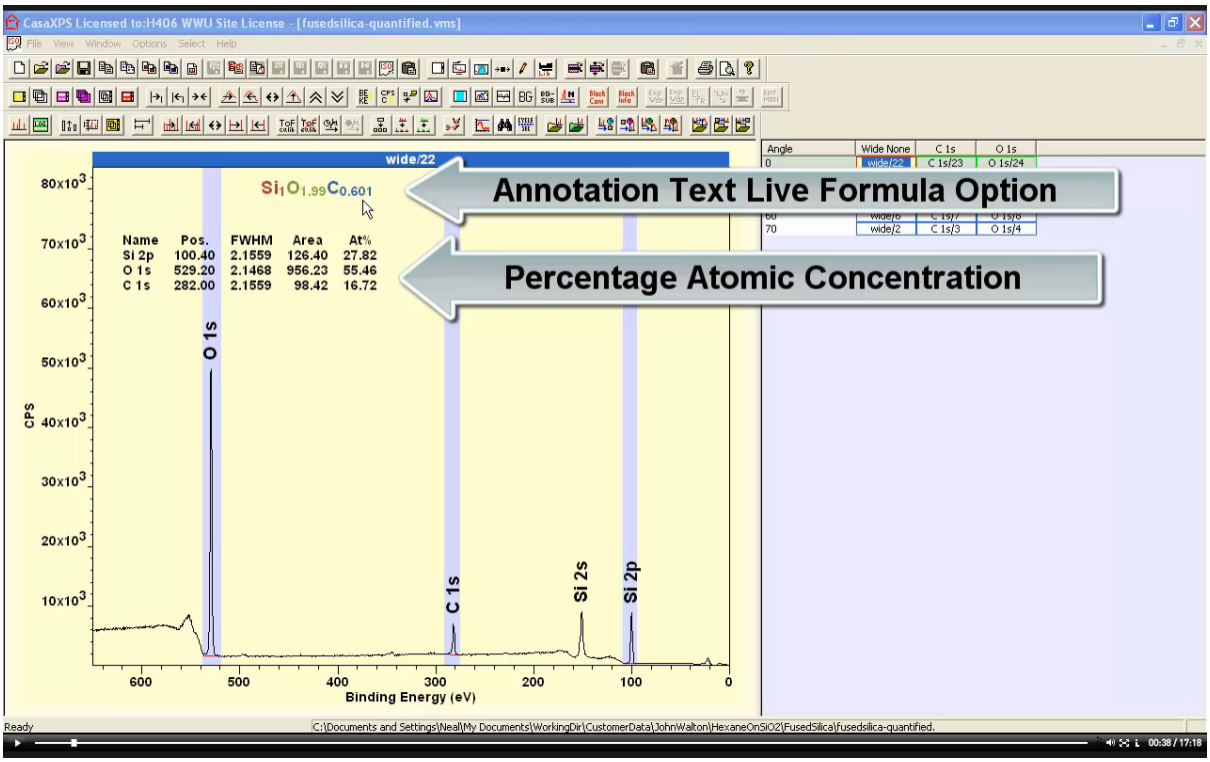

Quantification results from regions are display over data by adding annotation using the Annotation Dialog Regions property page table specification and the Formula option on the Annotation Dialog Text property page.

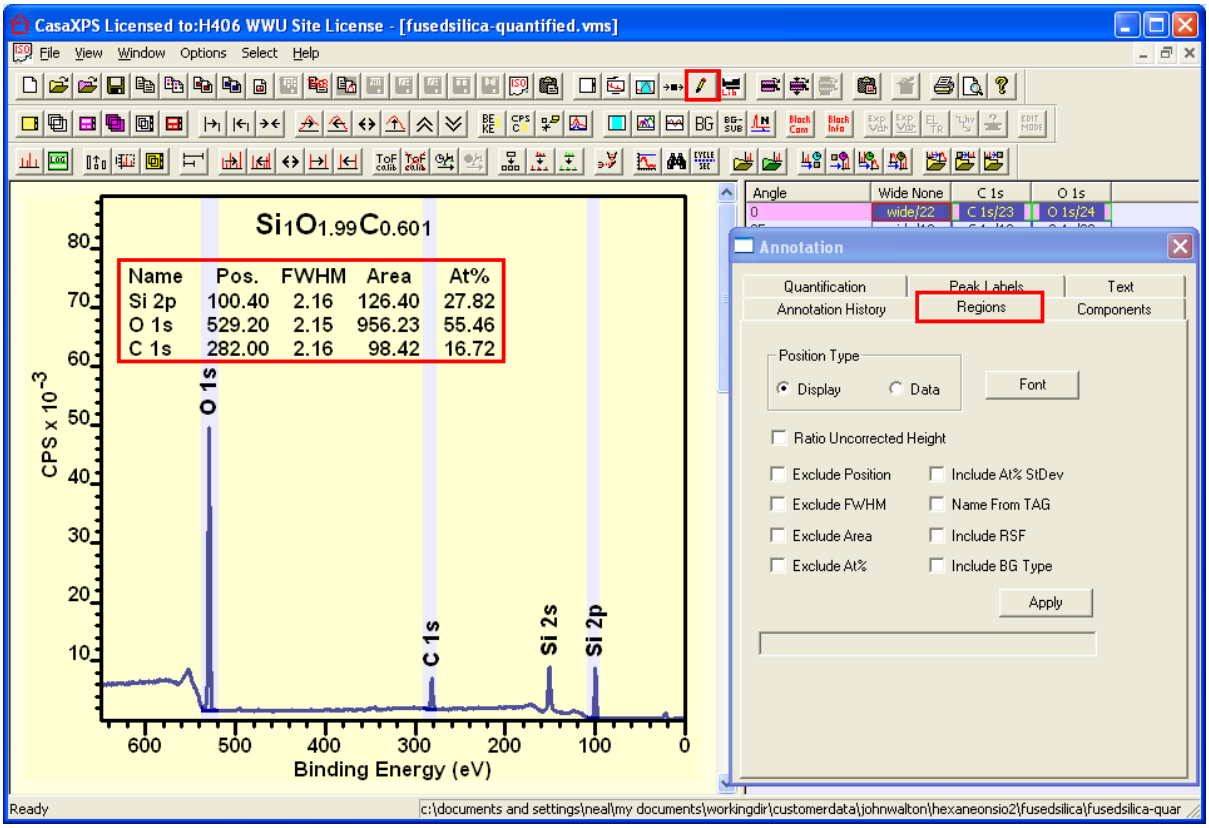

Annotation dialog Regions property page.

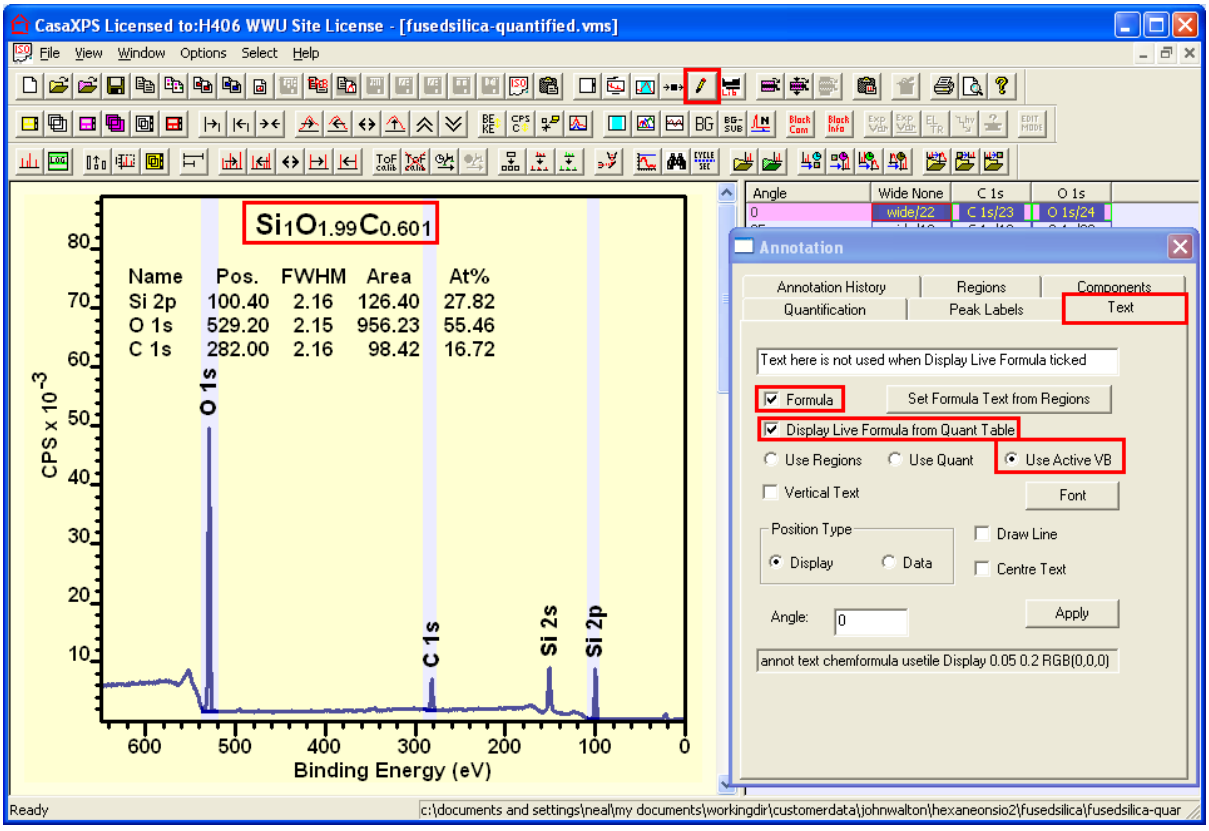

Annotation dialog Text property page making use of options for extracting the displayed text from quantification results gathered from regions.

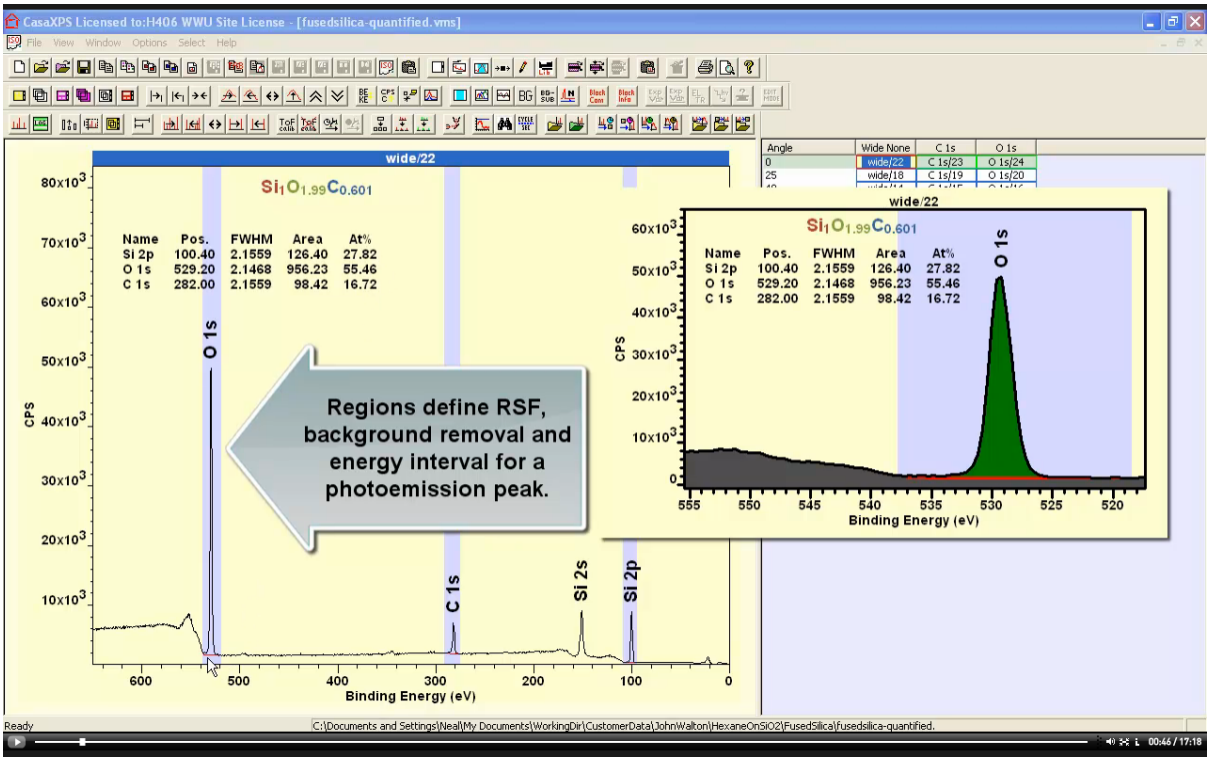

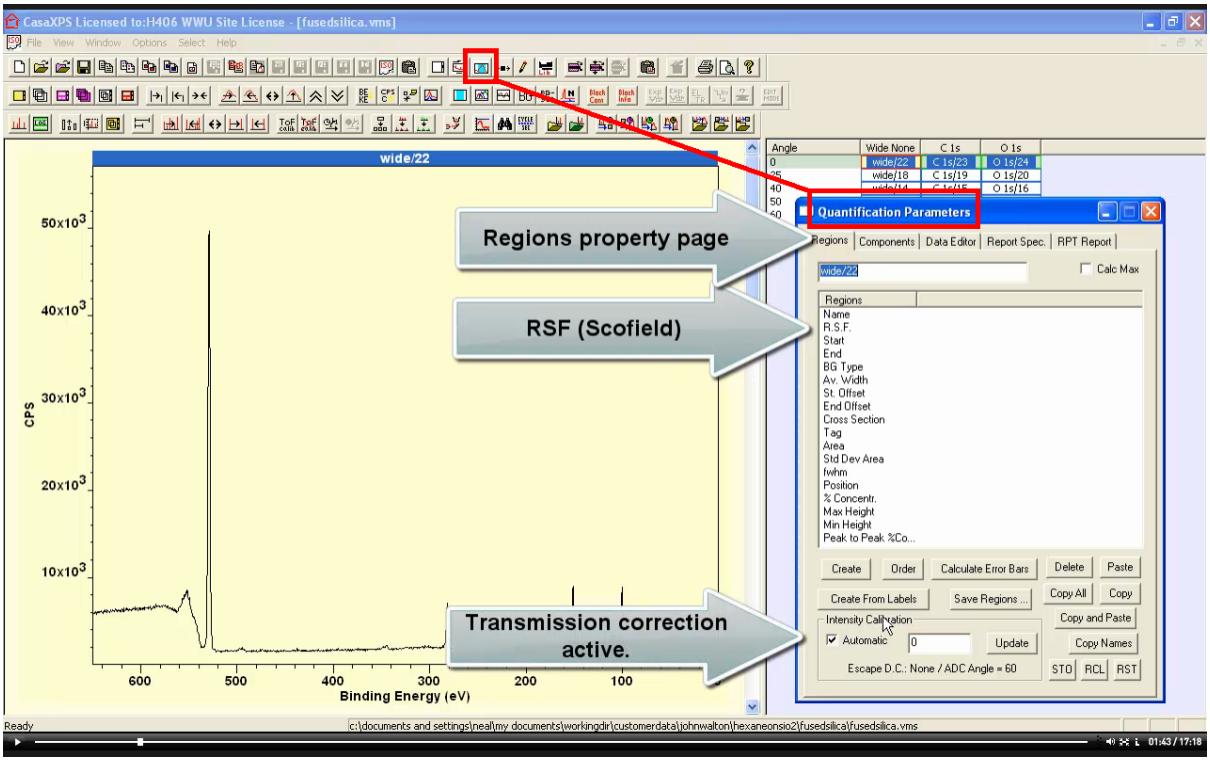

The Quantification Parameters dialog window Regions property page allows the specification of quantification information specific to a photoemission peak (RSF, background and energy interval) and displays the currently active intensity calibration options in the form of transmission, escape depth and angular distribution corrections.

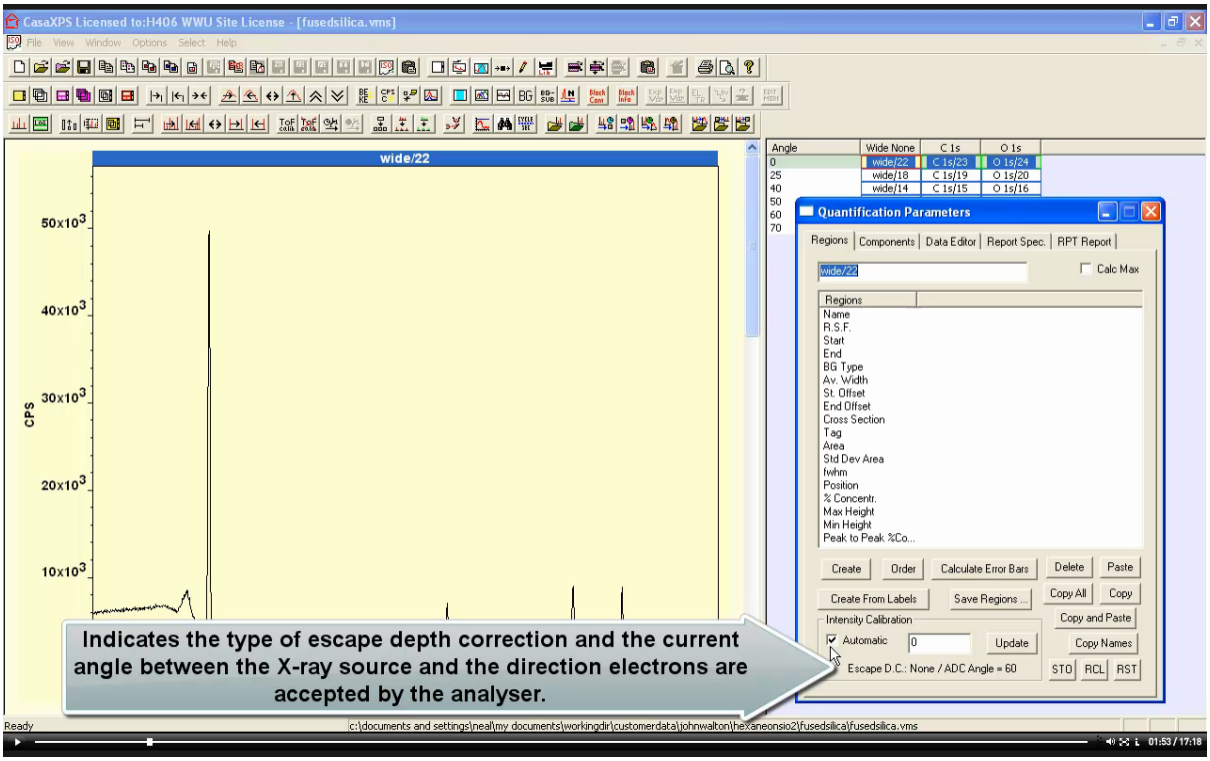

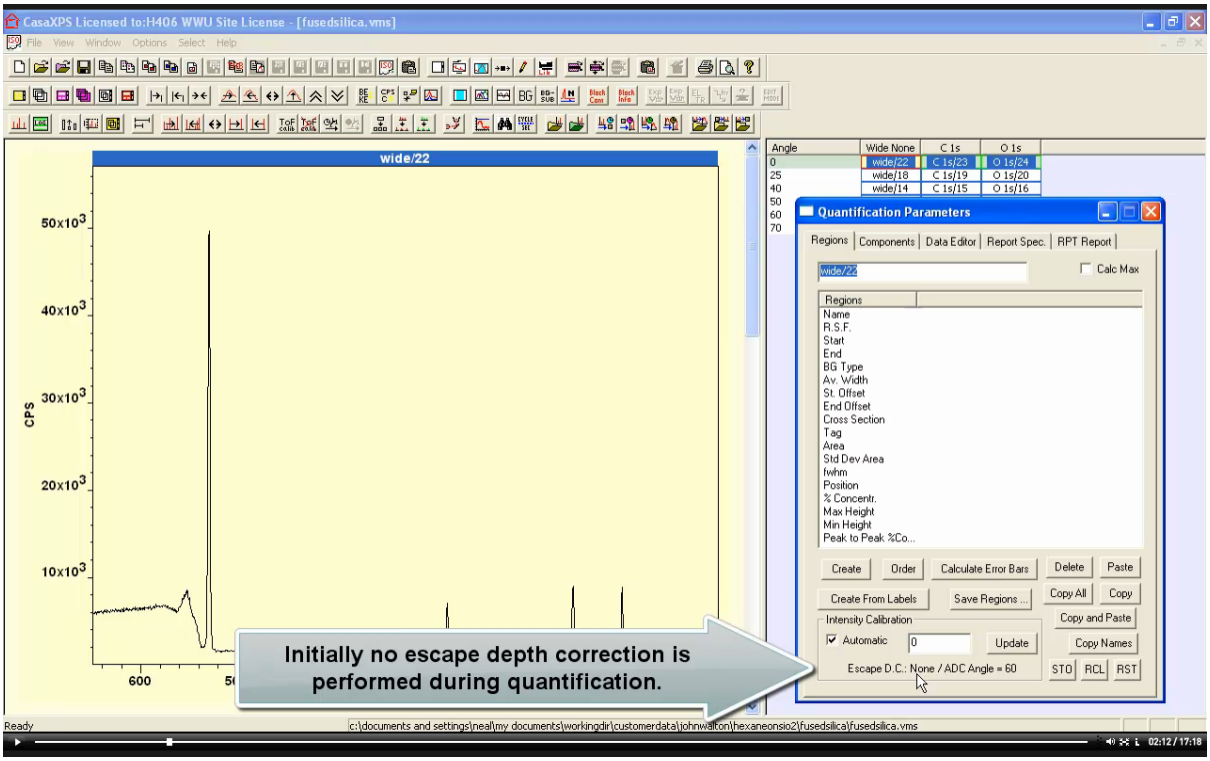

During the course of this video quantification regions are defined and intensity calibration steps are progressively added resulting in traceable quantification for a fused silica sample. Initially transmission correction based on an NPL computed transmission function is active.

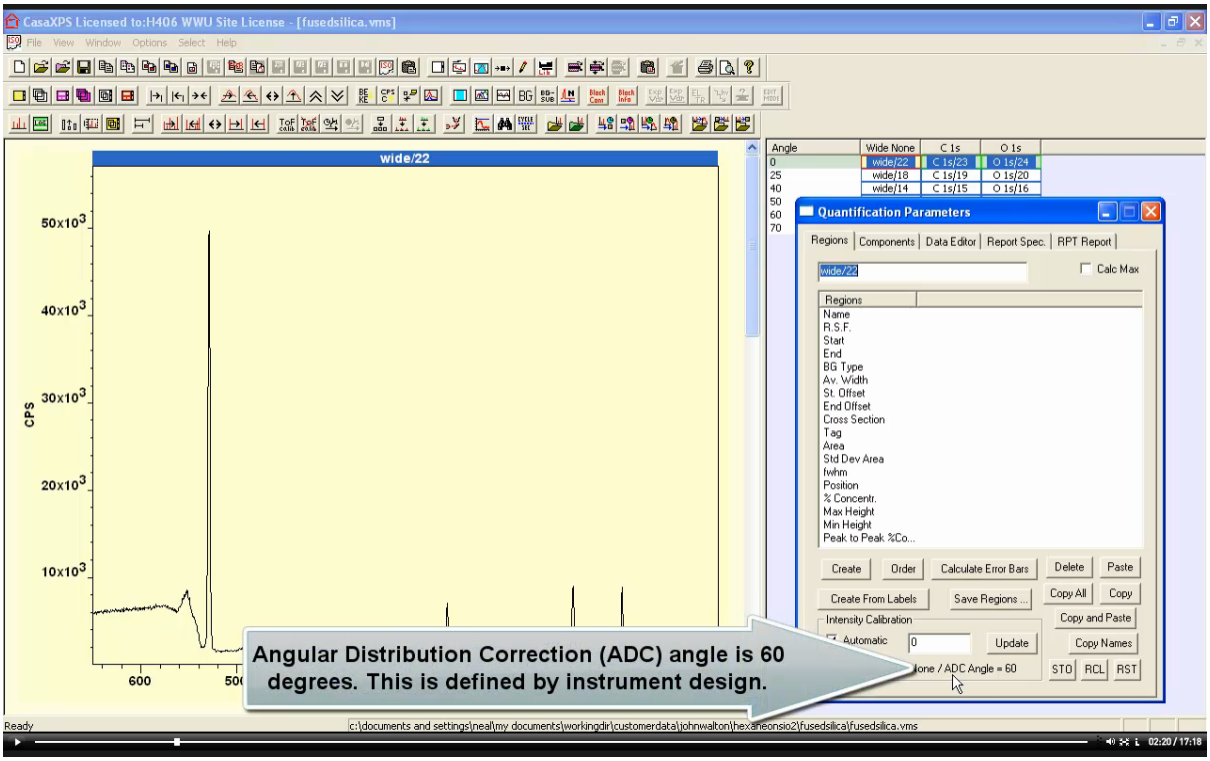

Angular distribution correction is active too making use of an angle of 60° between the direction for electrons collected by the transfer lens system and the x-ray source. ADC information is used to adjust the relative sensitivity factor for a region at the time a region is created.

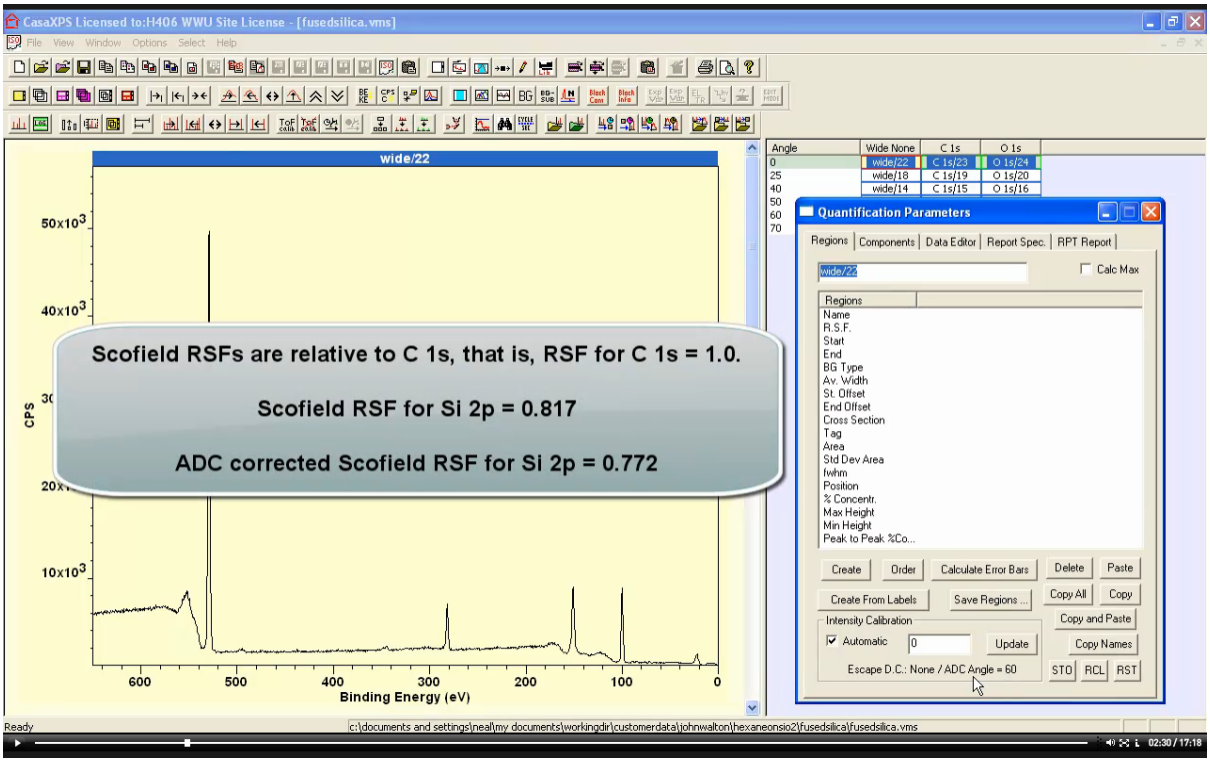

The element library contains an RSF for Si 2p equal to 0.817. This value for the Si 2p RSF is computed by Scofield using quantum mechanics to compute the photoionisation cross-section for Al anode x-rays exciting a Si atom initially in the ground state.

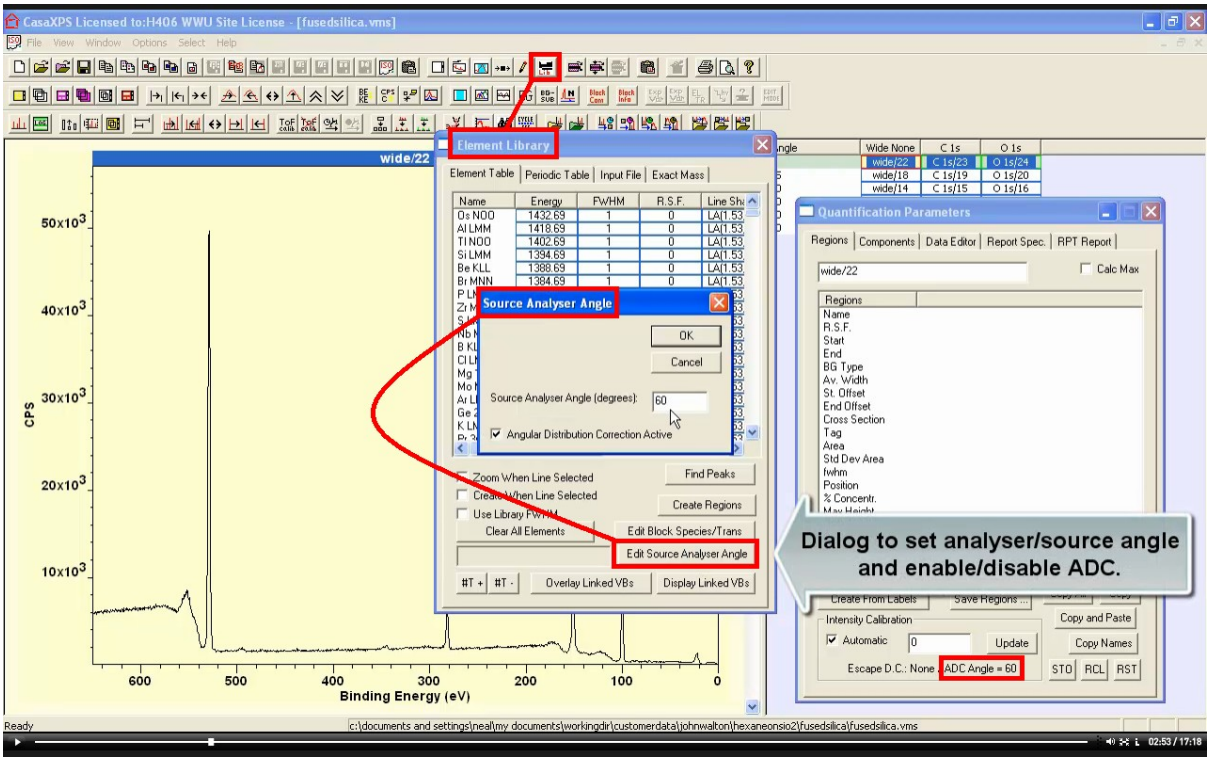

Values for the ADC angle can be adjusted using the Element Library dialog window Element Table property page.

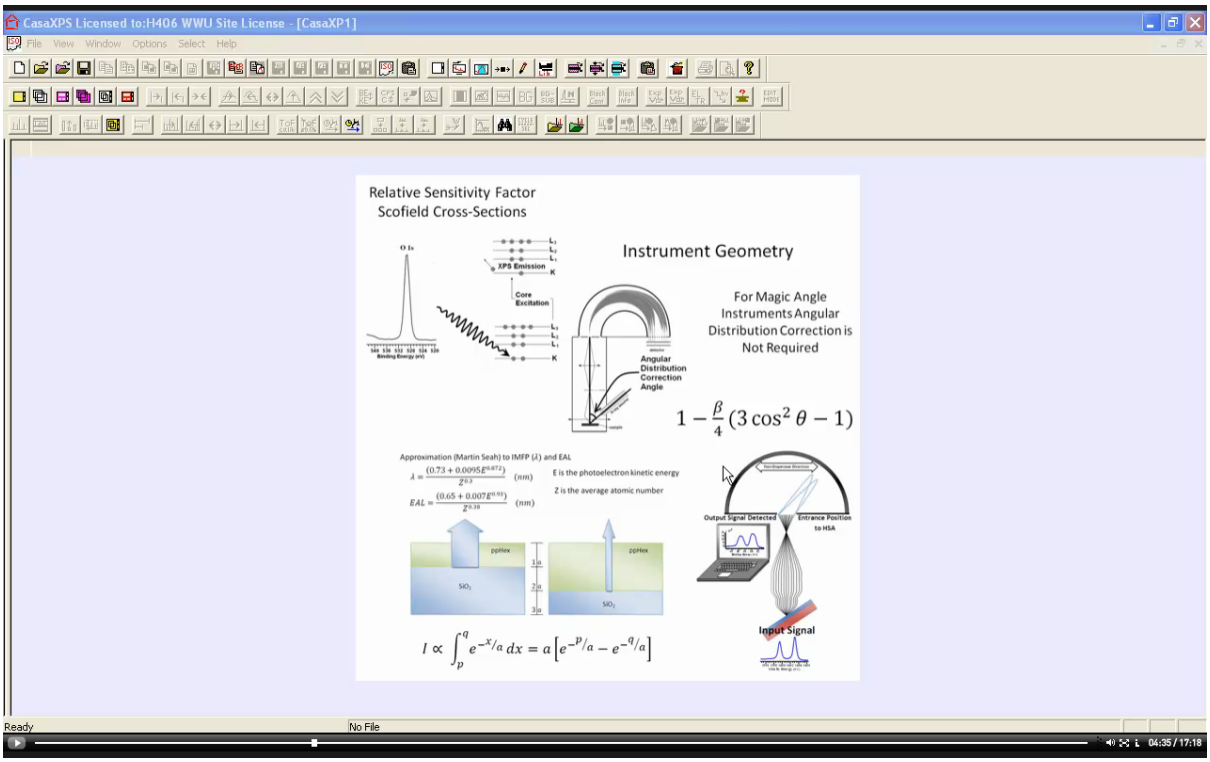

For each region a total sensitivity factor is computed based on Scofield RSF, transmission function for the photoemission energy, escape depth for the photoemission energy and the source analyser angle instrument geometry.

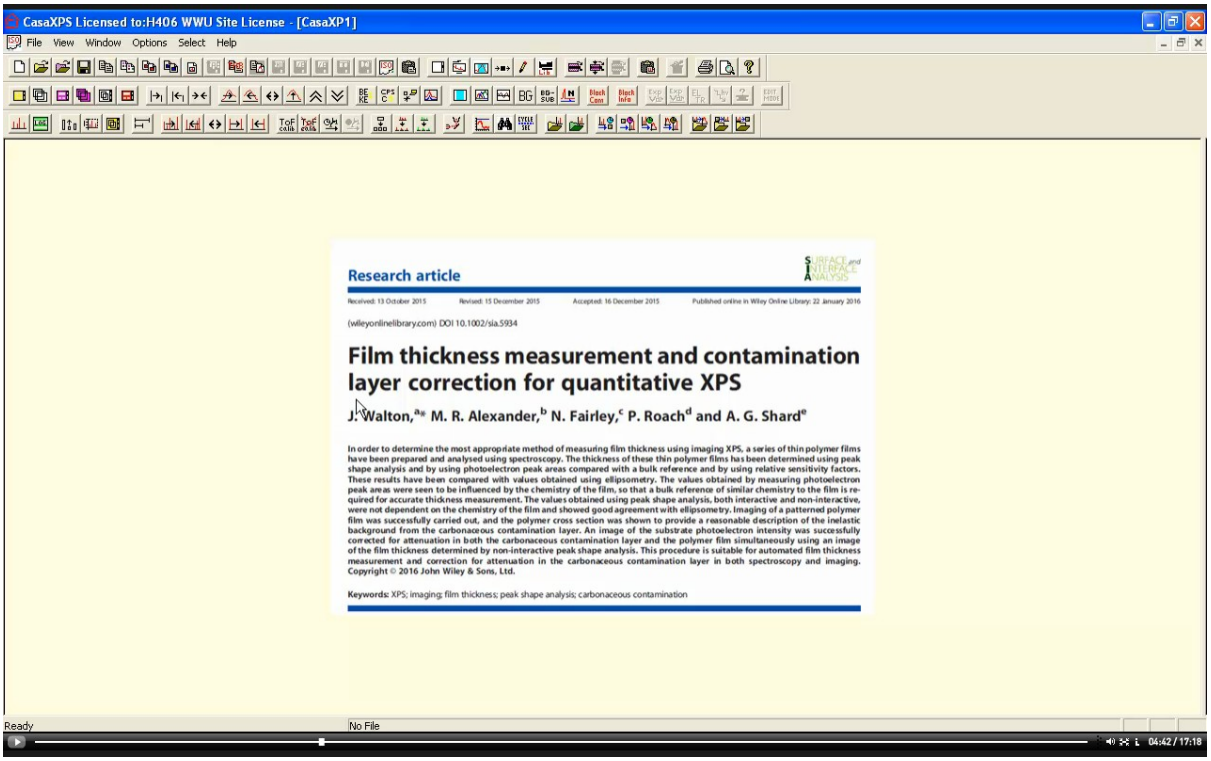

Information about escape depth corrections and how escape depth can be used to understand sample composition by XPS is described in Walton et al (SIA 2016).

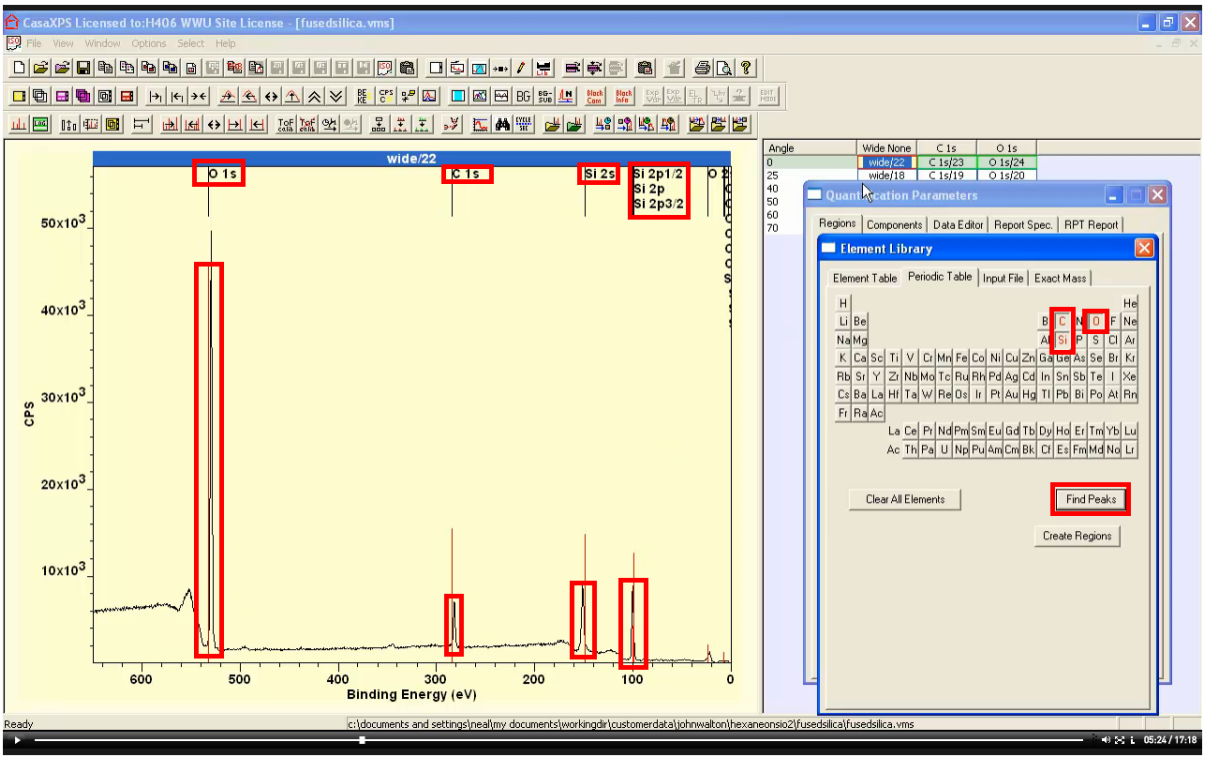

Quantification regions can be created by marking each element of interest using the Element Library dialog window via the Element Table and Periodic Table property pages. The Find Peaks button marks any peak with element markers for which a possible match occurs. This is a superset of elements rather than attempting to identify the most likely.

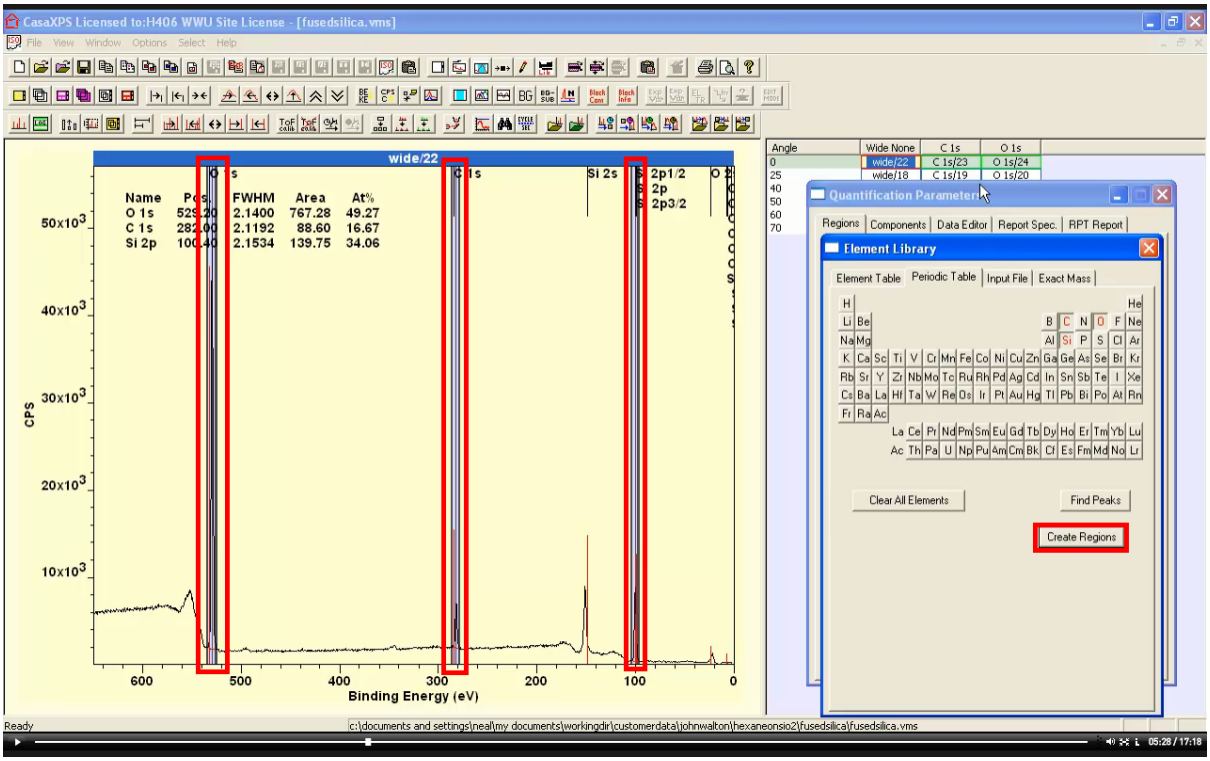

Once the user assesses the superset of elements and limits the element markers to the most likely elements (in this case C 1s, O 1s and Si) regions are created using element markers by pressing the Create Regions button on the Periodic Table or Element Table property pages.

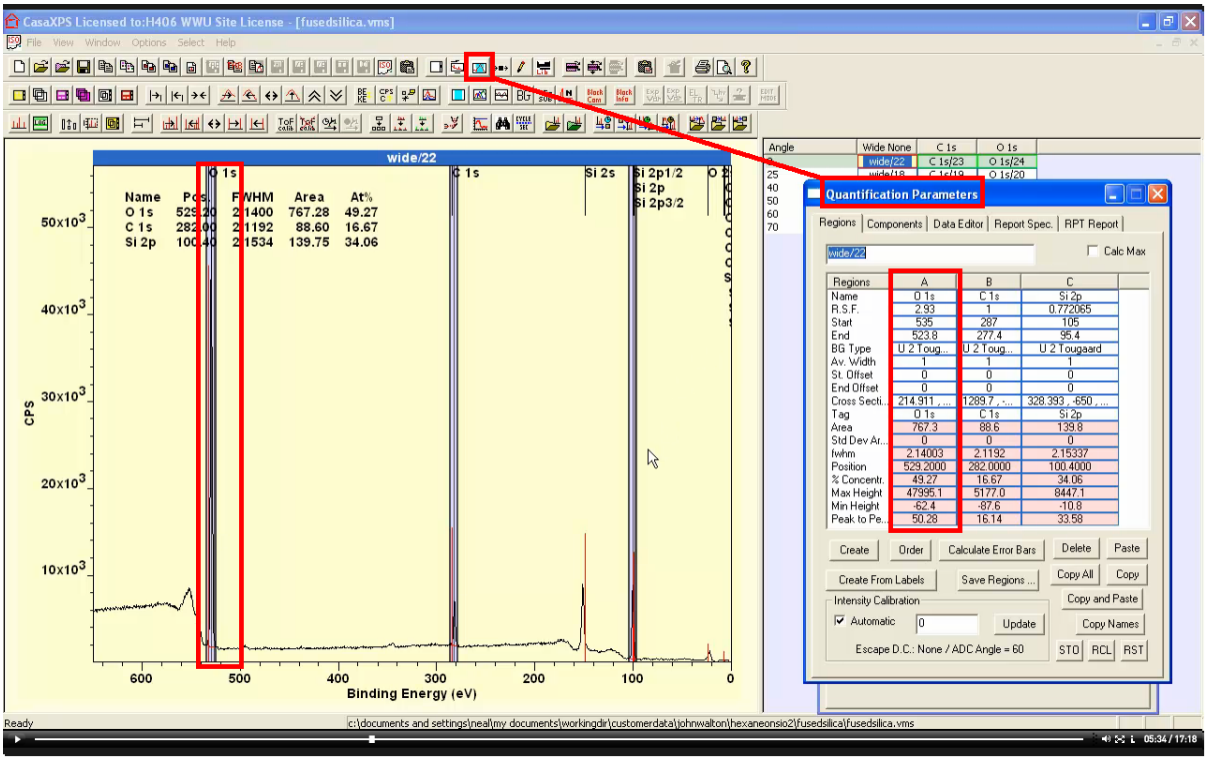

Regions are created and can be edited using the Quantification Parameters dialog Regions property page.

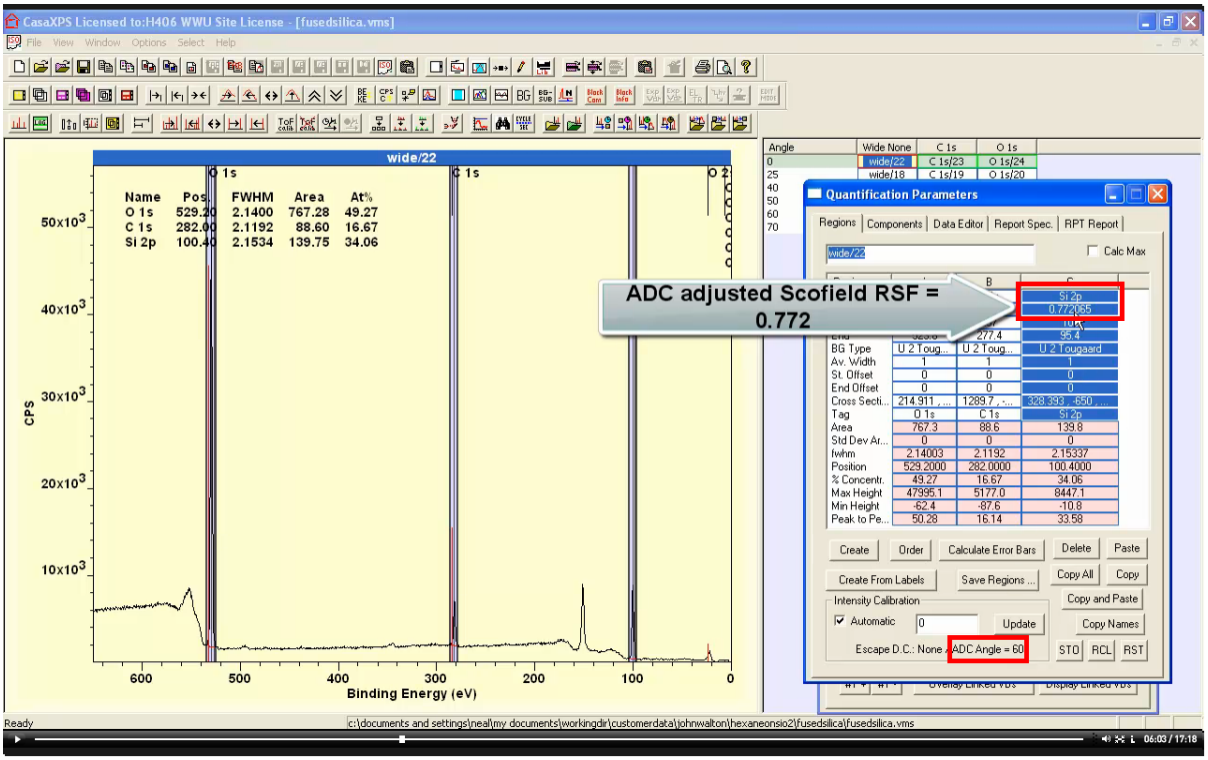

Note the Si 2p is the only region with an ADC corrected RSF. RSFs in the Scofield library are relative to C 1s sensitivity and ADC for electrons with s orbital angular momentum the correction is identical for all elements. Differences occur in ADC for p, d, f orbital angular momentum therefore the Si 2p RSF is the only RSF out of C 1s, O 1s and Si 2p that requires ADC adjustments.

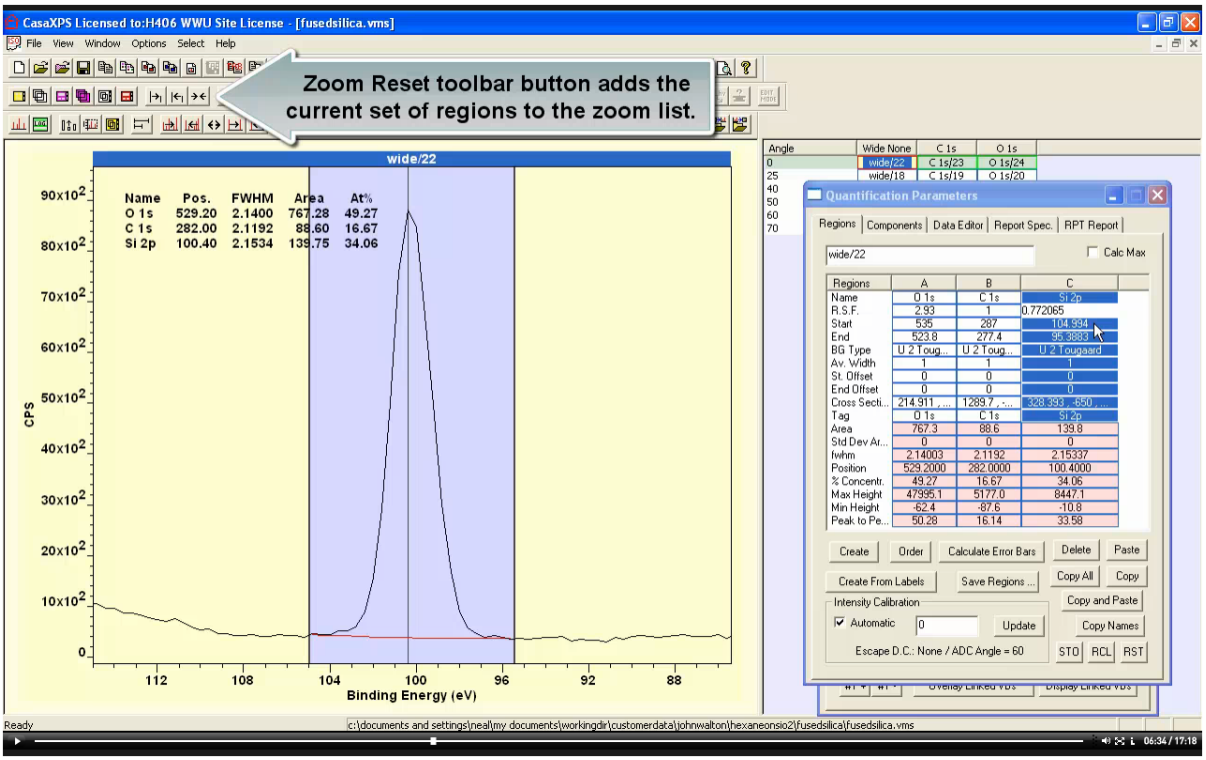

Each time a zoom action occurs the dimensions for the display in terms of energy and intensity intervals is added to a zoom list. Toolbar buttons allow the zoom states to be used to view data in

sequence. When regions are defined on a VAMAS block and the Reset zoom list toolbar button is pressed the energy intervals defined by the current set of regions is used to initialise the zoom list. Cycling through the zoom list allows each region to be viewed in turn.

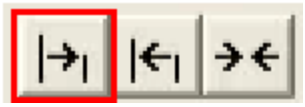

Zoom In toolbar button creates a new zoom state using a box drawn using the mouse and the left mouse button to drag a box over the left hand display tile. The new zoom state is added to the current zoom list.

Zoom Out toolbar button steps through the zoom states currently active for the left hand display tile. The set of current zoom state are cycled through repeatedly by pressing the Zoom Out toolbar button.

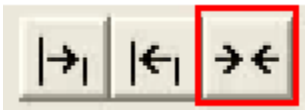

Reset Zoom List toolbar button will empty the zoom list or if regions are defined on the active spectrum in the active display tile, energy intervals defined by these regions are added to the zoom list to allow the easy inspection of newly created region limits.

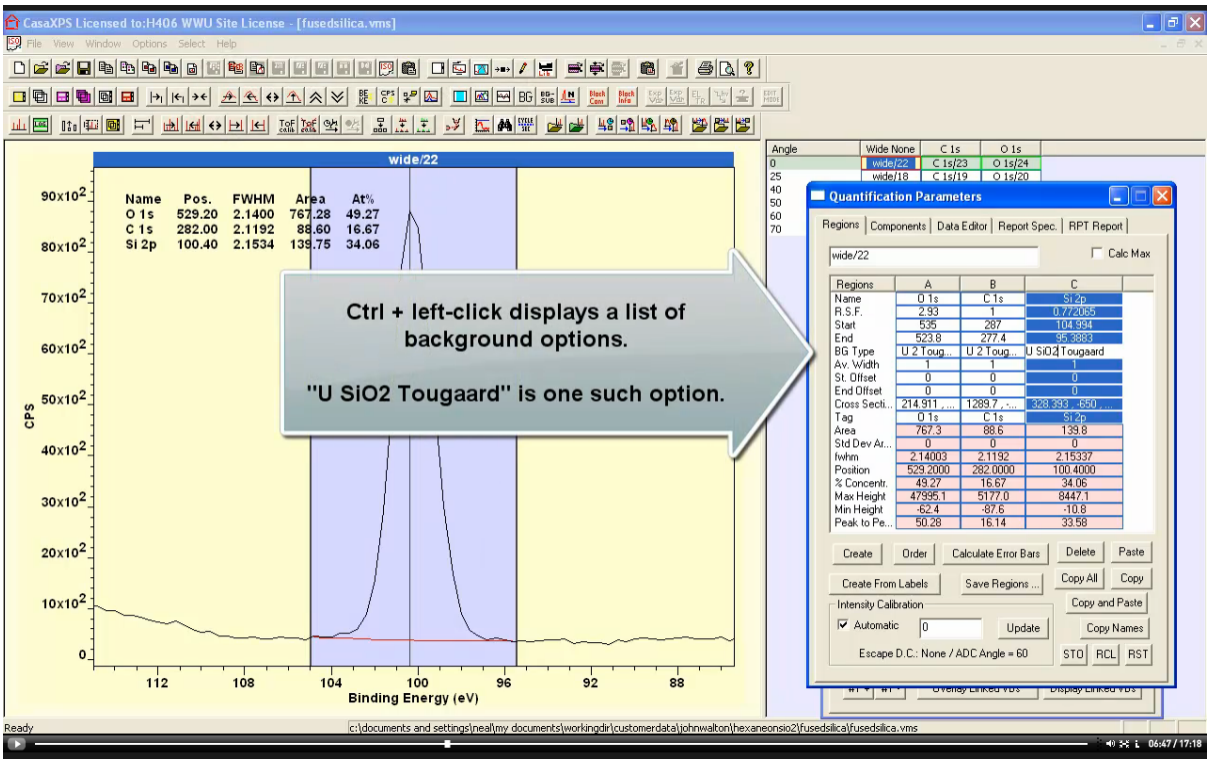

BG Type refers to the type of approximation used to remove inelastic scattered background signal from intensity due to primary zero-loss photoemission signal used to quantify sample composition. There are many background types available including basic linear, Shirley and Universal Tougaard backgrounds, however there are more sophisticated backgrounds for materials such as fused silica established by Tougaard. These can be viewed and selected via a dialog window associated with the BG Type field within a region specification.

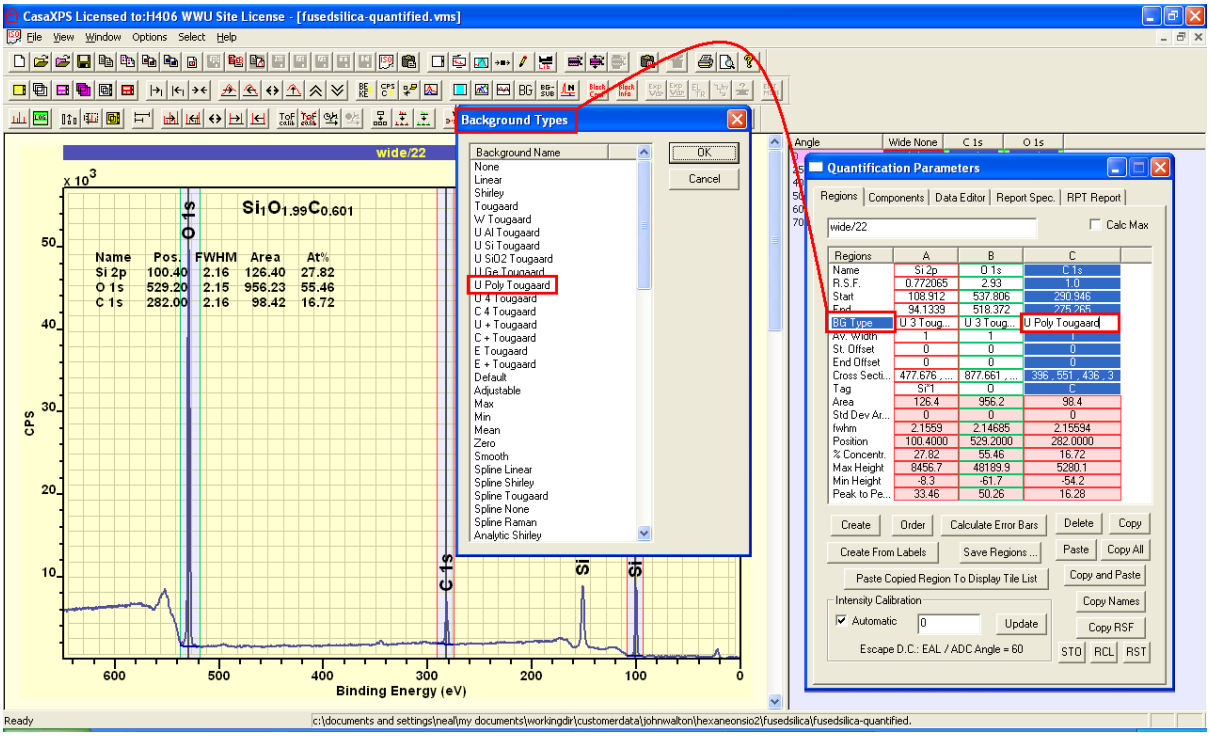

New features in CasaXPS 2.3.22 invoke the Background Type dialog window by selecting a BG Type field for an existing region before left clicking on the BG Type label within the Regions property page table of region parameters.

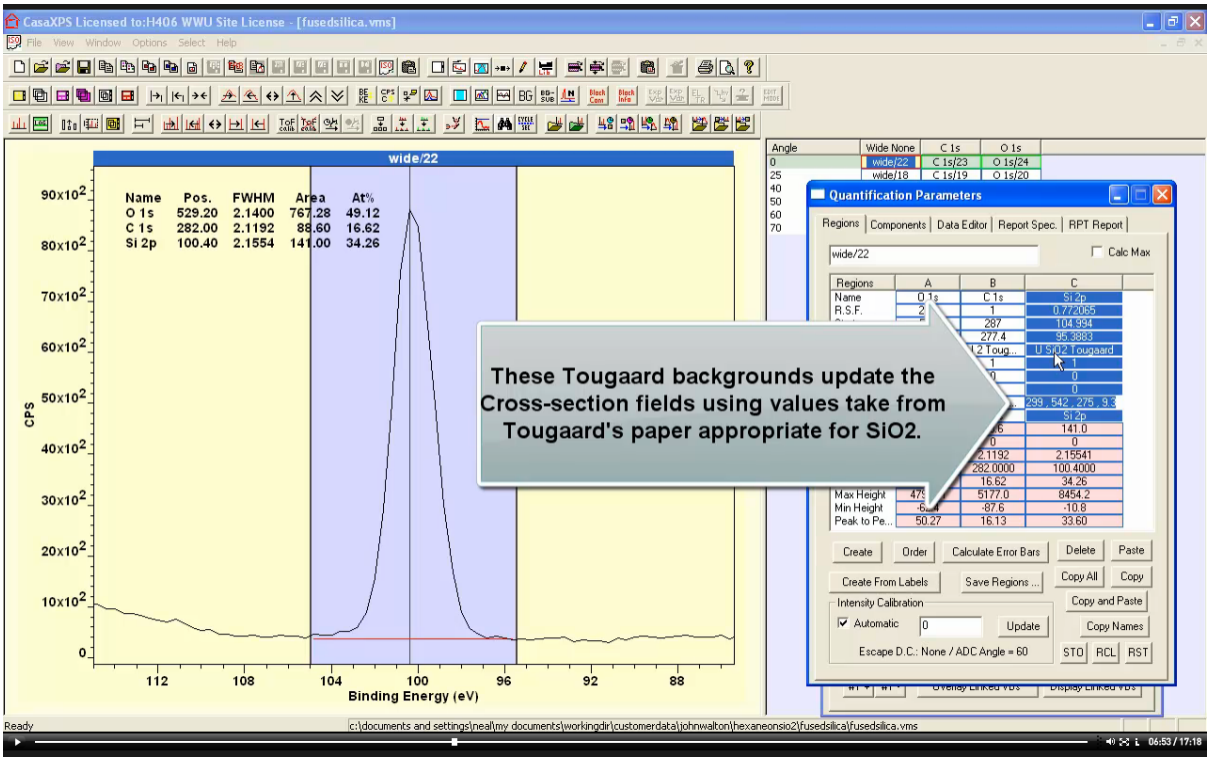

After a specific Tougaard background type is selected, the cross-section field is updated with four parameters defined by Tougaard. The values for U SiO2 Tougaard are entered in the cross-section field. The cross-section functional form for the U 3 Tougaard background type is identical to the U SiO2 Tougaard cross-section however when the background type is set to U 3 Tougaard the cross-

section fields can be manually adjusted, if required, and the B cross-section parameter is automatically computed for the specific interval of spectra defined by the region.

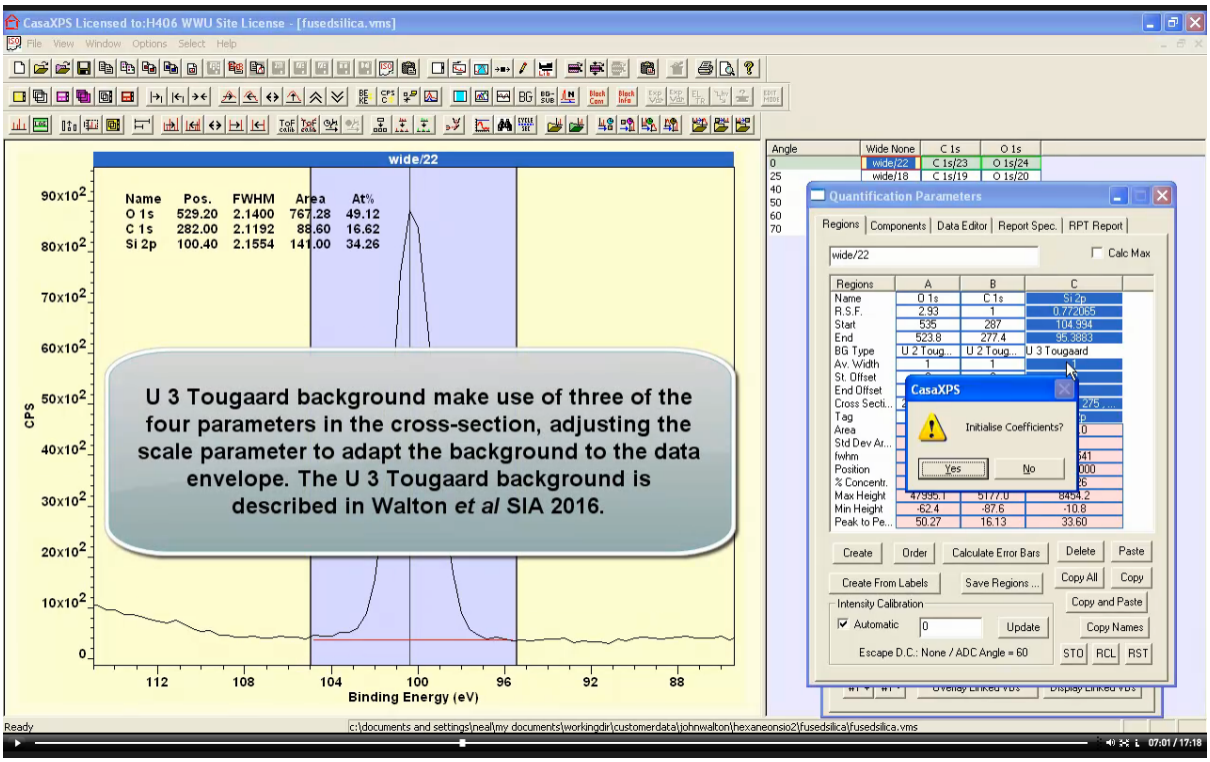

When the BG Type is changed from U SiO2 Tougaard to U 3 Tougaard a dialog window asks if the cross-section coefficients should be initialised. Since the U SiO2 Tougaard cross-section values are already appropriate for these data, the reply is to select the No button.

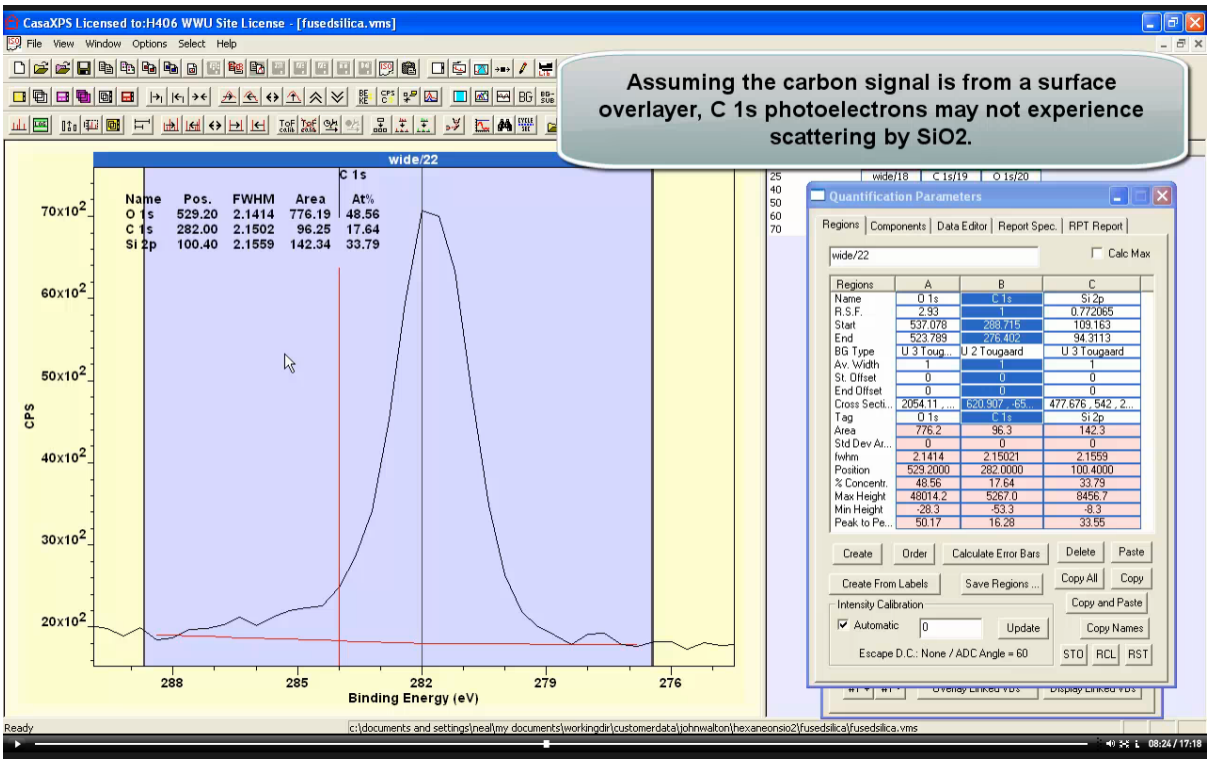

Inelastic scattering of photoelectrons depends on the material through which these electrons must pass en route to the vacuum. Photoemission from a surface contamination layer may experience different scattering events to those from a substrate. We assume for fused silica carbon is an overlay to SiO_2 and therefore only Si and O signal experiences scattering by Si and O electrons bond to these elements. C 1s signal is predominantly scattered by carbon atoms so may require a different background to Si 2p and O 1s peaks.

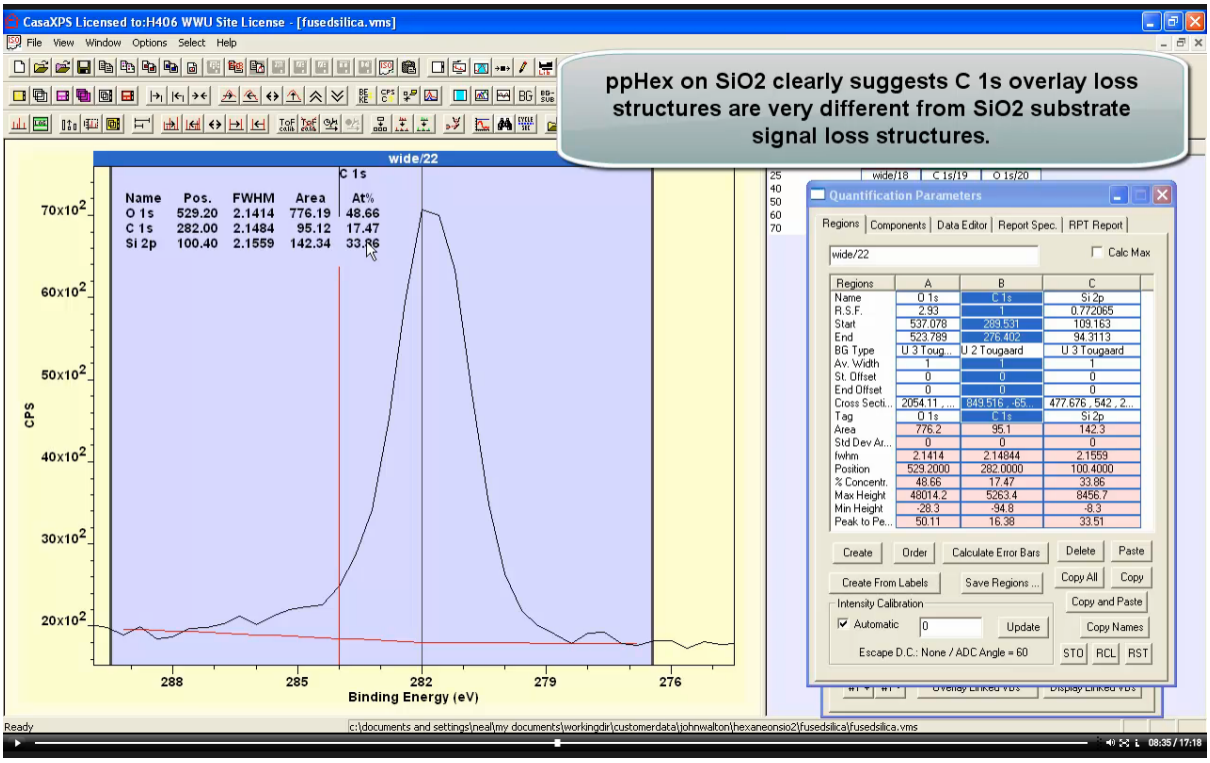

Backgrounds for these data are not important as both SiO_2 and carbon contamination result in relatively flat backgrounds beneath photoemission peaks. The significance of the background becomes more apparent when heterogeneous materials are analysed such as a layer of plasma-polymerised hexane on SiO_2.

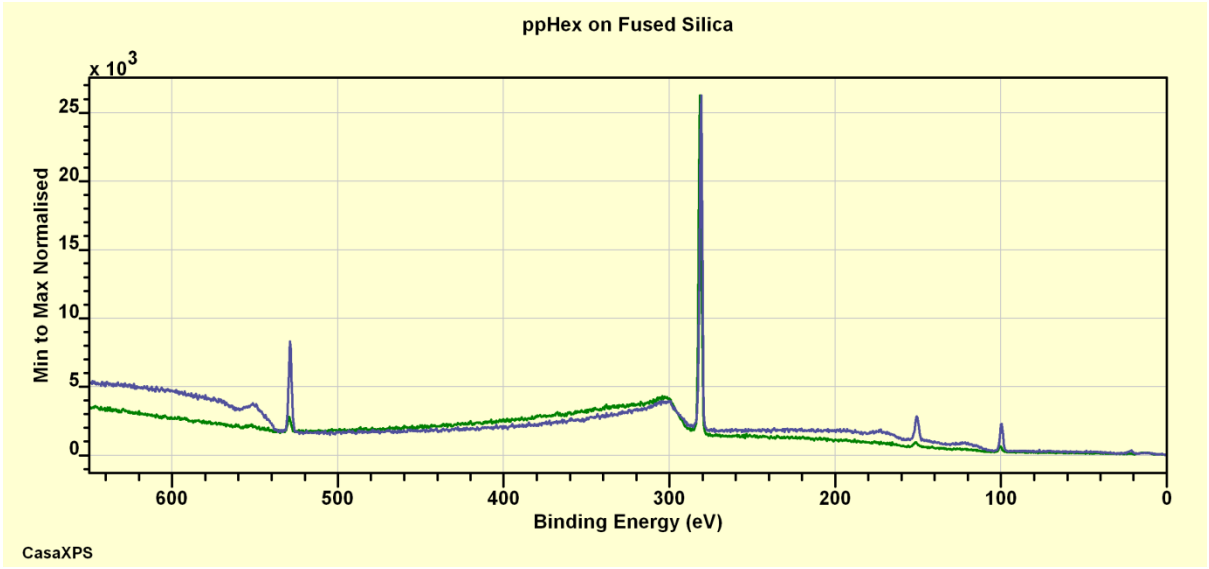

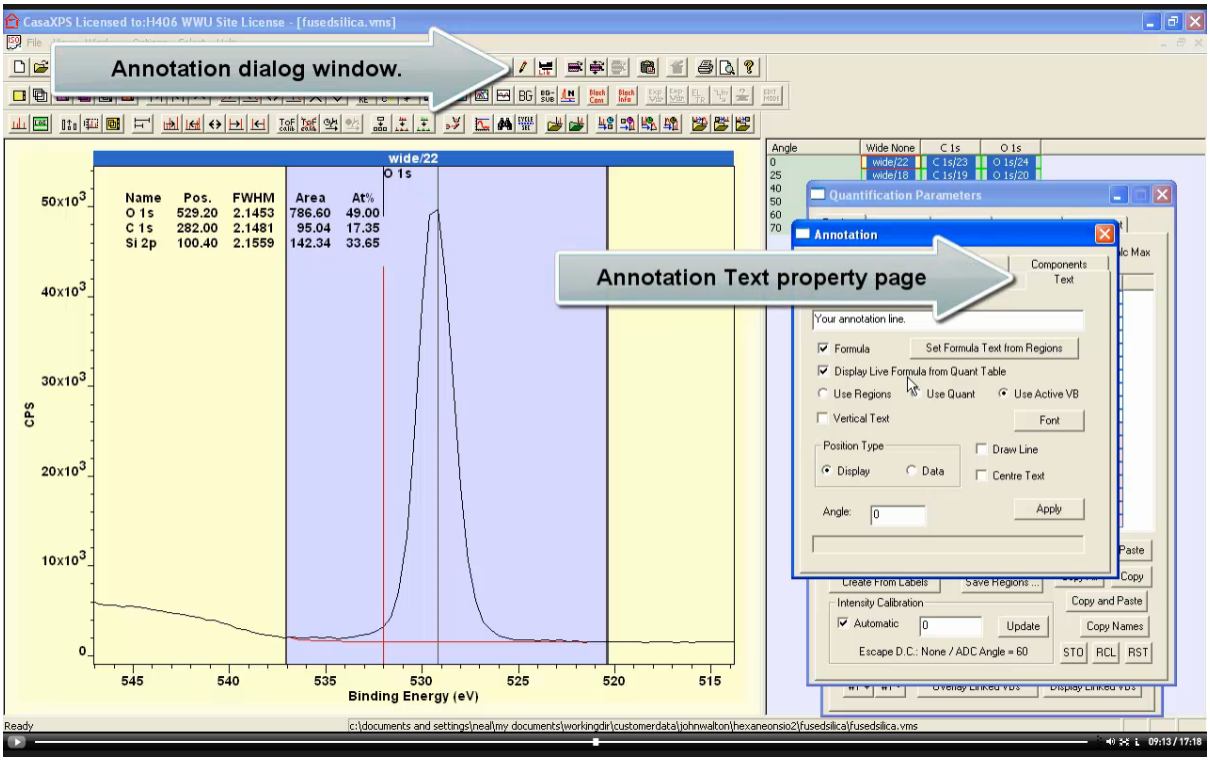

An alternative perspective to atomic concentration when viewing sample composition based on regions is the use of an option on the Annotation dialog window Text property page. The Formula option allows text to be displayed using subscripts and other formatting defined by expressions involving element symbols explicitly entered on the property page.

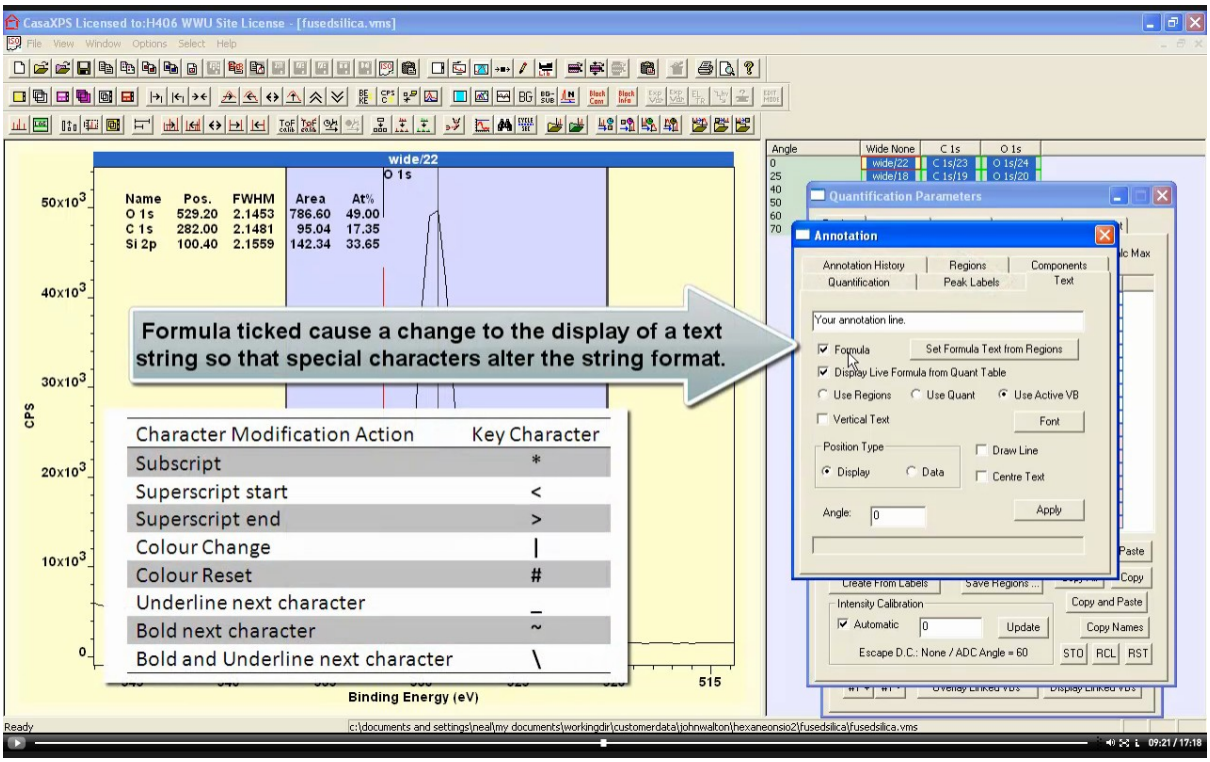

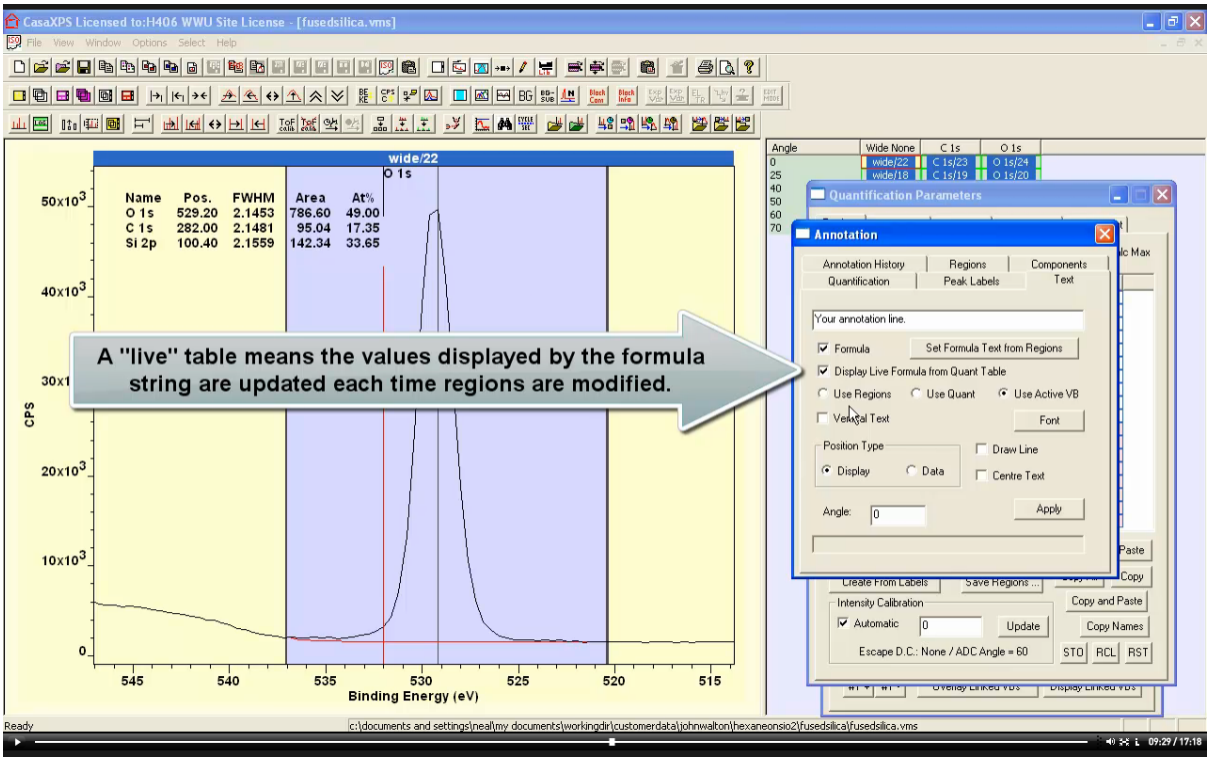

Formatting of elemental symbols is extended by the option labelled Display Live Formula from Quant Table. When active the annotation displayed over data is generated automatically from information gathered from quantification results.

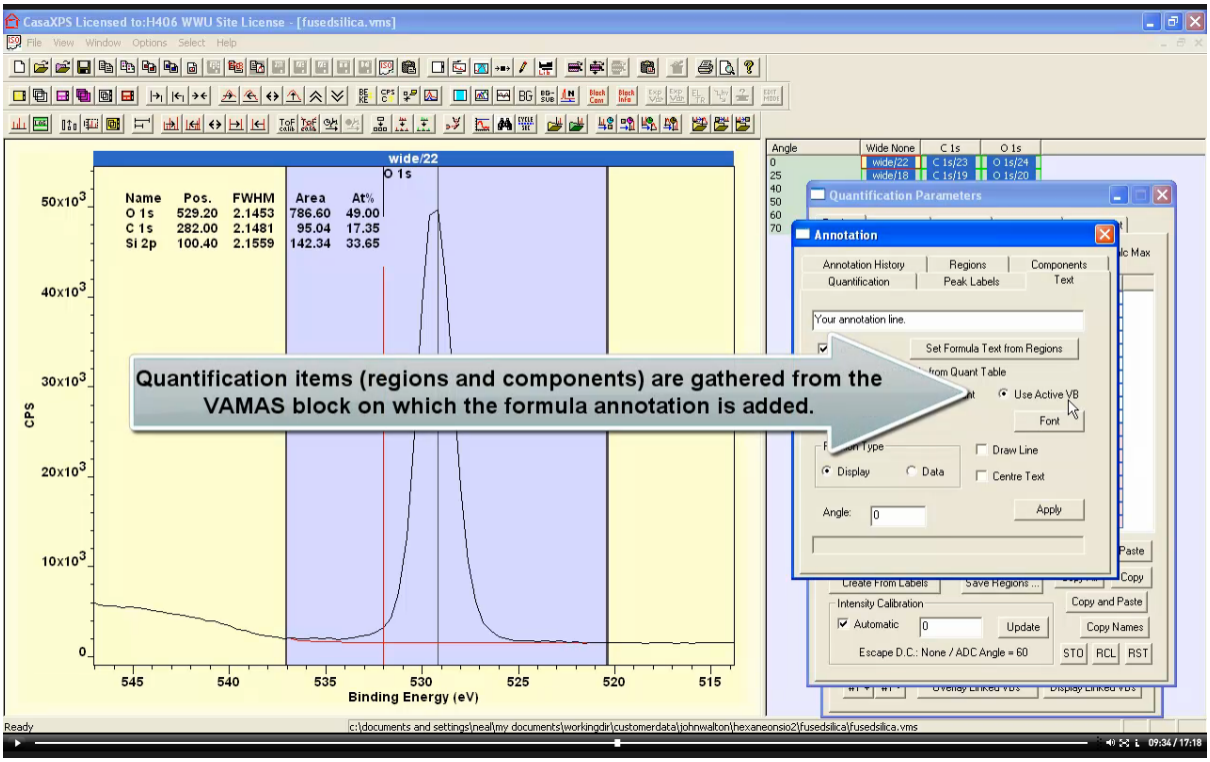

The most general form of quantification results derives from the selection made for VAMAS blocks in the right hand pane. Regions and components in a peak model are combined to create quantification tables. Both the Quantification Parameters dialog window Report Spec property page

and the Annotation dialog window Quantification property page display tabulated results based on selected VAMAS blocks in the right hand pane. There is however an option on the Annotation dialog window Text property page that allows quantification from only the active VAMAS block in the active display tile. The radio button labelled Use Active VB enables gathering of quantification results based on the Active VAMAS block displayed in the active display tile.

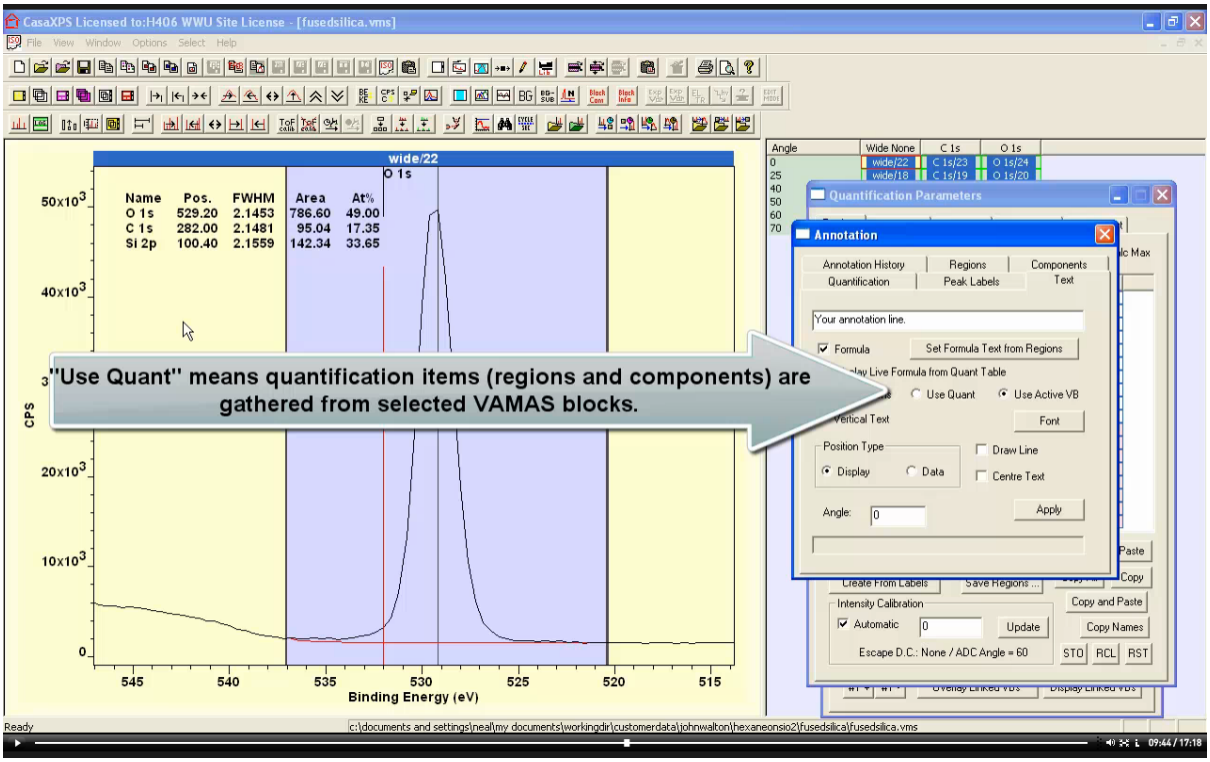

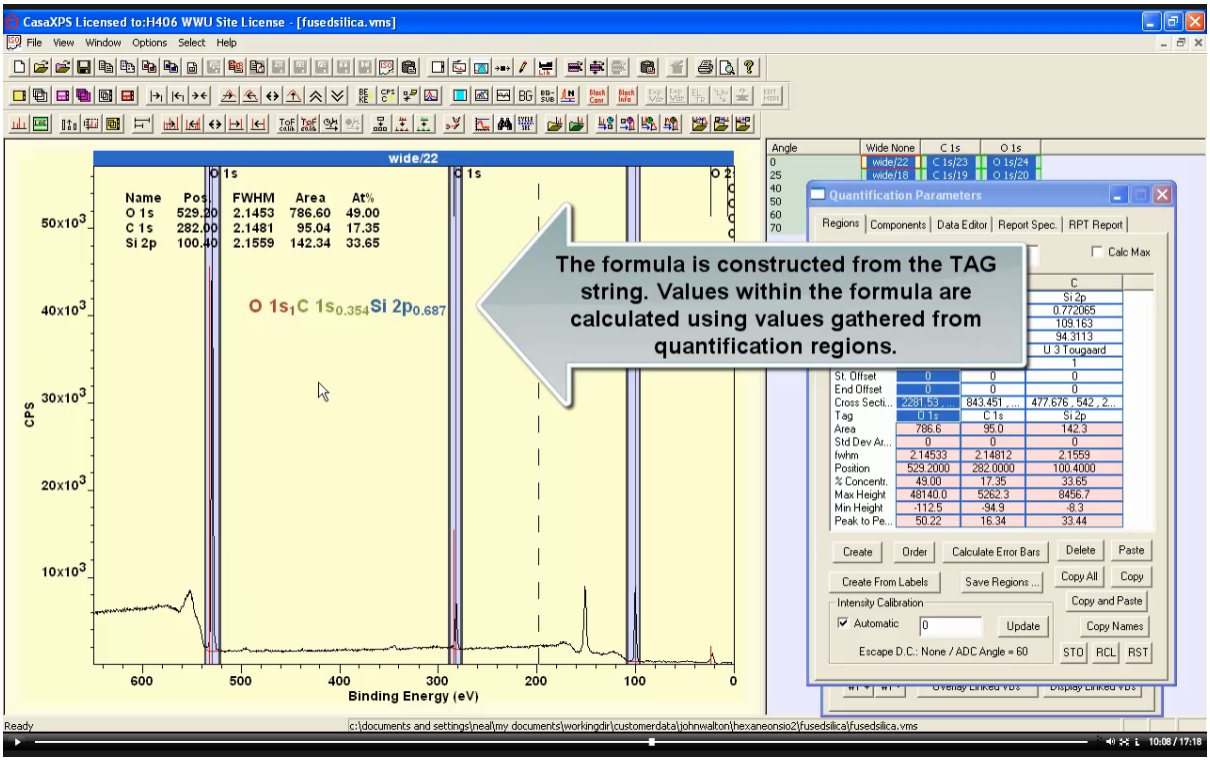

Text strings used to by formula based annotation text are the strings entered in the TAG fields for regions. TAG string and the use of * character allow changes to the order and numerical values associated with labels entered into the TAG field for each region.

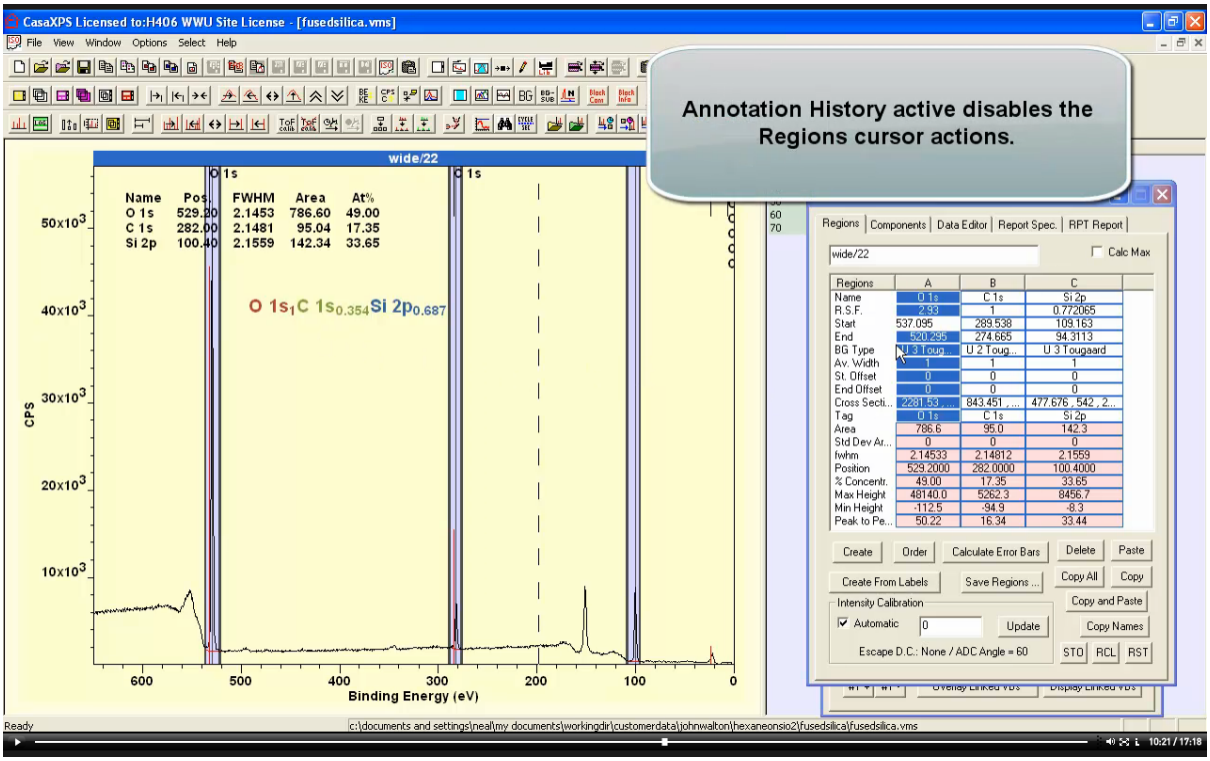

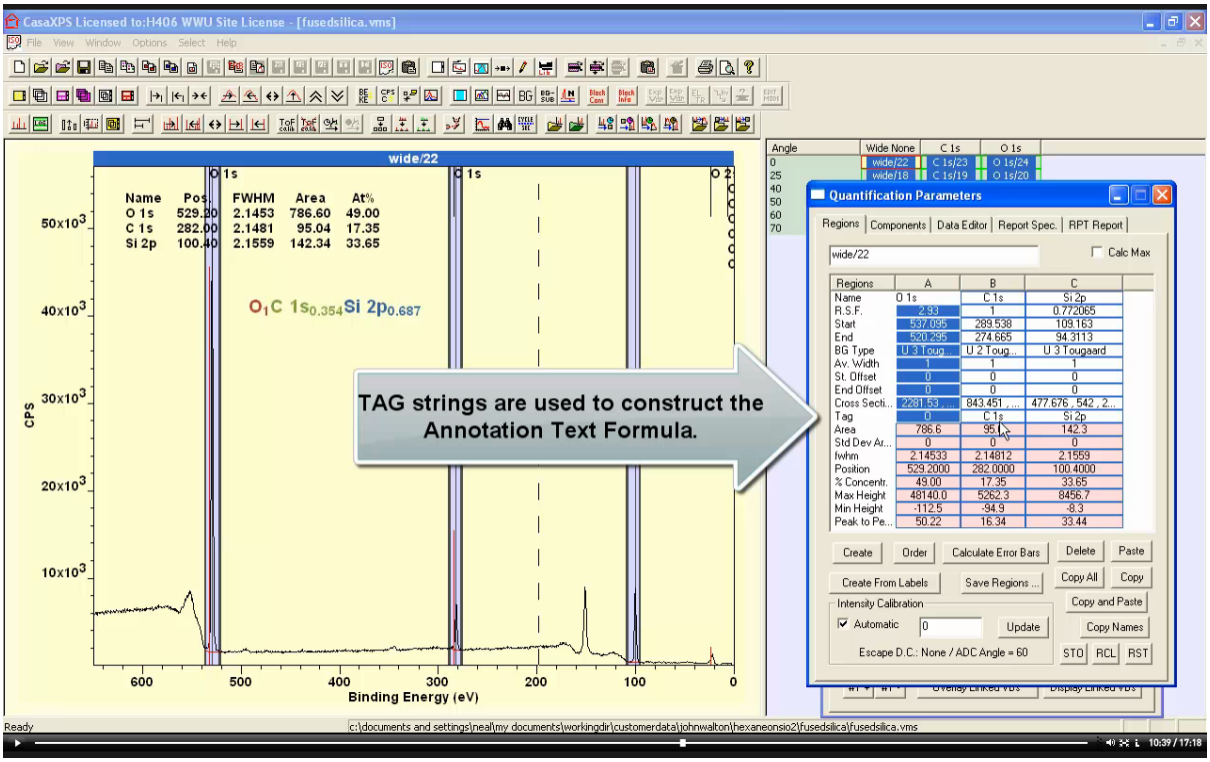

Initially the formula is constructed assuming O appears with a multiplicity of unity, hence the formula is constructed with O_1. If it is preferred to display the formula using the number of silicon atoms is indicated as unity then the TAG field for Si 2p can be adjusted by entering Si * 1.

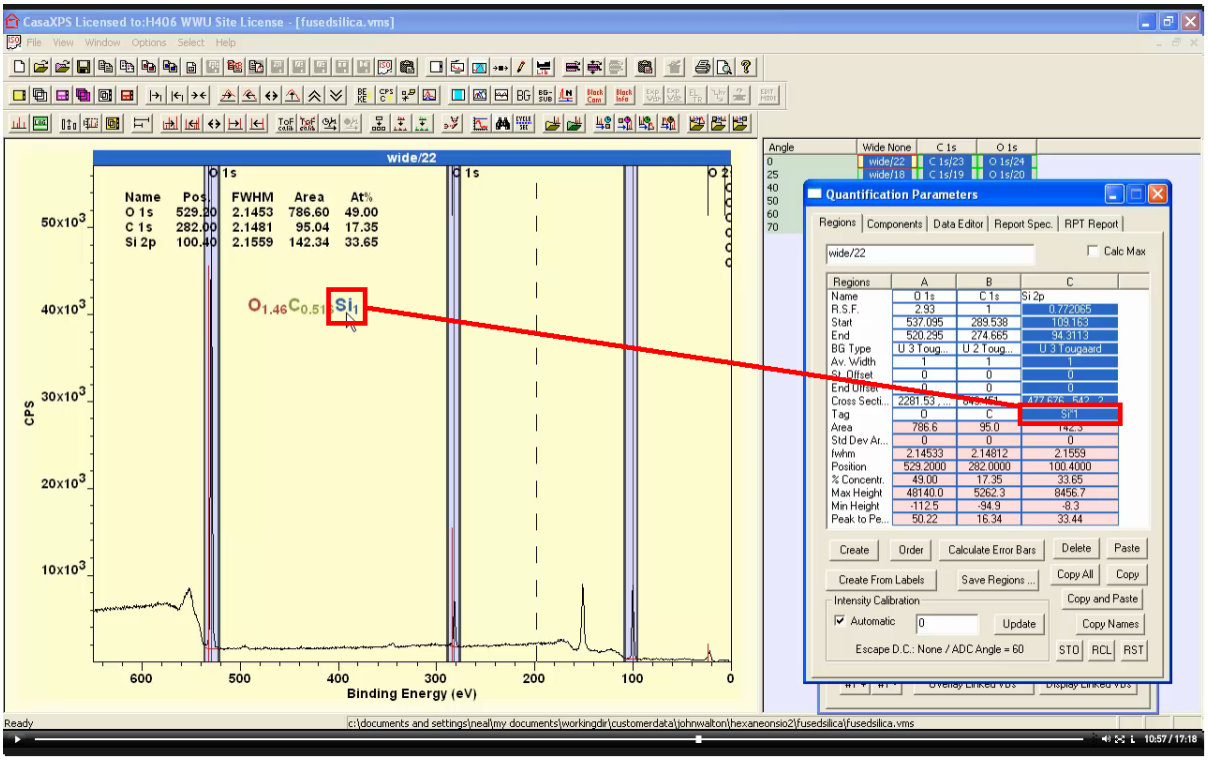

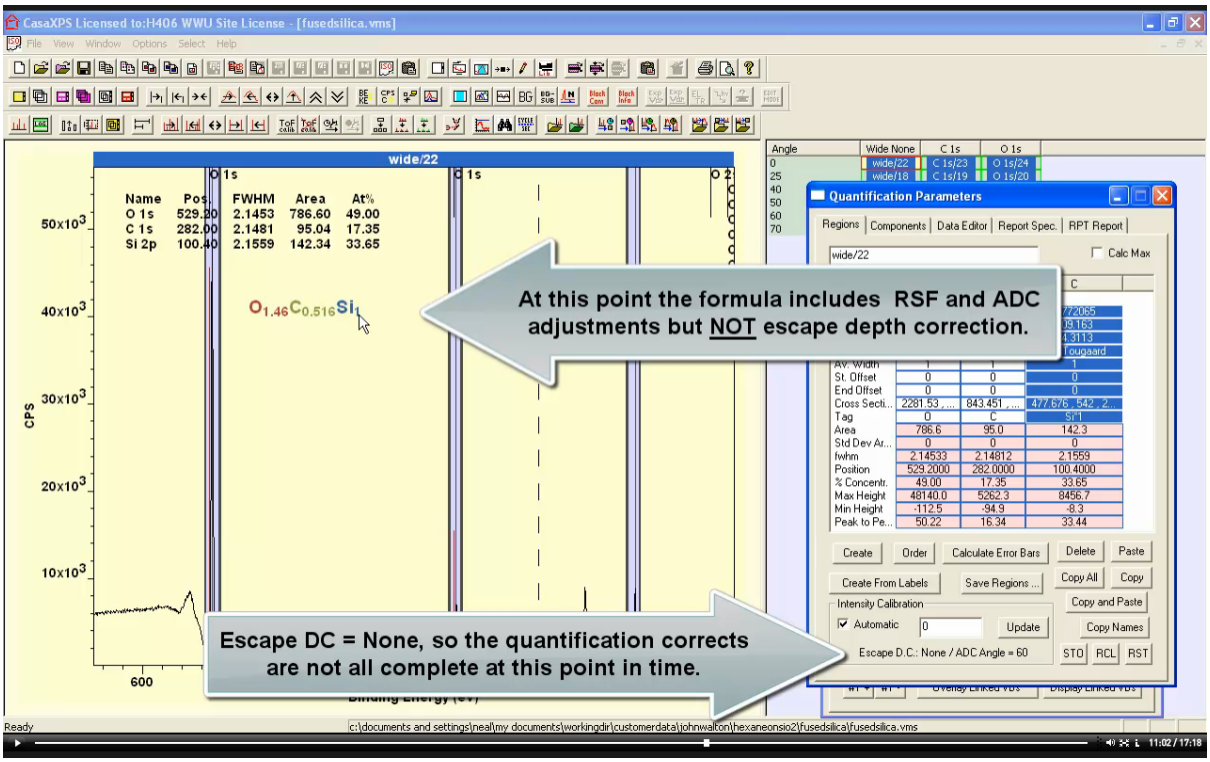

As indicated in the Regions property page Intensity Calibration section, the results so far include transmission correction, relative sensitivity corrected for angular distribution but not escape depth correction. Escape depth correction is an important part of quantification and without the correct adjustments for escape depth the correct stoichiometry of two oxygen and one silicon for silica is not returned.

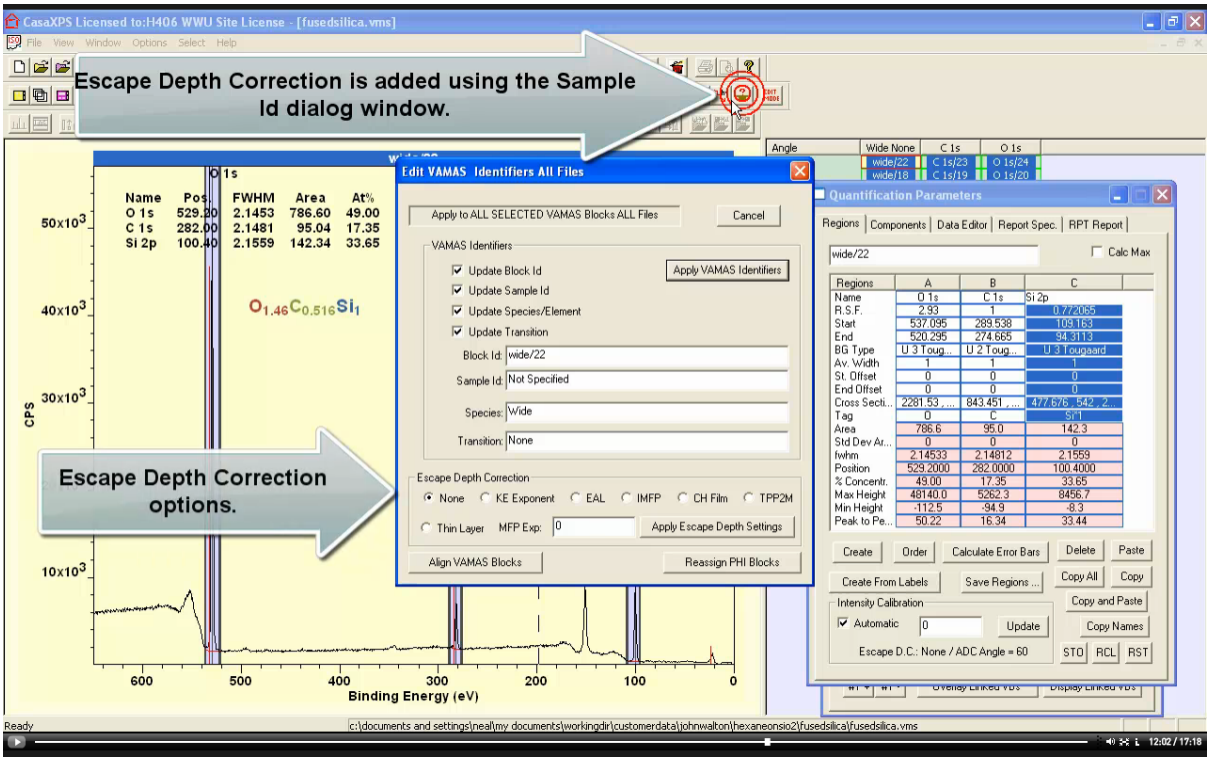

Escape depth correction is introduced via selecting VAMAS blocks in the right hand pane then invoking the Edit VAMAS Identifiers dialog window from the toolbar button. For fused silica it will be assumed the material is bulk in nature and therefore EAL (effective attenuation length) correction is appropriate.

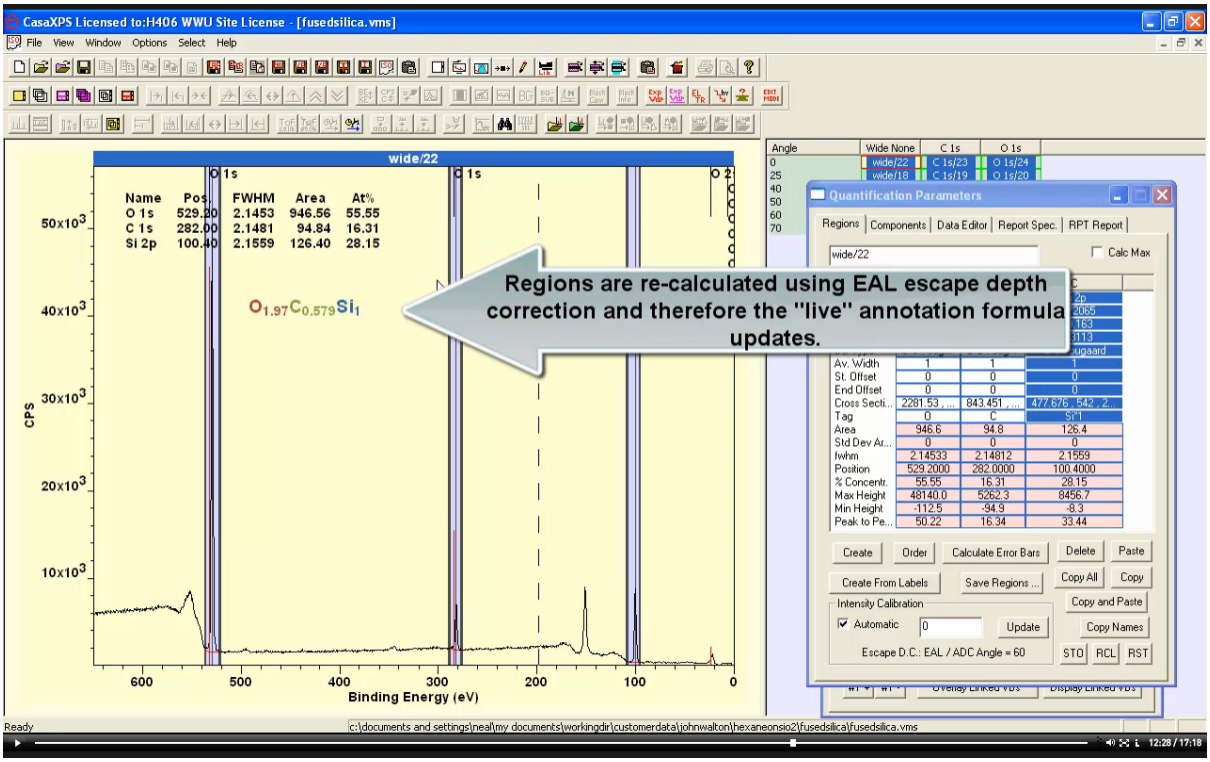

Since regions and annotation text are defined using data collected from quantification regions, once the EAL correction is applied both the atomic concentration table and text are updated.

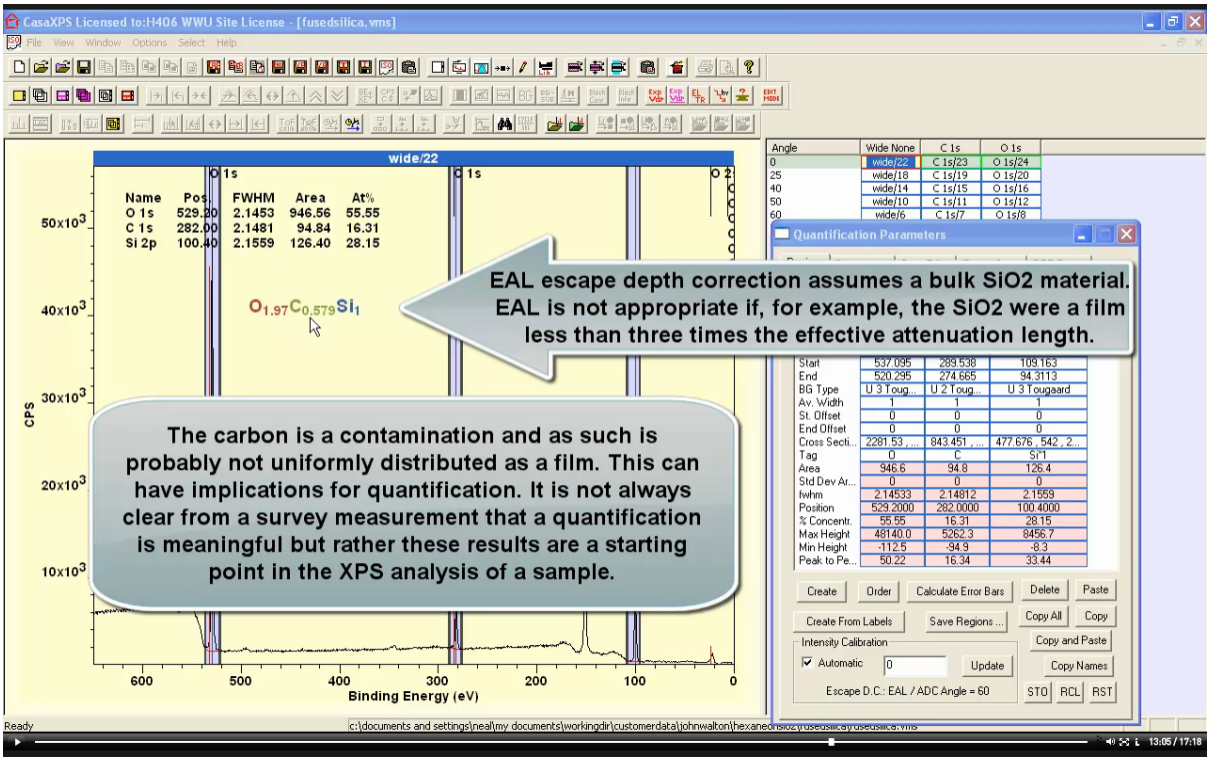

The expected ratio for silicon and oxygen is returned for these data. It should be noted that survey data can be misleading when quantified in isolation. For example the carbon contamination may also include carbon bonded to oxygen so one might expect more oxygen than silicon given the amount of carbon measured by XPS. An alternative argument might be made where it is assumed the contamination by carbon is not uniformly spread over the fused silica but appears as islands of thickness about 10nm. If islands of carbon exist then silicon signal from beneath the contamination would be attenuated less than O 1s signal so one might conceive as scenario where silicon appears more intense than oxygen. It is also possible elemental silicon is involved and this too could shift the composition measure by XPS towards silicon. High energy resolution spectra for Si 2p would remove this possibility.

These fused silica data represented a control experiment for a set of samples prepared with films of plasma polymerised hexane (ppHex) on SiO_2. These samples of interest to the paper by Walton et al also provide some insight into the influence of escape depth on general quantification by XPS. By considering how these quantification steps applied to fused silica, when applied to samples with known films alter quantification for a substrate of similar composition to fused silica, it is clear quantification of samples of less well defined origin requires careful consideration.

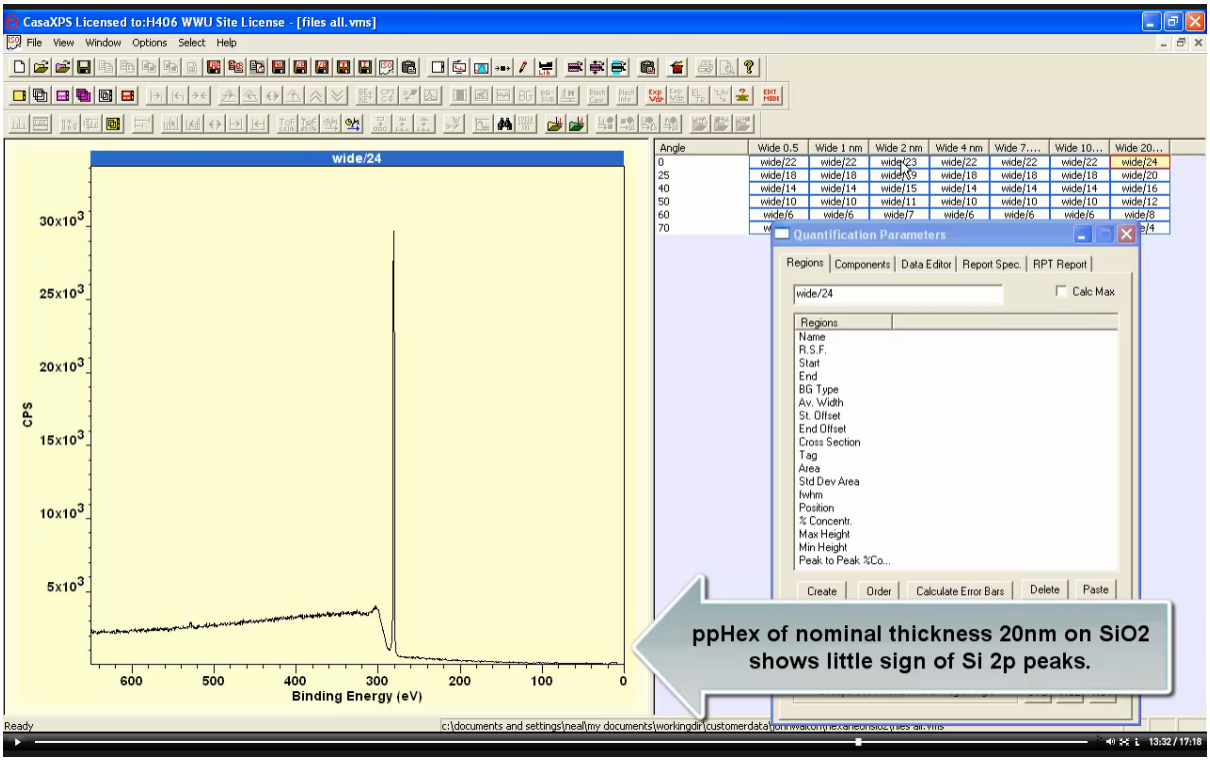

A thick film of ppHex greater than the sampling depth for Si 2p and O 1s the influence of SiO_2 substrate on XPS data is only visible in shapes observed in the inelastic scattered background. That is to say, almost all electrons from Si 2p and O 1s undergo energy loss events therefore these photoemission peaks are absent from the spectrum.

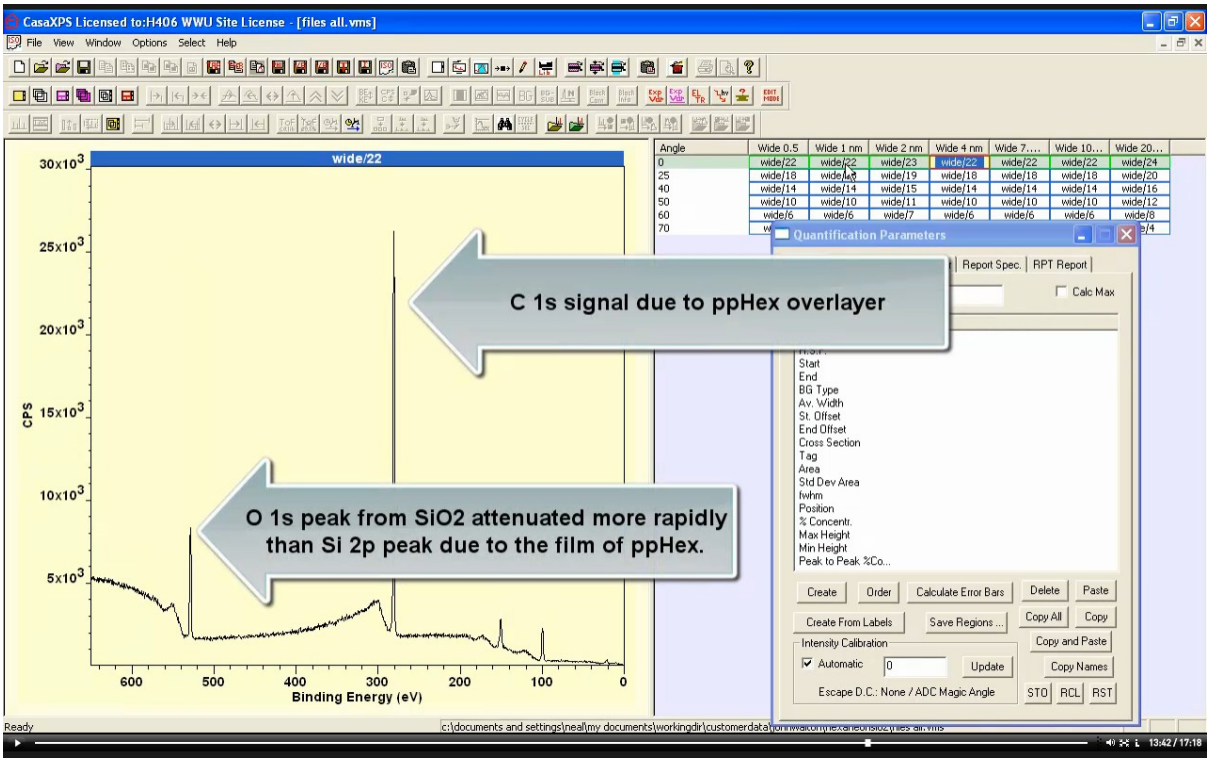

A sample prepared with ppHex depth less than the sampling depth for Si 2p and O 1s electrons, peaks are evident within the spectrum and background shapes indicate an overlayer that does not contain silica.

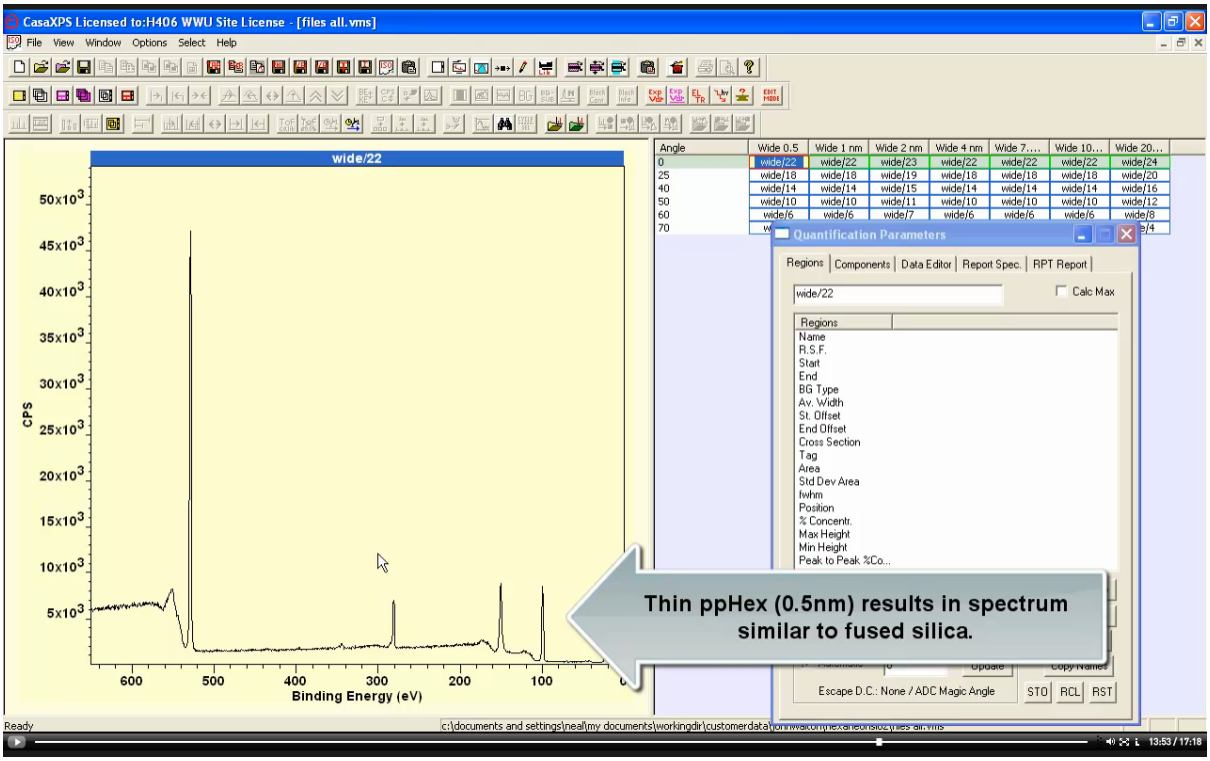

For very thin ppHex on SiO_2 it is difficult by-eye to see the difference from as received fused silica.

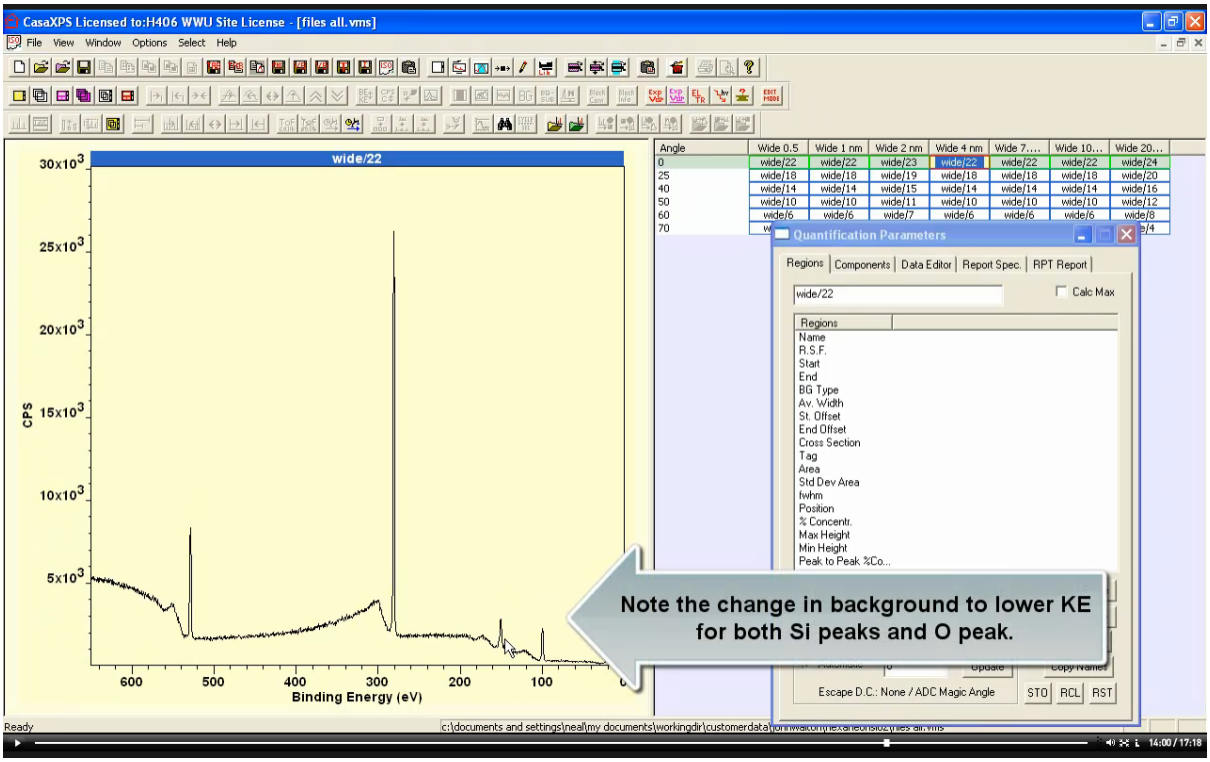

Note how the background to the C 1s overlay of ppHex is very different from background to lower kinetic energy for Si 2p and O 1s photoemission.

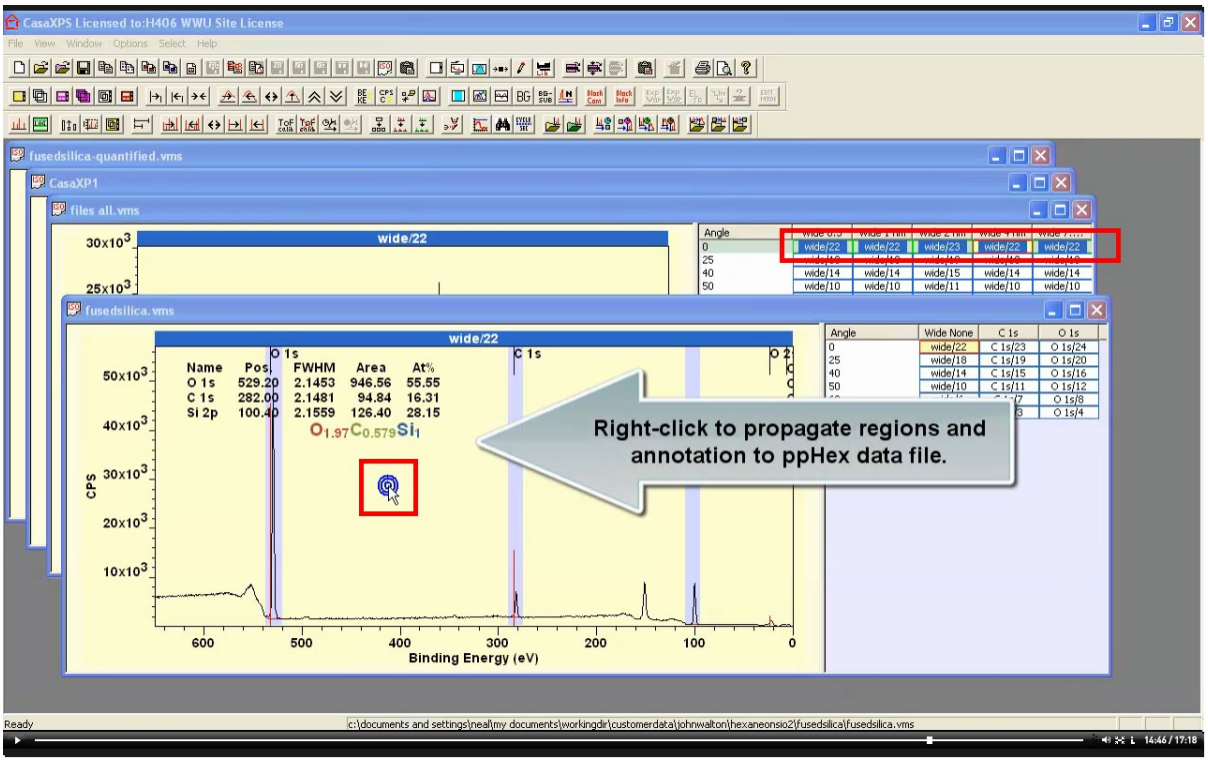

Regions and annotation previously defined for the fused silica VAMAS block are transferred to the ppHex spectra making use of the Browser Operations dialog window.

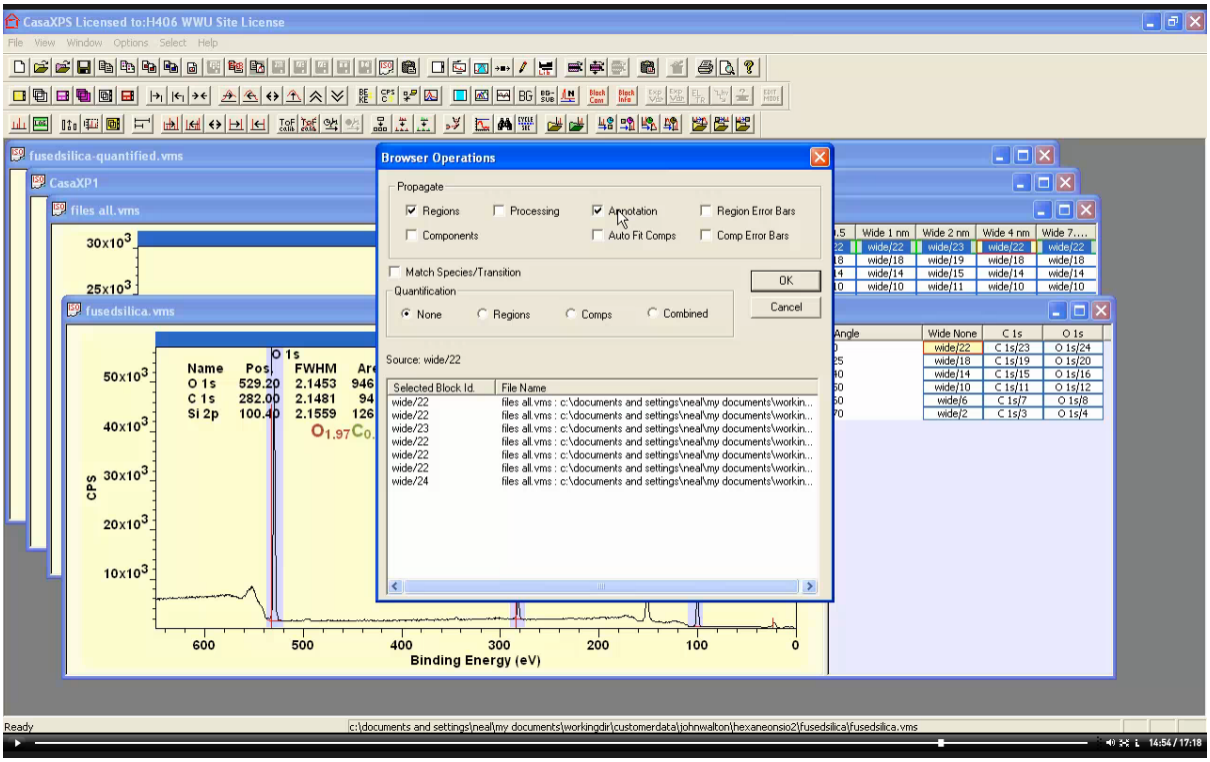

VAMAS blocks selected in the right hand pane receive regions and annotation from data displayed in the active tile.

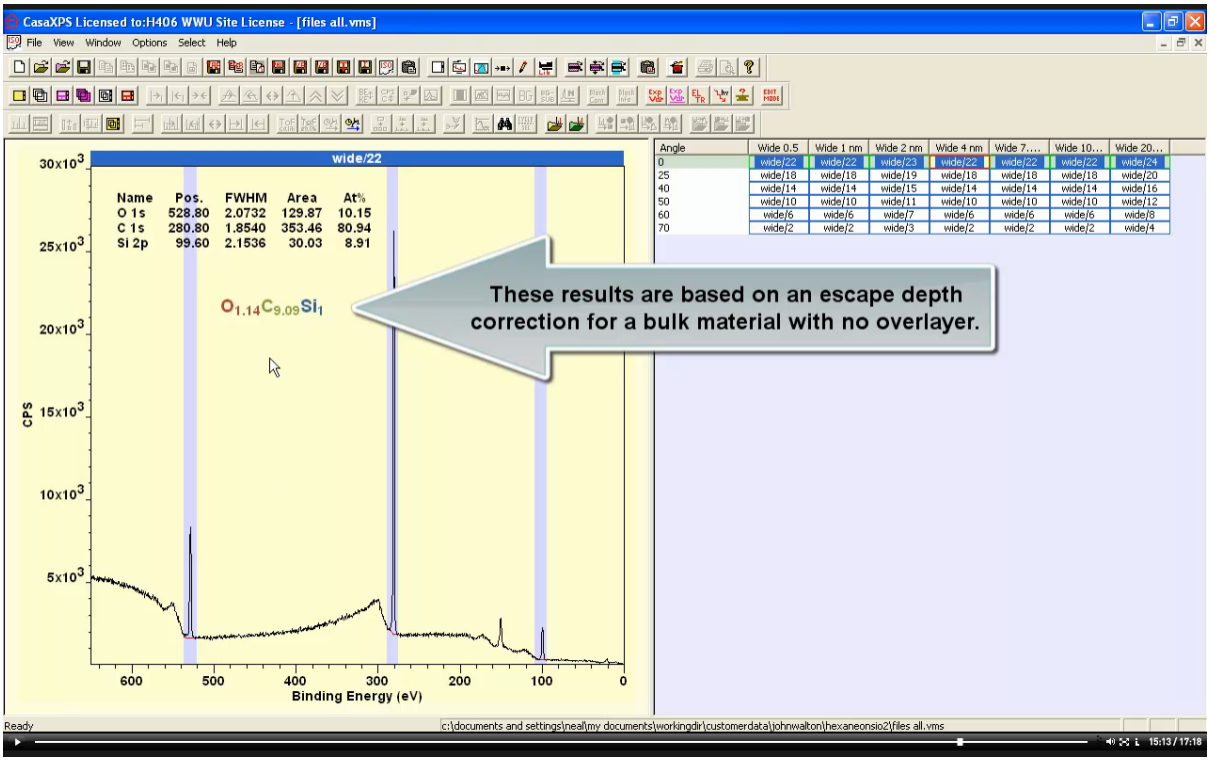

Quantification propagated from fused silica includes all the intensity corrections used to quantify fused silica. Therefore these ppHex samples are quantified making an assumption that is false, namely, the samples are homogeneous in lateral and depth distribution.

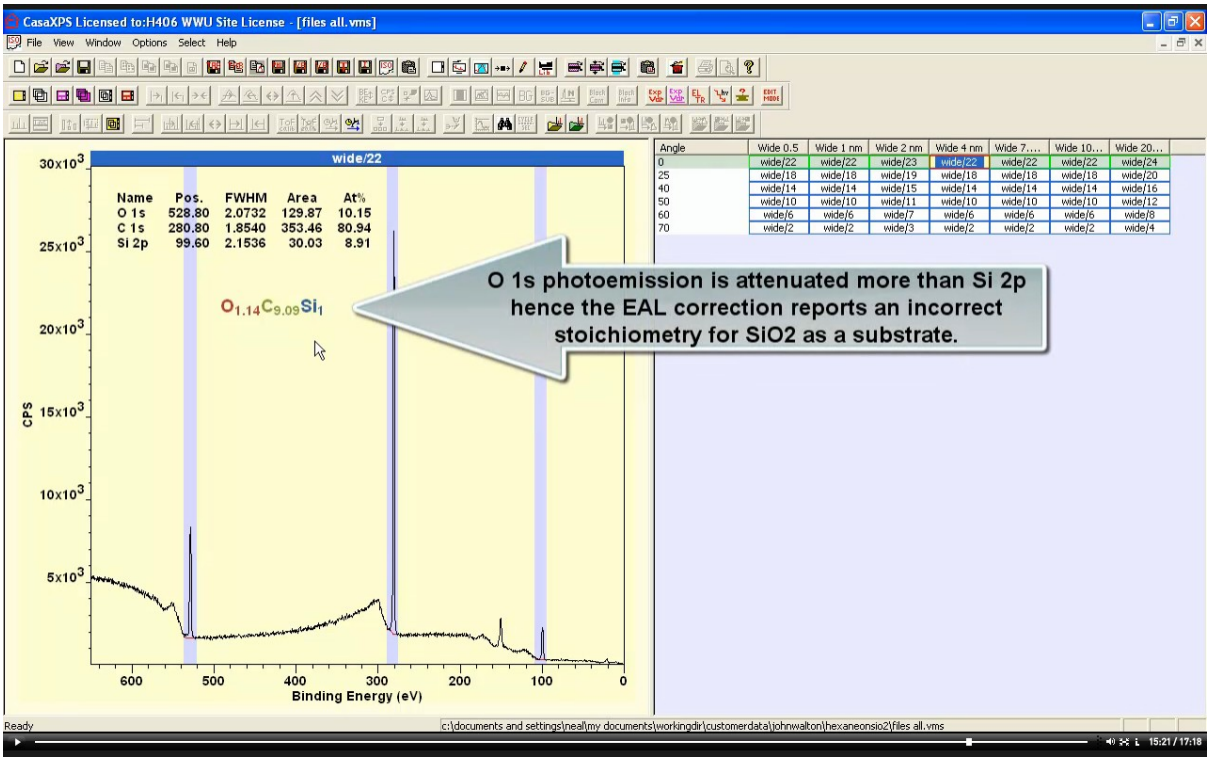

Since these ppHex samples are layers of ppHex on silicon dioxide when the ratio of oxygen to silicon is reported by the annotation the expected ratio for silicon and oxygen is not achieved.

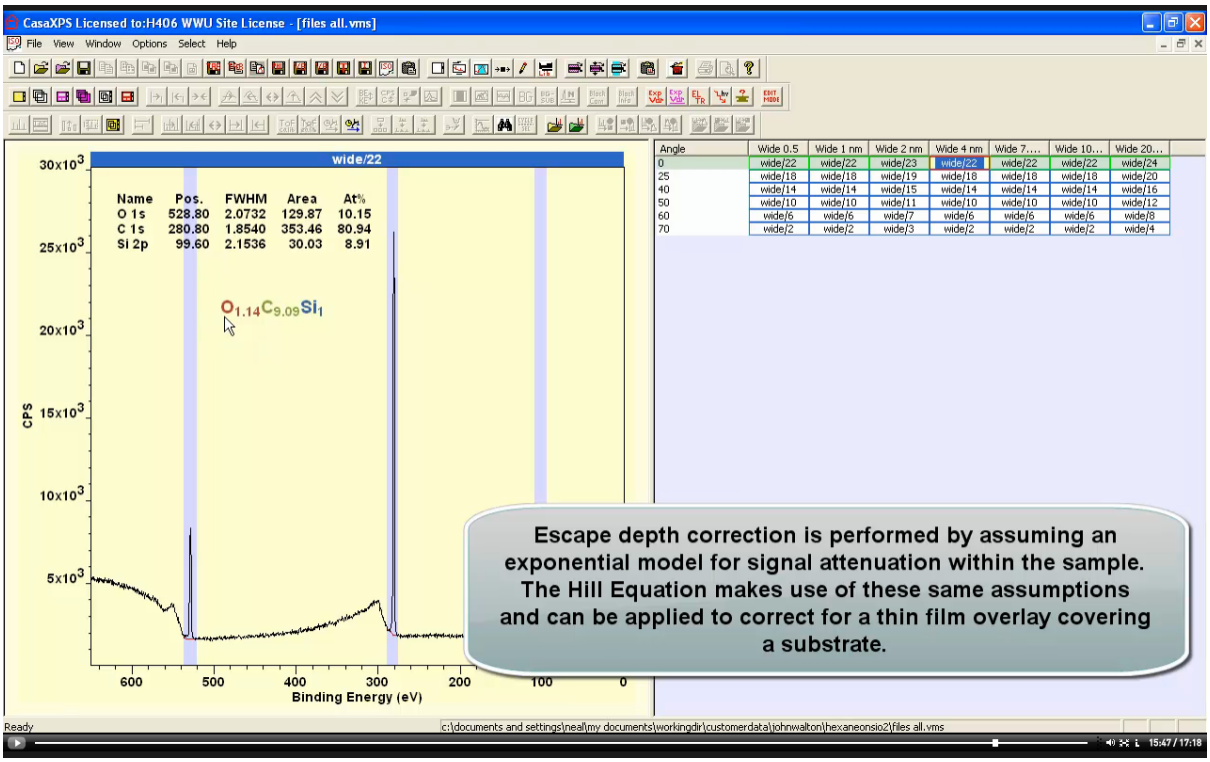

There is an option for correcting a substrate signal for an overlayer. The overlayer ppHex is a CH film so correcting signal from the SiO_2 substrate provides a measure for the film thickness of ppHex.

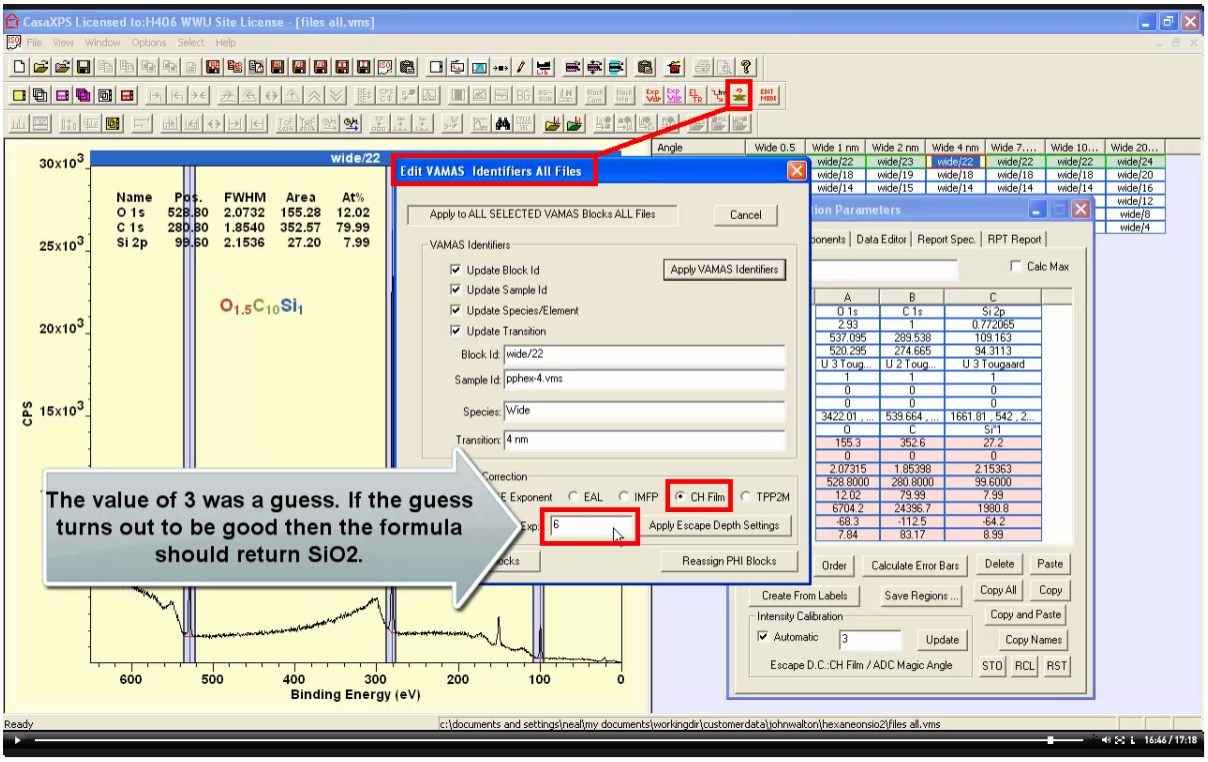

The value entered for the overlayer thickness is based on attenuation assuming an exponential attenuation model. It should be noted that after making such a correction the signal from the overlayer, namely, C 1s is no longer correct as shown in these tables and annotation text.

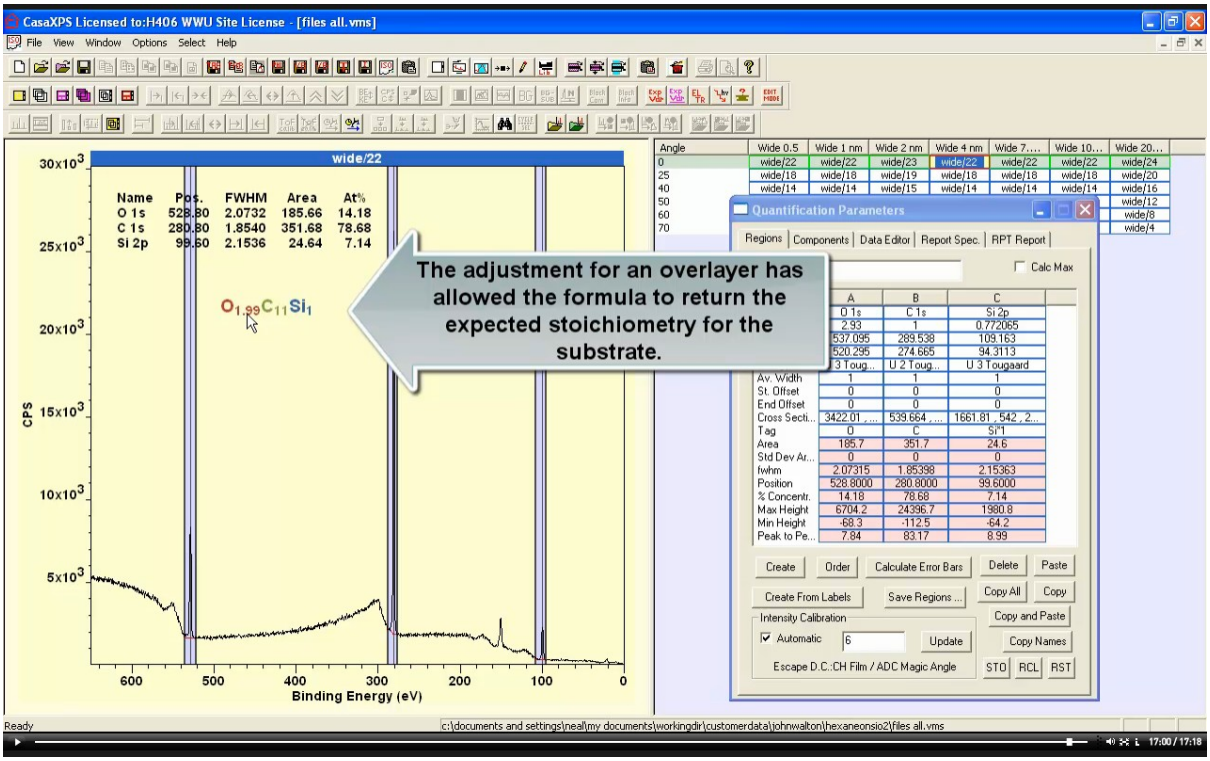

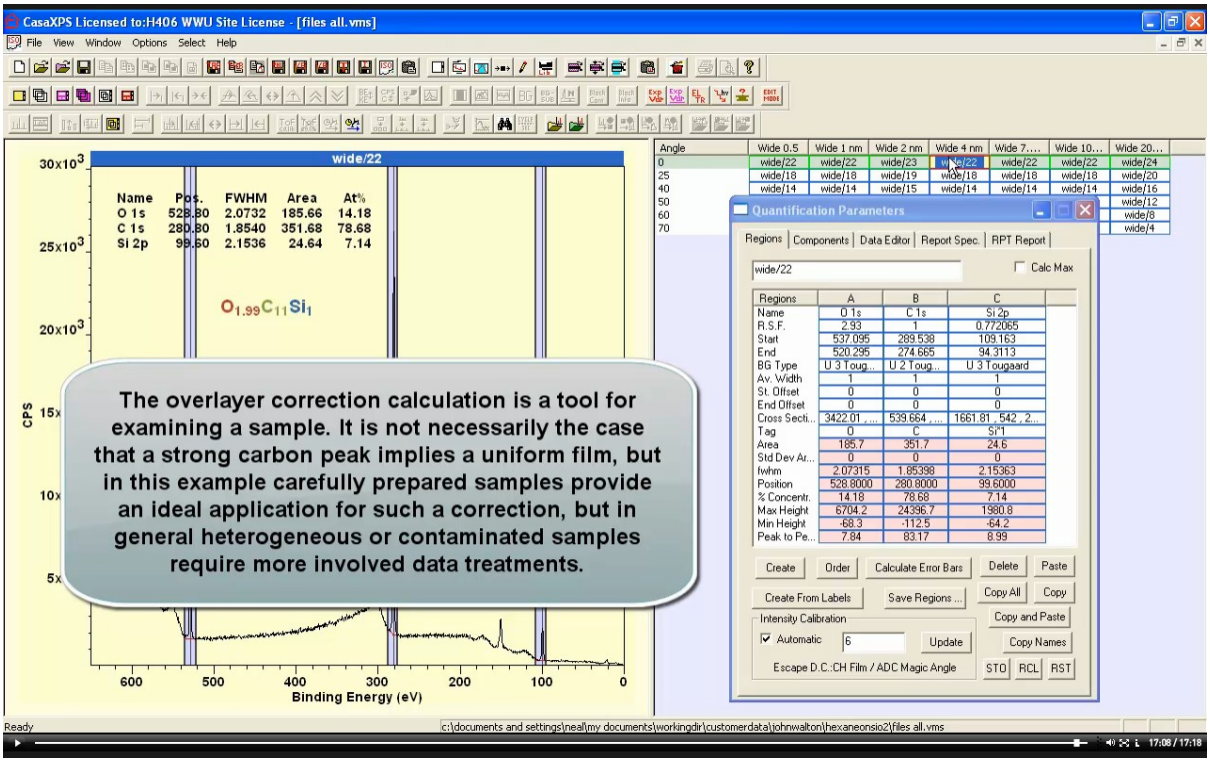

Creating Peak Models: Quantification Parameters Dialog Window Components Property Page

Within in the video a peak model is created based on a spectrum for N 1s photoemission from a sample formed from a mixture of two ionic liquids of known composition. This spectrum is one of eleven N 1s spectra measured from a set of ionic liquid samples representing mixtures of these two well defined ionic liquids and represent a data set for which it can be shown how parameter constraints are created and how these parameter constraints influence optimisation outcomes when fitting components to data.

Structures for a) $[C_8C_1im]$ $[Tf_2N]$ and b) $[C_4C_1Pyrr]$ $[Tf_2N]$ used in the mixtures experiments and ionic liquid samples on the Kratos sample bar, left-right 1) 100% $[C_8C_1im]$ $[Tf_2N]$ and mixtures increasing towards 11) 100% $[C_4C_1Pyrr]$ $[Tf_2N]$

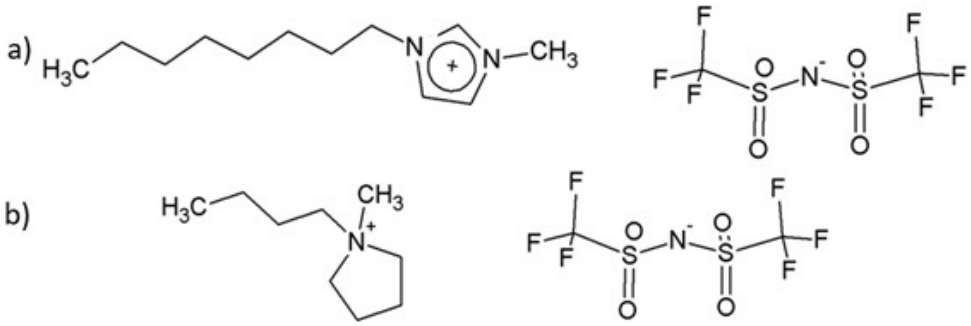

A peak model is constructed using the Quantification Parameters dialog window. The Regions property page is used to define a background required to remove the influence of inelastic scattering and other energy loss processes not attributed to photoemission from N 1s electrons.

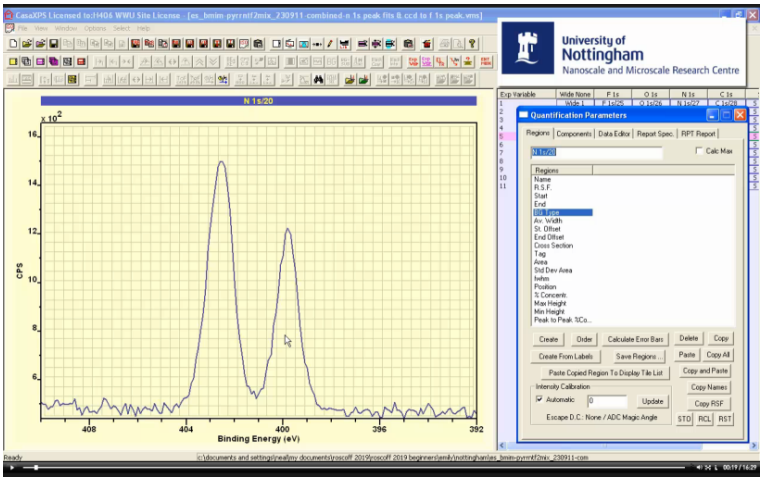

The basic forms for backgrounds include linear, Shirley and Tougaard Universal Cross-section. Many other background approximations are available, but for these data where the background is flat

beneath these N 1s photoemission peaks the selection of background type is not as important because all three basic background types turn out similarly flat.

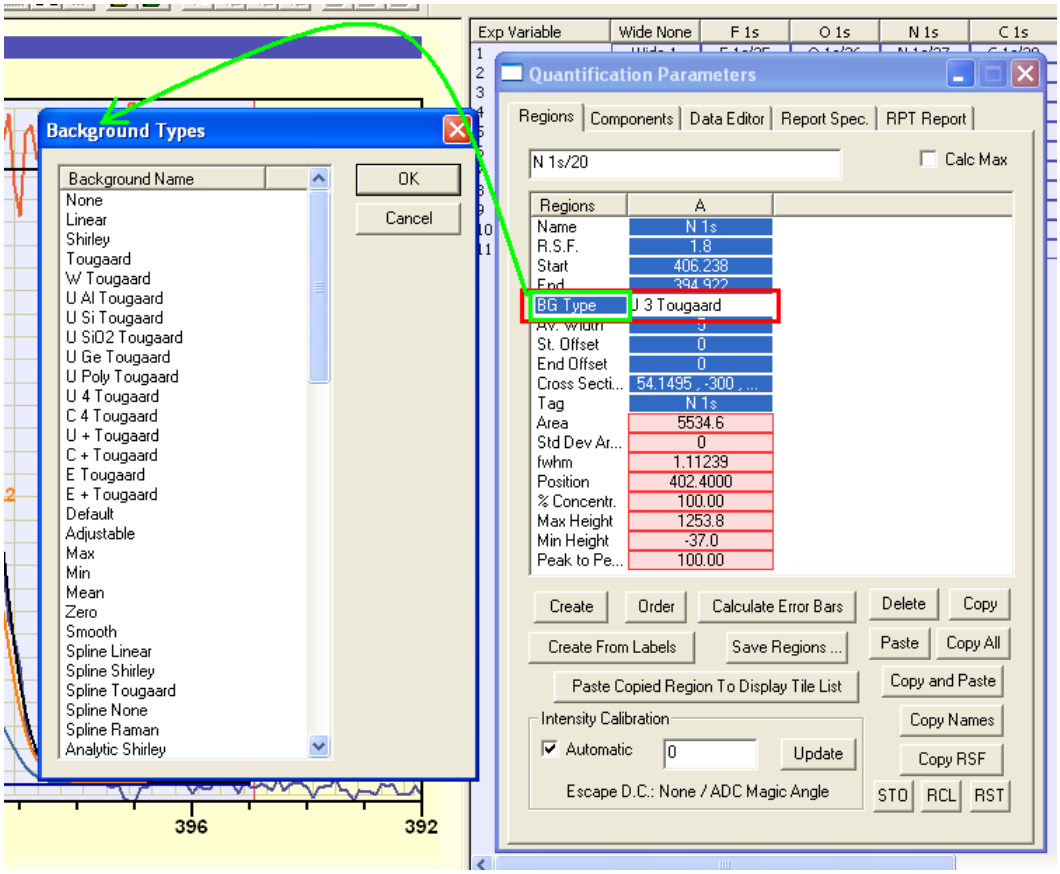

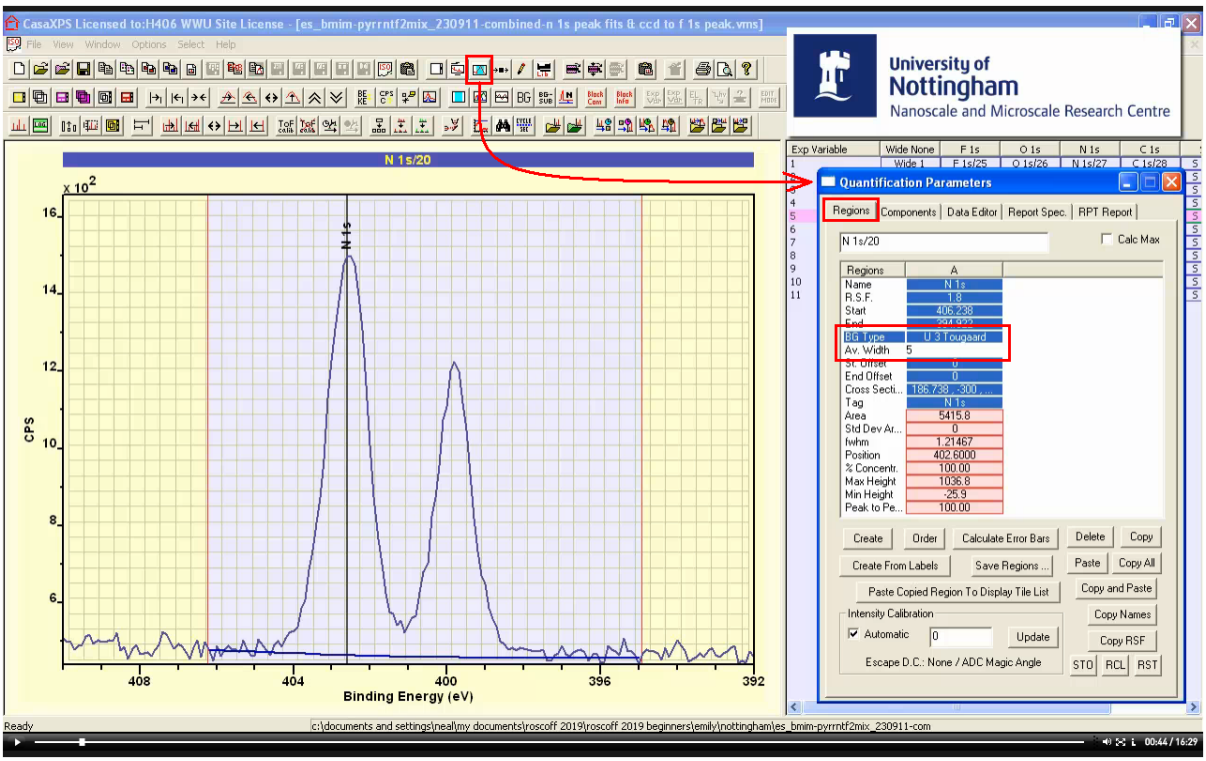

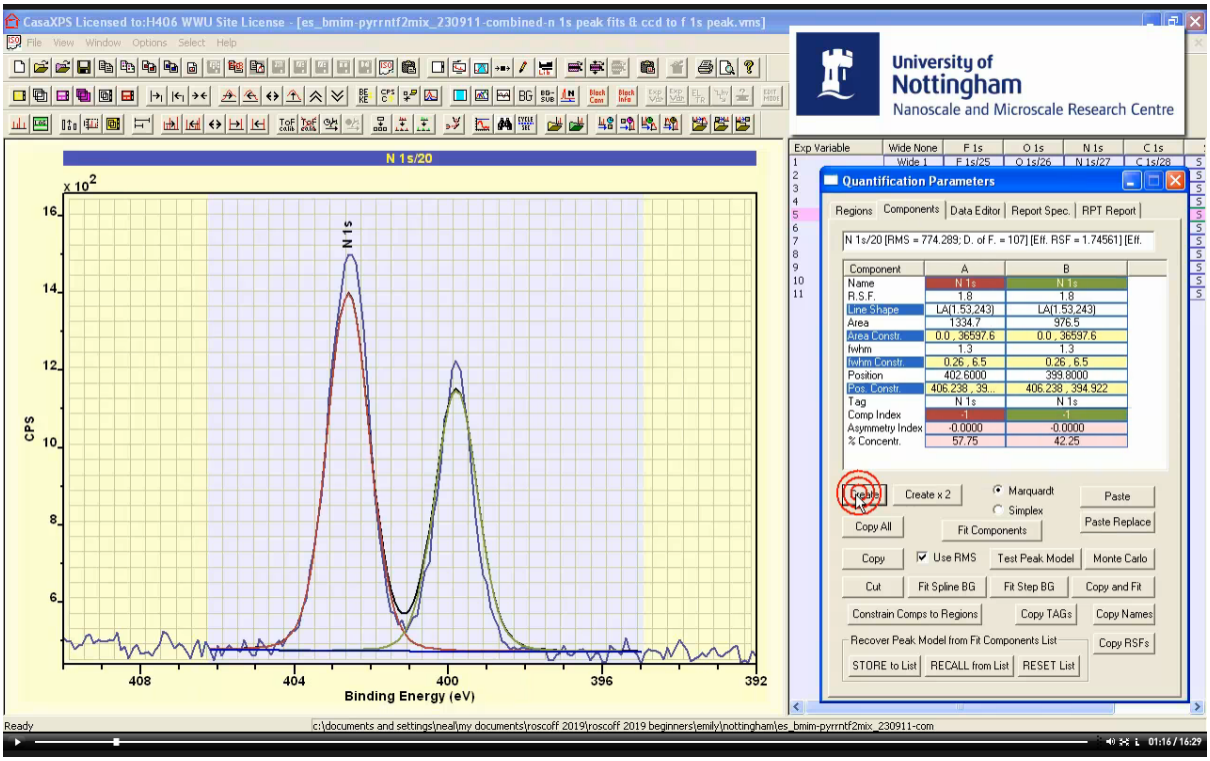

Component peaks are added to a peak model by pressing the Create button on the Components property page. Each new component is added to the list of components as a column of parameters. At the top of each column of component parameters is an alphabetic label. These labels are used to specify constraints between components. Component constraints are illustrated during the video.

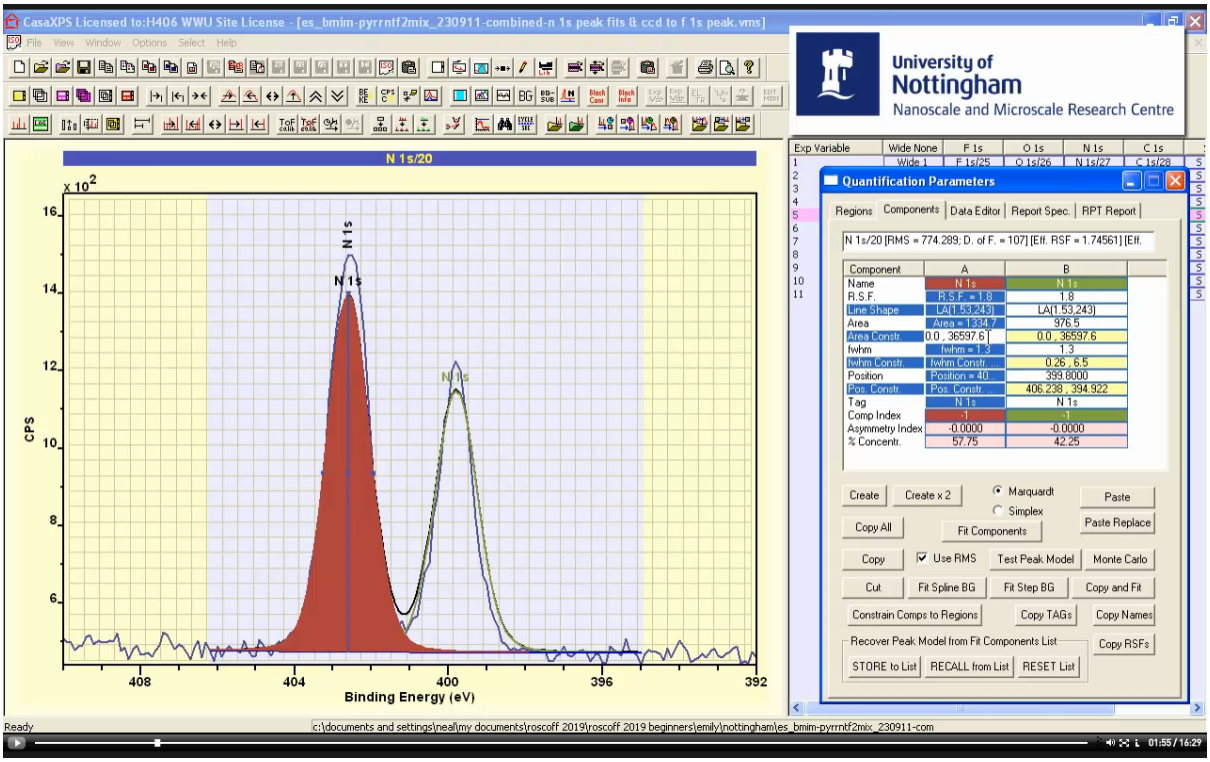

Component peaks are fitted to data by adjusting fitting parameters (Area, FWHM and Position) within intervals for these parameters defined in the corresponding constraints text-field.

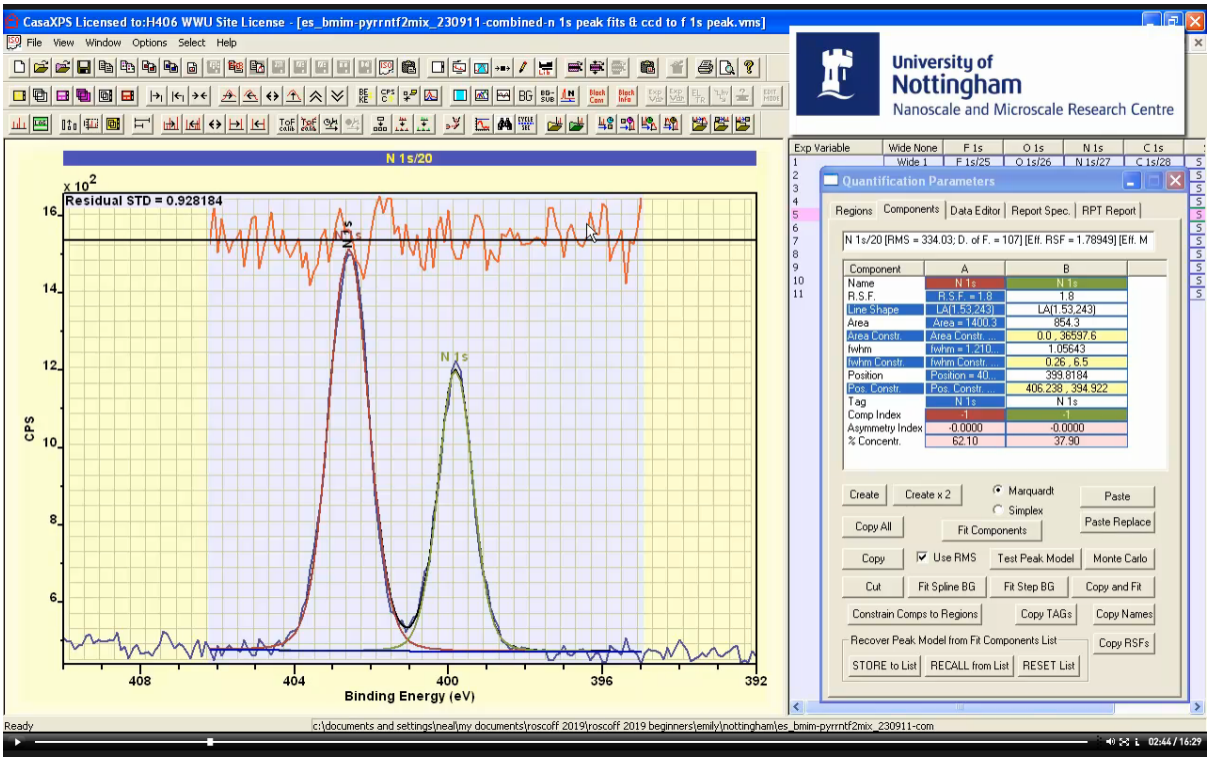

Component peaks are fitted to data in the active display tile by pressing the Fit Components button on the Components property page. Fitting of components to data is also performed by giving focus to the display tile with the use of a left-mouse click within the display tile and then holding down the Control keyboard key before pressing the G key (Ctrl+G).

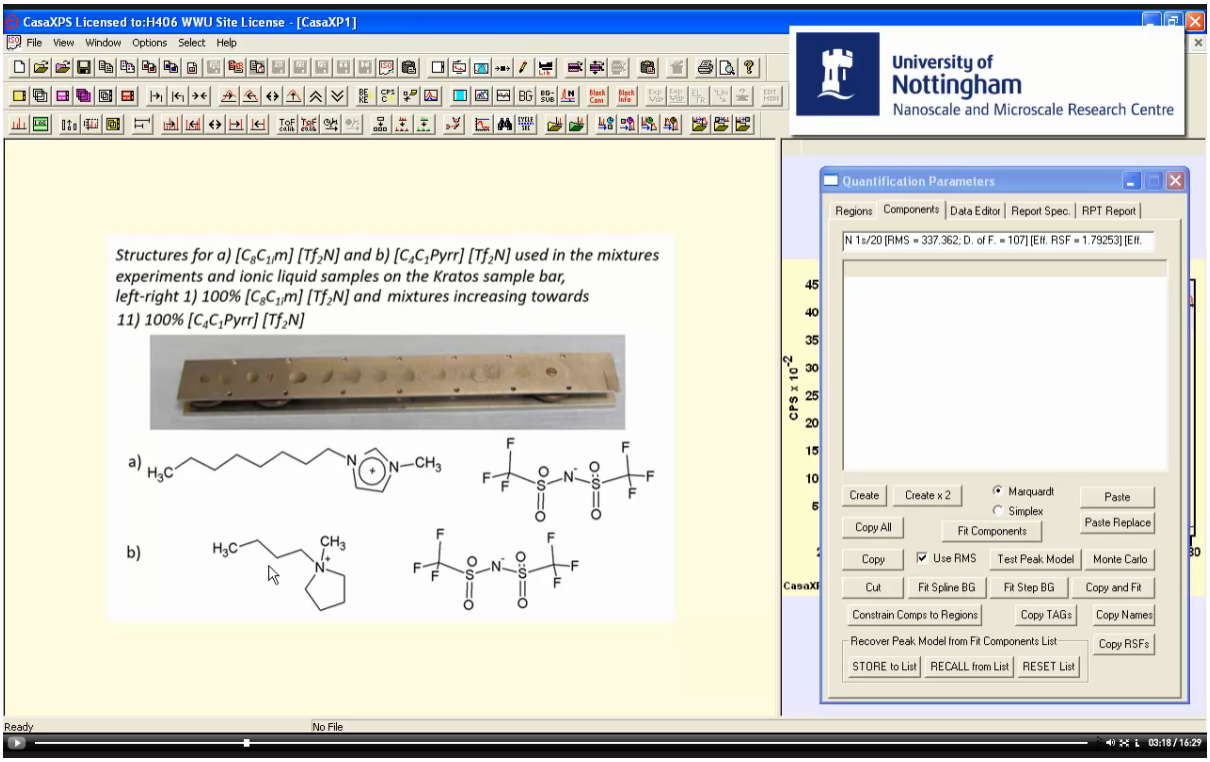

Given that these samples are prepared by mixing two ionic liquids with a common negative ion but different positive ions the number and relative intensities for component peaks should differ from the two peaks currently used to reproduce data from a mixture spectrum.

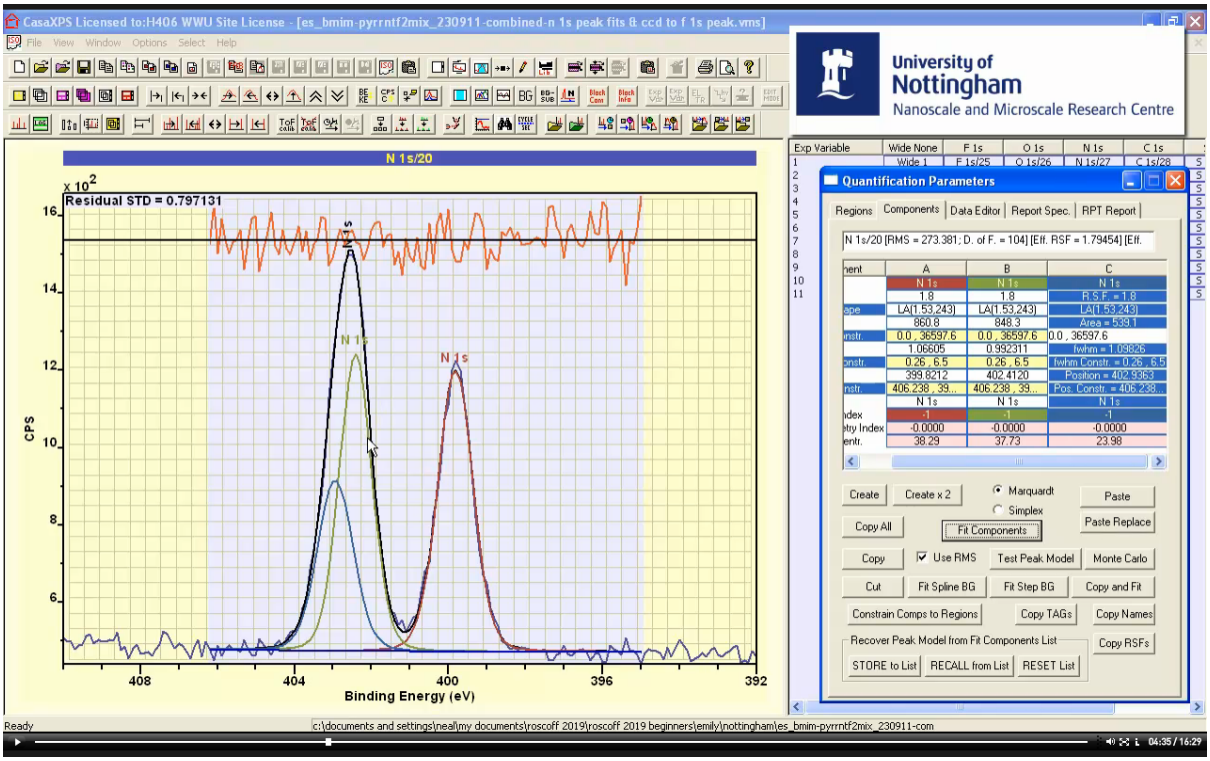

Adding more component peaks allows constraints to reflect the expected stoichiometry for these ionic liquid samples.

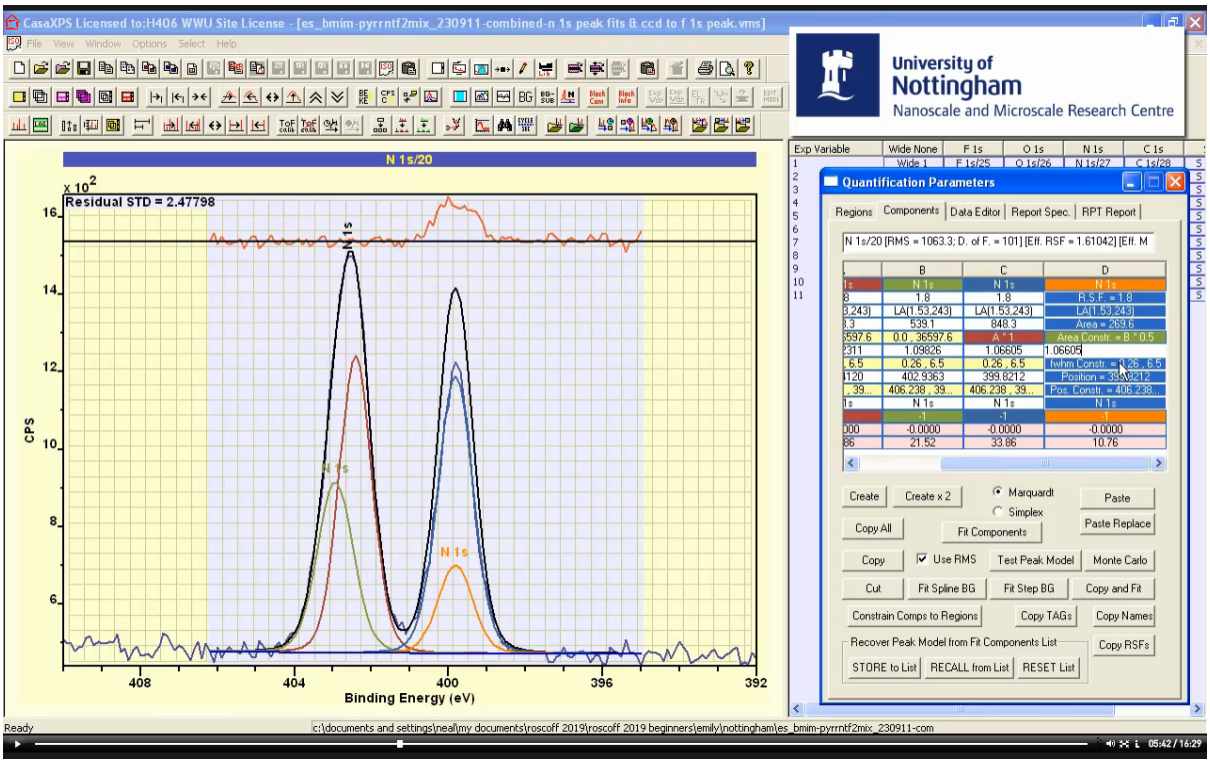

It is expected that two peaks are required for the positive ion contribution to N 1s spectra. It might also be possible to consider signal deriving from negative ions is accounted for by making use of two components provided these two components are linked in FWHM and Position to be identical for both components. Two perfectly correlated peaks would be of little value unless area constraints are also used to force a relationship between negative and positive ions.

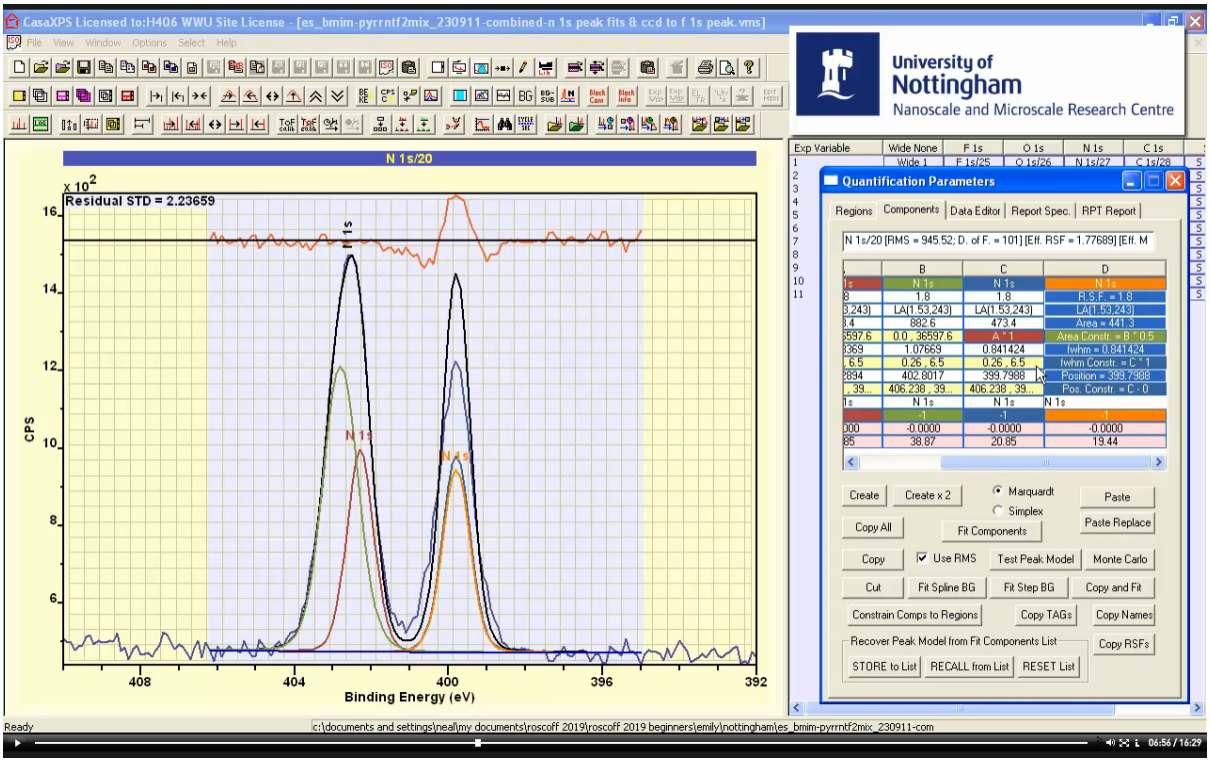

The negative ion N 1s peaks in Column C and Column D are constrained to have identical FWHM and Position by entering into the FWHM constraint field within Column D the string “C * 1” and in the Position constraint field “C + 0”. These two peaks represent all photoemission from negative ions but allowing two area parameters for the same signal permits intensity from two different positive ions to scale the area for these negative ion peaks to be consistent with the two pure forms for the ionic liquids from which these mixtures were formed. While the use of two component peaks for negative ion signal would appear to increase the number of fitting parameters, introducing Area constraints of the form “A*1” and “B*0.5” together with constraining the FWHM and Position parameters reduces the freedom from potentially six fitting parameters for negative ion signal down to two fitting parameters for the combined FWHM and Position for negative ion signal.

Component	A	B	C	D
Name	N 1s IL1	N 1s IL2	N 1s IL1	N 1s IL2
R.S.F.	1.8	1.8	1.8	1.8
Line Shape	LA(1.53,243)	LA(1.53,243)	LA(1.53,243)	LA(1.53,243)
Area	345.3	1040.0	345.3	520.0
Area Constr.	0.0 , 36597.6	0.0 , 36597.6	A * 1	B * 0.5
fwhm	1.08556	1.05761	1.07236	1.07236
fwhm Constr.	0.26 , 6.5	0.26 , 6.5	0.26 , 6.5	C * 1
Position	403.0141	402.4732	399.8226	399.8226
Pos. Constr.	406.238 , 394.922	406.238 , 394.922	406.238 , 394.922	C - 0
Tag	N 1s	N 1s	N 1s	N 1s
Comp Index	-1	-1	-1	-1
Asymmetry Index	-0.0000	-0.0000	-0.0000	-0.0000
% Concentr.	15.34	46.21	15.34	23.11

These constraints are introduced based on sample knowledge. Introducing these constraints represents user bias as we assume these ionic liquids once mixed can be considered as unaltered from the ionic composition for the two pure forms of these liquids.

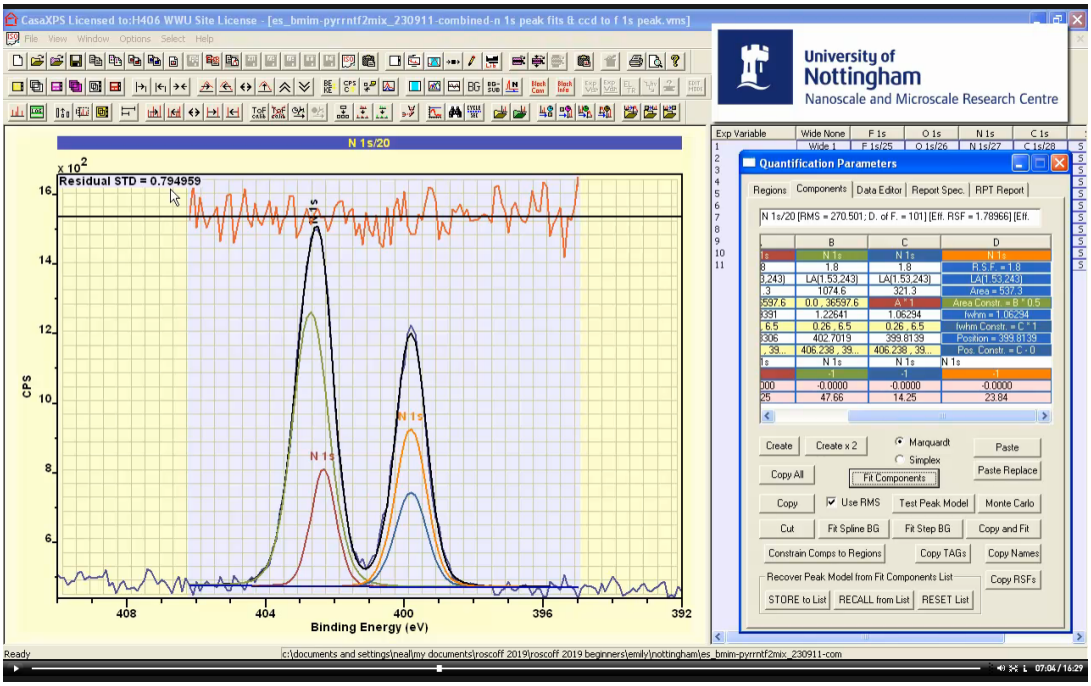

Parameter constraints thus far link negative ion intensity with corresponding positive ion intensity is accordance with the expected relationship for the two pure forms of ionic liquids mixed to create the sample from which these N 1s data are acquired. The two negative ion components are linked via a Position constraint, but to this point the pair of positive ion components may adjust independently of each other in terms of Position and FWHM parameters. Two highly correlated components with freedom to move in binding energy and component width should be a cause for concern.

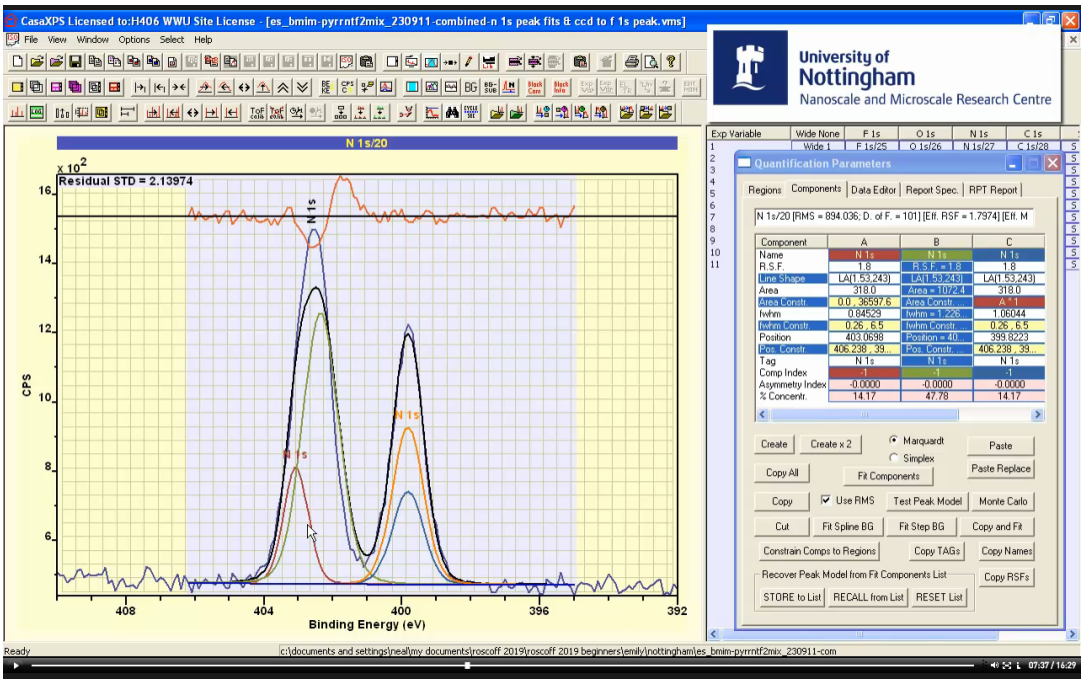

Adjusting the starting conditions for the peak model from the previous optimisation sequence allows us to test if a simple adjustment can produce a fit for these peaks to data with similar quality of fit but for which physically significant information changes to the point of negating the conclusion drawn from the previous fit to the same data.

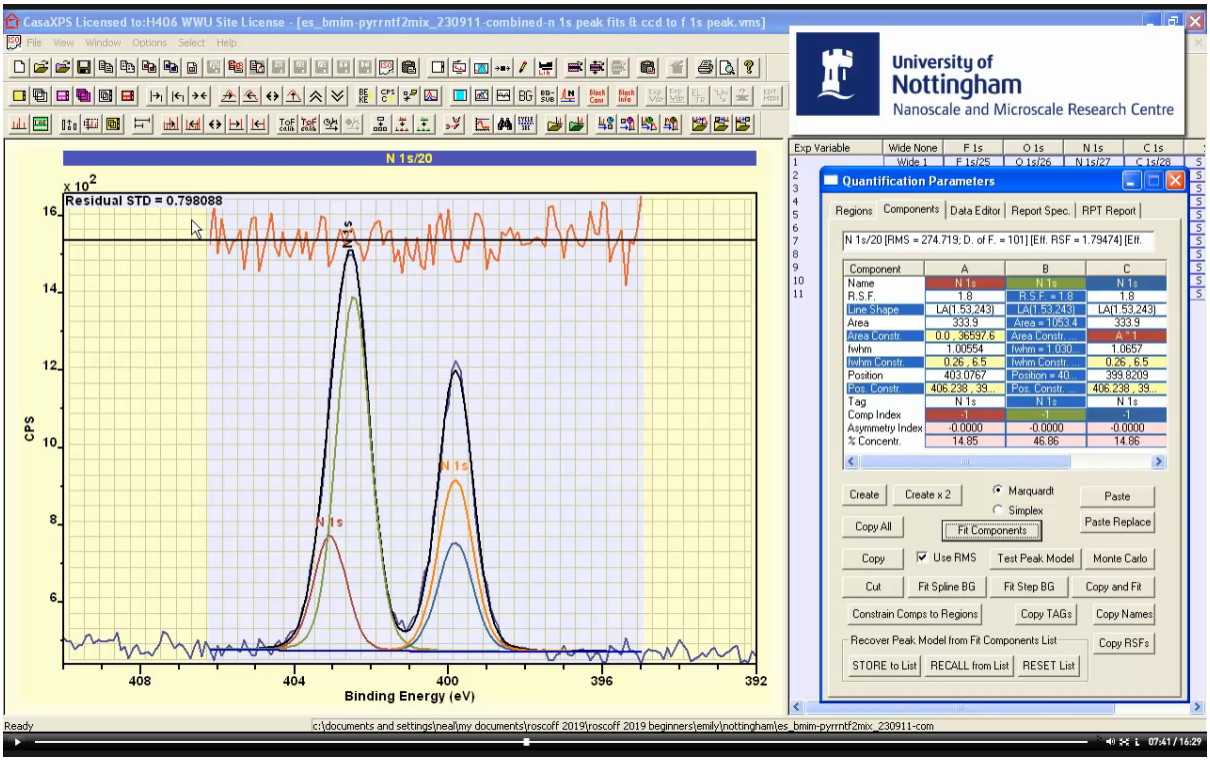

On fitting these same peaks using a different starting position for these two components representative of positive ion signal yields a similar quality of fit as measured by the residual standard deviation, but importantly for the analysis so far, the binding energy for these component peaks is reversed without altering the relative intensity of these components. Two different starting conditions for optimisation produce similar residual standard deviation but the outcome in terms of binding energy is very different. Such a test indicates the peak model, meaning number of peaks and constraints linking fitting parameters, is not capable of separating signal from positive ions for this particular mixture of ionic liquids.

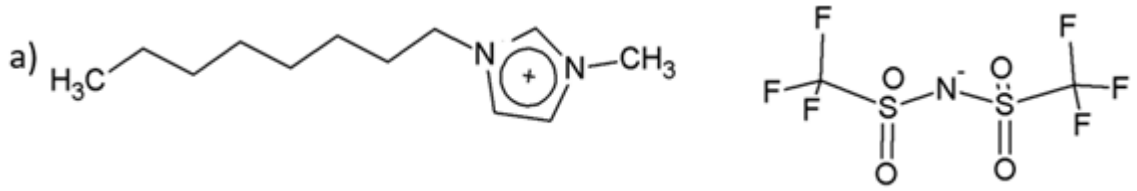

The objective for these data is to measure the relative proportions for positive ions within mixtures formed from the two pure ionic liquids. Currently the peak model would not be suitable for this purpose therefore additional constraints are required. Since data are collected from the pure forms for these two ionic liquids, and in both cases N 1s spectra exhibit well resolved peaks corresponding to positive and negative ions, it is therefore possible to support our assumptions about relative intensities for N 1s component peaks and, more importantly for this analysis, binding energy relationships can be assessed and computed.

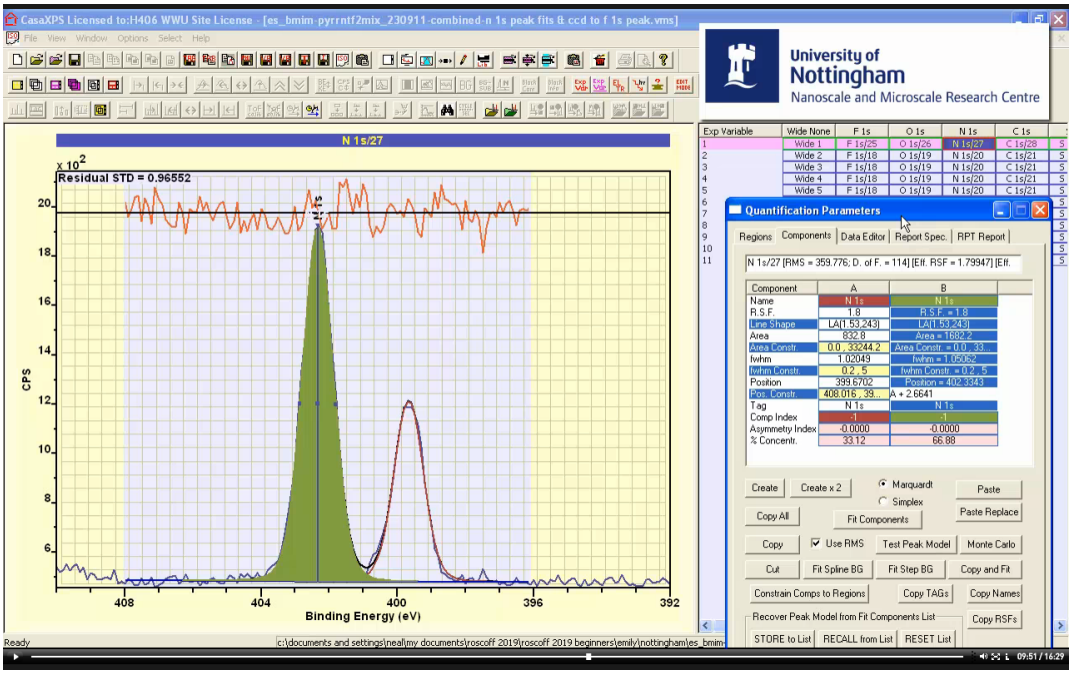

Adding two component peaks to an N 1s spectrum then fitting these components to these data facilitates the calculation for the offset between components. A binding energy offset between two component peaks is introduced using the Position Constraint field for a component by entering the heading label for a second component followed by an offset value in the form “A+2”, meaning set the position for the component in Column B by adding 2 eV to the position of the component in Column A. If the label for a component header is simply entered into a different component constraint and the Enter keyboard key pressed, then the constraint is updated by computing the relative offset between these components. To compute the offset between these two N 1s components the Position Constraint in Column B is entered as A. On pressing the Enter key the Position Constraint is updated with the string “A+2.6641”, thus indicating the binding energy offset is 2.6641 eV.

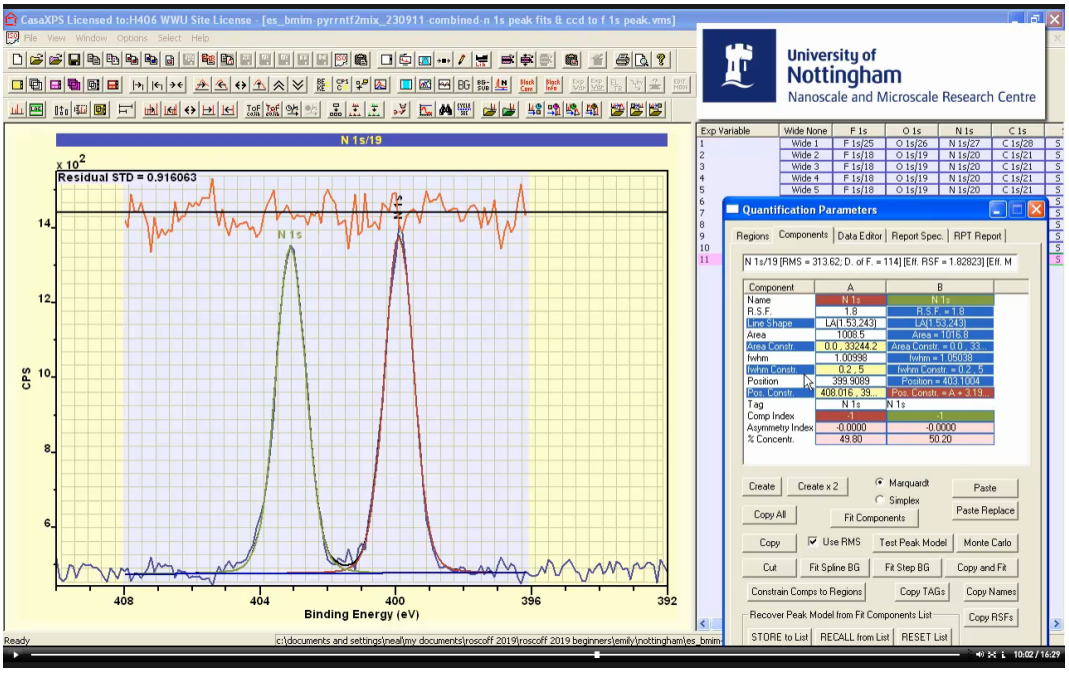

Creating a two component peak model and repeating the same offset calculation for the second pure ionic liquid results in an offset in binding energy of 3.1915 eV between two peaks of equal intensity. Armed with the binding energy offset for two peaks of equal area applying the same offset to equivalent peaks in the peak model for the mixture removes the binding energy issue with the ionic liquid peak model.

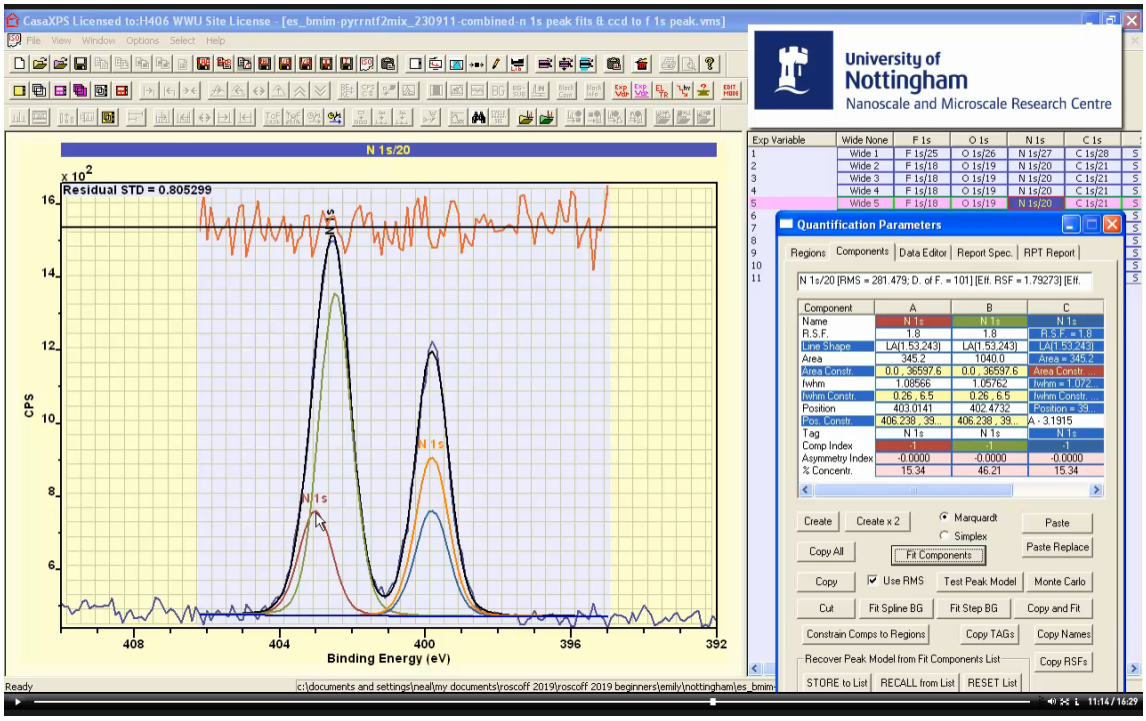

b)

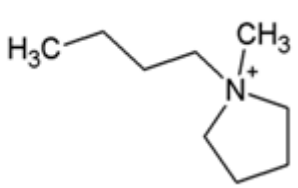

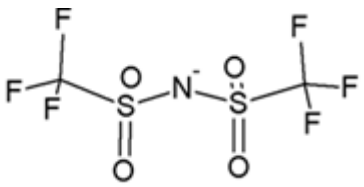

Regions | Components | Data Editor | Report Spec. | RPT Report

N 1s/20 [RMS = 270.49; D. of F. = 101] [Eff. RSF = 1.79244] [Eff. M

Component	A	B	C	D
Name	N 1s IL1	N 1s IL2	N 1s IL1	N 1s IL2
R.S.F.	1.8	1.8	1.8	1.8
Line Shape	LA(1.53,243)	LA(1.53,243)	LA(1.53,243)	LA(1.53,243)
Area	225.3	1315.7	225.3	657.9
Area Constr.	0.0 , 36597.6	0.0 , 36597.6	A * 1	B * 0.5
fwhm	0.953352	1.00899	1.03903	1.03903
fwhm Constr.	0.26 , 6.5	0.26 , 6.5	0.26 , 6.5	C * 1
Position	402.9048	402.3264	399.7133	399.7133
Pos. Constr.	406.238 , 394.922	406.238 , 394.922	A - 3.1915	A - 3.1915
Tag	N 1s	N 1s	N 1s	N 1s
Comp Index	-1	-1	-1	-1
Asymmetry Index	-0.0000	-0.0000	-0.0000	-0.0000
% Concentr.	9.29	54.27	9.30	27.14

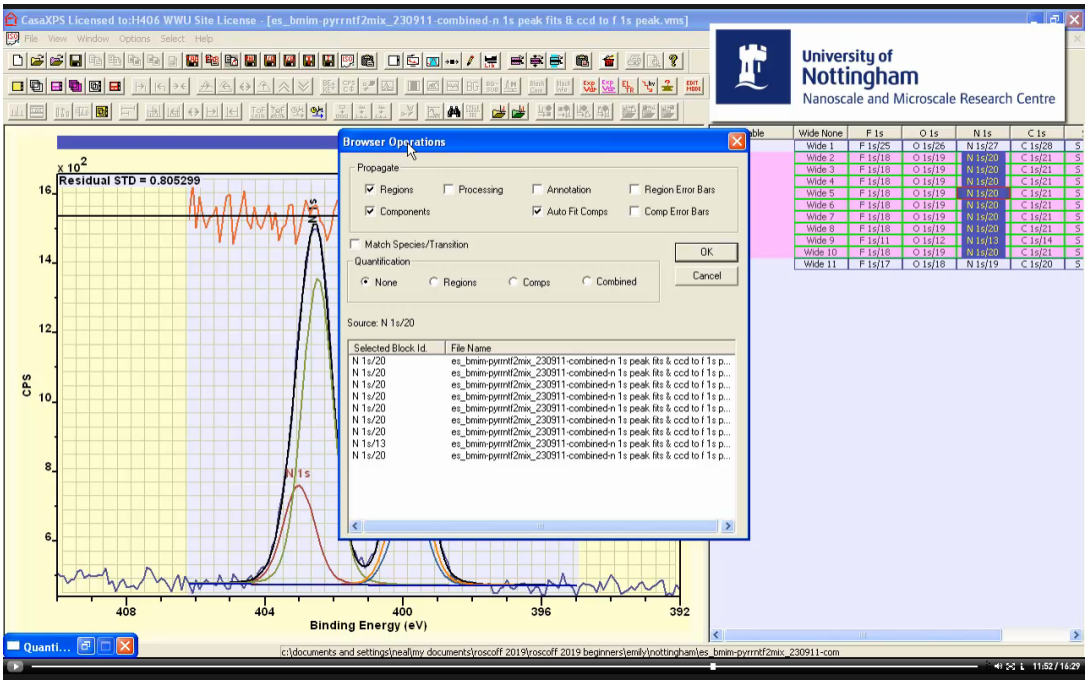

Confidence in a peak model is enhanced by testing the model using spectra with similar peak structure by fitting the peak model to all such data. In this example, N 1s spectra were measured from a range of nine samples formed by mixing different proportions of two ionic liquids. If it is assumed no chemical changes occur within these mixtures, the model as constructed based on this assumption should fit all data with similar data reproduction that has been obtained so far.

Selecting the set of VAMAS blocks in the right hand pane corresponding to mixtures of ionic liquids before placing the cursor over the active display tile containing the current peak model then pressing the right hand mouse button invokes the Browser Operations dialog window. Selecting the Regions, Components and AutoFit tick-boxes then pressing the OK button propagates the peak model from the active VAMAS block to the set of selected VAMAS blocks.

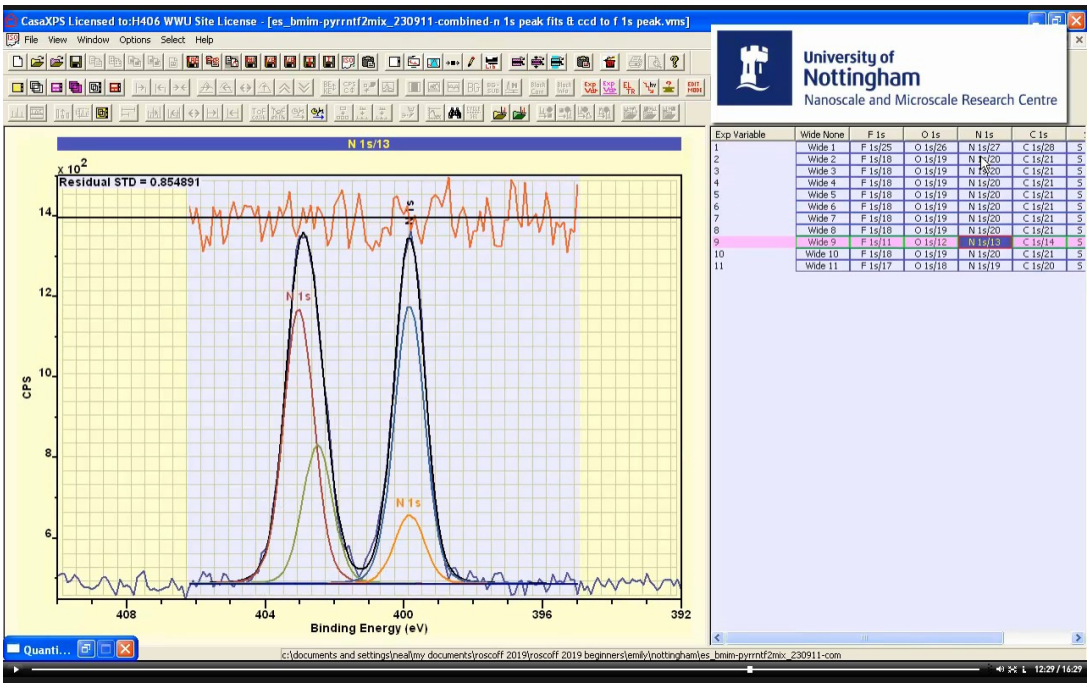

Visual inspection indicates data reproduction is comparable to the original data used to construct the peak model.

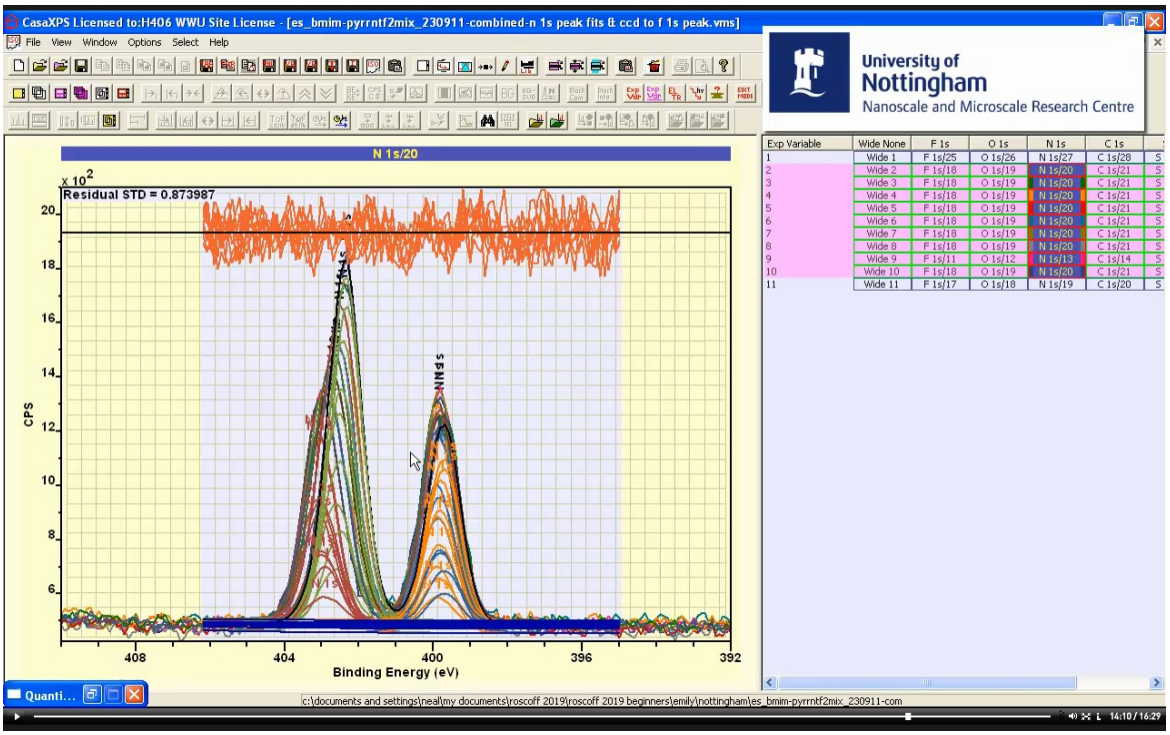

These N 1s spectra measured from different proportions of two ionic liquids exhibit different charge state resulting in shifts in binding energy for different measurements. The peak model prepared for one spectrum was propagated to all spectra without performing any charge correction processing step. The act of fitting this peak model to these data necessarily required the flexibility to shift the model in binding energy as well as adjust relative intensities of component peaks depending on spectrum. These types of adjustments in fitting parameters are the reasons non-linear least squares optimisation is required. Given the target of measuring proportions of ionic liquid mixtures, parameter constraints were necessary for this particular peak model where these constraints were added in turn to limit the flexibility of the model when fitted to data and these development steps demonstrated the need for such constraints for this application. Non-linear least square fitting of components to data is sometimes replaced by linear least squares fitting of standard spectra to unknown data. Linear least square fitting of these two pure ionic liquid spectra would require charge referencing to align all N 1s data in a physically meaningful way. Once energy shifts are performed as an independent exercise from optimisation, linear least squares would be equivalent to linking all fitting parameters within the component peak model with the exception of Area parameters. Finally FWHM and Position Constraints would need to be fixed to specific values before propagating the model to all other data. At which point, non-linear optimisation and linear optimisation are logically performing the identical calculation. Thus in using non-linear optimisation fitting of components to data with the least number of constraints permits a degree of flexibility that at times is required to allow for acquisition differences in spectra.

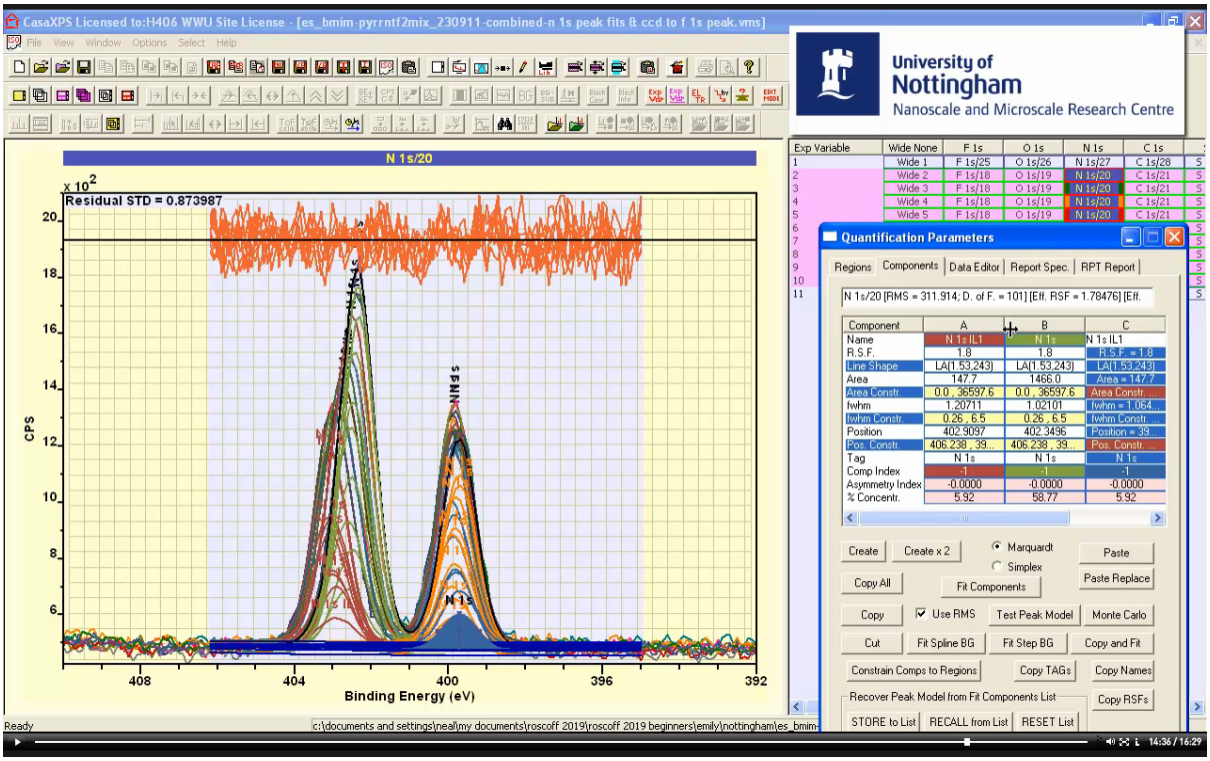

Once these spectra are fitted using the current peak model the next step might be to profile these samples in terms of component areas determined by the peak model for each of the standard ionic liquids used in the preparation of these mixtures. The Report Spec. property page includes a sections used to define Custom Reports for combining intensities from regions and components defined on VAMAS blocks selected in the right hand pane. The Custom Report allows the profiling of signal gathered from different components representative of the same material. Any component or region with the same name will have intensity summed to form the composition reported by the Custom Report section. Thus to make use of the Custom Report to calculate the proportions for these two ionic liquids in the mixtures, components representative of an ionic liquids must be assigned a unique name. Component name fields are therefore adjusted to “N 1s IL1” for one ionic liquid and “N 1s IL2” for the other. Note the region name is “N 1s” so it is important to make these component names different from that of the region name, otherwise component and region intensity will be summed incorrectly. A warning message is issued in the event a Custom Report is prepared with regions and components with identical names.

Changing name fields on the Components property page only adjusts names for components on the active VAMAS block displayed in the active tile. All component names for the models fitted to each of the mixture N 1s spectra must be updated too. Once the name field are updated with N 1s IL1 and N 1s IL2 on the active VAMAS block the alternative to propagating and fitting afresh is to use the Copy Names button on the Components property page. Component names are transferred to VAMAS blocks selected in the right hand pane for any peak model matching the number of components defined on the active VAMAS block. Copying names does not incur the cost of refitting components to data.

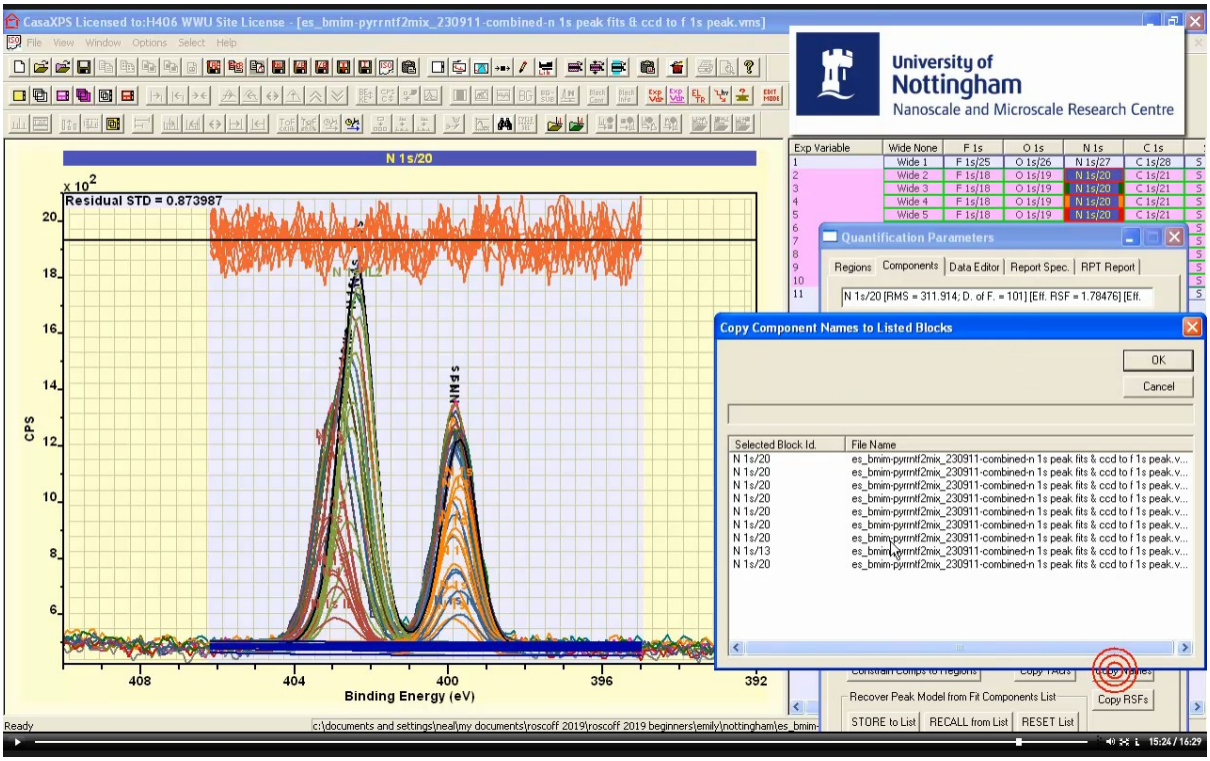

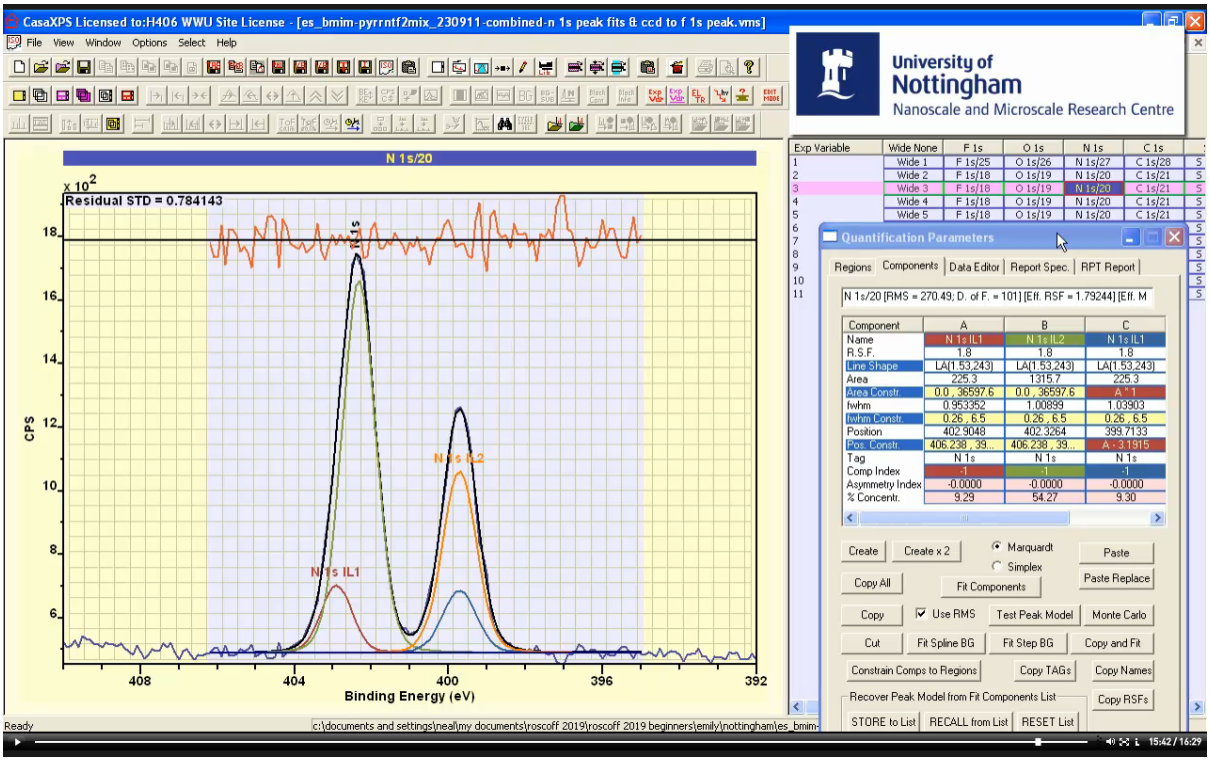

After names are copied using the Copy Names button, stepping through the VAMAS blocks previously selected before pressing the Copy Names button verifies names are appropriate for use with the Custom Report.

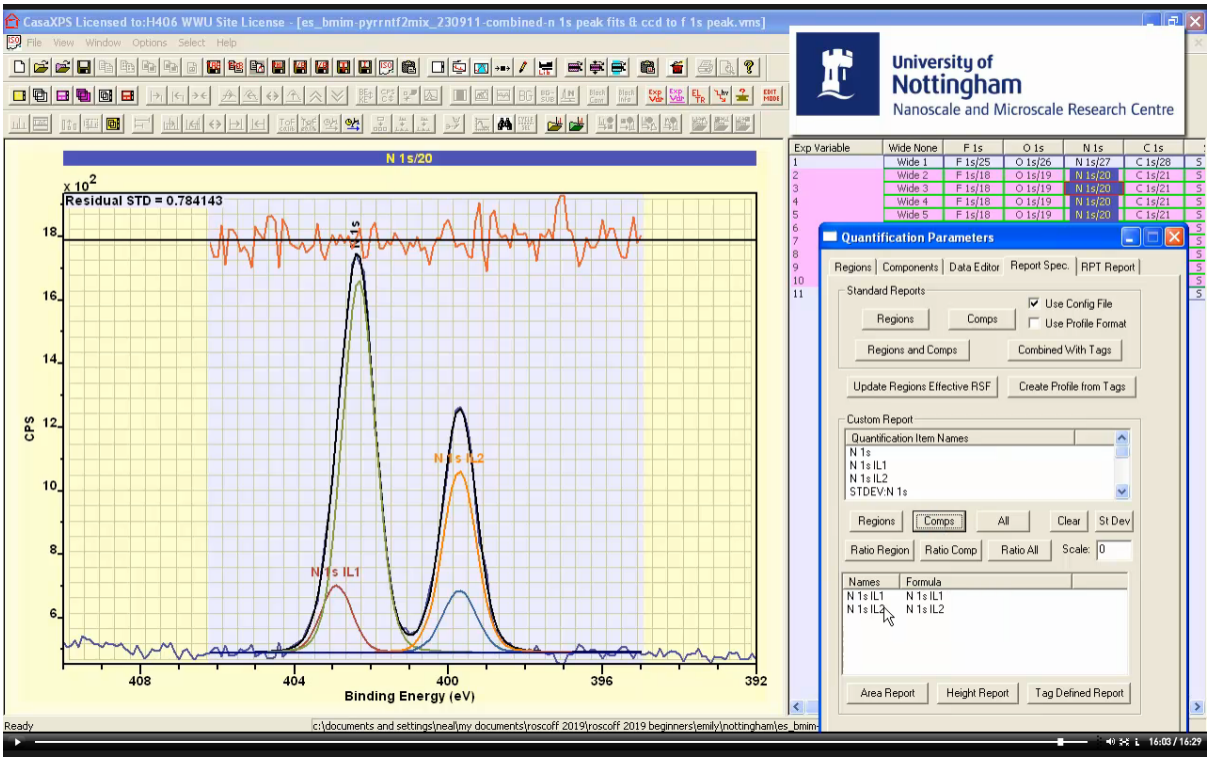

Quantification Parameters dialog window, Report Spec property page makes use of VAMAS blocks selected in the right hand pane. The Quantification Items table is a list of names assigned to components and regions defined on the selected VAMAS blocks. The Names/Formula is a subset of these quantification items that will be used to compute a quantification table. The Names columns is a user defined string not necessarily the name of a component or region. The Formula column is an expression defined in terms of component or regions names that allows the intensity to be specified from more than one region or component, if necessary, but in this example these formulae are simply the names for components assigned to each of the ionic liquids.

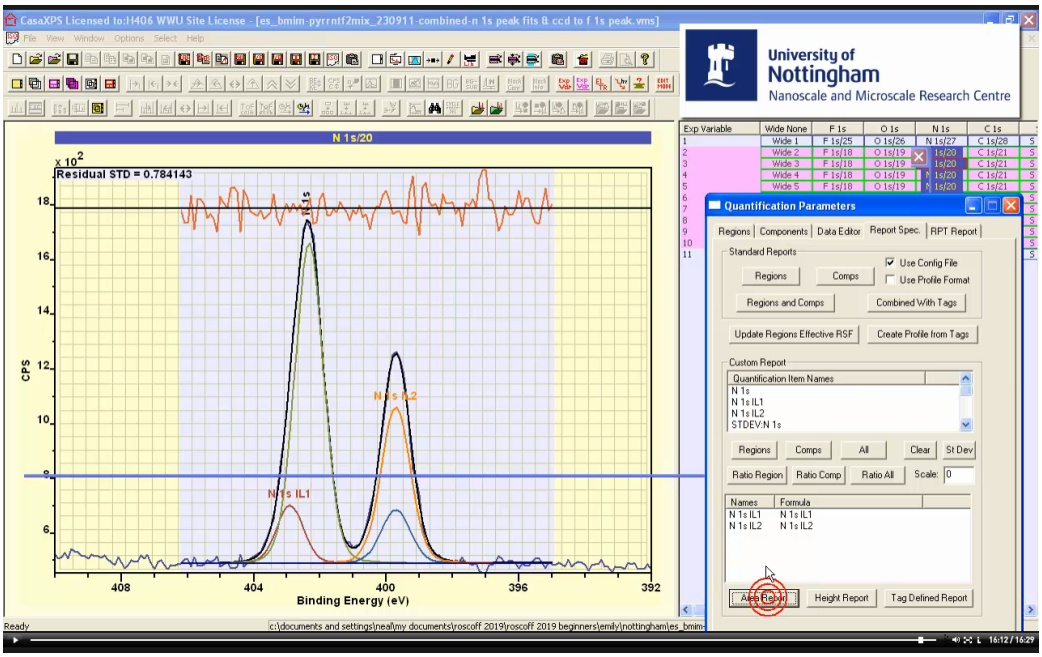

A quantification table making use of the Name/Formula table applied to selected VAMAS block is created by pressing the Area Report button.

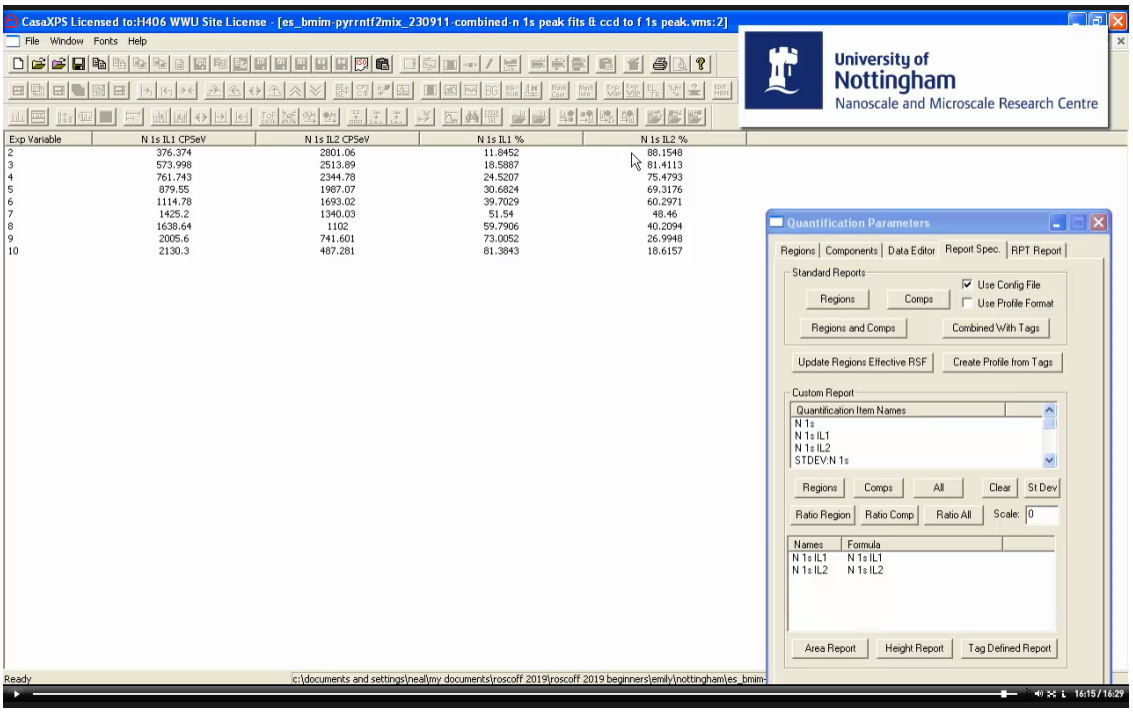

Text from the report can be copied to the clipboard as tab spaced ASCII data suitable for use in a spreadsheet program.

Relative Sensitivity Factors and Doublet Peaks

The objective for this video is to illustrate the relationship between Scofield cross-section RSFs and the appropriate use of RSFs for doublet peaks when used as part of quantification results.

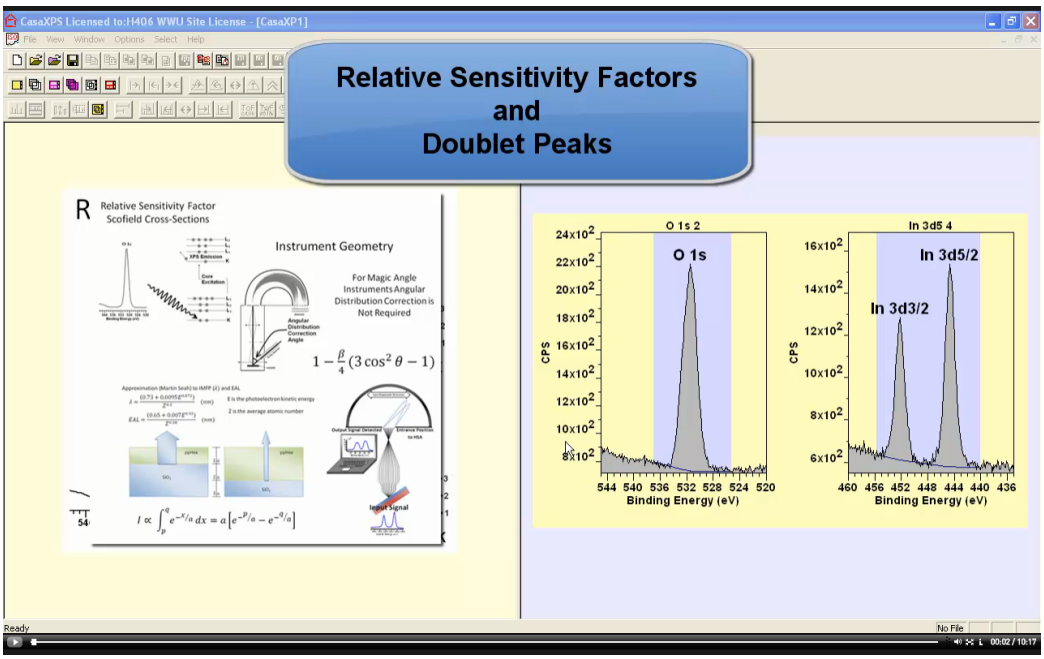

The Scofield element library in CasaXPS includes three entries for every photoemission process involving spin-orbit split doublet peaks. These library entries include relative sensitivity factors for each of the doublet peaks separately, and one corresponding to both peaks combines as one entity. The reason for three element library RSFs is quantification for a given element and photoemission line can be performed even when one part of a doublet overlaps another photoemission line. For best signal to noise the preferred option is to make use of both peaks in a doublet, but circumstances may prevent the use of both peaks for quantification.

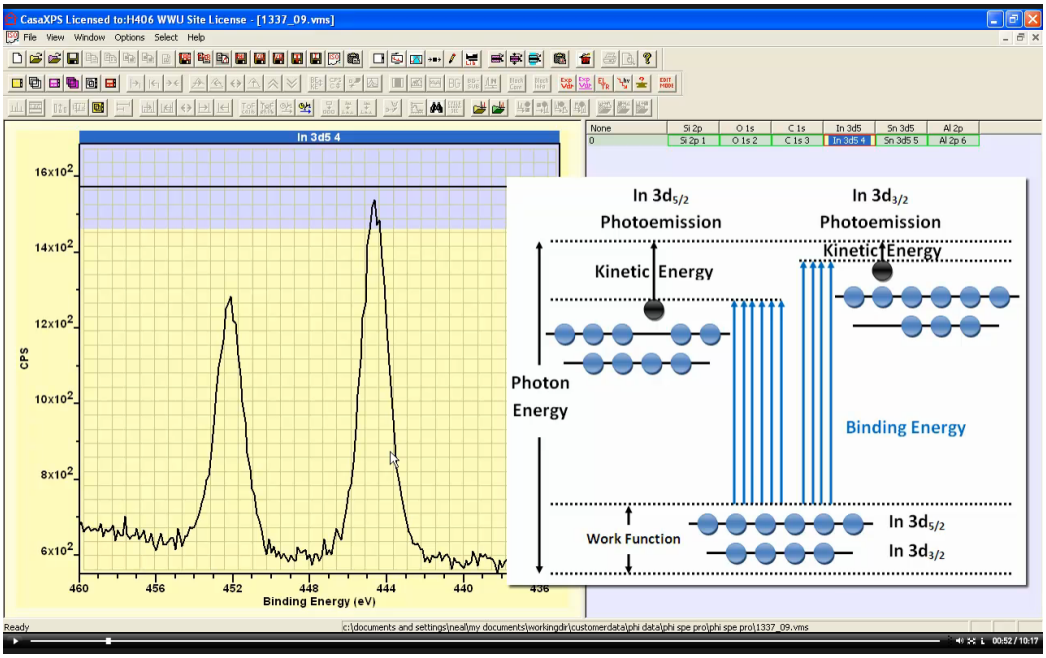

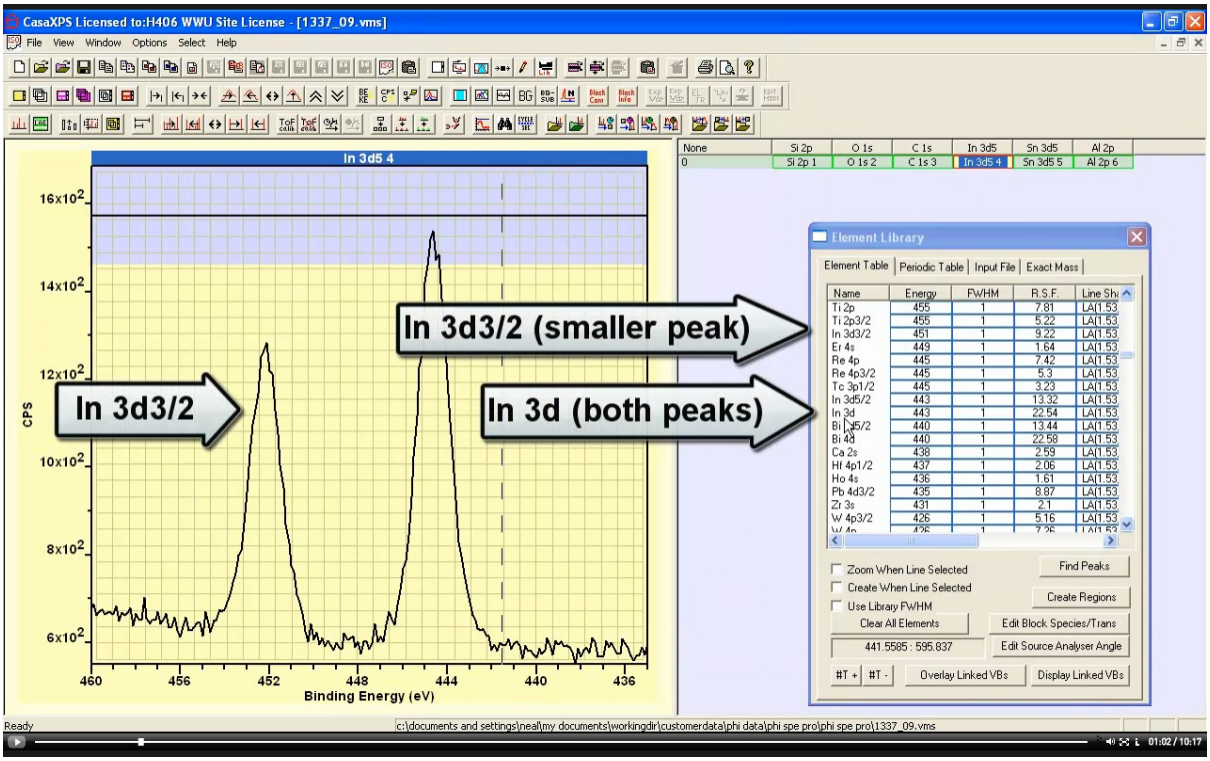

The most intense photoemission signal from indium is due to photoemission of In 3d electrons. The element table scrolls to the position where the cursor is positioned over the active display tile before left-clicking the mouse button. Three entries in the element library table are labelled In 3d, In 3d3/2 and In 3d5/2. Doublet peaks for the same orbital angular momentum assignment are distinguished by means of the total angular momentum quantum numbers 3/2 and 5/2. Emission of a 3d electron leaves the final state for the ion with one of two possible energies.

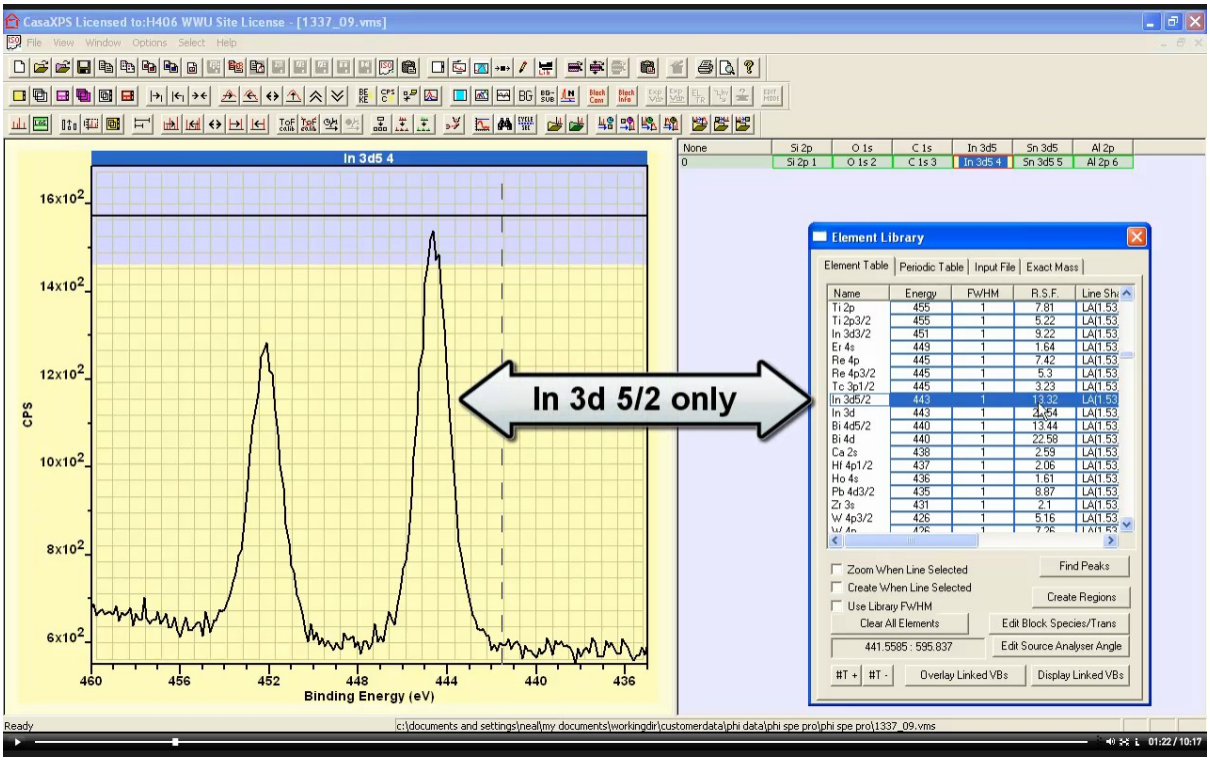

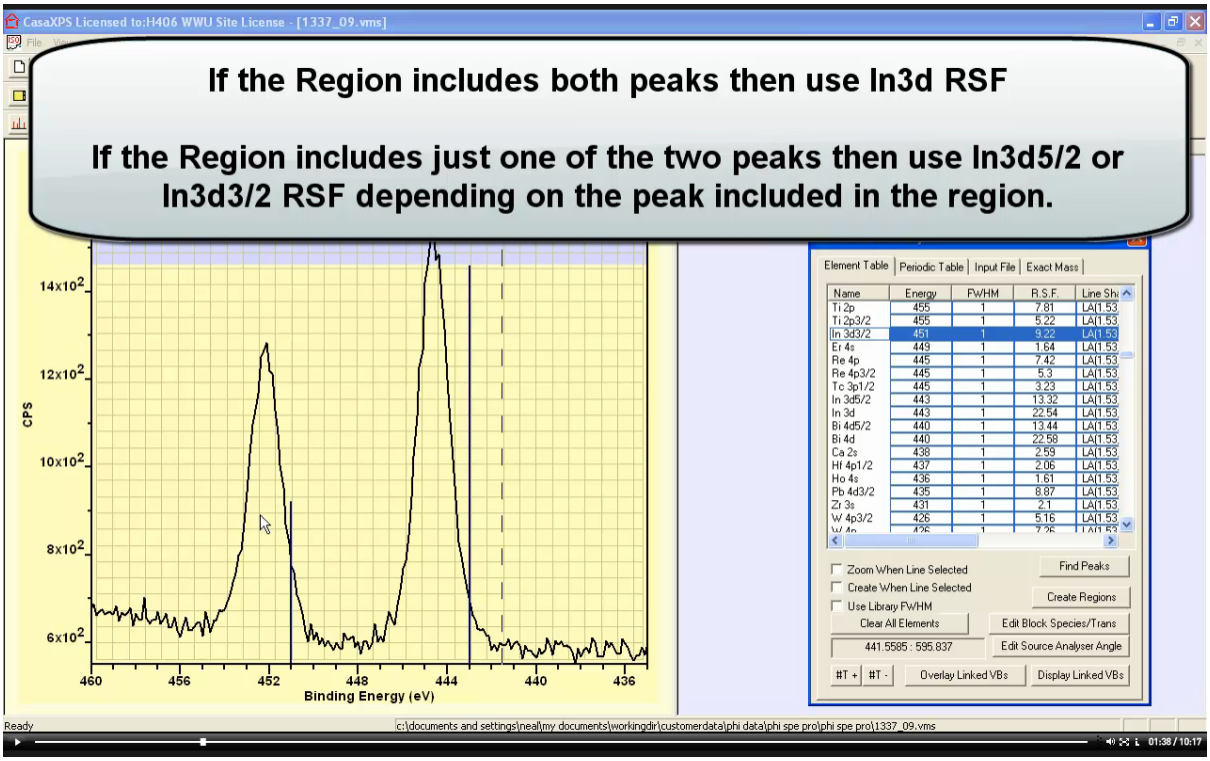

The probability for the final state ion being left in one or the other of these two possible energy levels is computed using Hartree-Slater wave functions by Scofield and these are the two RSFs assigned to In 3d3/2 and In 3d5/2 where the values are reported relative to the probability of the emission of a C 1s electron.

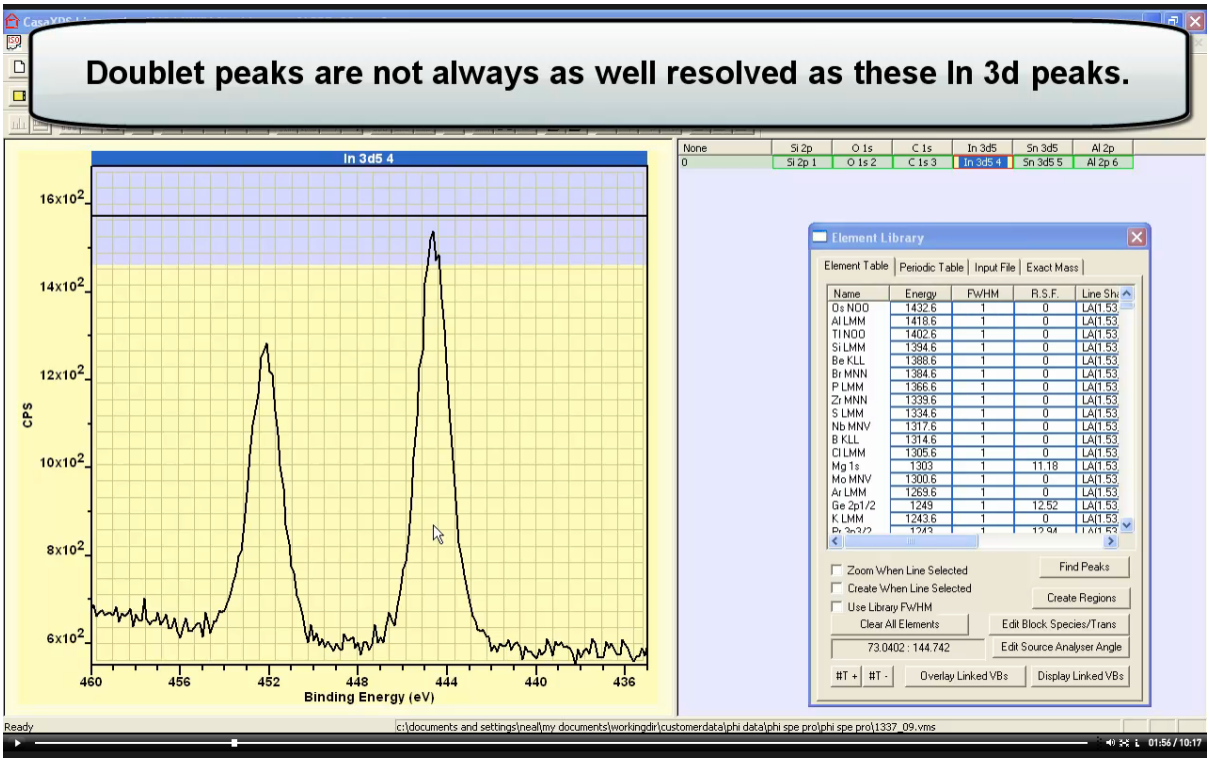

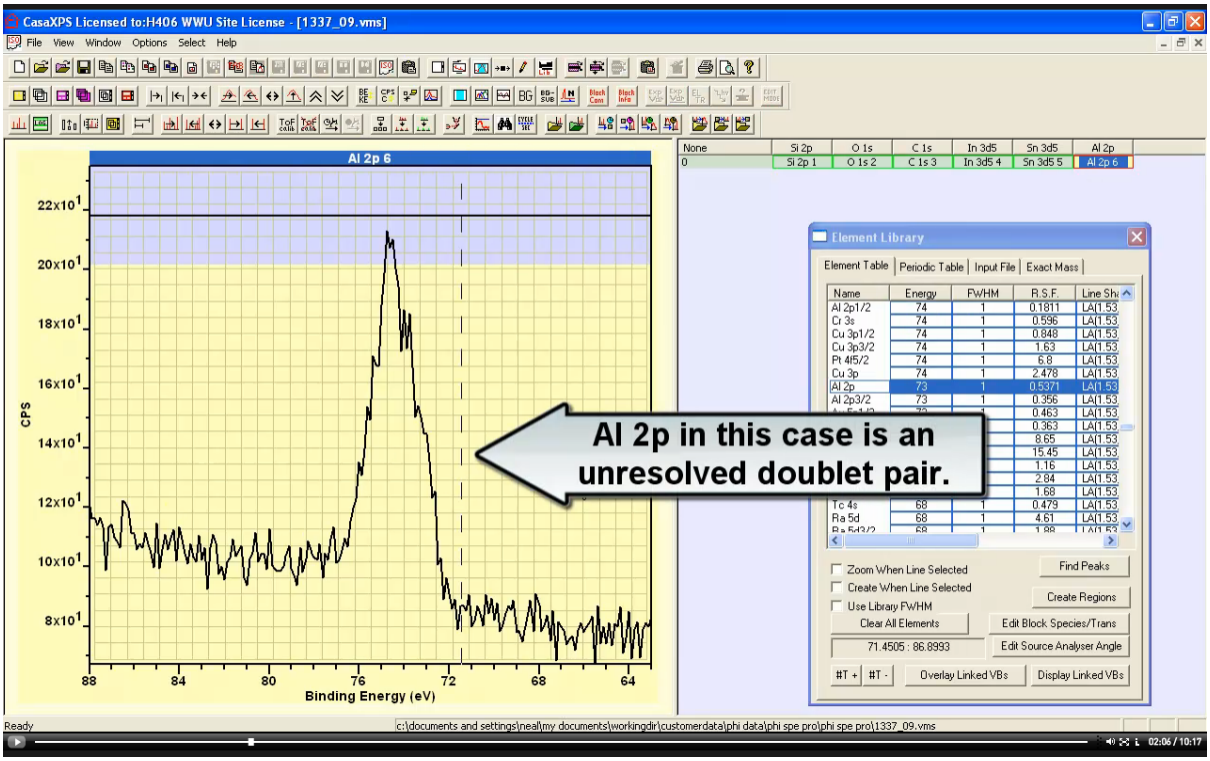

In 3d doublet peaks are well separate in energy compared to full width half maximum and allow both peaks to be defined without the need for modelling using component peaks. This situation is not always the case for doublet peaks. For example, aluminium oxide Al 2p doublets are broad (FWHM ~ 1.3 eV) and separated in energy by about 0.6 eV. As a result, quantification for aluminium oxide via a region requires the use of the combined Al 2p RSF.

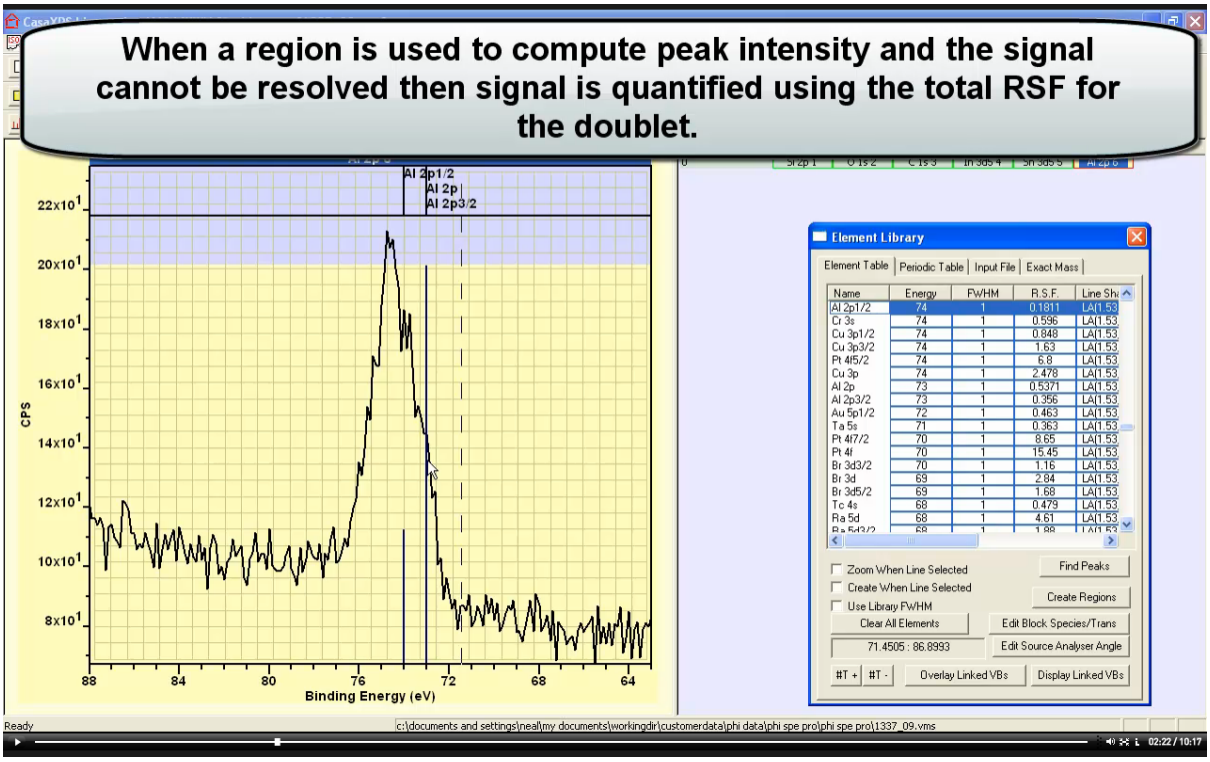

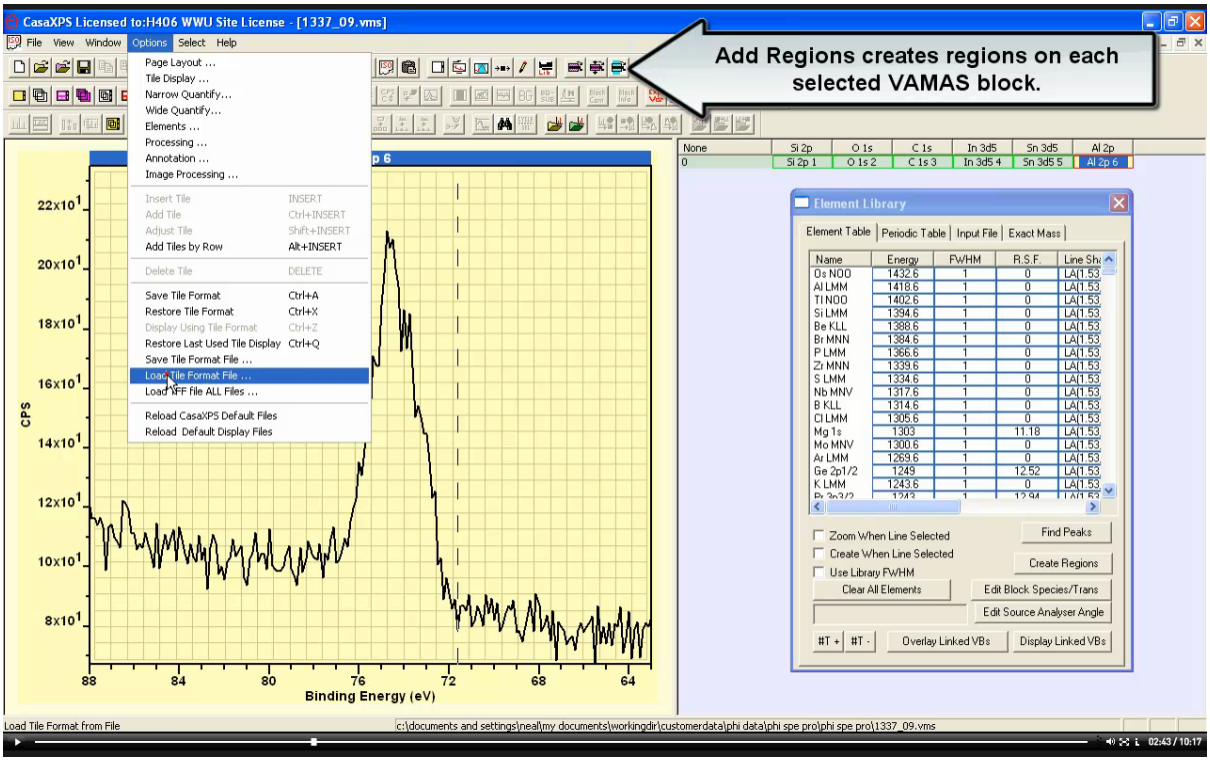

The display state for a VAMAS file can be prepared using the Page Tile Format and Display Tile Parameters dialog windows and then saved to disk as a Tile Format File (TFF). At a later time the display state for a VAMAS file is recovered from the TFF file by loading the saved file using either the File menu or the Options menu by selecting the menu option labelled Load Tile Format File.

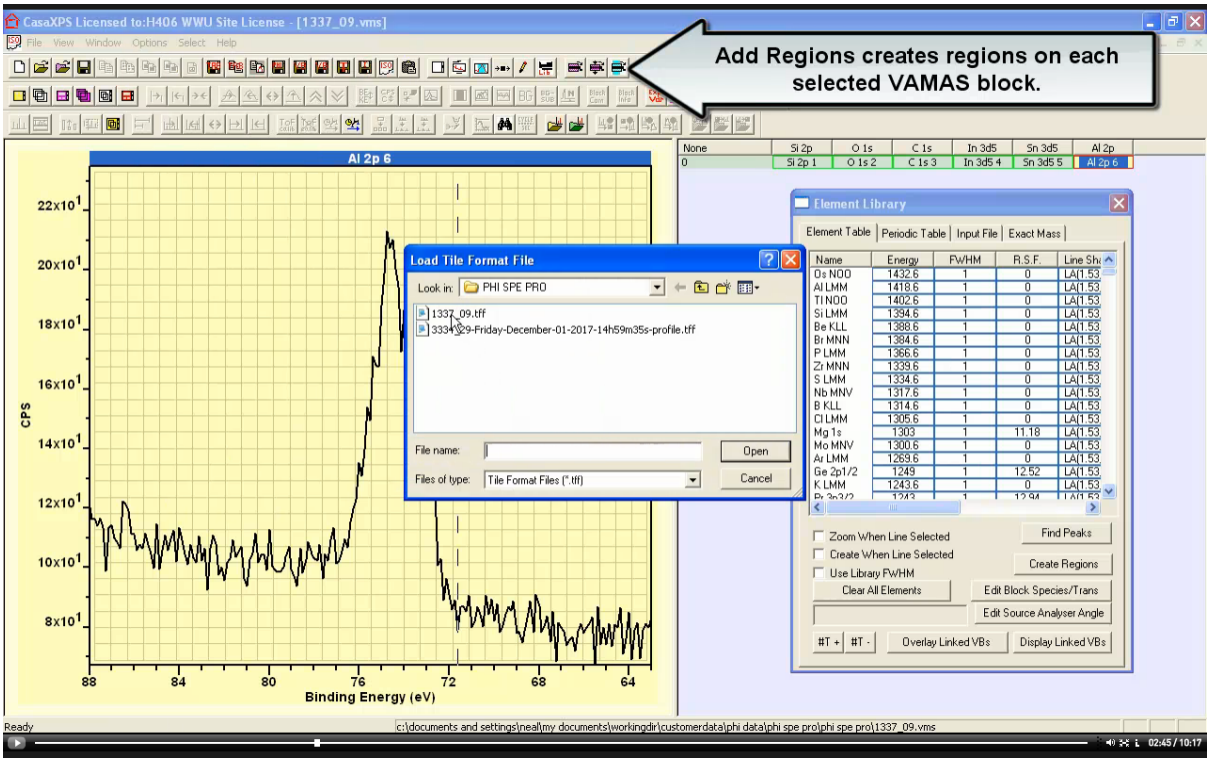

A TFF file is saved with the file extension .tff and is typically saved with the original file basename with .tff replacing .vms.

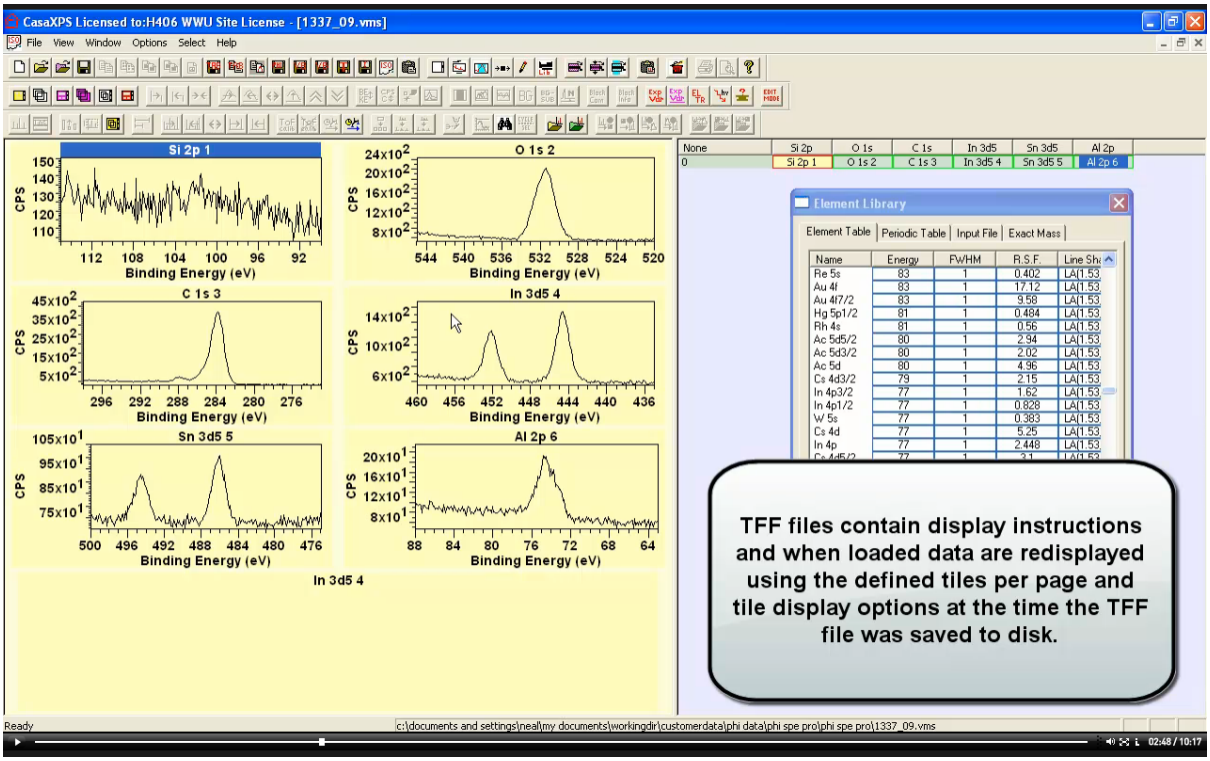

These TTF specifications include the number of tiles per page, fonts, colours and a range of display setting active at the time the TTF file is saved to disk. These six VAMAS blocks where originally displayed using seven display tiles. Selecting these VAMAS blocks in the right-hand pane before pressing the Add Regions toolbar button provides a means of adding a region to each selected VAMAS block. The blue zone indicated the limits for each created region.

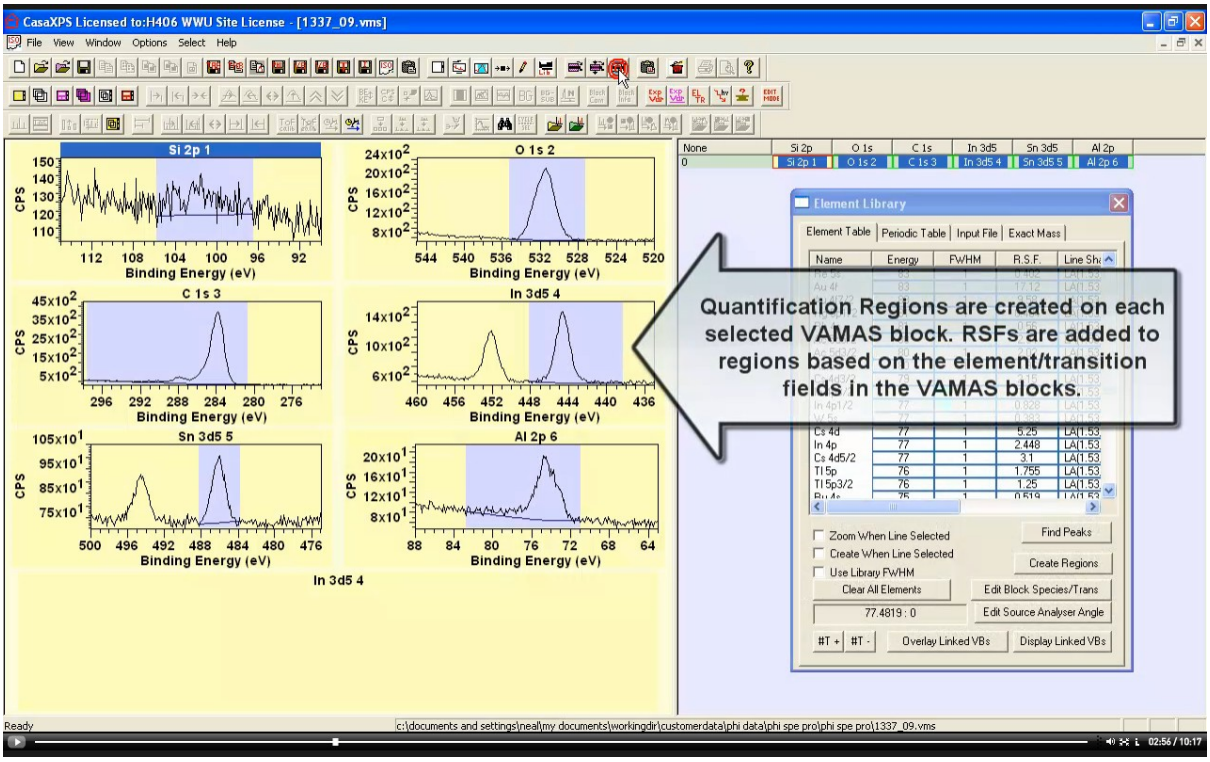

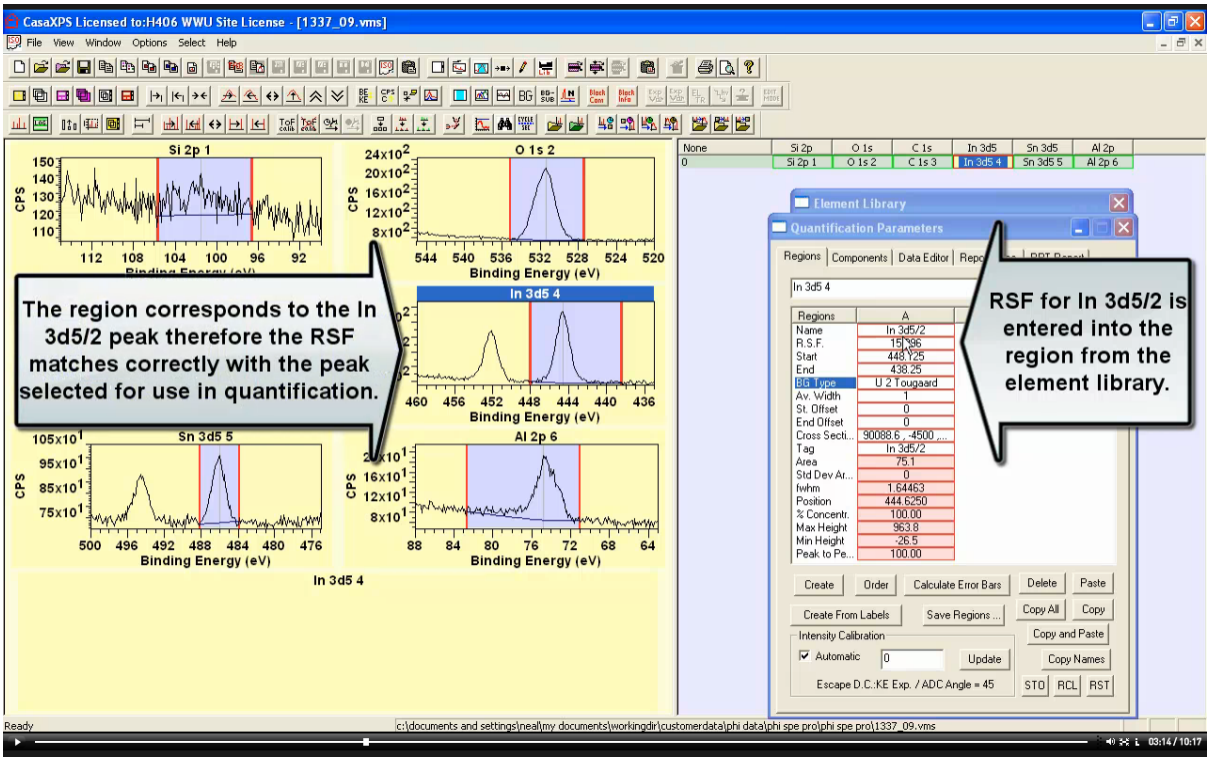

When regions are created for VAMAS blocks created with appropriate element/transition VAMAS fields (e.g. In 3d5/2 or as in this case In3d5), then these element transition fields are used to match an entry in the element-library element-table to permit the correct assignment of RSF to the region parameter field on the Quantification Parameters dialog window, Regions property page, Region table entry.

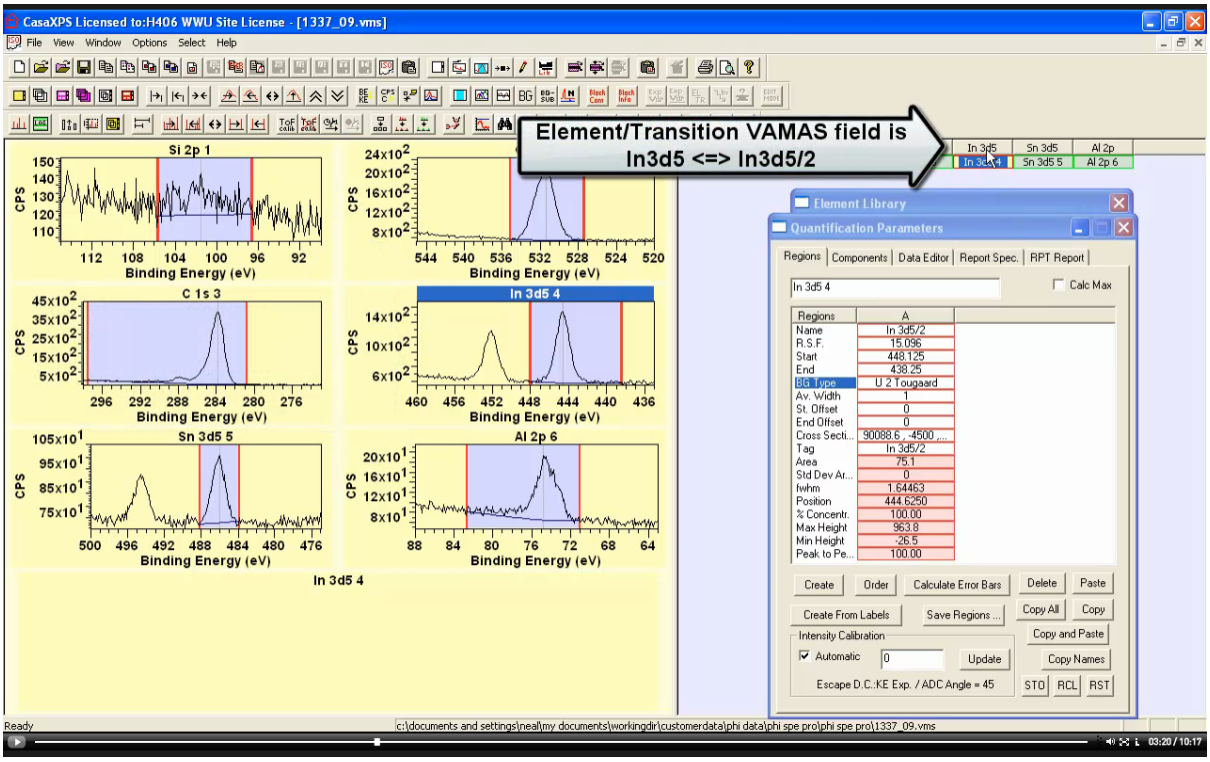

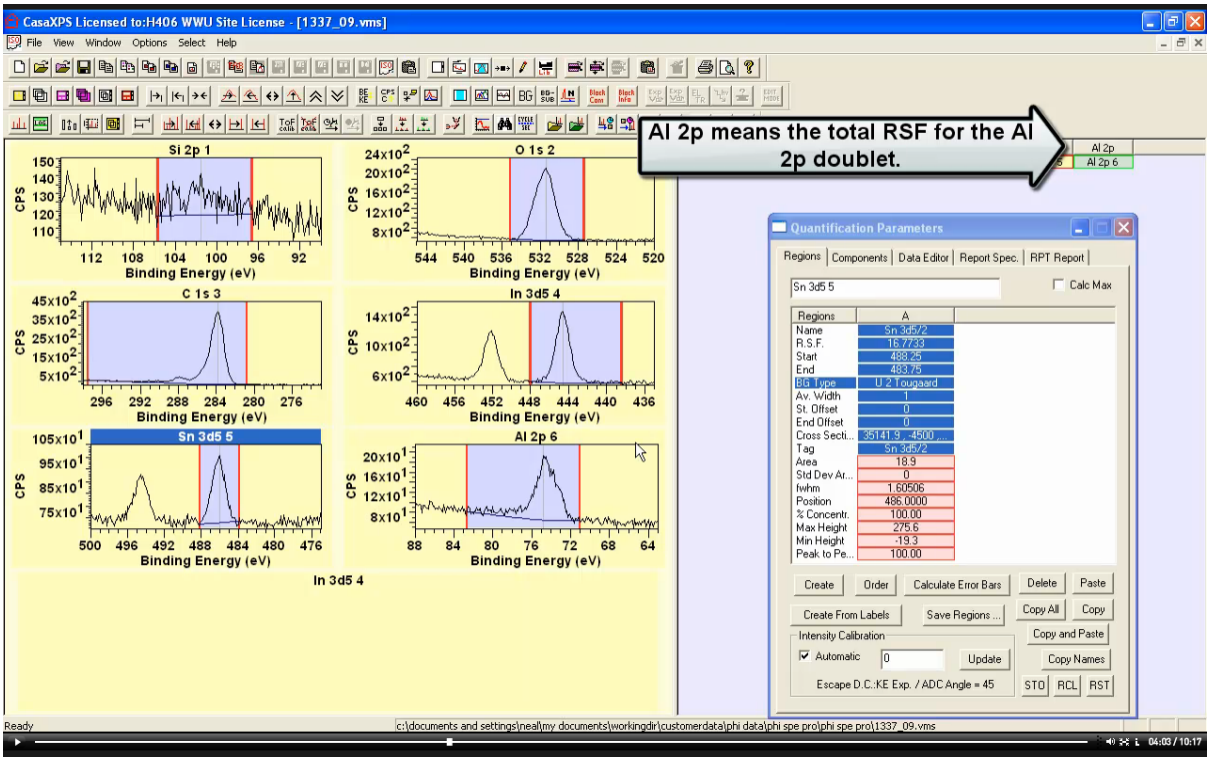

The automatic identification of a peak found the In 3d5/2 signal and ignored the In 3d3/2 signal. Fortunately the element/transition VAMAS field for these data is set to In 3d5 which is an abbreviation for In 3d5/2 and as a consequence the correct RSF is extracted from the element library. In the case of Al 2p, the entire Al 2p signal has been identified and since the element/transition field is assigned Al 2p too, the appropriate RSF for both Al 2p doublet peaks is used in the region defined on the Al 2p VAMAS block, namely, the sum of Al 2p1/2 and Al 2p3/2 RSFs.

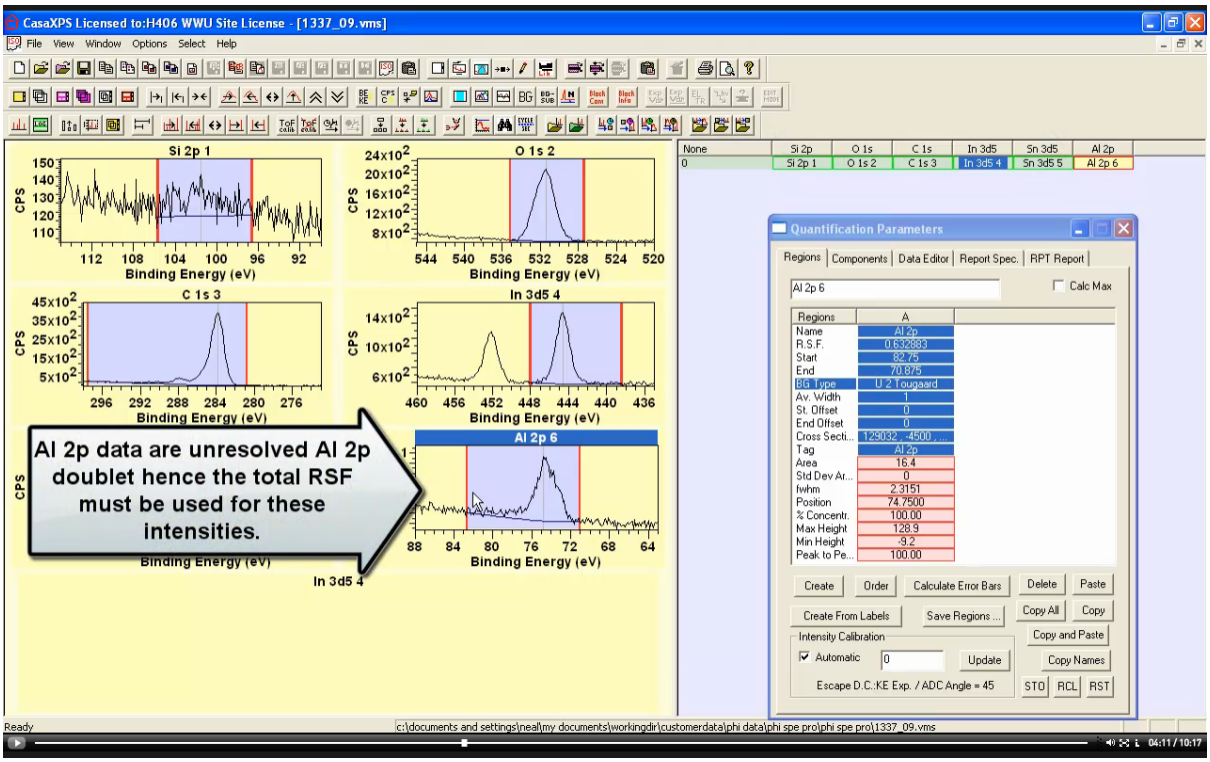

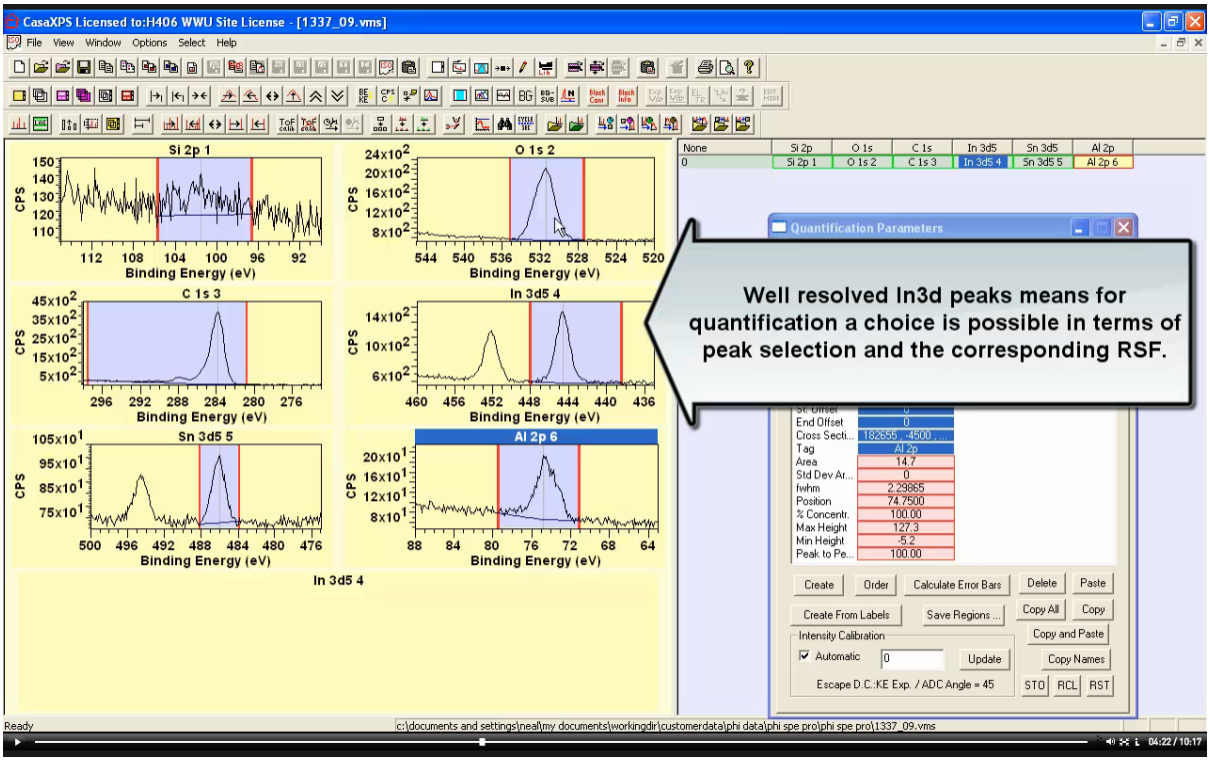

Since these In 3d doublet peaks are well resolved it would be possible to quantify indium by making use of both peaks in the In 3d doublet applying the total RSF for In 3d, or In 3d3/2 peak only and ensuring the RSF corresponds to the In 3d 3/2 entry in the element library or by defining the regions as shown where only the In 3d 5/2 peak is within the energy interval specified by the region. Successful quantification depends on matching the correct RSF with the selected energy interval.

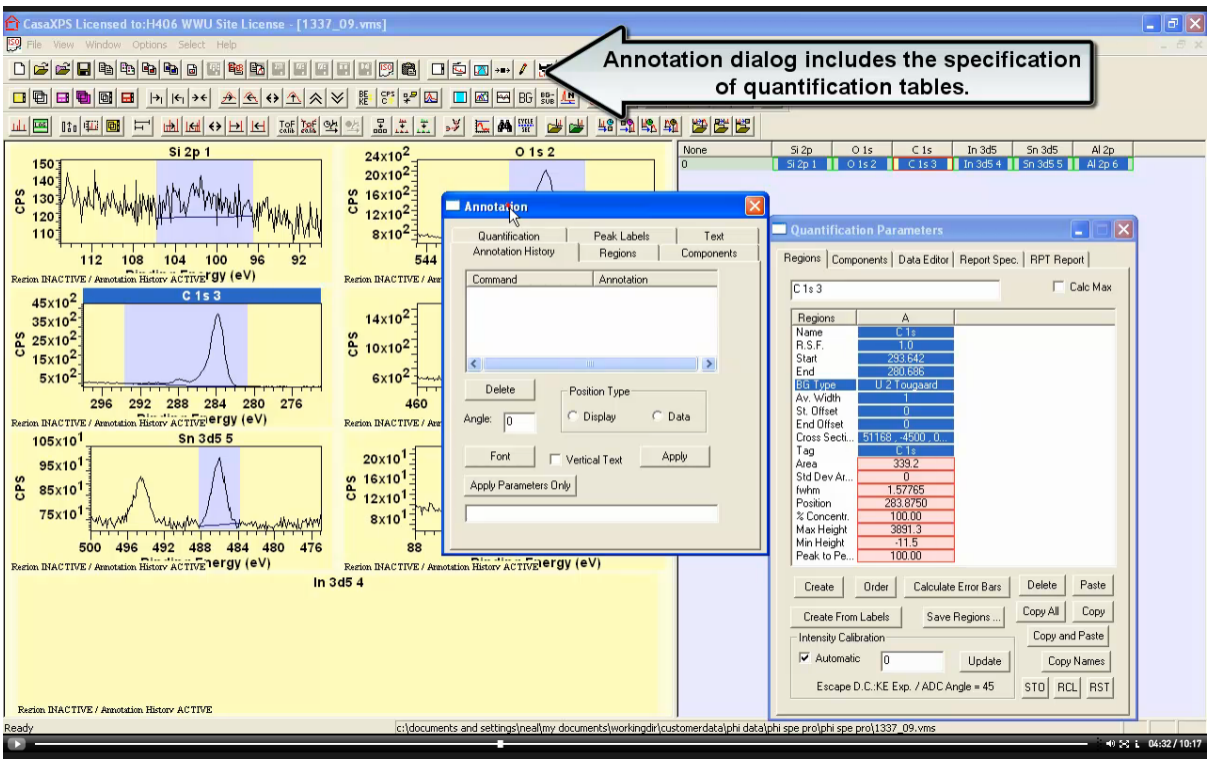

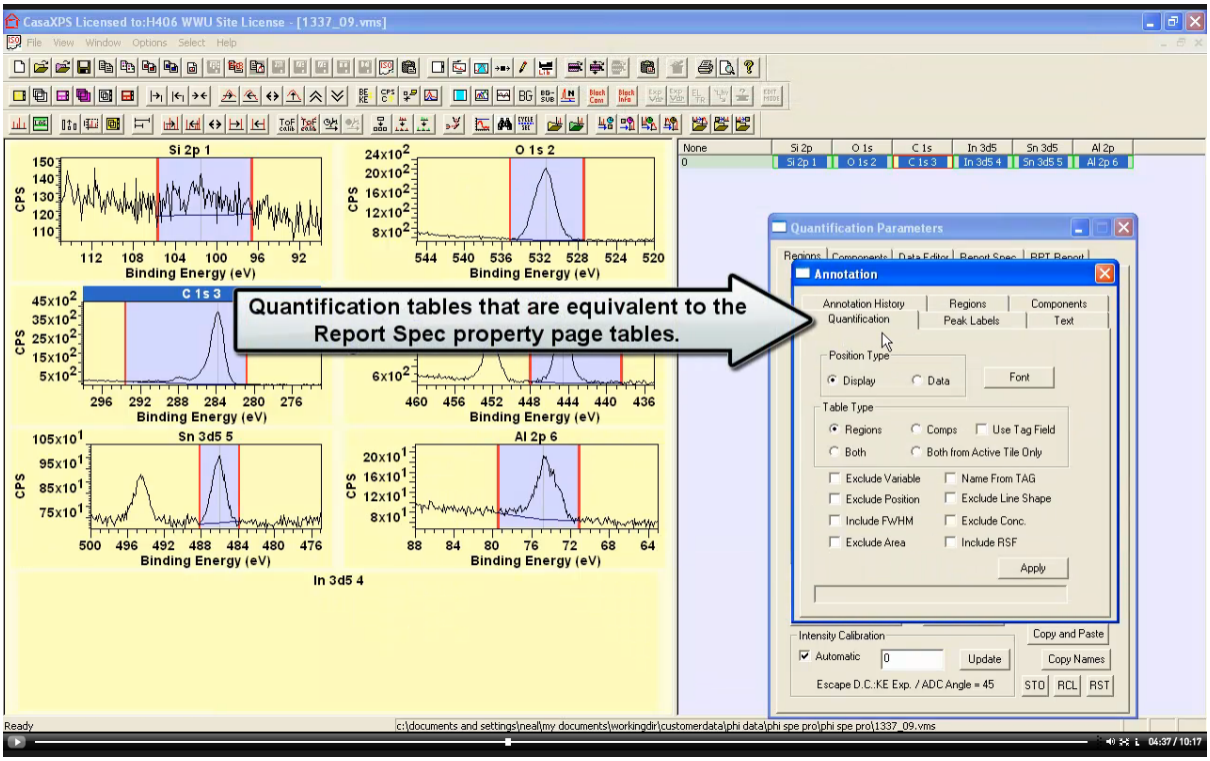

Quantification tables based on regions, components or regions and components is performed by making a selection of VAMAS blocks in the right-hand pane then generating a text based report via the Quantification Parameters dialog window, Report Spec property page. The same mechanism for generating text reports via the Report Spec property page also generate annotation tables displayed over spectra defined using the Annotation dialog window, Quantification property page.

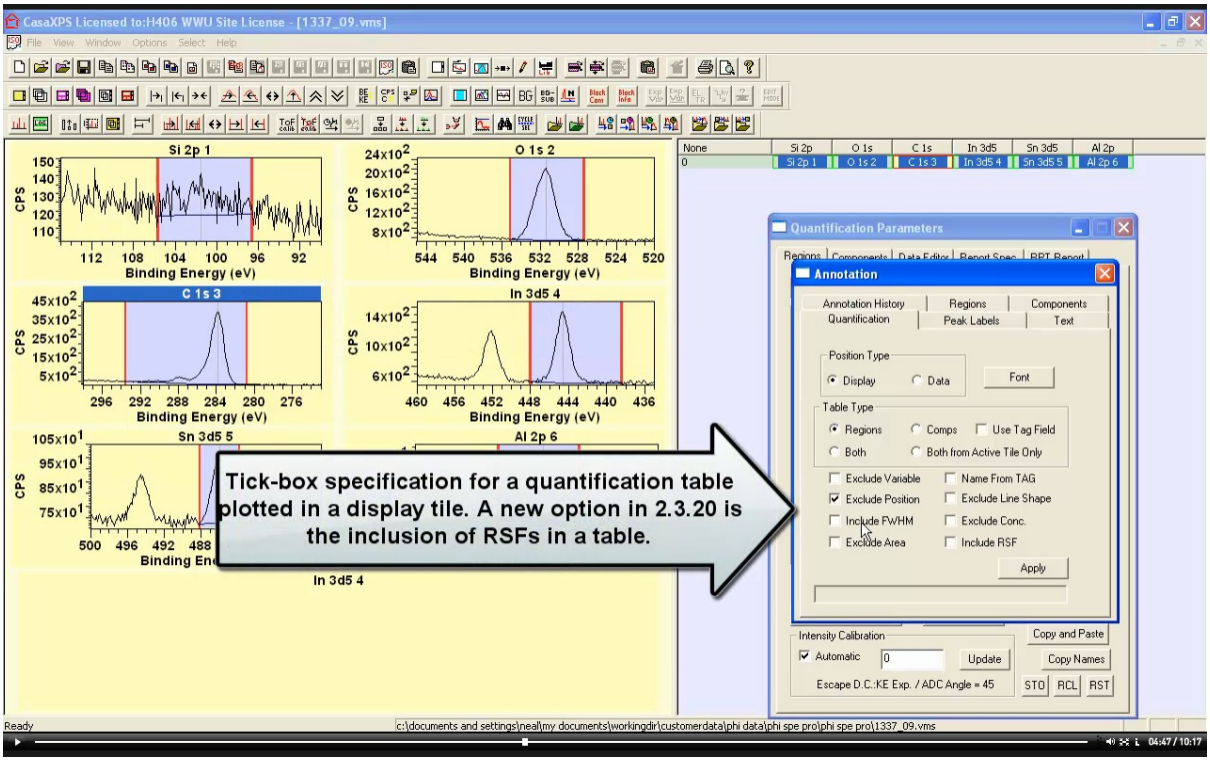

Tick box options allow the customisation of an annotation table added to the display of spectra.

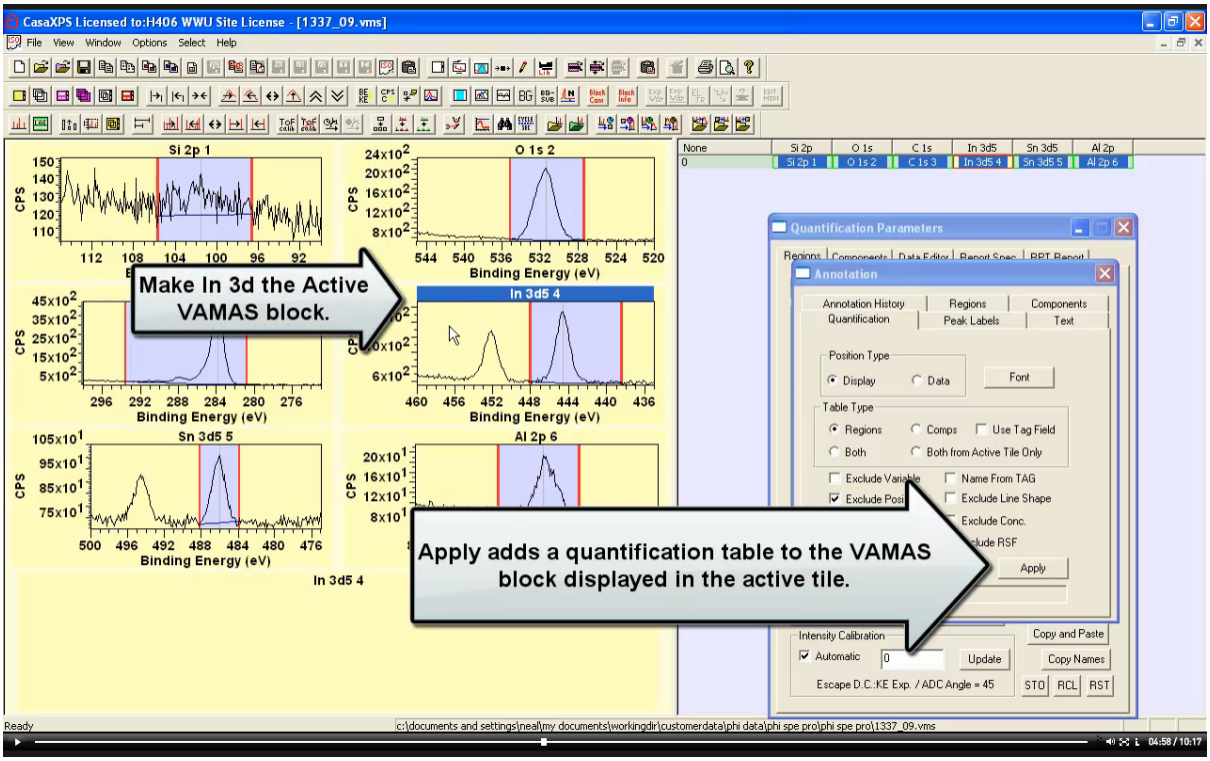

Display tiles are controlled by the Tile Display Parameters dialog window. It is possible to arrange display tiles and then specify display settings resulting in the omission of spectral data and only the display of annotation tables defined on the active VAMAS block associated with a display tile. The VAMAS block for In 3d is includes twice in the set of display tiles, hence there are six VAMAS blocks displayed, one for each spectrum, plus an additional In 3d display tile configured to display annotation tables only.

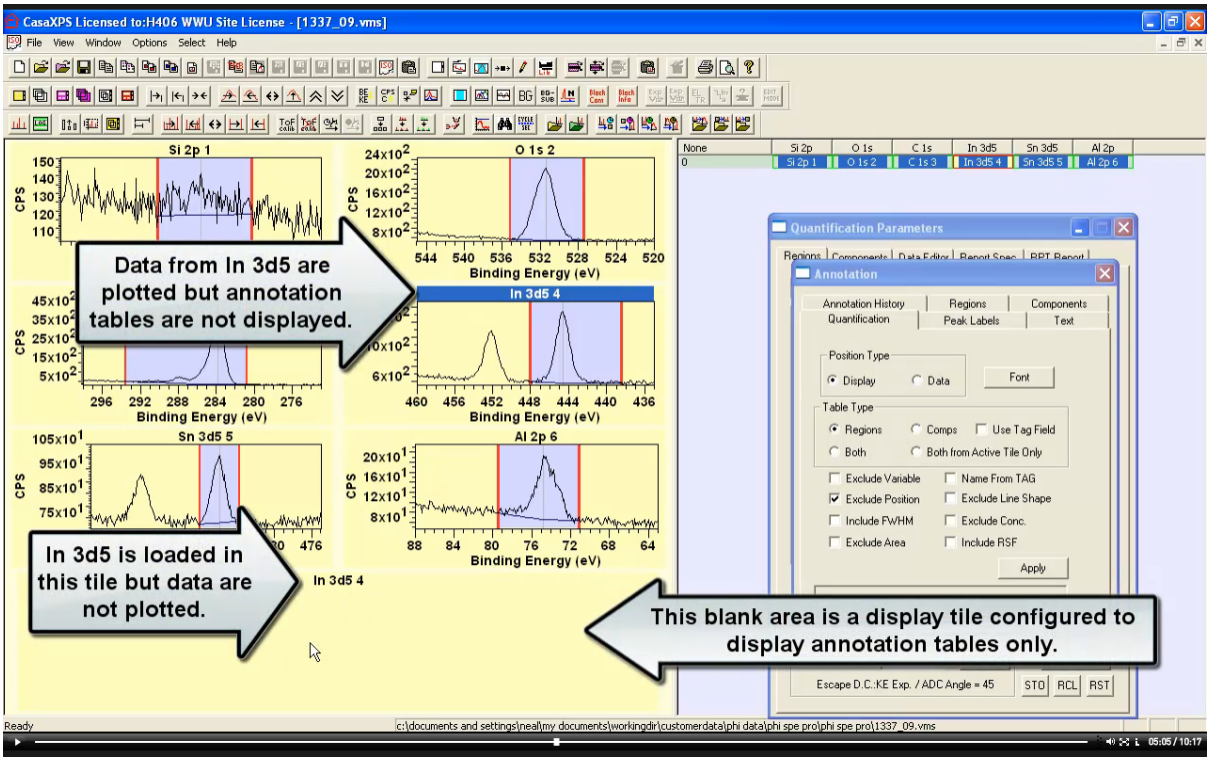

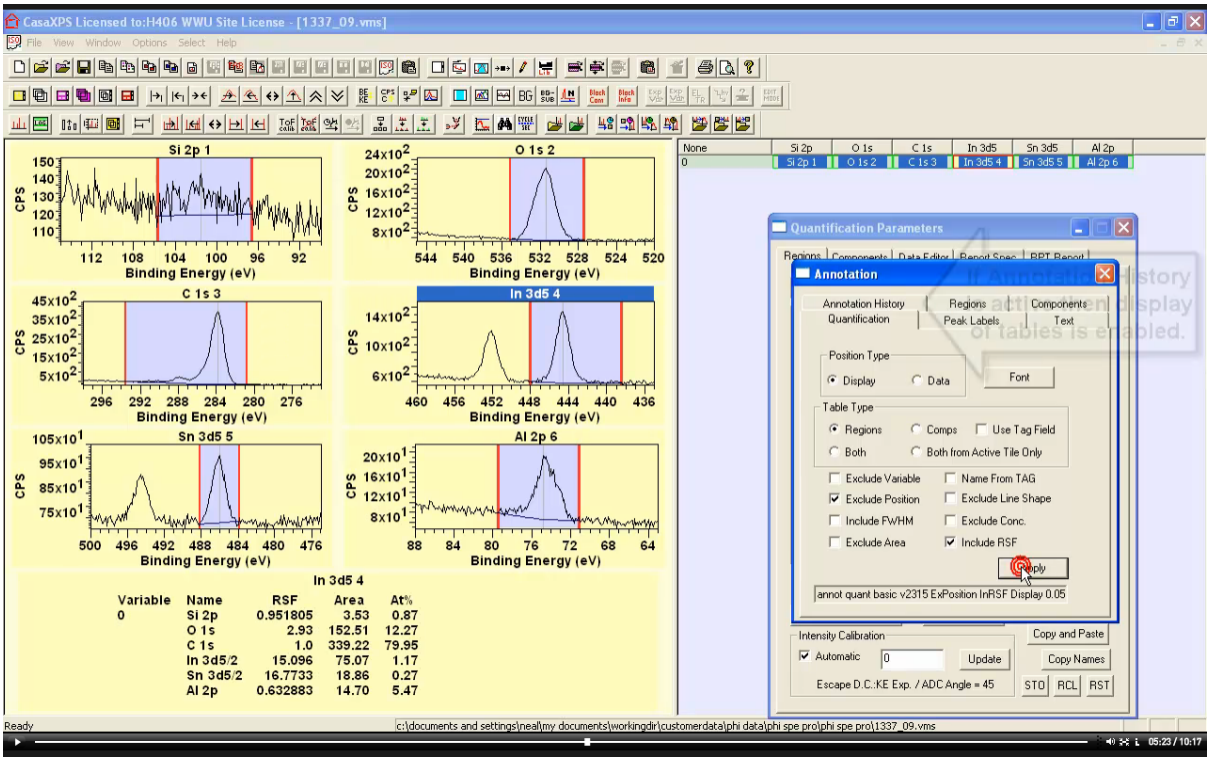

Creating an annotation table using the Annotation dialog window, Quantification property page gathers information from each region defined on VAMAS blocks selected in the right-hand pane. The table displayed in the bottom display tile is defined on the In 3d VAMAS block, but due to the selection of VAMAS blocks in the right-hand pane the table is quantification prepared from all VAMAS blocks in the VAMAS file. Quantification between VAMAS blocks requires these VAMAS blocks to appear in the right-hand pane all in the same row.

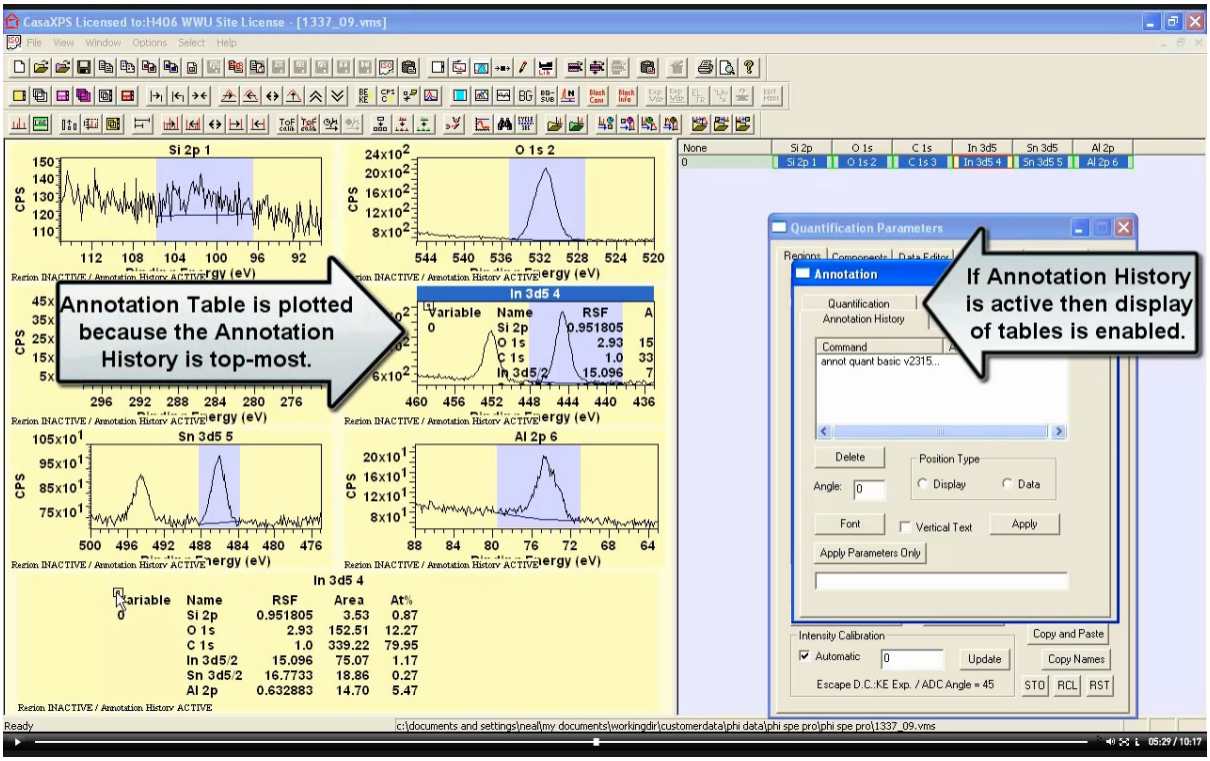

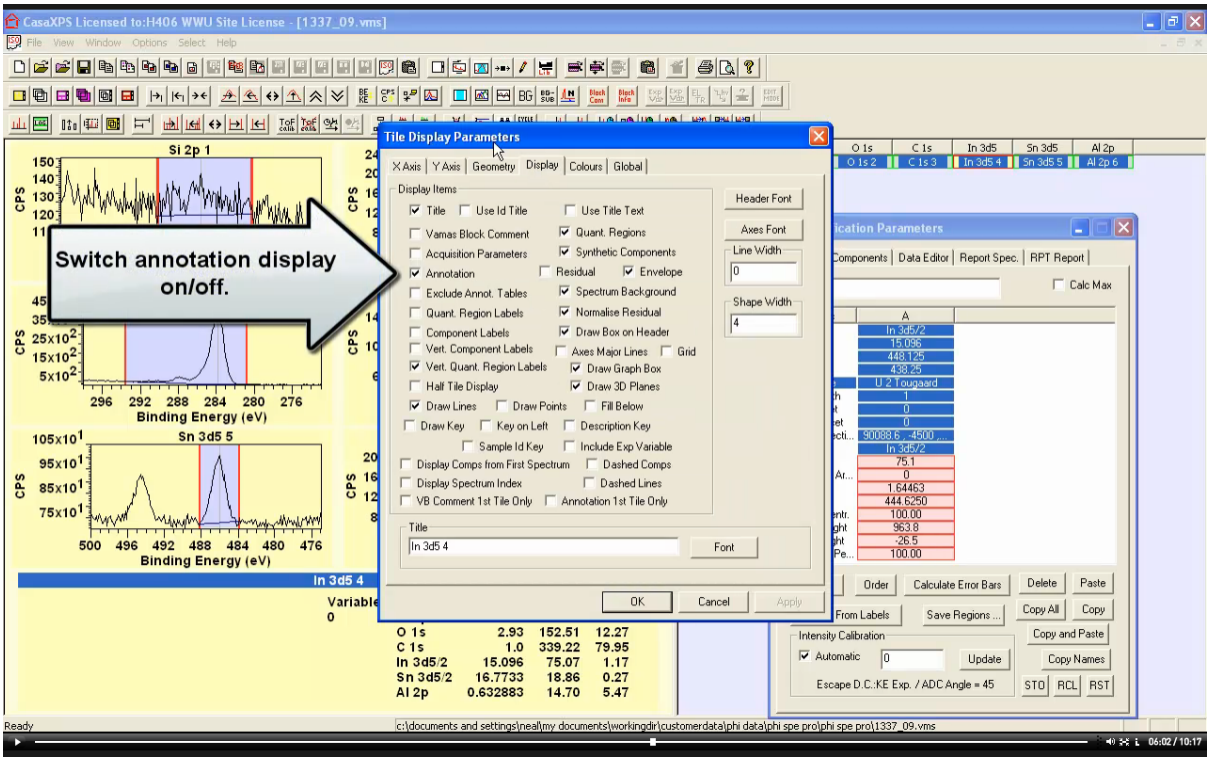

Options on the Tile Display Parameters dialog window, Display property page include a tick box that enables or disables the display of Annotation. It is also possible to exclude annotation tables from the display. The active display tile, indicated by the highlight bar positioned at the top of a display tile, is the bottom display tile. For the bottom display tile the annotation display option is enabled.

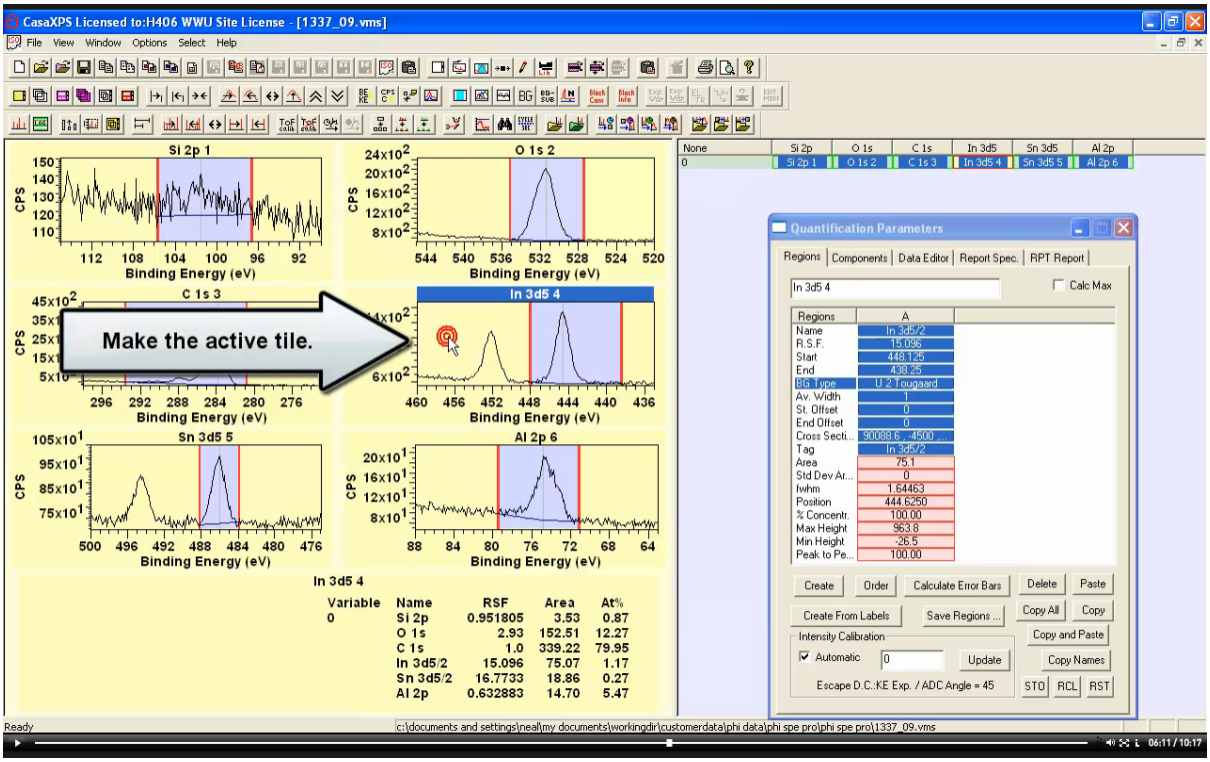

When the display tile displaying the In 3d spectrum is made the active tile, the display setting can be viewed via the Tile Display Parameter dialog window. For this particular display tile the Annotation

tick-box is disabled, thus the annotation table from the In 3d VAMAS block does not appear over data.

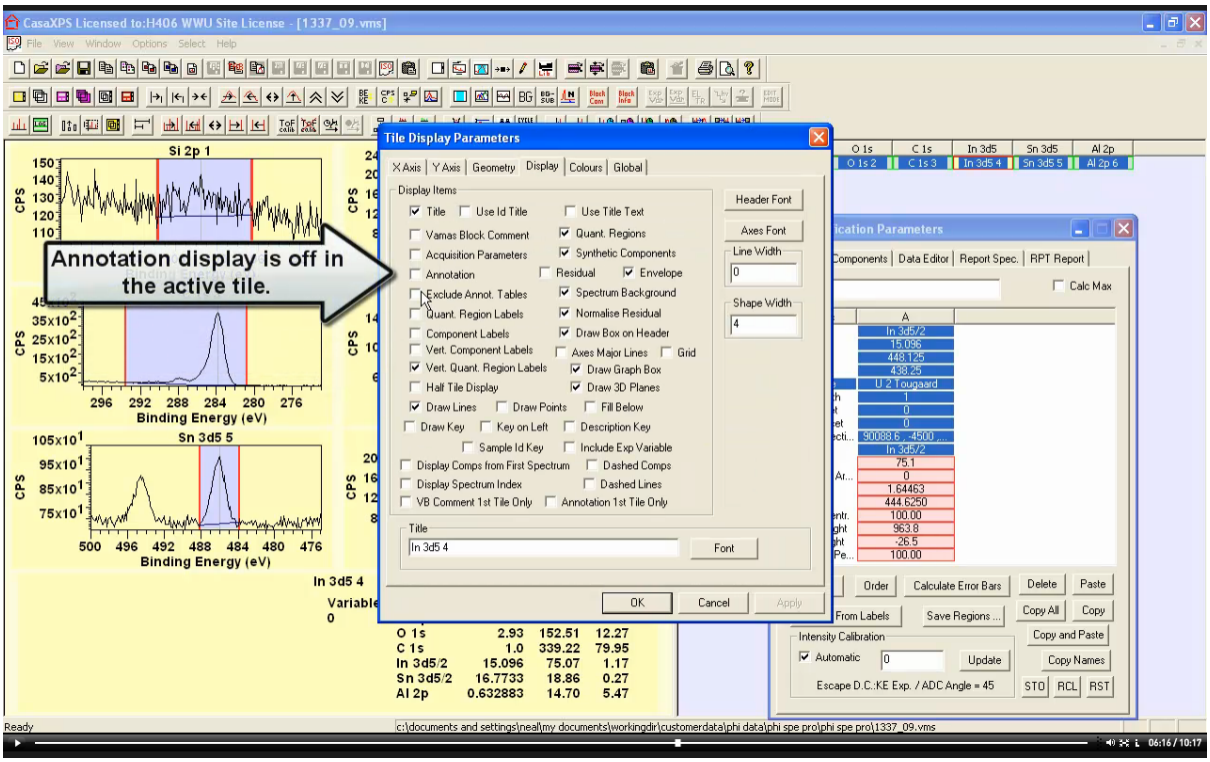

There is in addition to the display options a property page where a display tile can be switch to display annotation tables only. That is to say display options are almost completely disables with the exception of Annotation tables.

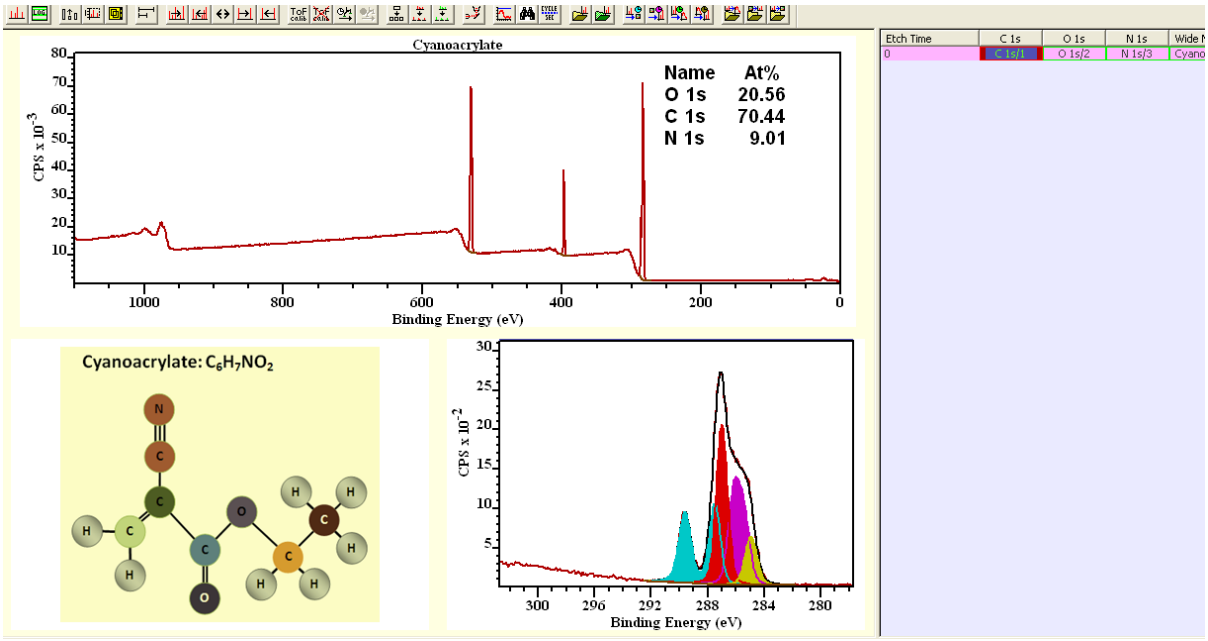

It is also possible to display one of a set of images from a set of bitmaps saved in the configuration directory CasaXPS.DEF/SlideShow. These display mode changes are selected via the Tile Display Parameters dialog, Geometry property page.

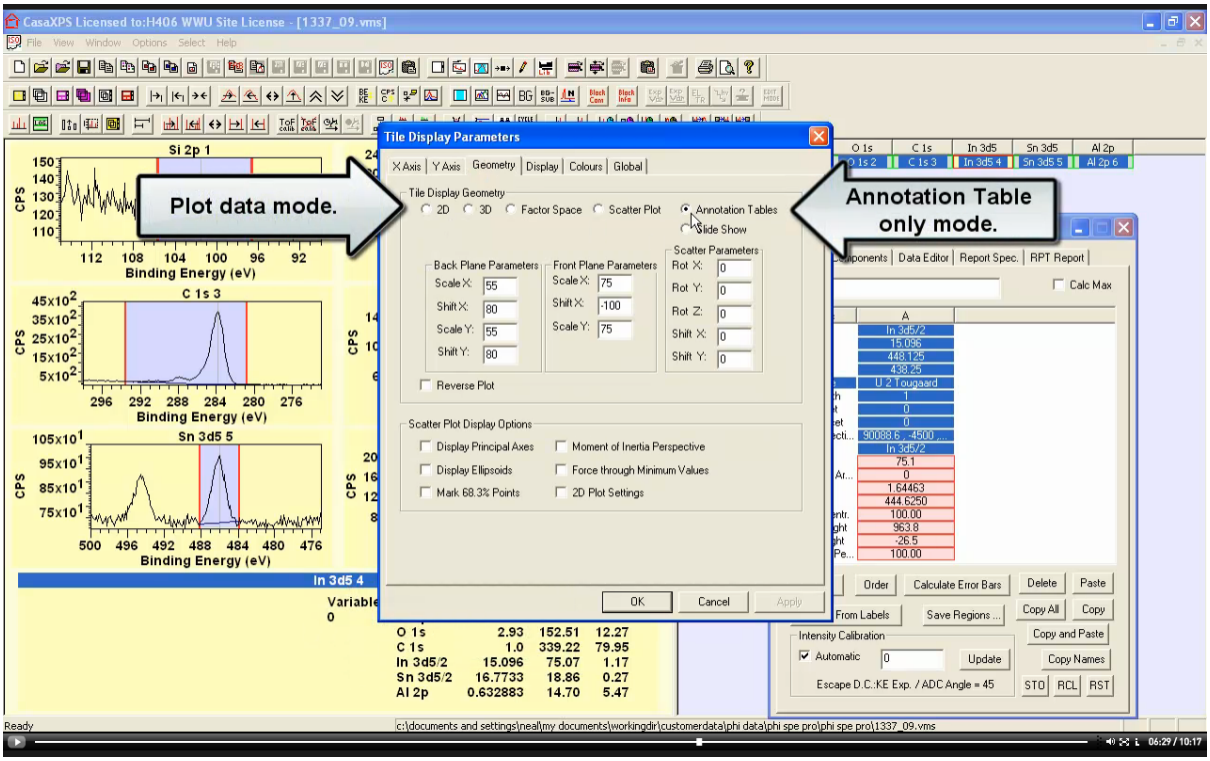

The difference between the two display tiles displaying information from In 3d VAMAS block is for the bottom tile the Tile Display Parameters dialog window Geometry property page radio button is selected for Annotation Tables where as the other In 3d display tile is selected for display of 2D spectra.

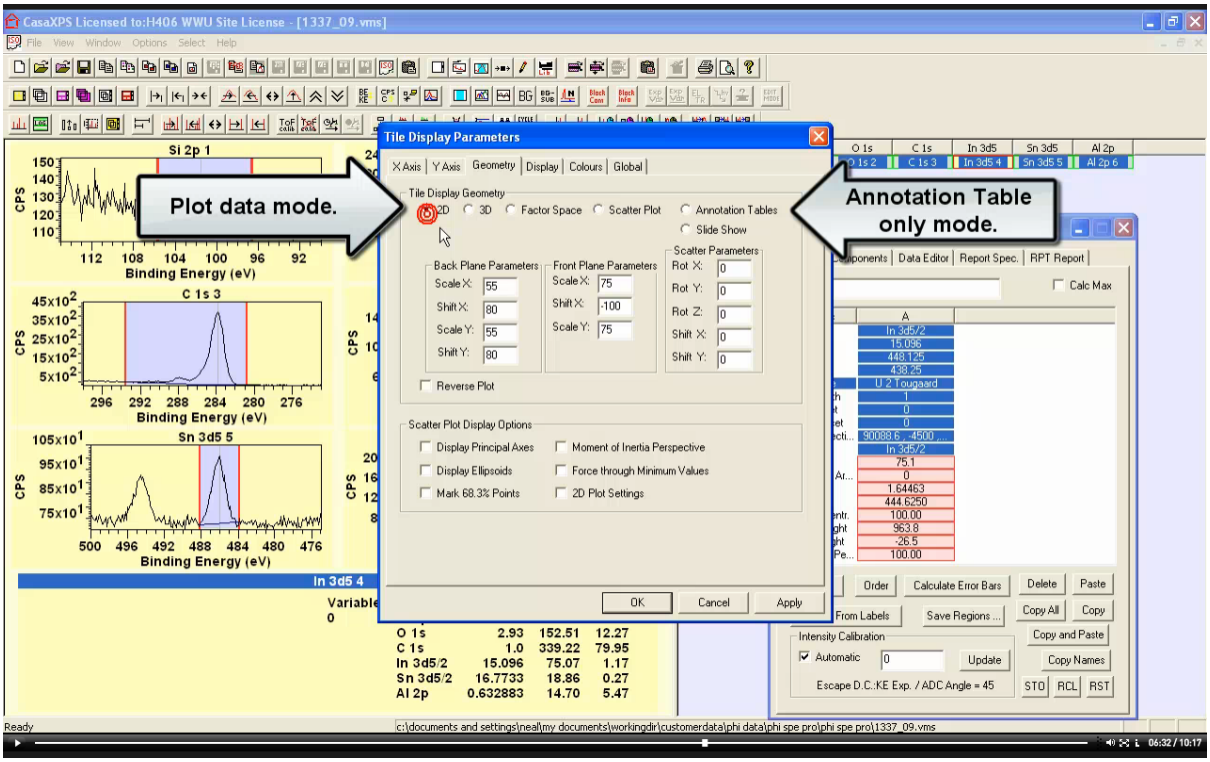

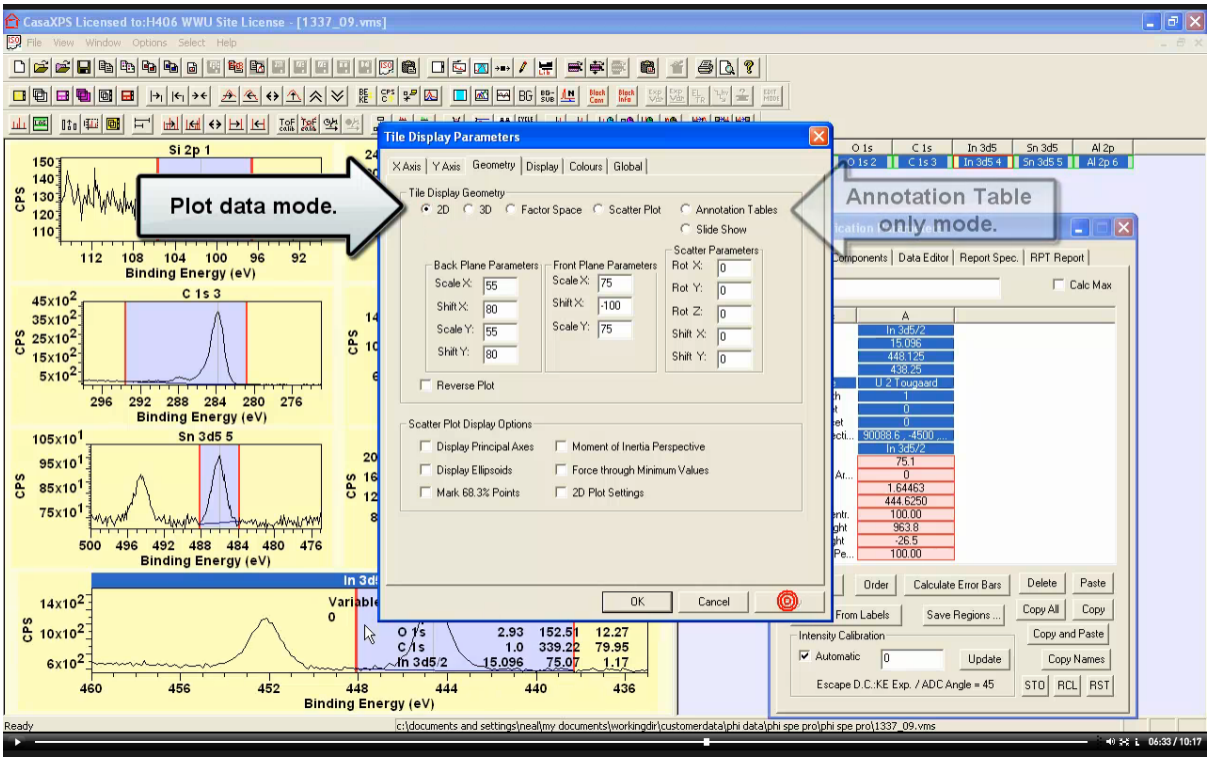

Switching the bottom display tile from Annotation Tables to 2D enables the display of In 3d data in the bottom display tile.

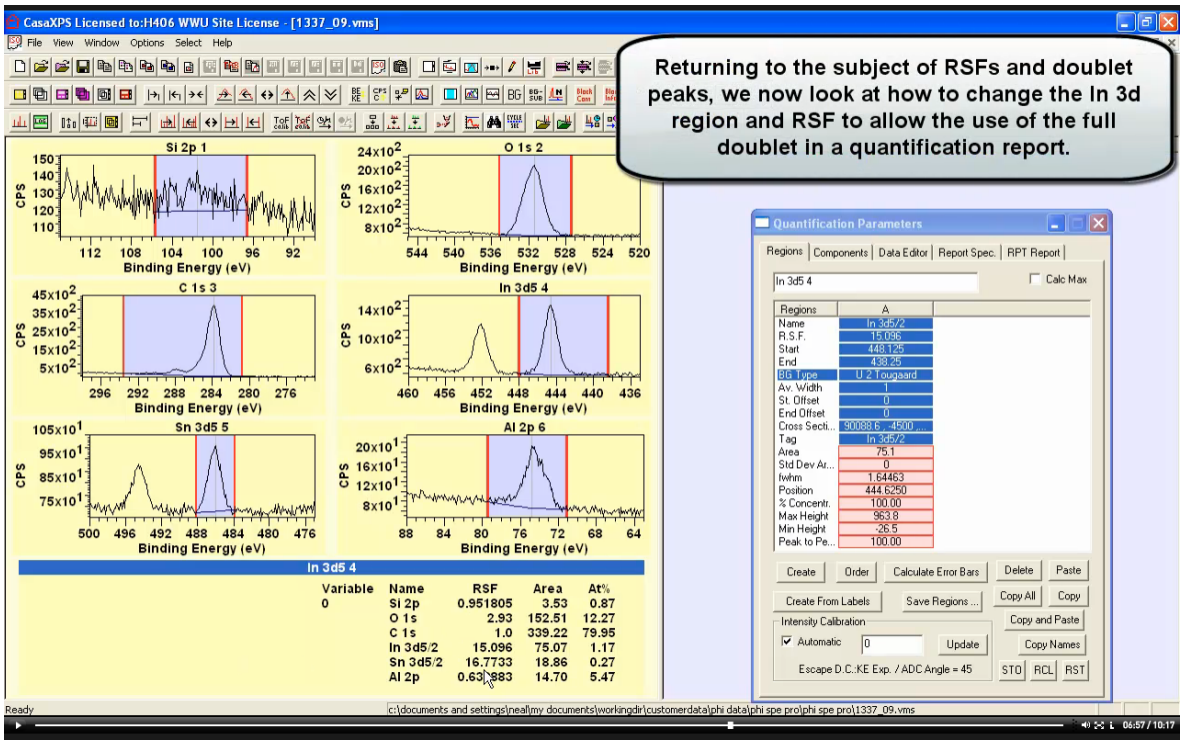

The following actions are intended to illustrate the relationship between region energy intervals, RSFs and quantification results. Currently the In 3d data are defined with a region energy interval corresponding to the larger of the two doublet peaks. The RSF within the region is assigned using the library RSF corresponding to In 3d 5/2. As a consequence the atomic concentration reported in the quantification table is 1.17%.

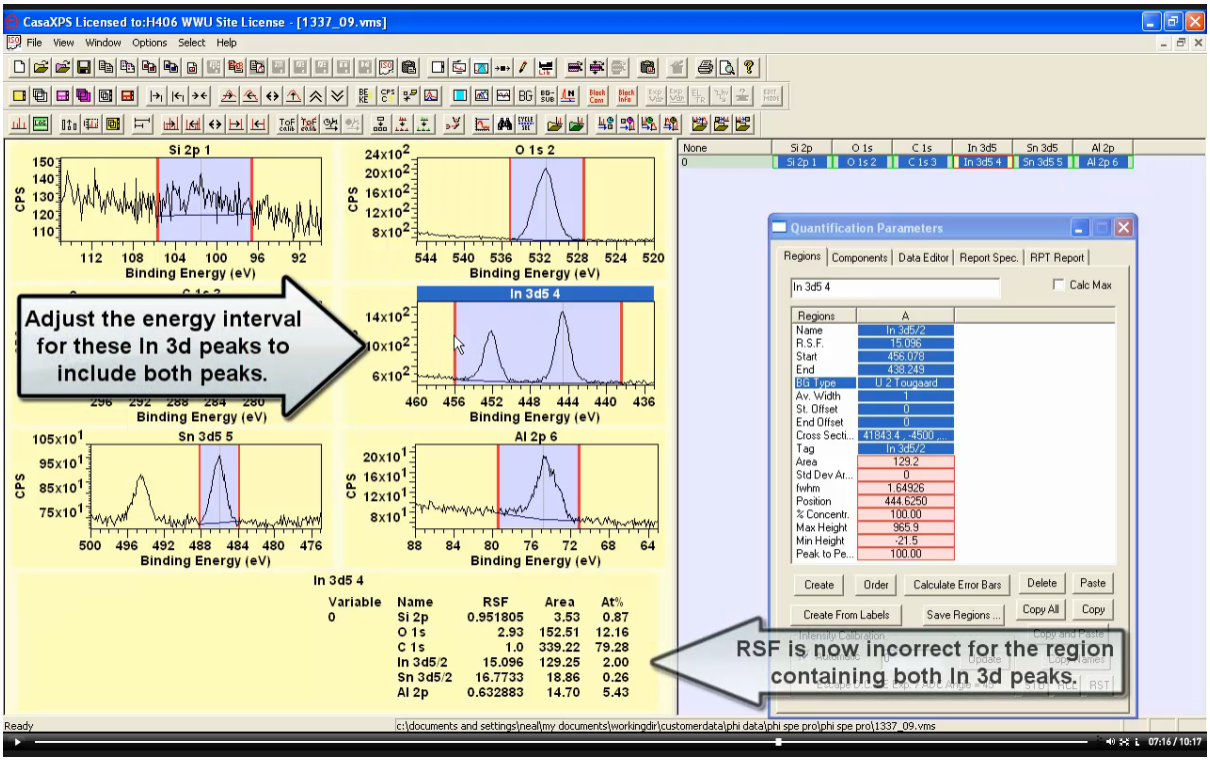

Changing the energy interval for In 3d to include both doublet peaks alters the atomic concentration percentage to 2.0% because the RSF is still assigned the value for In 3d 5/2 which is now incorrect for the energy interval defined.

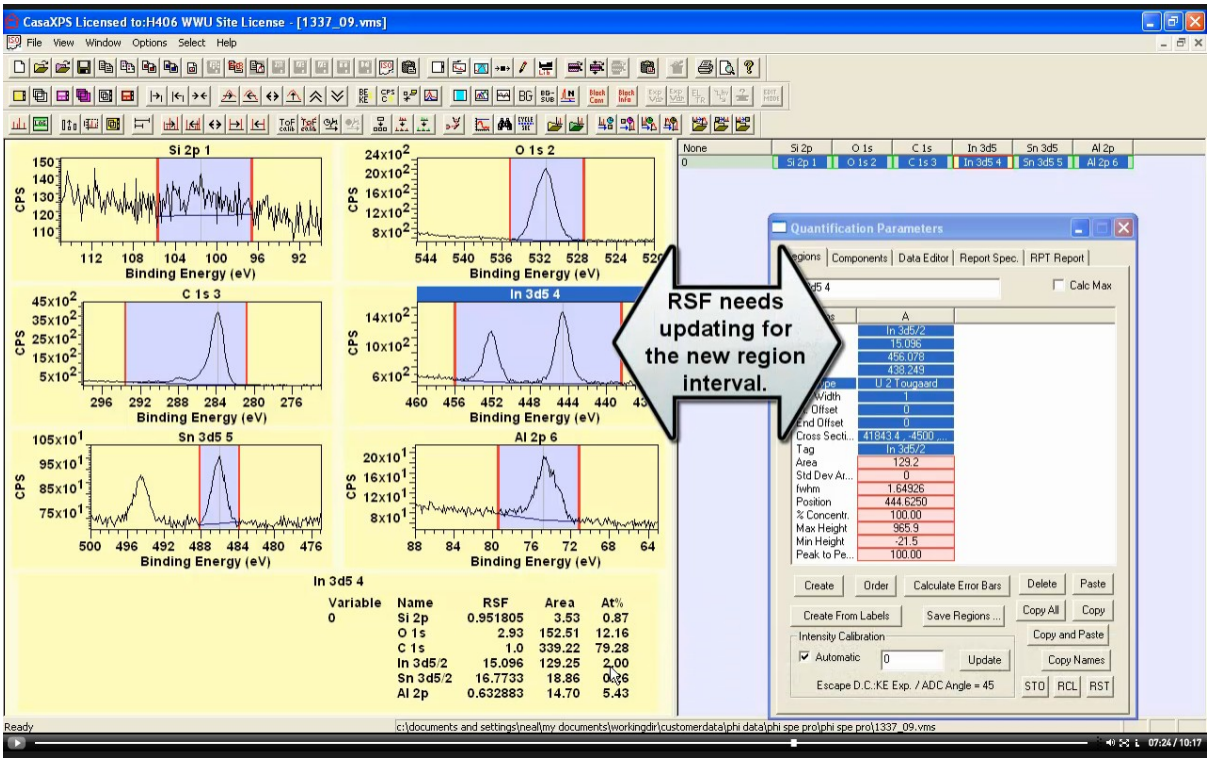

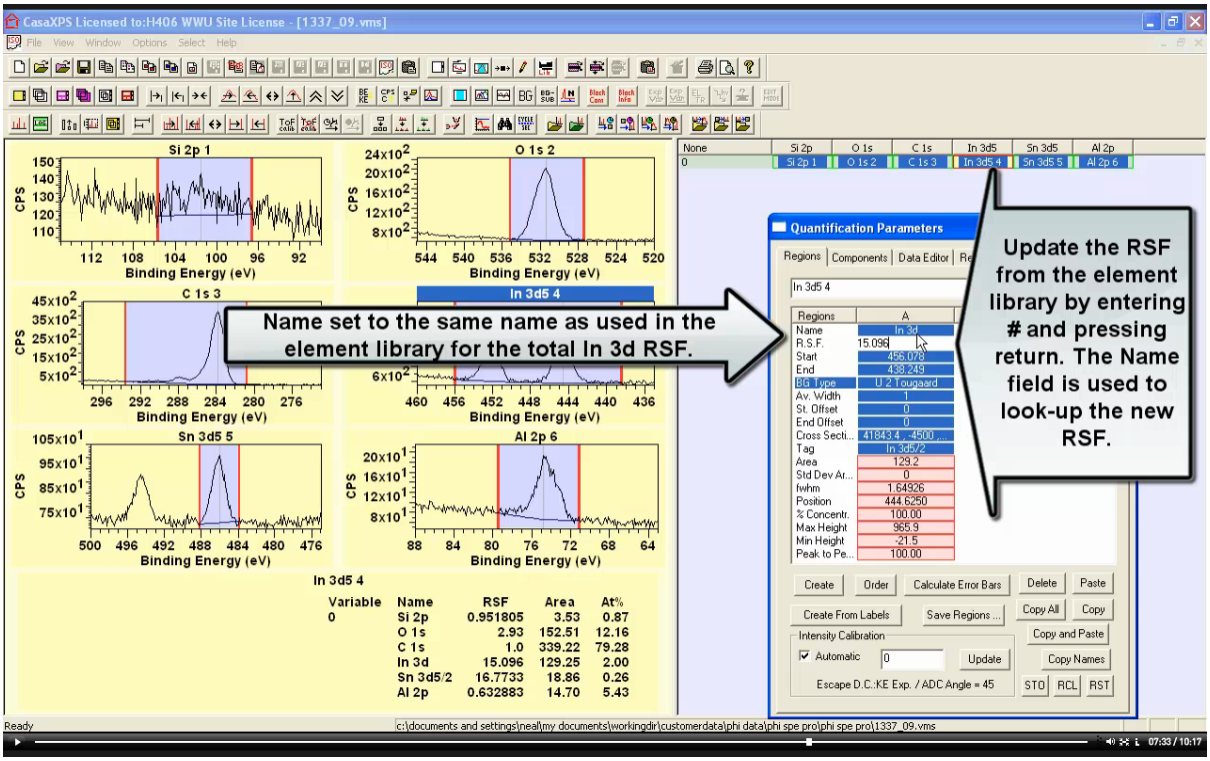

The RSF for In 3d where both peaks are included in the energy interval can be updated from the element library by changing the region name field from In 3d5/2 to In 3d and then within the RSF text-field the current values is replaced with the # character. On pressing return, the string entered in the name field is used to lookup the matching entry in the element library and the new RSF is entered into the RSF field. These data are measured from a PHI Quantum 2000 and therefore the library RSF is adjusted for angular distribution resulting in a value of 25.5453 for both In 3d peaks.

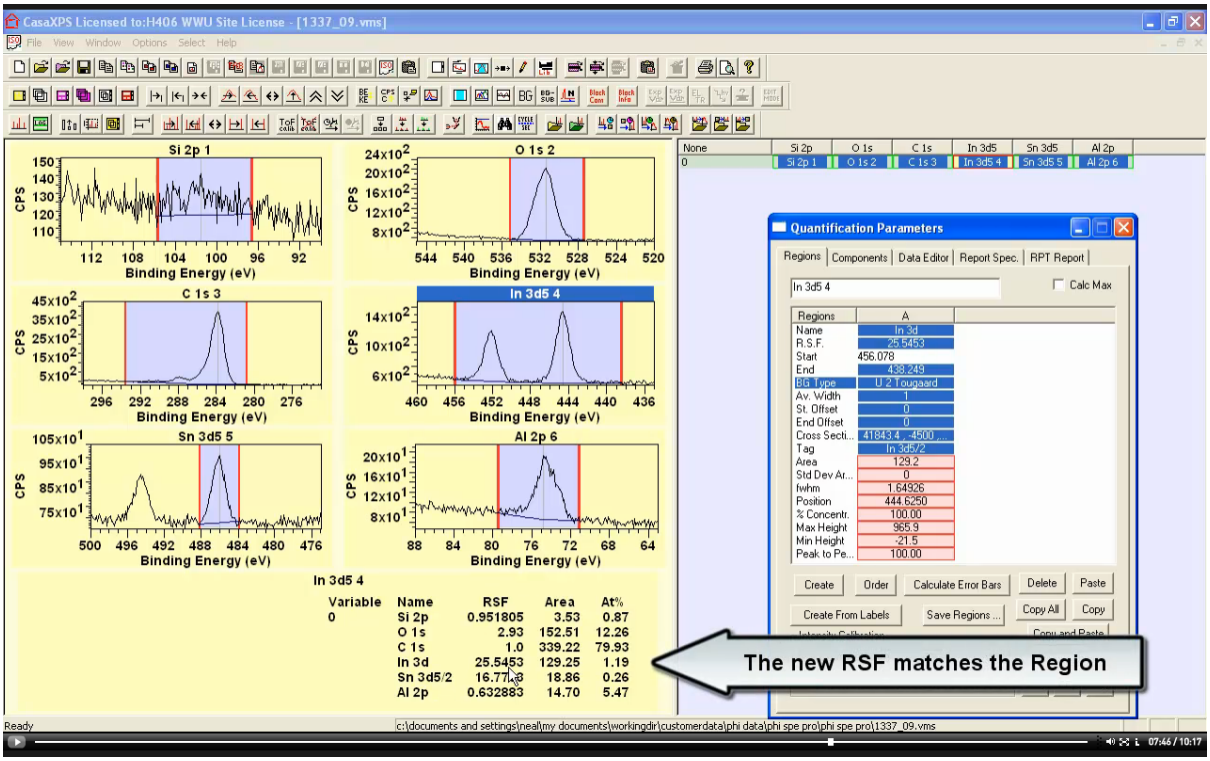

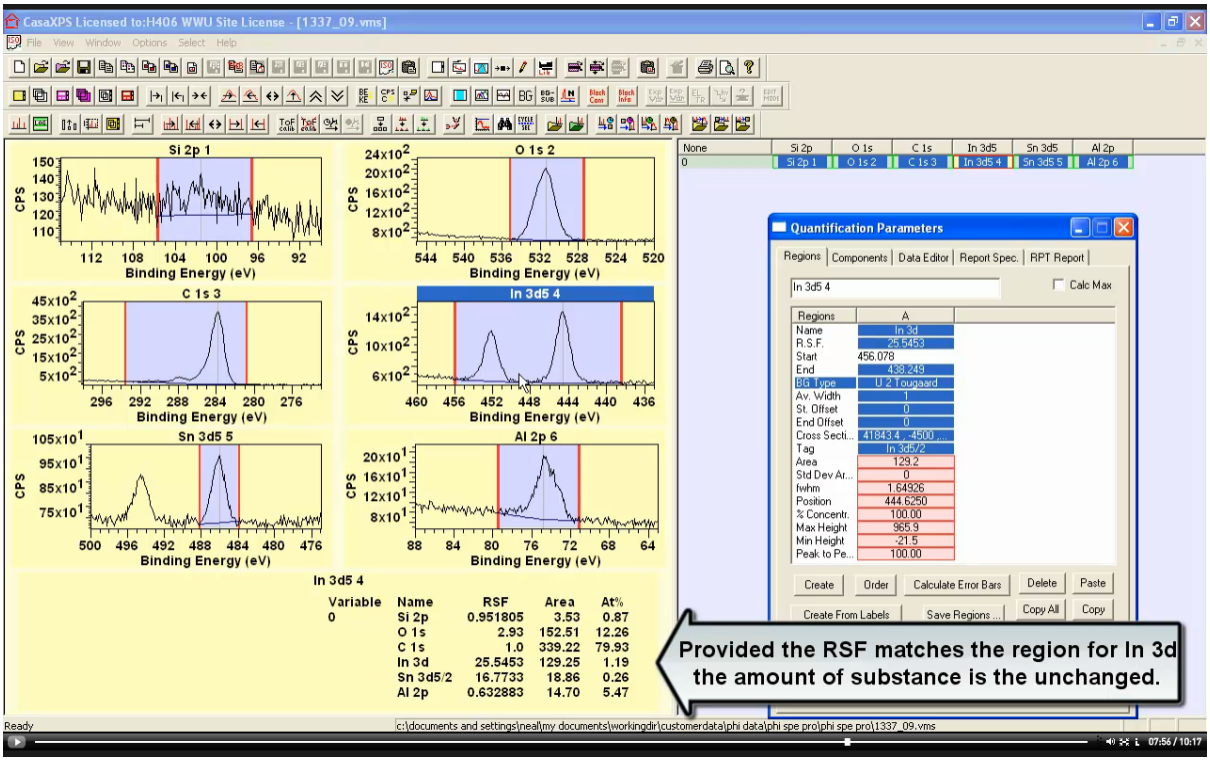

Once the correct RSF is entered for both doublet peaks the atomic concentration reports 1.19% for indium, which is consistent with the quantification computed using the In 3d5/2 peak and RSF.

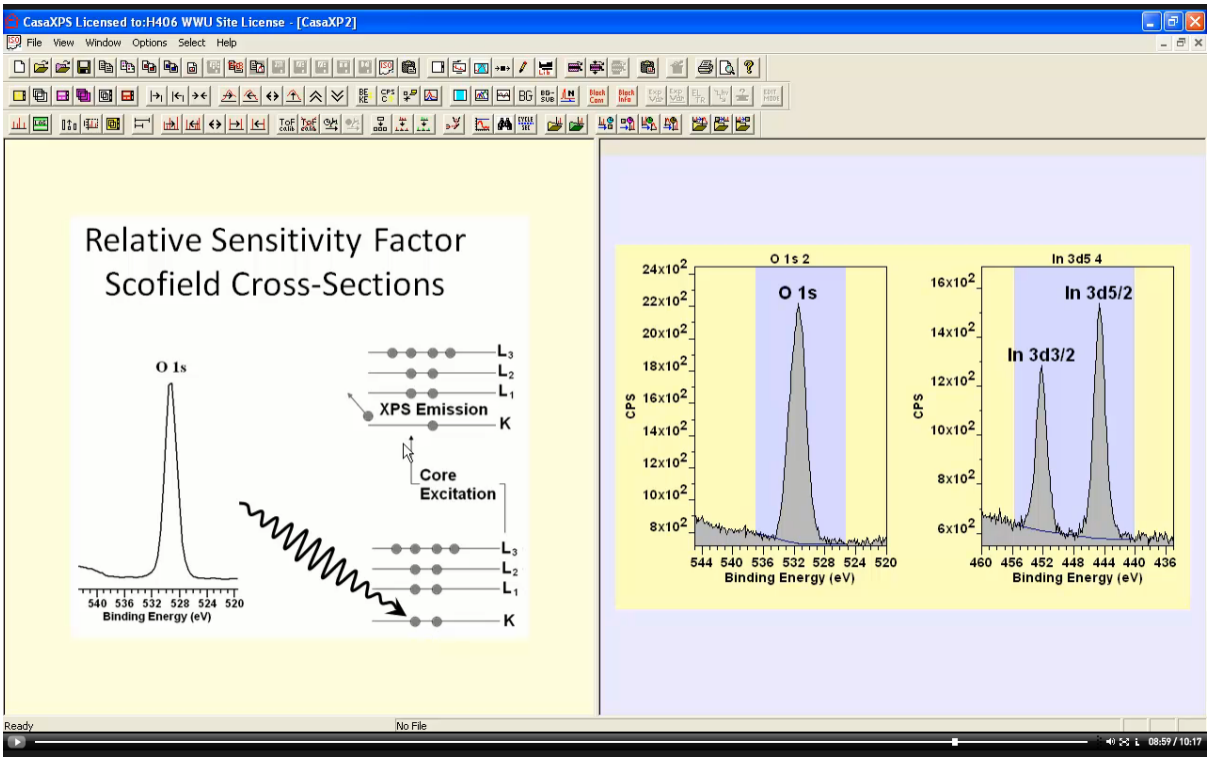

Photoemission from s-orbital result in a single energy for the atom and a single energy for the final state ion, hence s-orbitals nominally result in one peak.

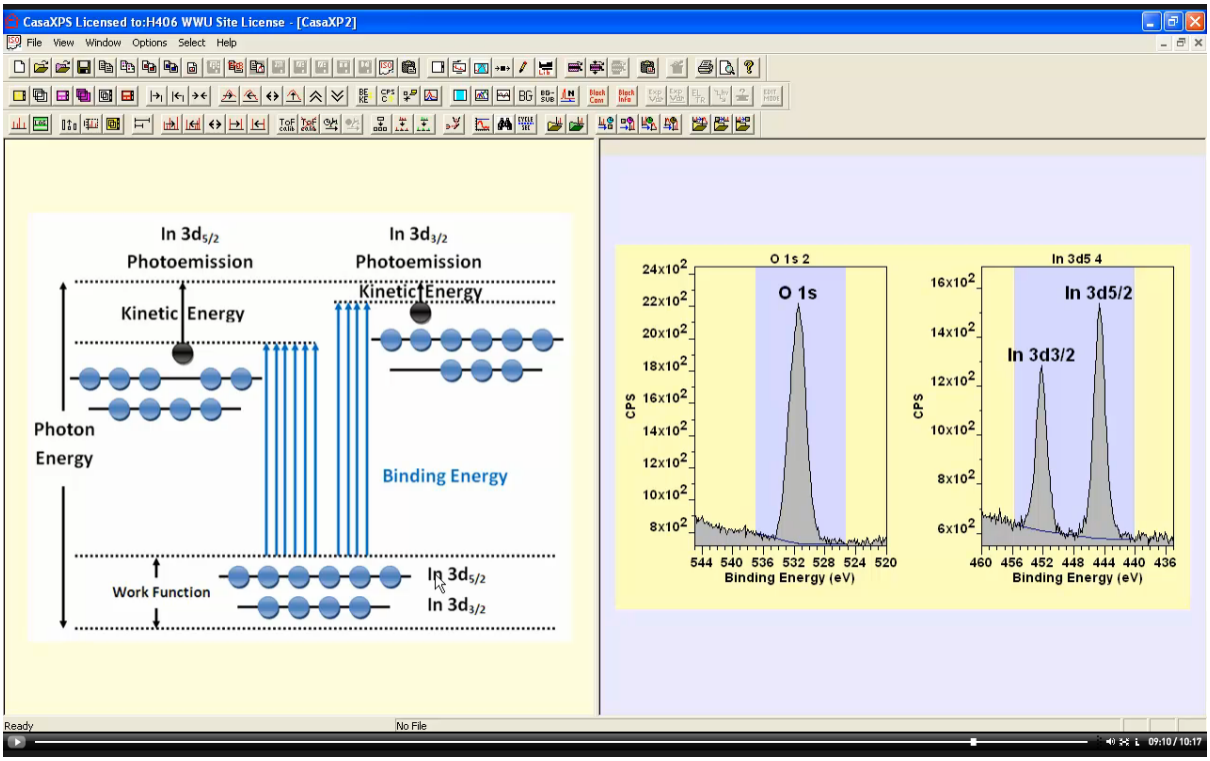

Photoemission corresponding to orbital angular momentum greater than zero (p, d ,f …) allows final state splitting of energy due to spin orbit interactions and these result in doublet peaks in XPS.

Test Peak Model: A Tool for Estimating Line Shape

This video looks at line shapes and how line shapes can be estimated from data.

The example used to illustrate how a line shape can be modified to reflect shapes in data via the Test Peak Model option on the Quantification Parameters dialog window Components property page is a Si 2p doublet. Data are measured using an acquisition mode optimised for quality of signal rather than for sensitivity. High sensitivity means high count rates which are achieved by compromising signal quality and therefore energy resolution. Quality of signal means restricting apertures allowing focused image quality signal to enter the hemispherical analyser (HSA) operating at low pass energy to provide maximum energy dispersion. The Si 2p doublet used throughout this video is recorded using medium magnification transfer lens mode limited to a 55um analysis area by a selected area aperture, the image of which projects signal spot of size equivalent to two thirds the width of the entrance aperture into the HSA. The silicon sample is assumed to be and evidence supports the assumption of a clean oxide free elemental silicon surface.

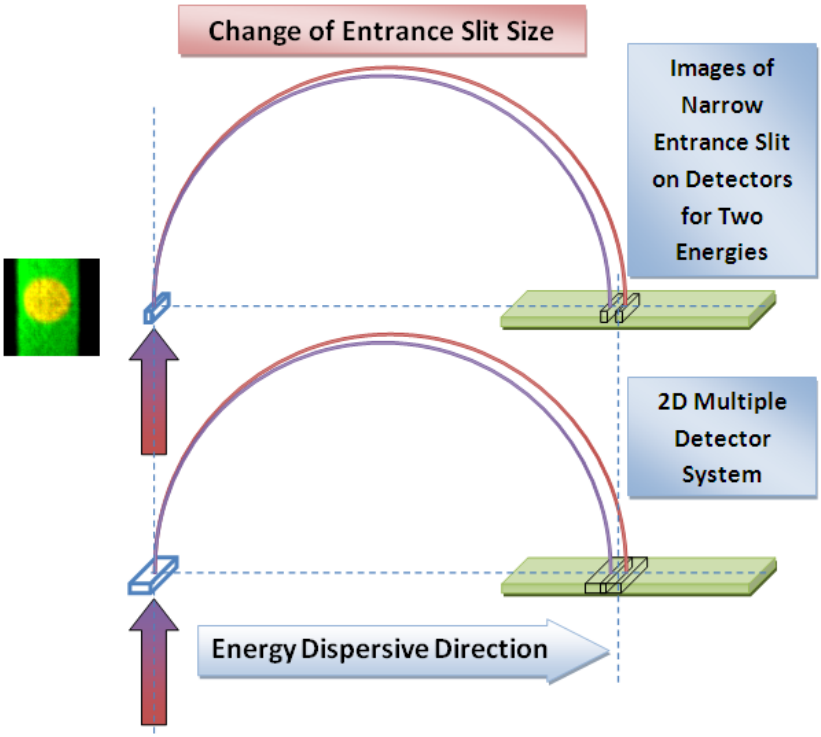

The shape modelled in this video is asymmetric in both Si 2p doublet components. The origin for this asymmetry is not entirely clear from these data, but the two most likely reasons relate to the semiconductor nature of Si 2p following a photoemission response observed in similar materials and/or these narrow Si 2p peaks include instrumental artefacts such as geometric aberration for HSA instruments that is a potential explanation of signal originating with a given energy but is recorded at a lower kinetic energy by the detection system. Regardless of origin, these doublet peaks provide an example where asymmetry in a synthetic line shape is an appropriate tool for estimating photoemission signal attributed to silicon.

The line shape used to model asymmetry is as follows.

Underlying Asymmetric Lineshape:

$$T(x:\alpha,\mu)=\left[\frac{1}{1+4x^2}\right]^{\alpha}\times\frac{1}{2}\left[\frac{\pi}{2}-tan^{-1}(2x)+\frac{\pi}{\mu}\right]\cdots\quad \mu>0\ \&\ \alpha>0$$

Gaussian Modified Lineshape:

$$TLA(x:\alpha,\mu,\omega)=N\int_{-\infty}^{\infty}T(\tau:\alpha,\mu)g(x-\tau:\omega)d\tau$$

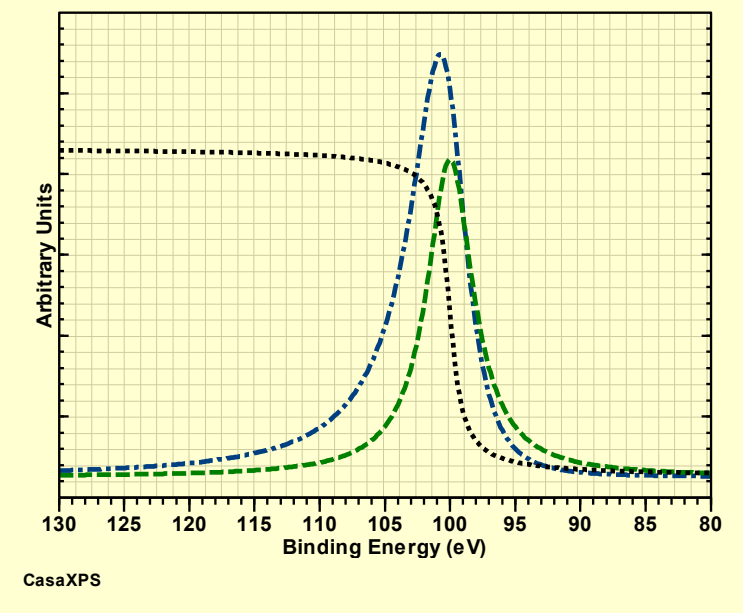

Step curve $\left[\frac{\pi}{2}-tan^{-1}(2x)+\frac{\pi}{\mu}\right]$ (dot, $\mu=1$), Lorentzian $\left[\frac{1}{1+4x^2}\right]^{\alpha}$ (dash, $\alpha=1$) and product of step curve with Lorentzian $\left[\frac{1}{1+4x^2}\right]^{\alpha}\times\frac{1}{2}\left[\frac{\pi}{2}-tan^{-1}(2x)+\frac{\pi}{\mu}\right]$ (dot/dash) (not drawn to scale).

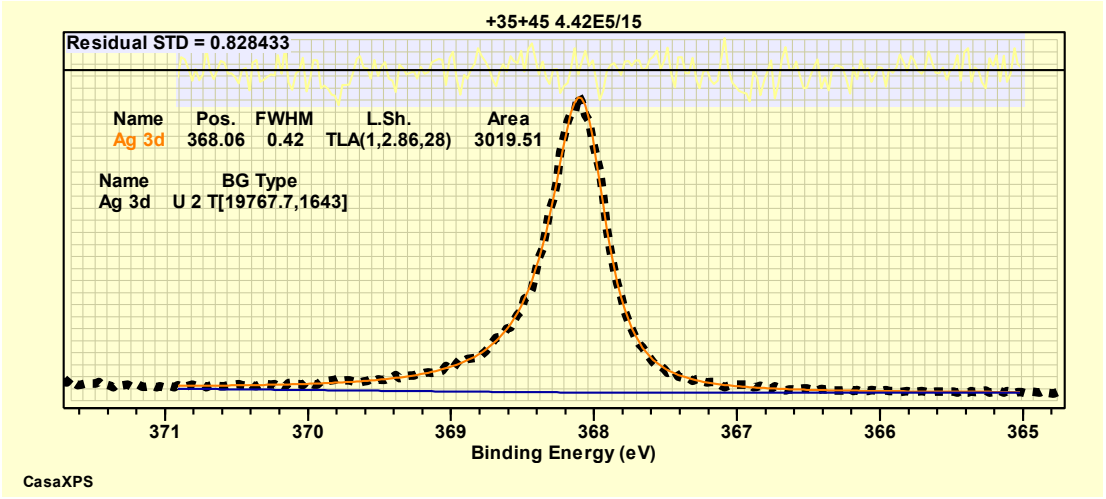

Ag $3d_{5/2}$ spectrum measured from Kratos Axis Ultra, PE5 in Hybrid lens mode using a limited and selected range of DLD logical detectors.

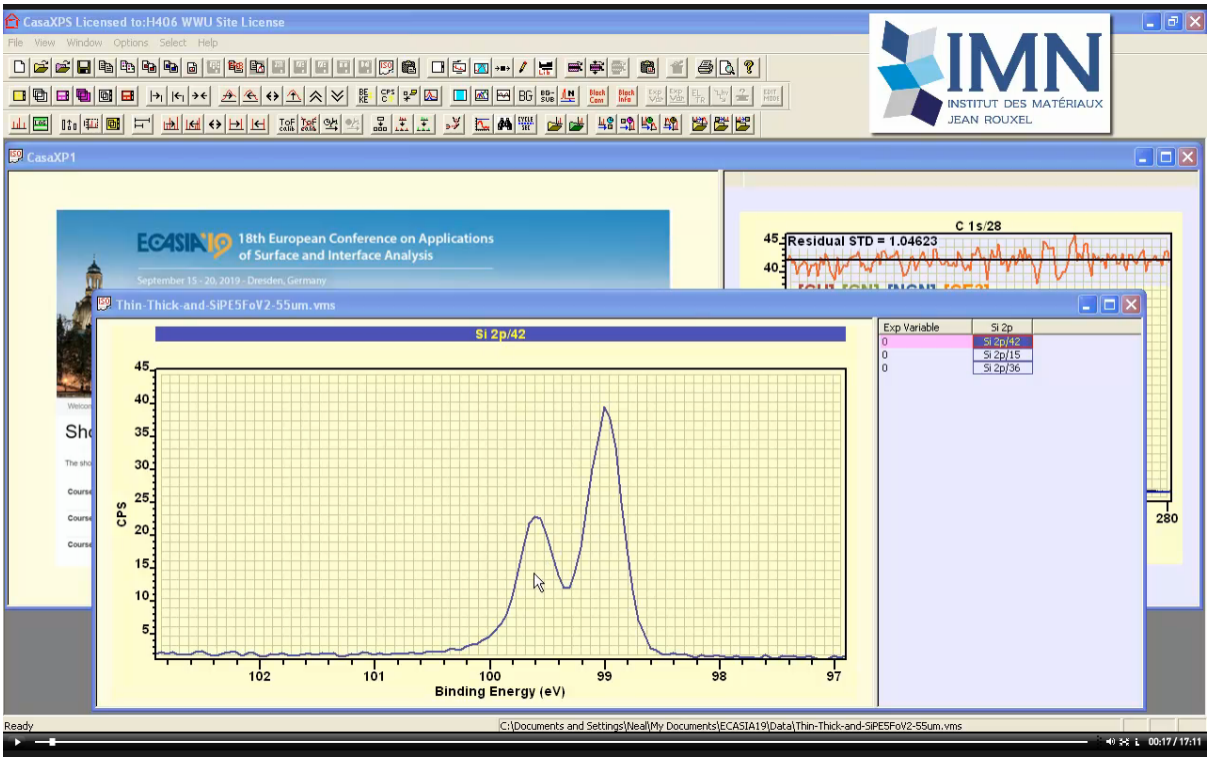

Si 2p represents a photoemission process slit by spin-orbital interactions into two component peaks. In this video data measured from a clean elemental silicon surface result in two energy resolved peak exhibiting asymmetry. The first task when considering data is the possibility peak shapes are the result of chemically shifted signal. Comparisons with samples similar to the clean silicon are made via Si 2p spectra as a means of estimating the potential influences of chemical state.

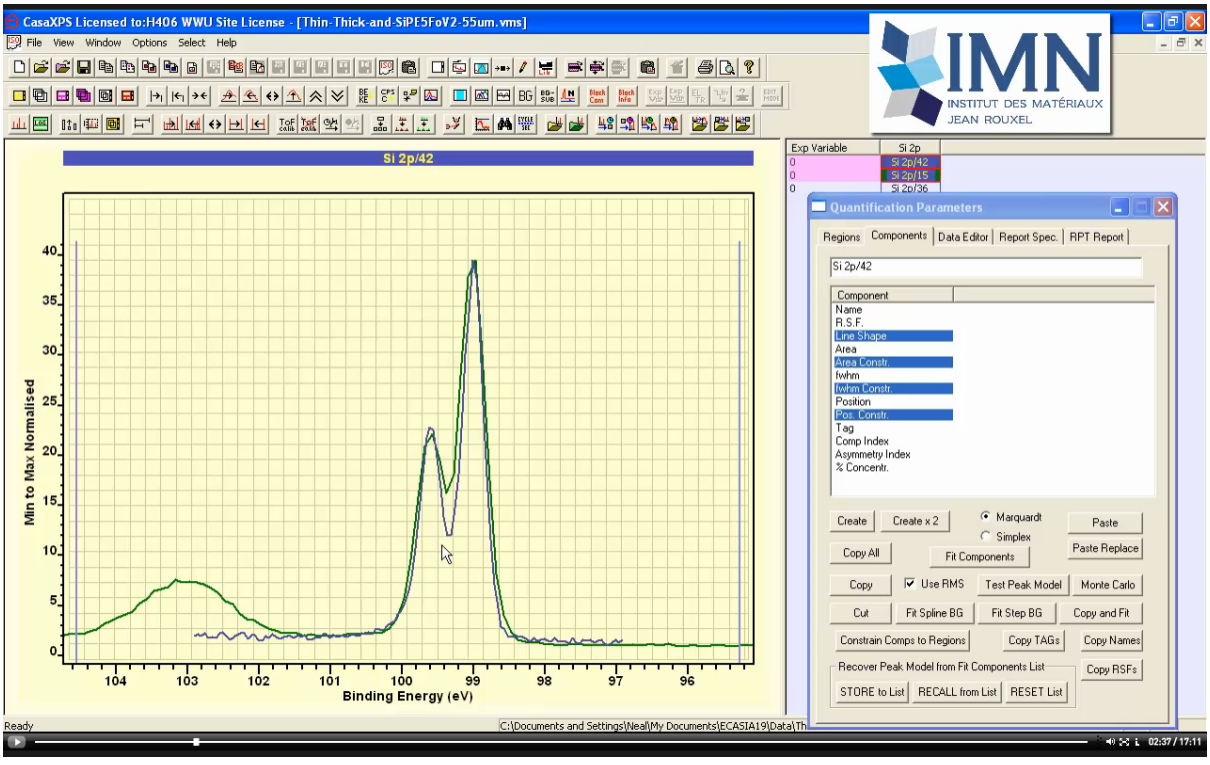

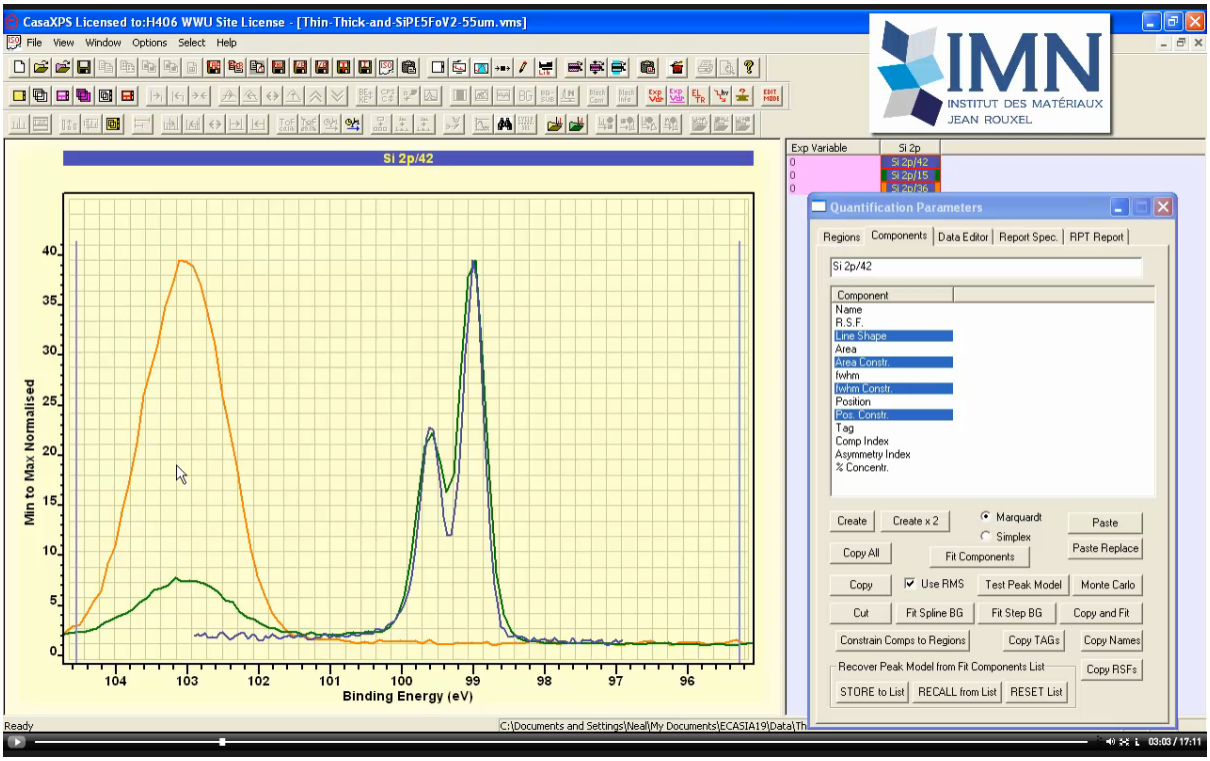

Si 2p data measured from clean silicon appears to be without significant oxide so the assumption is made that these peaks can be assigned to photoemission from silicon only.

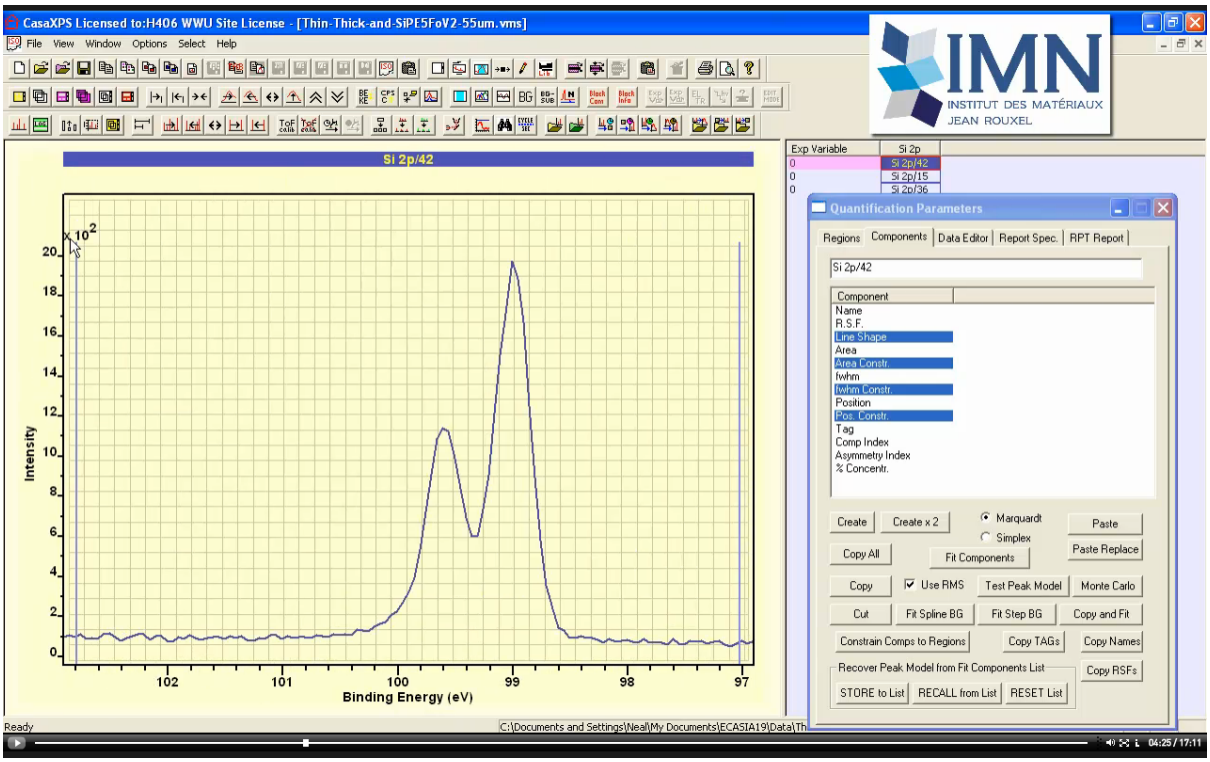

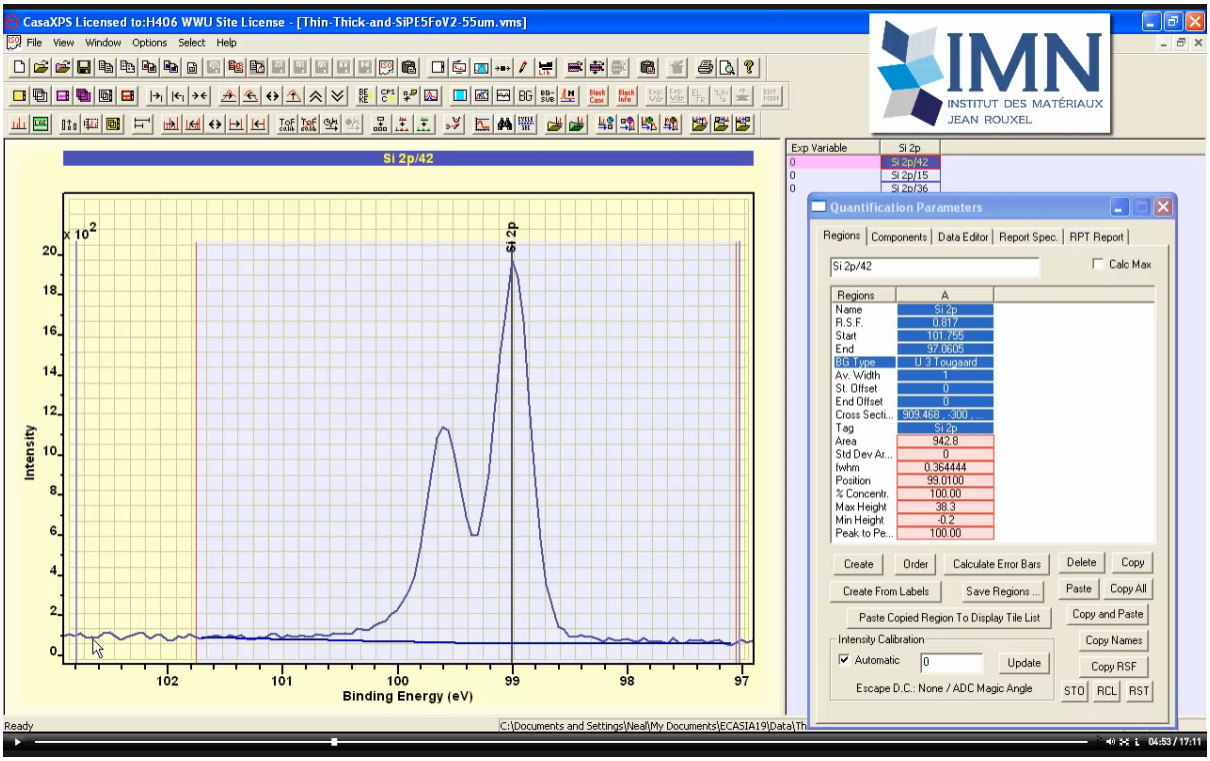

A single region is added to the VAMAS block containing Si 2p data from clean silicon. U 3 Tougaard background type is used to create an approximation to inelastic scattered background beneath Si 2p photoemission signal.

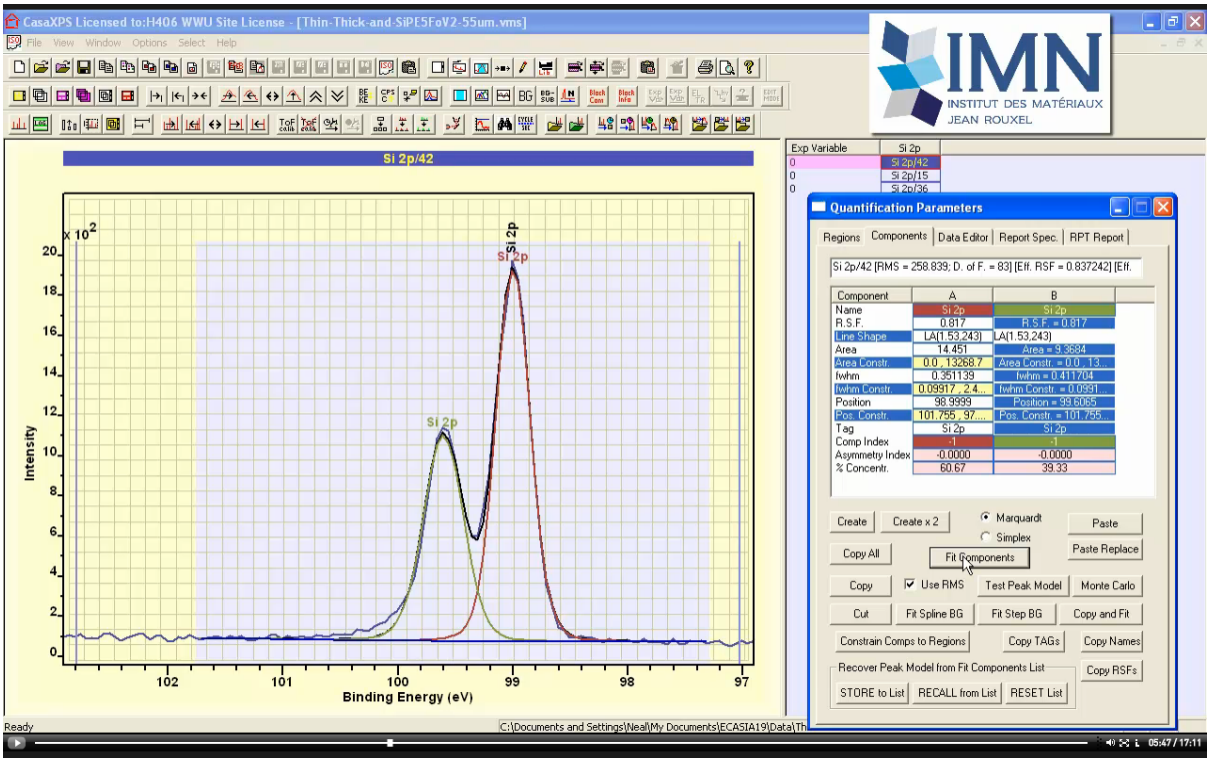

Initially, two component peaks with symmetric line shapes are added to the VAMAS block containing Si 2p data. These components when fitted do not produce expected data reproduction.

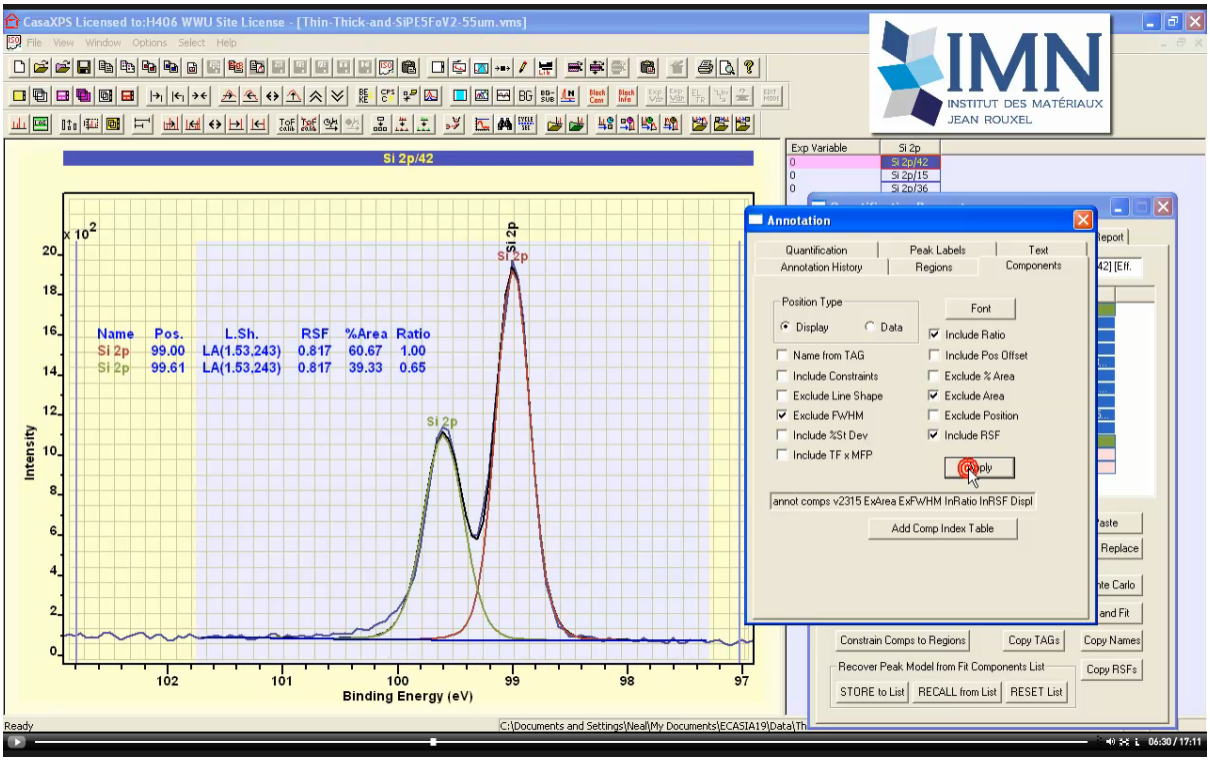

Adding an annotation table gathered from data displayed in the active display tile illustrates that these symmetrical peaks not only fail to reproduce these data the physical relationship between p-orbital photoemission doublets, namely, 2:1 intensity ratio is also less than perfect.

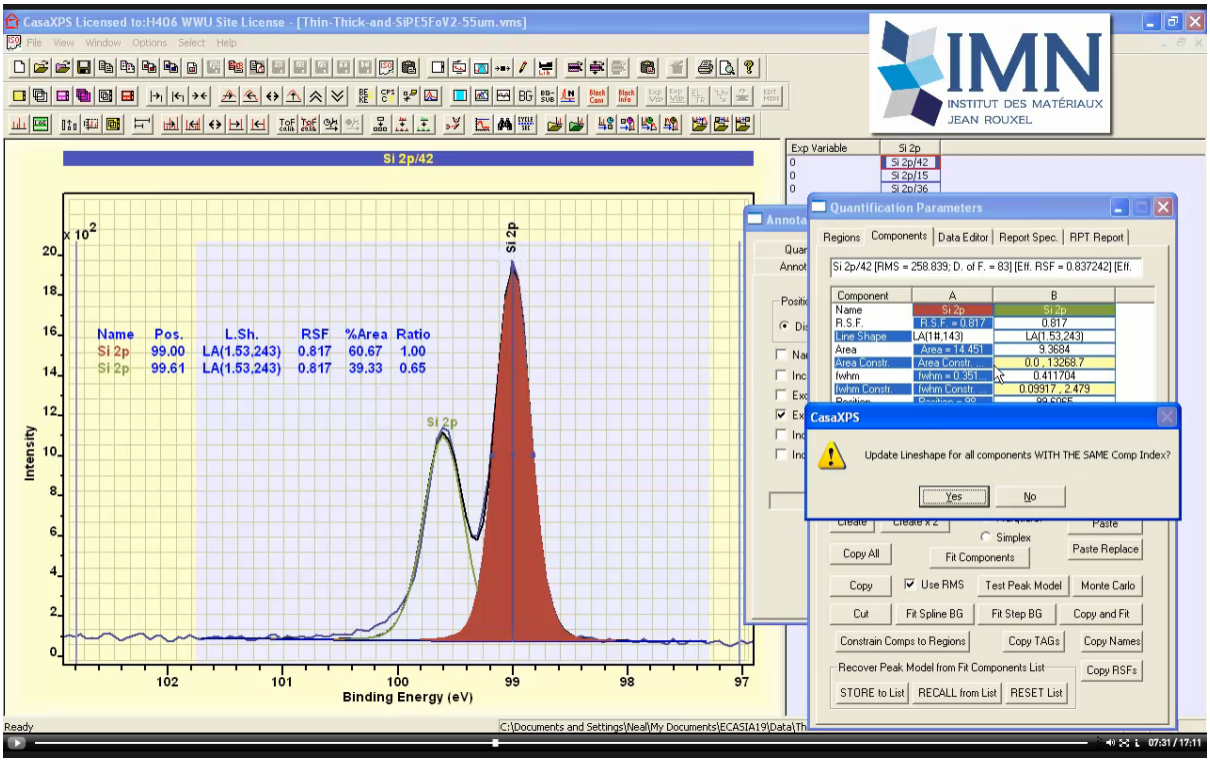

A more Lorentzian shapes lineshape is introduced in an attempt to model signal spread towards higher binding energy not accounted for by the initial line shape. A # character is used to copy the line shape entered in column A to the component in column B too.

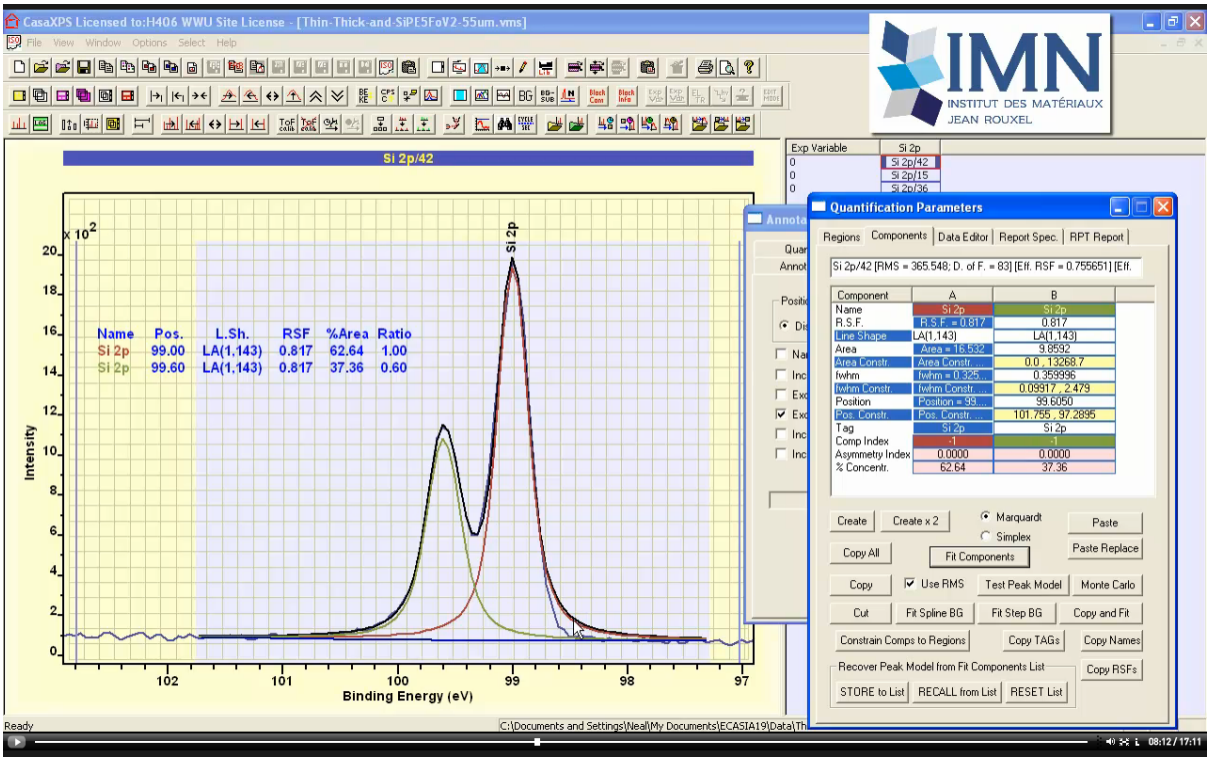

The new line shape, when fitted to these data, models peak maxima well and also accounts for signal to higher binding energy, but unfortunately introduces an error in terms of data reproduction to lower binding energy for these data.

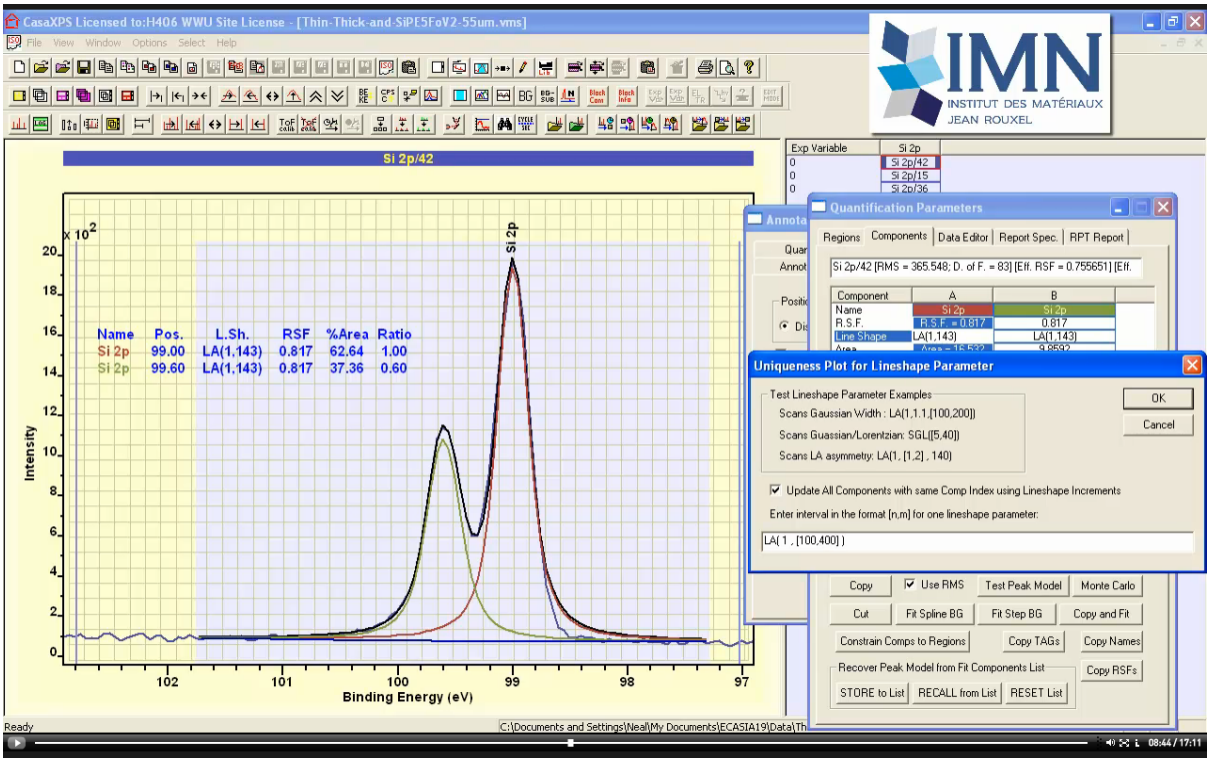

As a means of testing adjustments to the current line shape, the Test Peak Model button is made use of to scan a line shape parameter and perform a fit of the new peak model to Si 2p data. A line shape text-field is selected prior to pressing the button on the Components property page labelled Test

Peak Model. The result of such a line shape scan is a new file contain the original spectra fitted with a range of line shapes defined by adjustments to the parameter for which a value is specified using an interval within a pair of square brackets. The first example for the use of Test Peak Model is an interval for the Gaussian width parameter specified using the lineshape LA(1 , [100,400]).

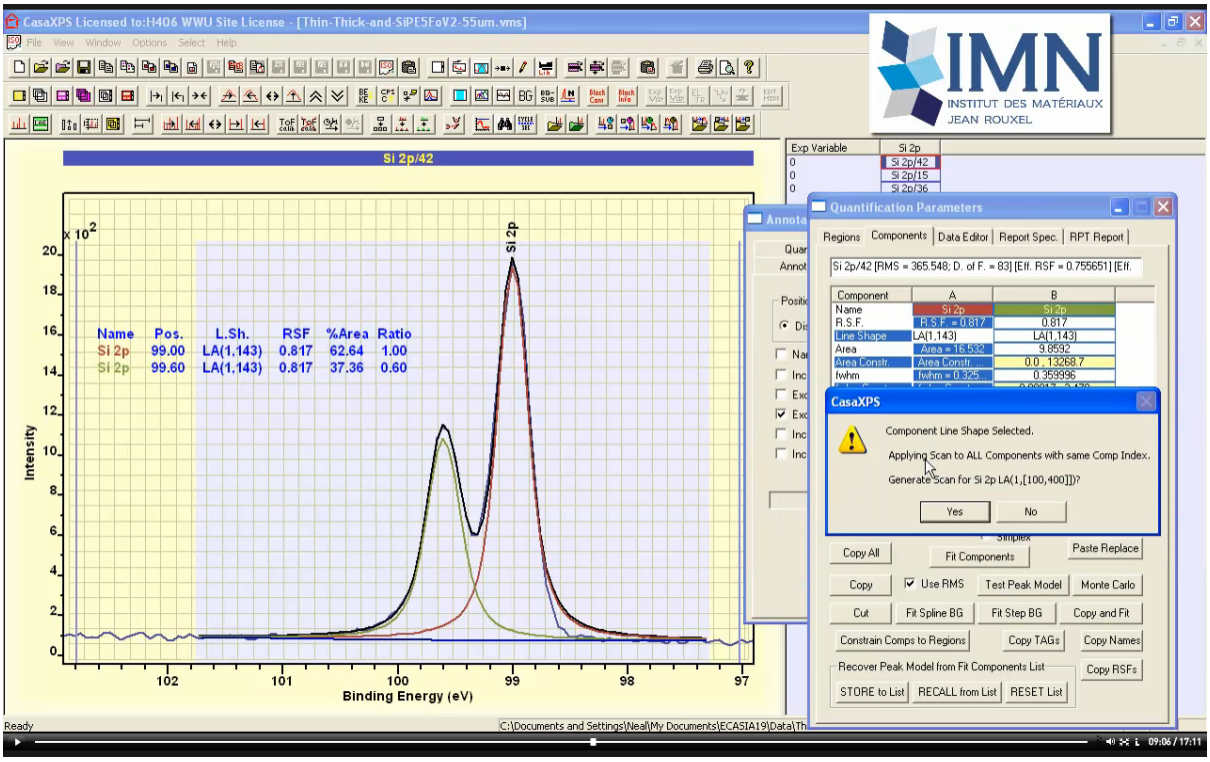

The result of scanning the Gaussian parameter is a plot for the figure of merit obtained by optimising the peak model including the new line shapes. Each spectrum fitted with a new peak model is also added to a new file. These spectra and fits of different peak models to the original spectrum is designed to allow line shapes and their influence on physical values to be assessed rather than simply relying on a figure of merit to identify the optimum choice for a line shape parameter.

Line shape parameters alter a very important property for a component peak that, when fitted as part of a peak model to data, significantly alters the physical parameters such as component binding energy or component intensity, both of which are typically significant to understanding sample chemistry. The property altered is the shape used to model photoemission signal and, in terms of optimisation, accurate photoemission shape represents the best chance of returning scientifically significant results by fitting components to data without user bias. A good figure of merit indicates good data reproduction but does not imply a correct peak model. Line shapes and the correct number of component peaks making use of correct line shapes and background fitted to data with a good figure of merit does imply scientific meaning can be assigned to binding energies and component intensities. A study of potential line shapes for a given sample and a given instrument is therefore an essential part of XPS data analysis based on the fitting of data by peak models.

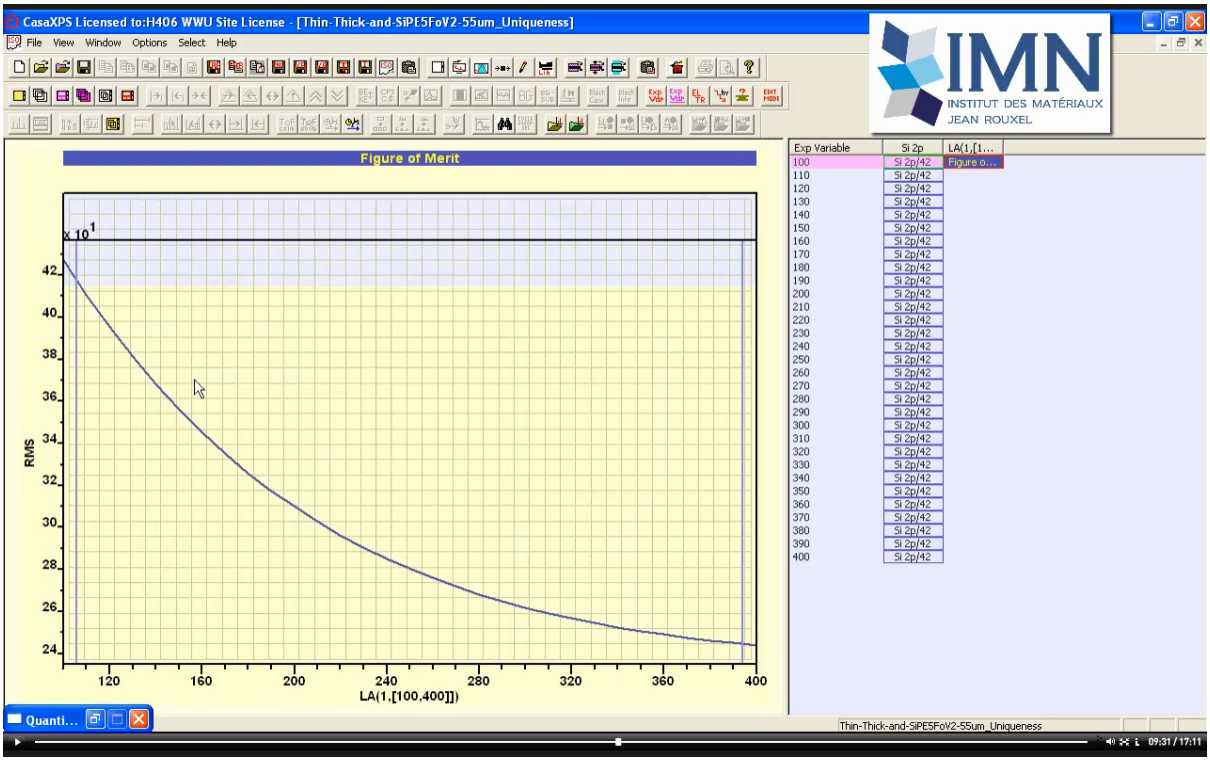

A figure of merit plot as a function of line shape parameter offers a tool for assessing changes induced by adjustments to a line shape parameter. However, observing the trend in terms of physical properties, such as the ratio for the p-orbital spin-orbit split doublet signal, is more important than the figure of merit. Scanning through these VAMAS blocks fitted with slightly different line shapes observing figure of merit, ratio of peaks and the way line shapes alter the fit to data provide guidance to best guess line shapes and subsequent line shape tests.

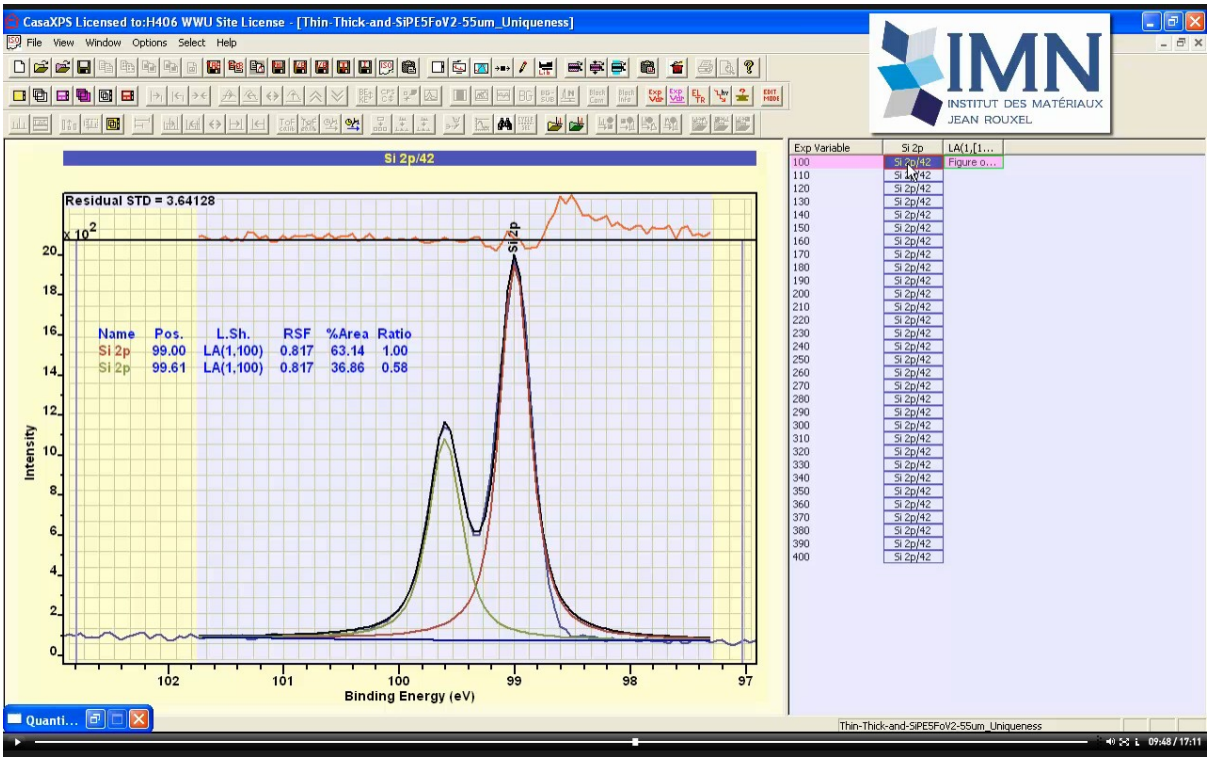

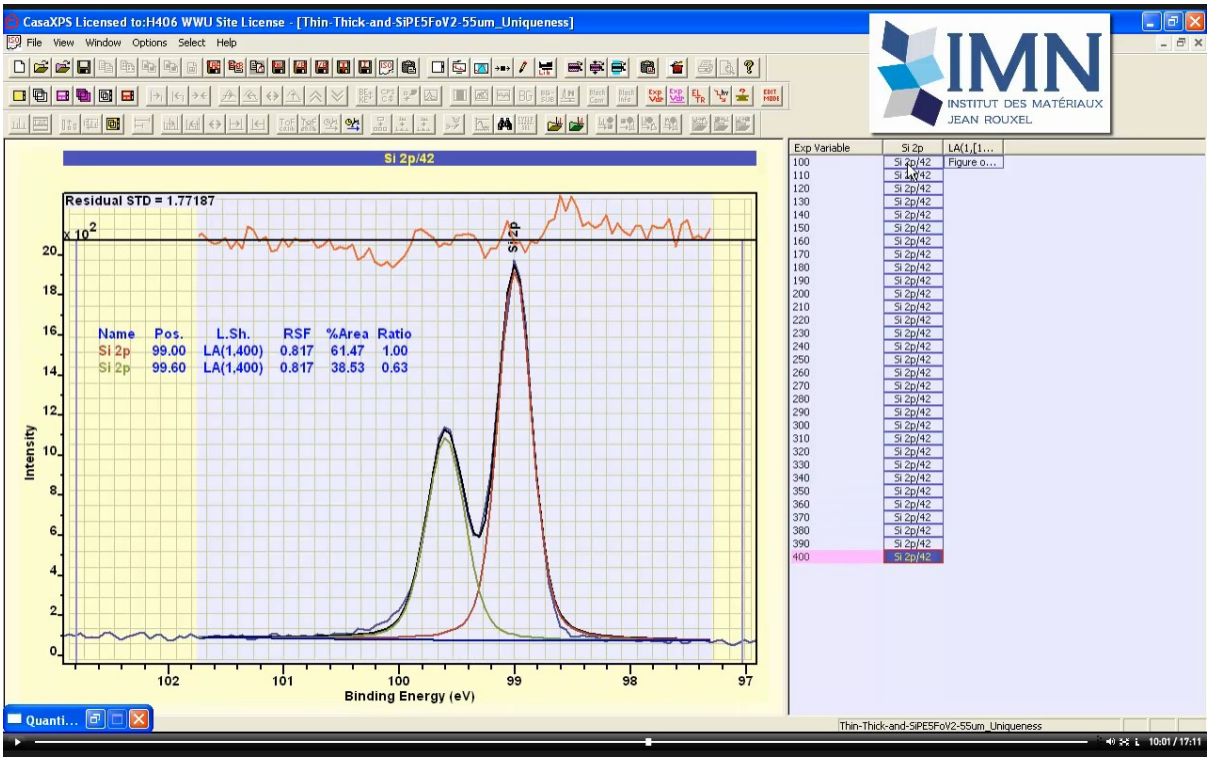

The first line shape within the scan and the last coupled with the shape for the figure of merit plot suggest the line shape is not best suited to fitting of these data using two component peaks.

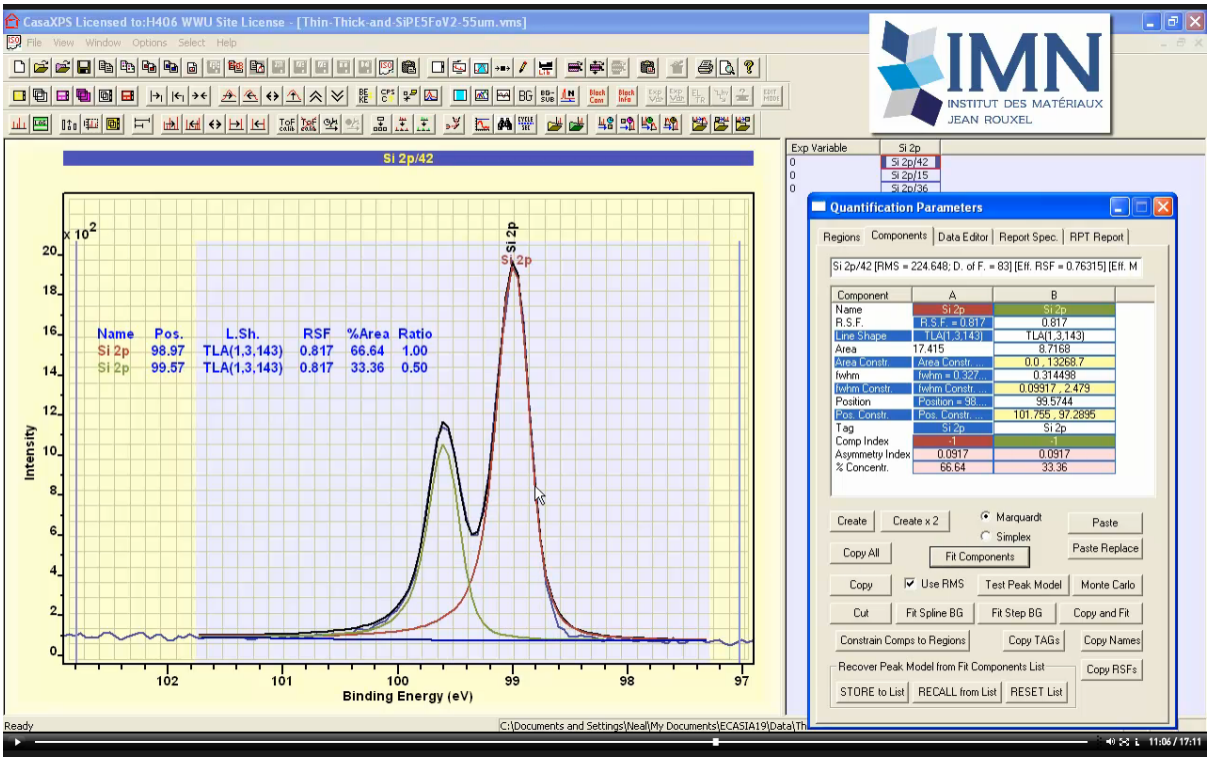

Returning to the original data using the Windows menu or simply closing the VAMAS file created by the Test Peak Model option allows a new line shape to be examined where the line shape is designed to accommodate asymmetry in a component peak.

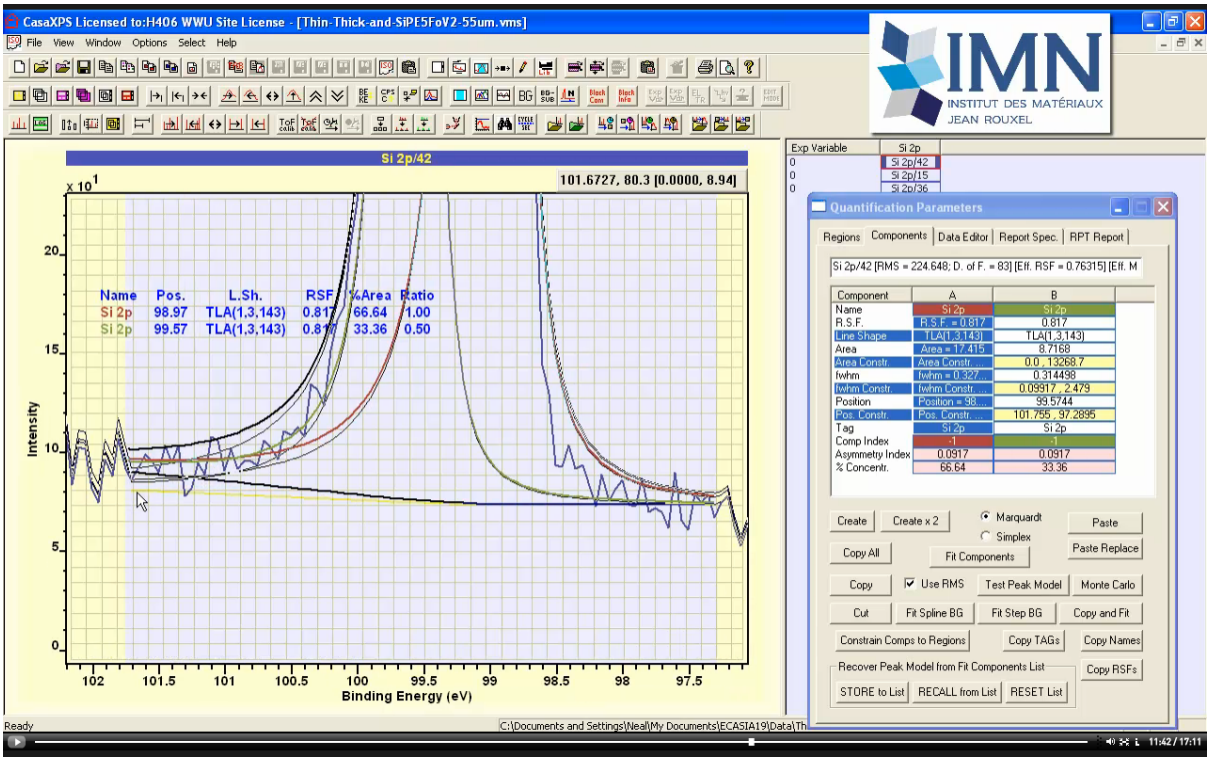

The logic behind the TLA line shape is a Lorentzian shape underpins photoemission peaks but when measured by XPS instruments and energy loss events associated with photoionisation signal, signal moves to lower kinetic energy compared to the energy for a purely Lorentzian process. What is more, a Lorentzian photoemission line models signal spread for the peak maximum and allowing a background to abruptly align with the perceived background is inconsistent with the use of a Lorentzian. Hence start and end offsets are used to allow the use of Lorentzian like line shapes.

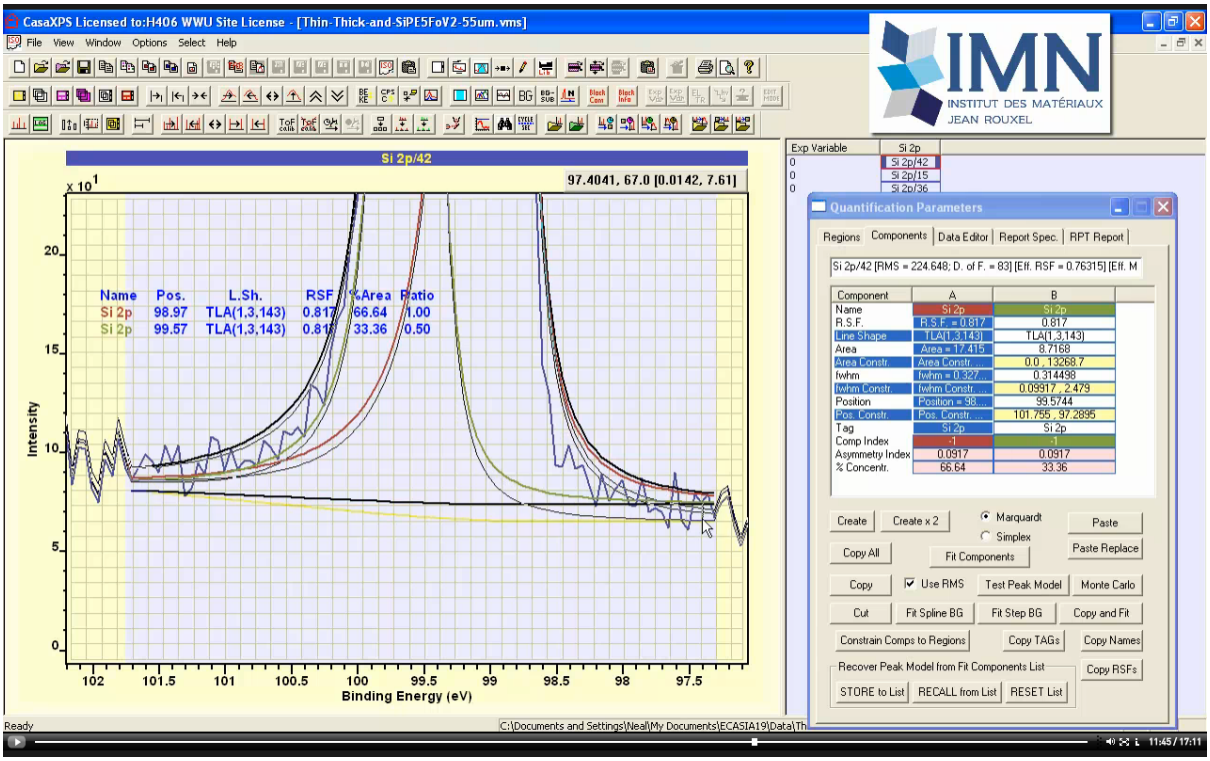

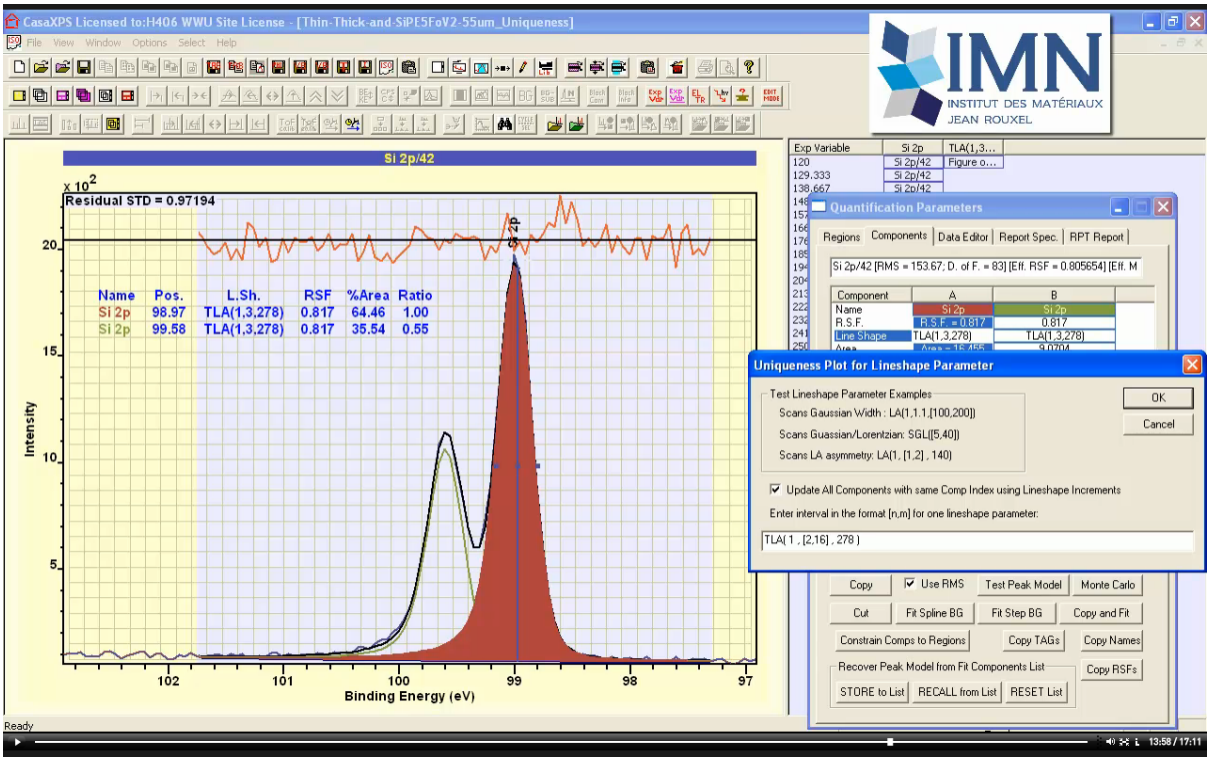

TLA line shape can be specified with three parameters. The second of these parameters alters the movement of signal from right to left side of a generalised Lorentzian resulting in an asymmetric line shape. Scanning the second parameter for a TLA line shape between 2 and 16 results in a figure of merit plot with a minimum but indices the parameter is not sensitive to a range of values close to the minimum.

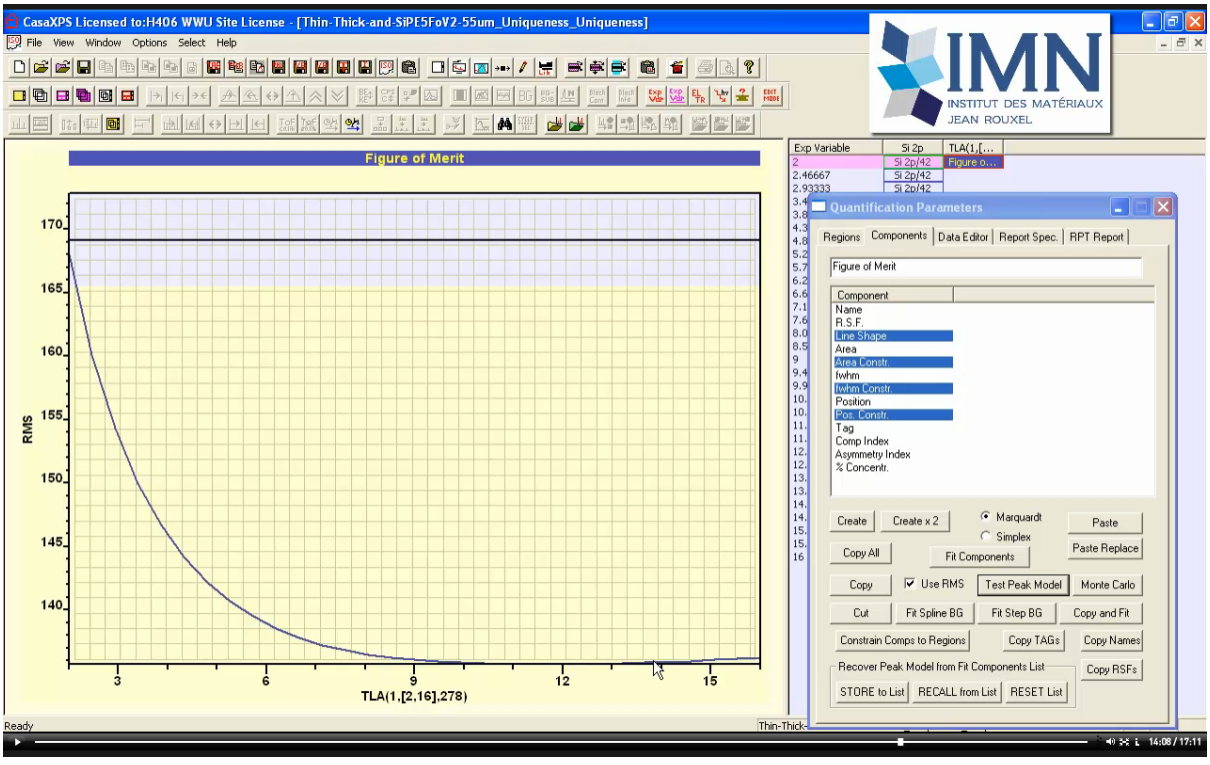

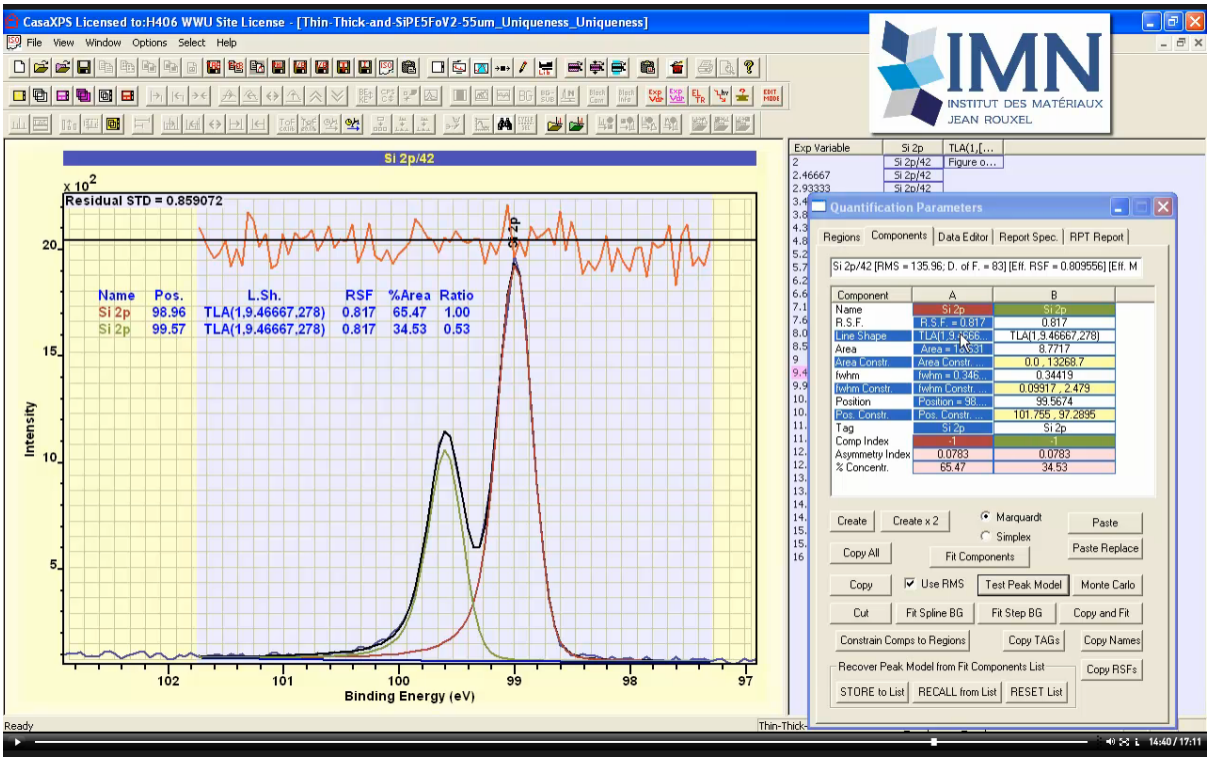

A new scan based on the Gaussian term in the TLA line shape making use of one of the results from the previous scan allows an investigation of adjustments centred around a promising values for the asymmetry parameter.

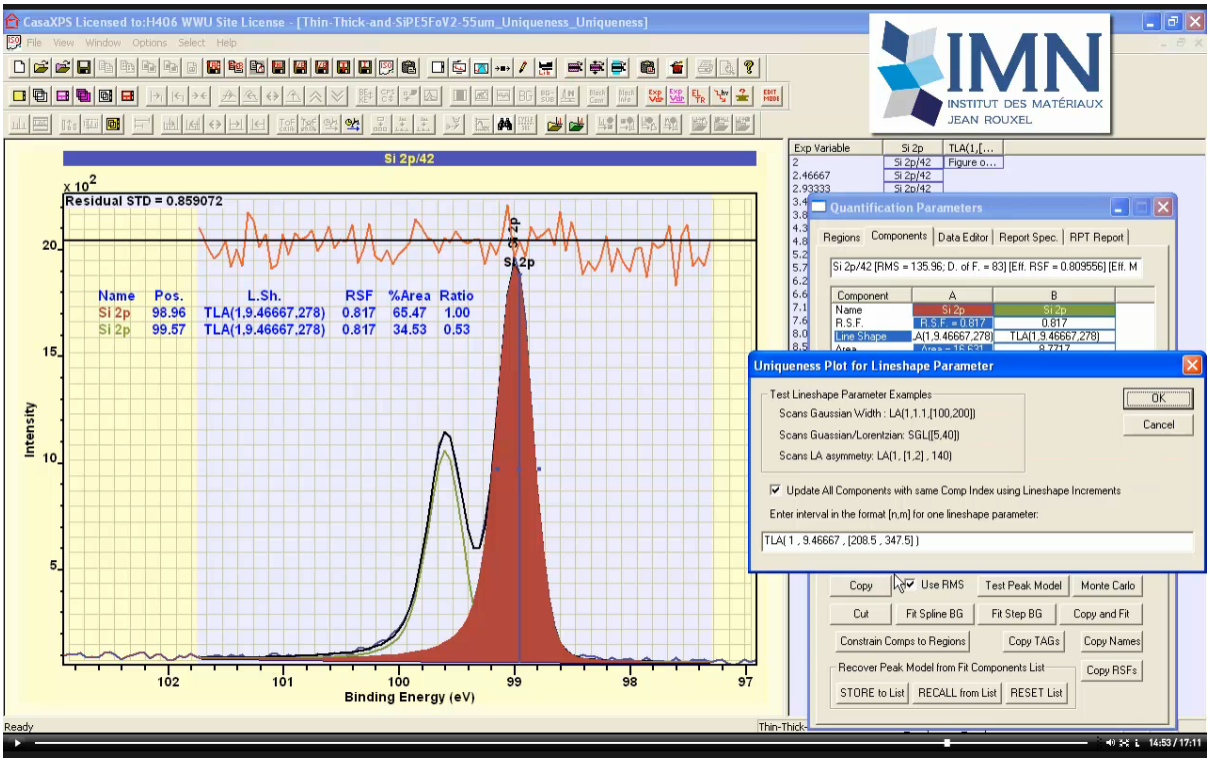

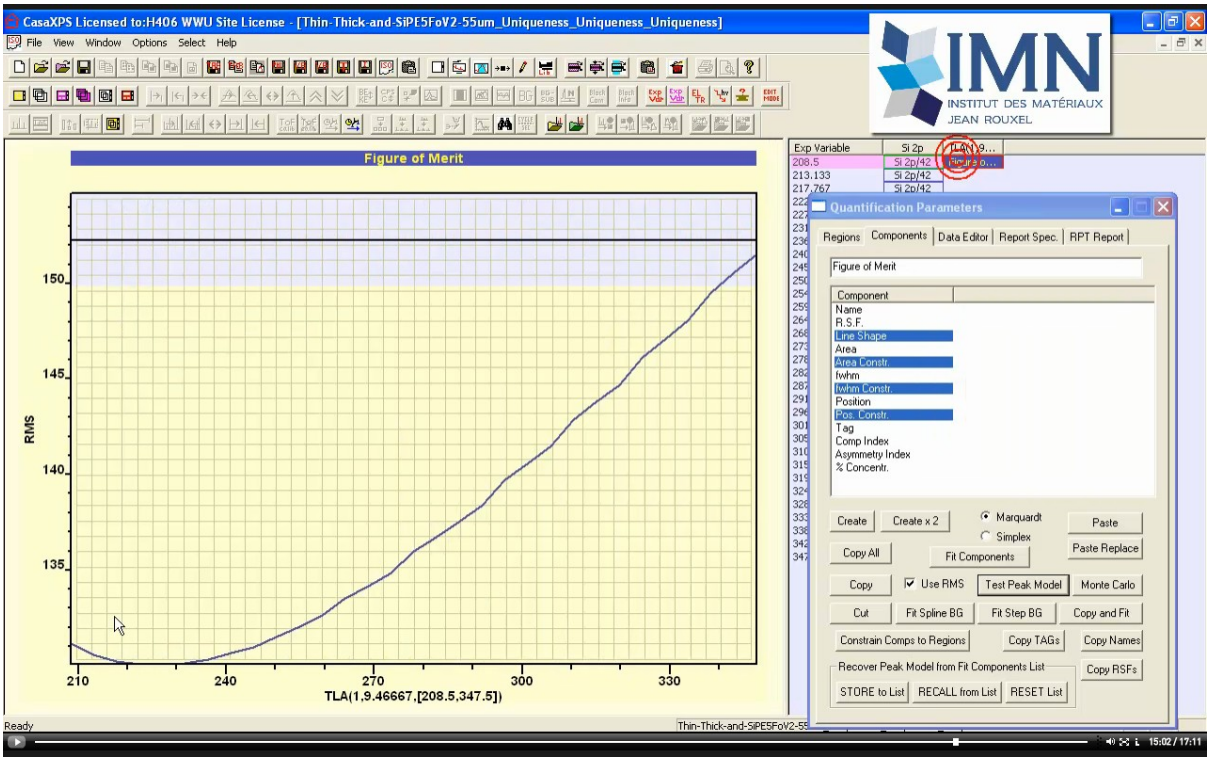

Ultimately these scans yield a line shape for which the figure of merit is consistent with pulse counted data collected using multiple detectors and the ratio for the doublet peaks matches expectation.

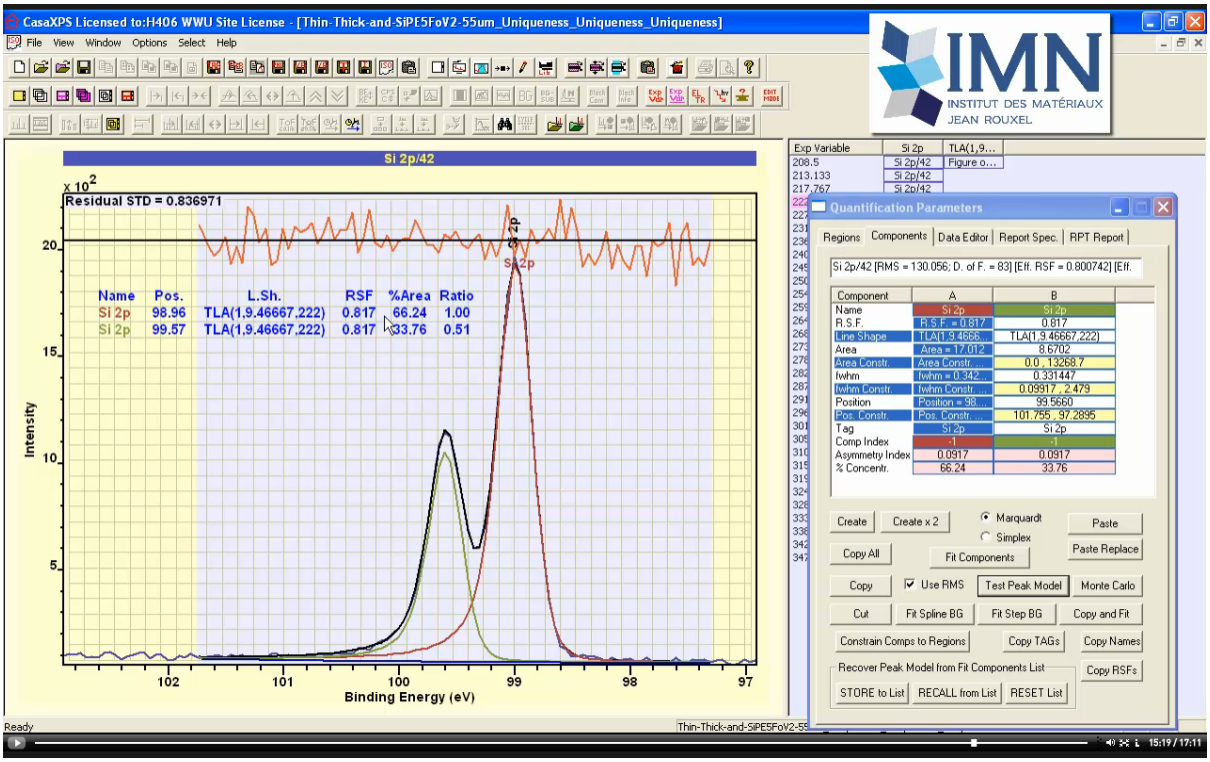

Si 2p peaks are nominally in the ratio 2:1 but are computed in terms of Scofield cross-sections to be slightly different from 2:1.

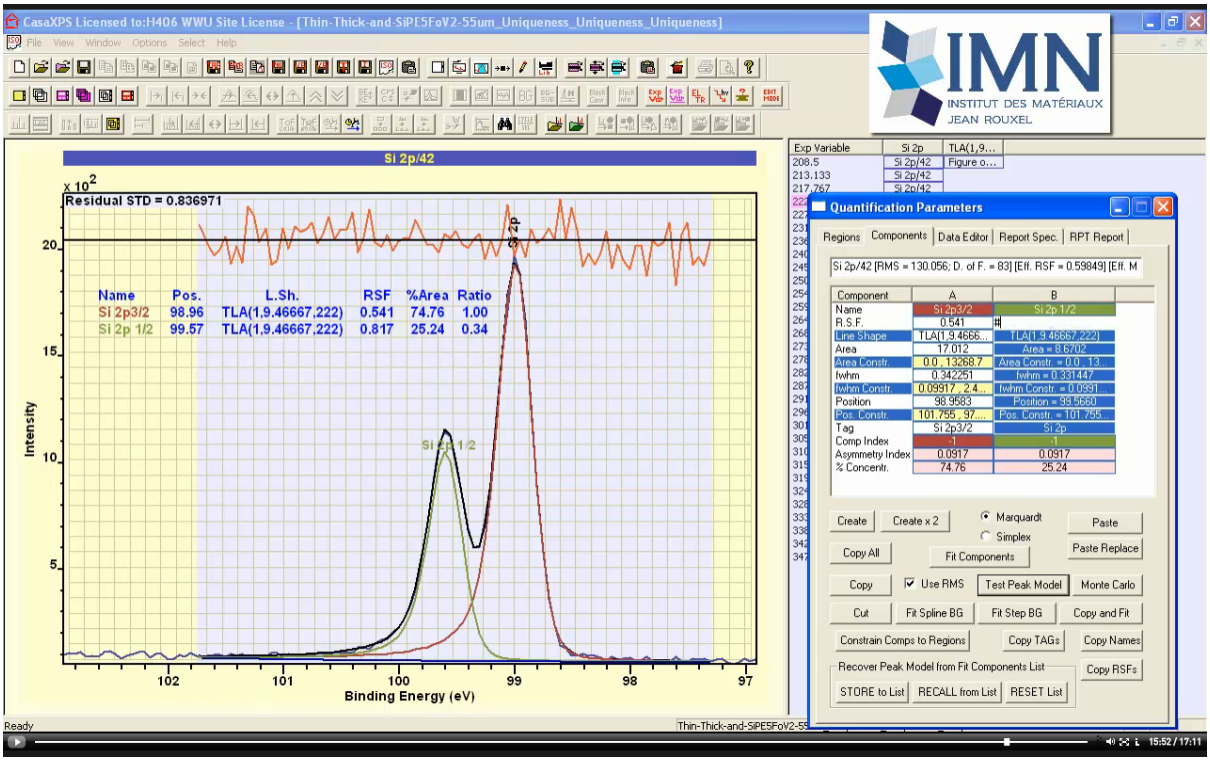

Updating the RSFs for individual doublet peaks with Scofield cross-sections allows a comparison in terms of component intensities consist with the probability for ionisation with different total orbital angular momentum in the final state. The result of applying these individual cross-sections to Si $2p_{3/2}$ and Si $2p_{1/2}$ component RSFs should be and does result in 50% to 50%.

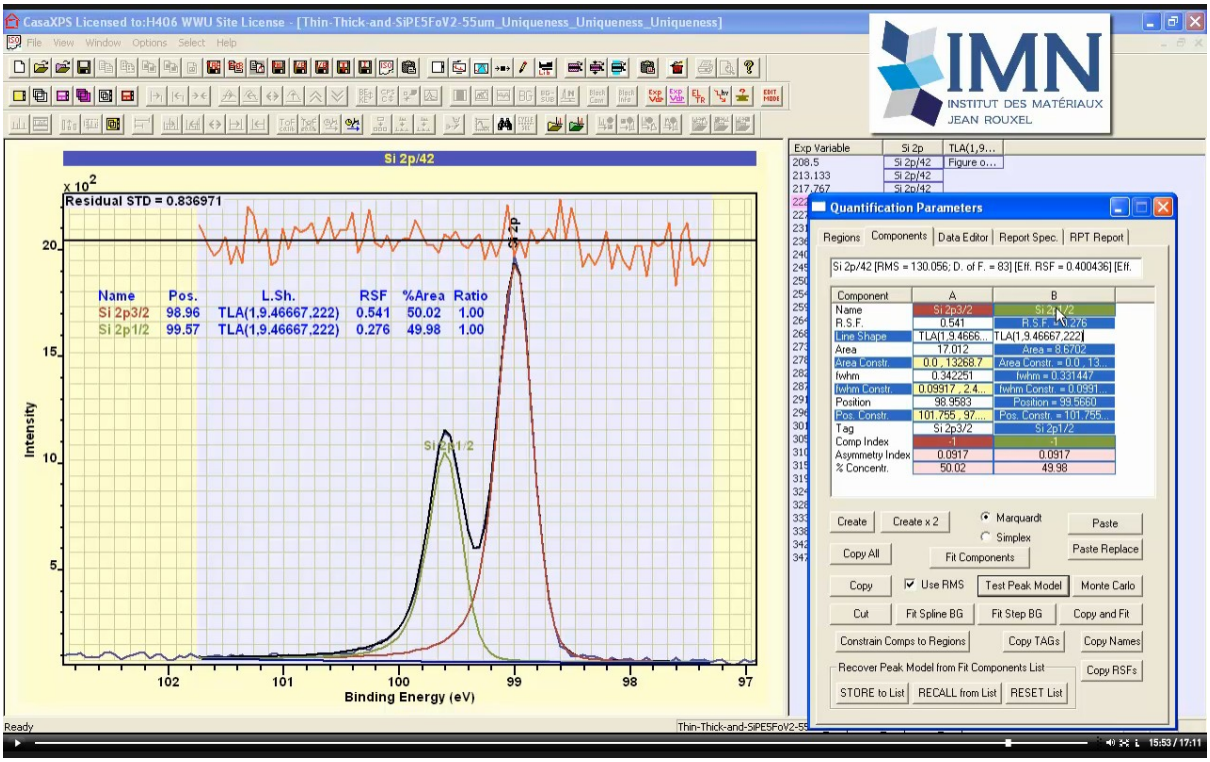

Data and Curve Fitting in XPS: Al 2s and Cu 3s

Thoughts on Data

The basic building blocks for a peak model are: an energy loss background approximation, the number of components and the line shapes for these components. One solution to uncovering these building blocks is the use of large data sets of spectra, preferably from samples with similar composition and also of composition similar to the sample of interest. The source for such data is best obtained by specific measurements from samples related to the material of interest performed on the same instrument, but availability of reference spectra of known origin is also a valuable tool when constructing peak models. By way of illustrating these points a material containing both copper and aluminium in the same sample is considered. The method used to obtain a large data set from related samples is via a sputter depth profile. Such a sputter depth profile provides multiple examples of spectra created from the same sample modified by argon ion gun sputtering, while reference in the La Trobe XPS database provides insight into line shapes and backgrounds appropriate to these data.

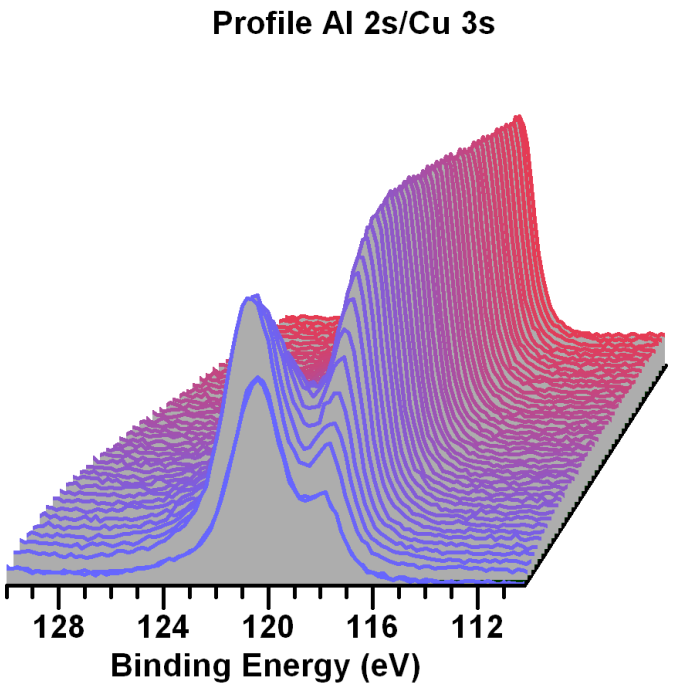

The use of spectra measured throughout a sputter depth profile is an advantage by virtue of numerous examples of evolving spectra as a consequence of modifications to surface composition by an ion gun. The disadvantage of a sputter depth profile is modifications to the surface include chemical changes induced by the action of the ion gun and topographical changes to the field of view analysed by XPS. For example, transition metal oxides often reduce when sputtered with an ion beam, some reduce simply as a consequence of measurement by XPS. Sputtering material from a sample before measurement by XPS may lead to signal collected from an uneven crater bottom, from crater sides and the original surface all at the same time. These and other artefacts should be considered when making use of such data to construct a peak model.

Database spectra measured from standard materials provide insight into line shapes and background characteristics. The La Trobe database includes examples of aluminium measured from a sputtered

metallic aluminium foil and also aluminium in a compound considered to be an insulator. These examples suggest for aluminium with delocalised electrons asymmetry is important and a rise in background signal close to photoemission peaks is possible, while aluminium materials with significant band gap is characterised by a flat background beneath photoemission peaks. It is important to appreciate all spectra include characteristics specific to acquisition modes and instrument design, but as a tool for assessing potential line shapes for a peak model comparisons to data of known origin is an essential part of constructing a peak model. The disadvantage of comparison with database spectra is samples may not yield spectra without artefacts of the measurement process, and understanding these artefacts may limit the usefulness of database spectra for a given analysis. In the context of the sputter depth profile described here, argon is implanted in the sample during sputter cycles and Ar 2p is measured throughout the experiment. While these argon spectra are not of primary importance to the analysis, argon measured by XPS does illustrate an important point. The La Trobe database includes an example of argon data measured from argon implanted in silicon. These argon spectra measured making use of silicon as the target for an argon ion beam include significant background shapes for argon that are characteristic of silicon. Background shapes to argon photoemission peaks change depending on matrix and are significantly different for other materials. In particular the background to argon photoemission peaks changes markedly between argon sputtered aluminium foil and oxidised or contaminated aluminium foil, both of which differ from background shapes generated by argon embedded in silicon. While argon is not the focus for the peak model discussed here, argon embedded in different materials illustrates the importance of appreciating the context for spectra and similar artefacts should not be overlooked when assessing spectra of interest against database spectra.

Making use of Data

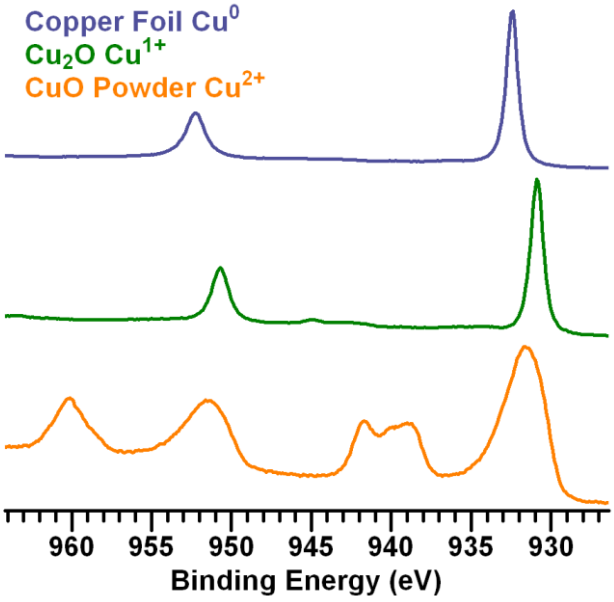

A peak model for Al 2s and Cu 3s requires a number of assumptions, not least the assumption that to each chemical state a synthetic component peak can be assigned and the ensemble of components selected for the peak model can be fitted to data envelopes to recover amount of substance for chemical states. This assumption is not always true and if used should be justified by some means.

For the case in point aluminium is a light element and for both metal and oxide while variation in FWHM is evident for these two cases, there is little evidence for complex data envelopes associated with chemical states for aluminium. That is to say component peaks are suitable for aluminium. The same is not true for copper. While metallic and Cu^{1+} generally appear as well formed signal easily identified as component peaks when in Cu^{2+} oxidation state copper spectra include structures of a more complex nature. If a material includes Cu^{2+} then assuming a single component representing Cu 3s would be a source for error when fitting data including aluminium and copper signal. The depth profile data set from which these Al2s/Cu3s spectra originate includes a measurement for Cu 2p and a survey spectrum. These additional data provide evidence that copper appear in either a metallic or a Cu^{1+} state, therefore assuming a single component for Cu 3s is reasonable when constructing the peak model for these data.

Constructing a peak model for an isolated spectrum is a challenge at best. Access to multiple spectra with evolving proportions of component peaks is an asset to developing a peak model. However in the case of a sputter profile spectra evolve in ways not entirely due to changing proportions for component peaks. The issue is establishing whether observed changes in binding energy for component peaks as a function of etch-time in Al 2s/Cu 3s spectra is due to chemical state changes or changing charge compensation state at the time each spectrum is acquired. The issue of charge compensation state is well known for sputter depth profiles but for the profile in question there is a further question of differential charging, meaning the possibility that charge state varies with location on the sample. Differential charging has consequences for relative component positions within a peak model, the influences of which are not always easy to interpret. For heterogeneous samples where an oxide layer is initially predominately at the interface between the sample and the vacuum on top of a substrate of metallic form, these layered structures can result in component peaks assigned to oxide moving relative to metallic components as a profile is acquired. There is evidence within this profile of altering surface potential with cycle time, offering one explanation for why the component assigned to Al 2s oxide appears to move relative to both metallic Cu 3s and Al 2s components.

Fitting component peaks to data is typically performed using non-linear least squares optimisation for precisely the reason that component peaks may vary in position and width. If components only adjusted in component height then linear least squares optimisation would be the preferred approach. Non-linear optimisation accommodating movements in position is necessary for fitting these Al 2s/Cu 3s data with three components.

Even if these shifts in an aluminium oxide component represent chemical changes, for a sputter profile these changes should not be considered representative of chemical state changes within the sample, but rather changes as a consequence of sputtering.

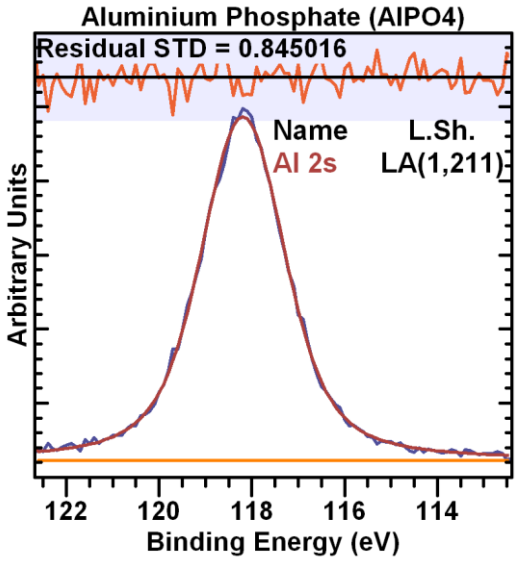

A peak model is constructed for these Al 2s/Cu 3s spectra by first considering the potential line shape for Al 2s when bond to oxygen. $AlPO_4$ spectra in the La Trobe database suggest a Voigt profile with little response to inelastic scattering should be expected beneath the aluminium component representative of aluminium bonded to oxygen.

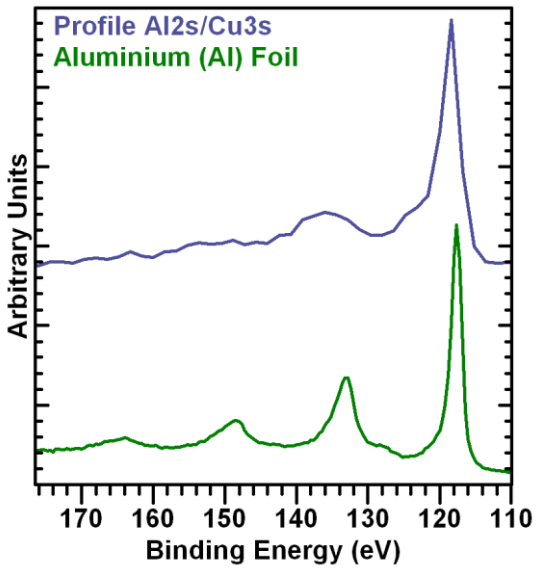

While the La Trobe database includes aluminium foil the plasmon loss structures characteristic of metallic aluminium do not appear to apply to the form of aluminium within the sample profiled. Survey data indicate plasmons correlated to aluminium and copper are significantly damped by comparison to sputter cleaned aluminium foil. Further, Cu 2p grows as the profile proceeds and takes the form of copper in either Cu^{1+} or Cu^{0} so rather than rely on line shapes purely based on database information the profile data can be used to infer a peak model for the limiting case where oxygen is eliminated from the sample. No such spectrum actually exists within the data set, but by manipulating spectra it is possible to compute a spectral form suggestive of copper and aluminium in the absence of aluminium oxide.

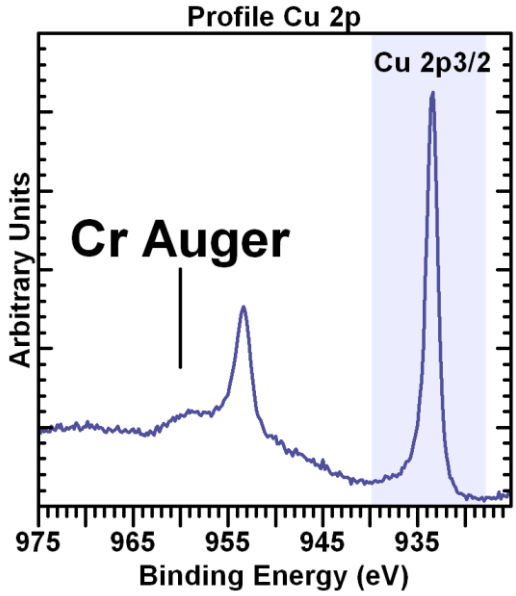

The peak model constructed from these Al 2s/Cu 3s data makes use of three components, namely, one component for each of the metallic Al 2s and Cu 3s plus a third component representative of a Shirley background computed assuming inelastic scattering is only possible for metallic components. By implication, making use of the Shirley component in a peak model removes any artefacts introduced by the Shirley algorithm when incorrectly applied to Al 2s oxide signal.

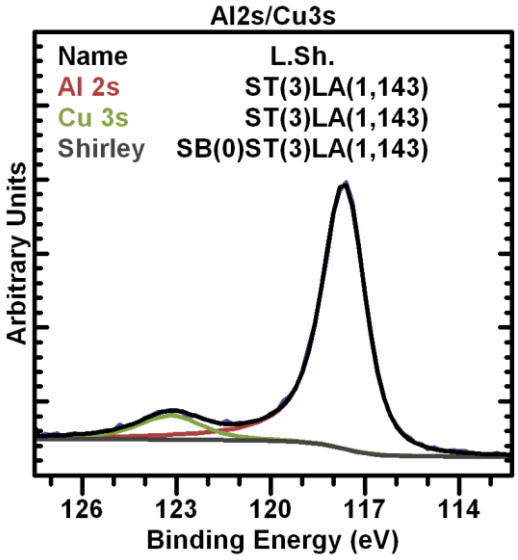

After experimentation with fitting the combination of three components plus a fourth Al 2s oxide to the Al 2s/Cu 3s spectra of the profile constraints were introduced to link relative FWHM and relative position for the three components corresponding to the metallic data but constraining FWHM of the Al 2s oxide relative to the metallic peaks only. Allowing optimisation to select the FWHM as well as position for the Al 2s oxide resulted in unacceptable shifts in the component position with respect to shifts in peak positions for equivalent O 1s and Ar 2p data. The value of additional data when constructing a peak model was therefore demonstrated by virtue of making comparisons in peak shifts and line shapes such as Cu 2p to infer the possibility of Cu^{1+} or Cu^{0} only. Survey data was also used to assess the damping of plasmon peaks from Al 2p/Cu 3p. Typically Al 2p is used to quantify

aluminium because of two factors. Firstly metallic Al 2p results in two narrow doublet peaks well separated from Al 2p oxide signal and secondly metallic Al 2p can result in low level plasmon peaks beneath the Al 2s. For the material in question, the first plasmon from Al 2p is significant, but subsequent plasmon peaks decay as seen by inspection of survey data.

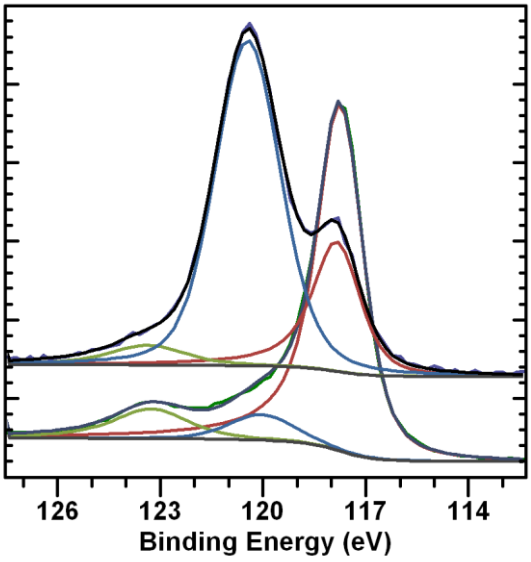

Name	L.Sh.
Al 2s Metal	ST(3)LA(1,143)
Cu 3s	ST(3)LA(1,143)
Al 2s BG	SB(0)ST(3)LA(1,143)
Al 2s Oxide	LA(1,443)

Exporting Bitmaps with Pixel Resolution suitable for publishing Data

Data and fonts for routine data treatment are rendered in display tiles of CasaXPS with dots per inch (dpi) of about 100. Graphical data equivalent to the set of display tiles (including the active display tile) corresponding to a page of display tiles is placed on the clipboard by pressing the Copy toolbar button.

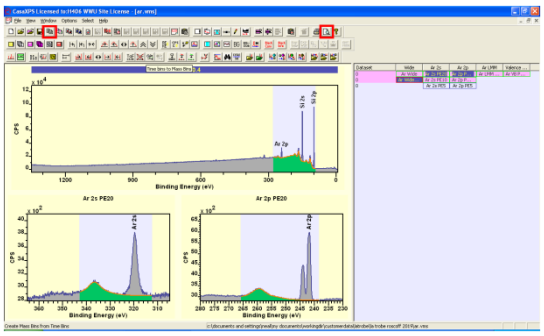

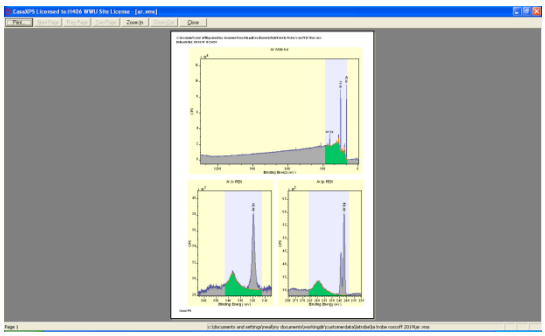

While 100 dpi is typically suitable for electronic documents, when printed on high resolution devices figures prepared using 100 dpi results in low quality printed graphics. Enhanced Meta Files are vector graphics objects and can be rendered with appropriate resolution for printing, however it is now possible to change modes for graphics when drawing into bitmaps to allow high resolution bitmaps of display tiles to be prepared and exported through the clipboard.

This video illustrates how a display tile can be exported via the Copy toolbar button as a bitmap with dpi of 300 and 600.

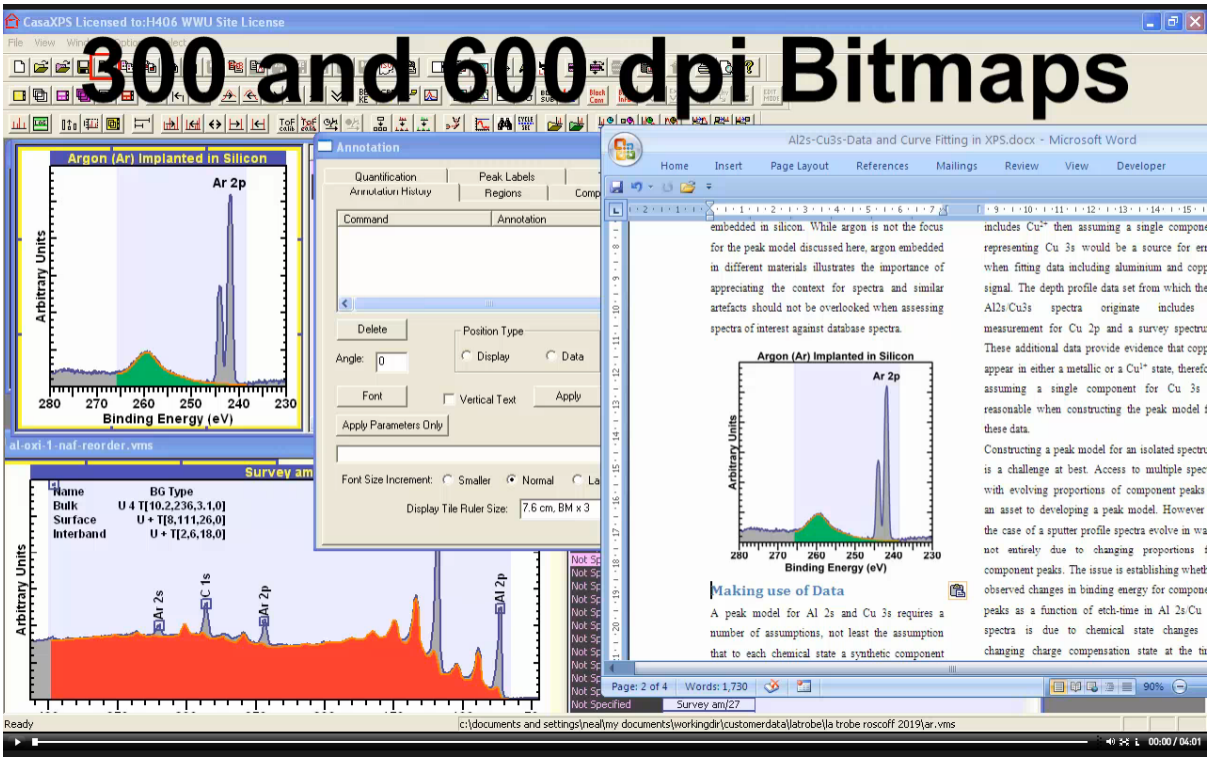

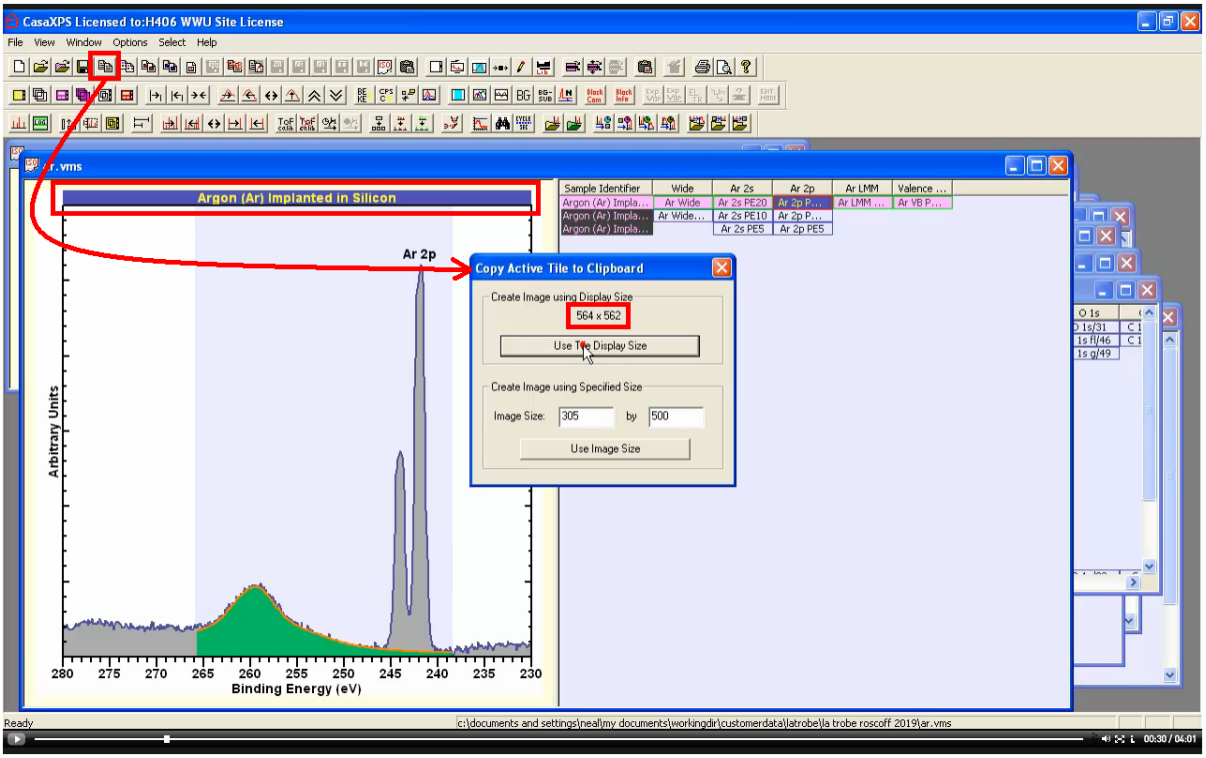

The active display tile determines which page of display tiles is placed on the clipboard by the Copy toolbar button. If the dialog window invoked by the Copy toolbar button indicates a bitmap width and height (e.g. 564 x 562) then the default pixel resolution will be used to place a bitmap on the clipboard. The pixel resolution for a bitmap exported from CasaXPS can be verified by making use of Microsoft Paint to display the actual bitmap size loaded on the clipboard.

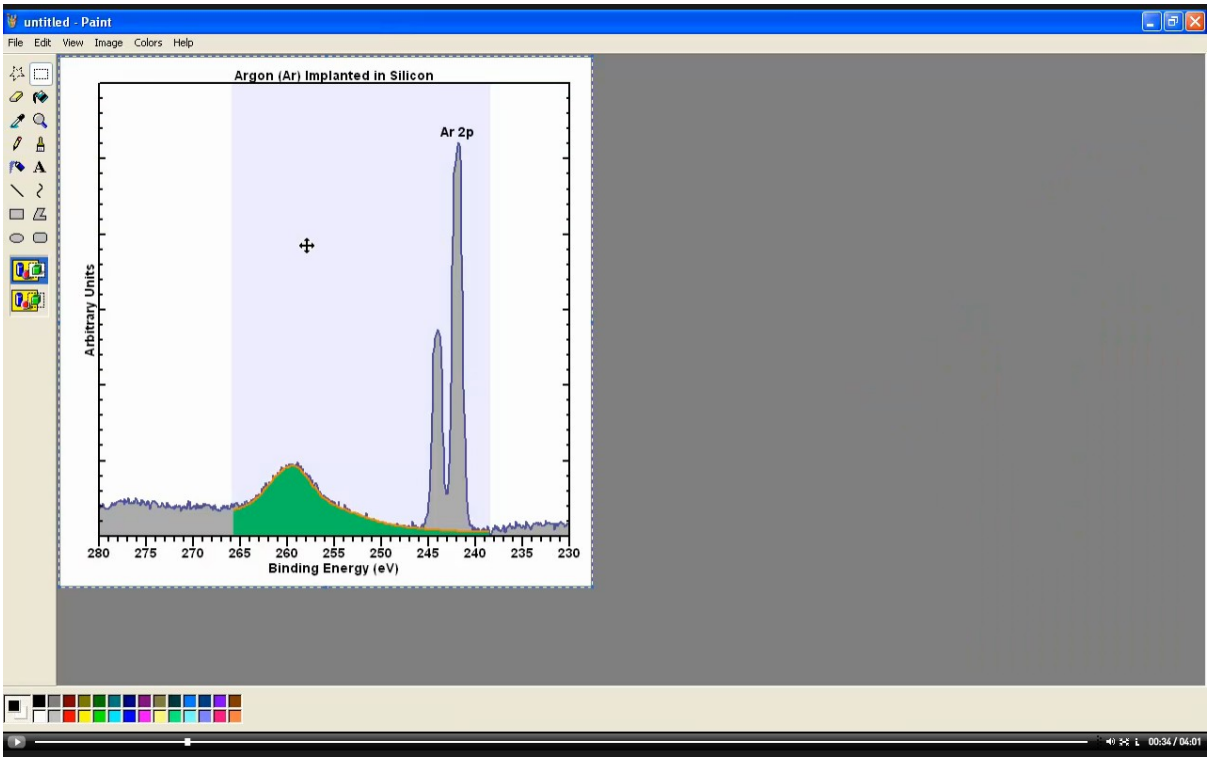

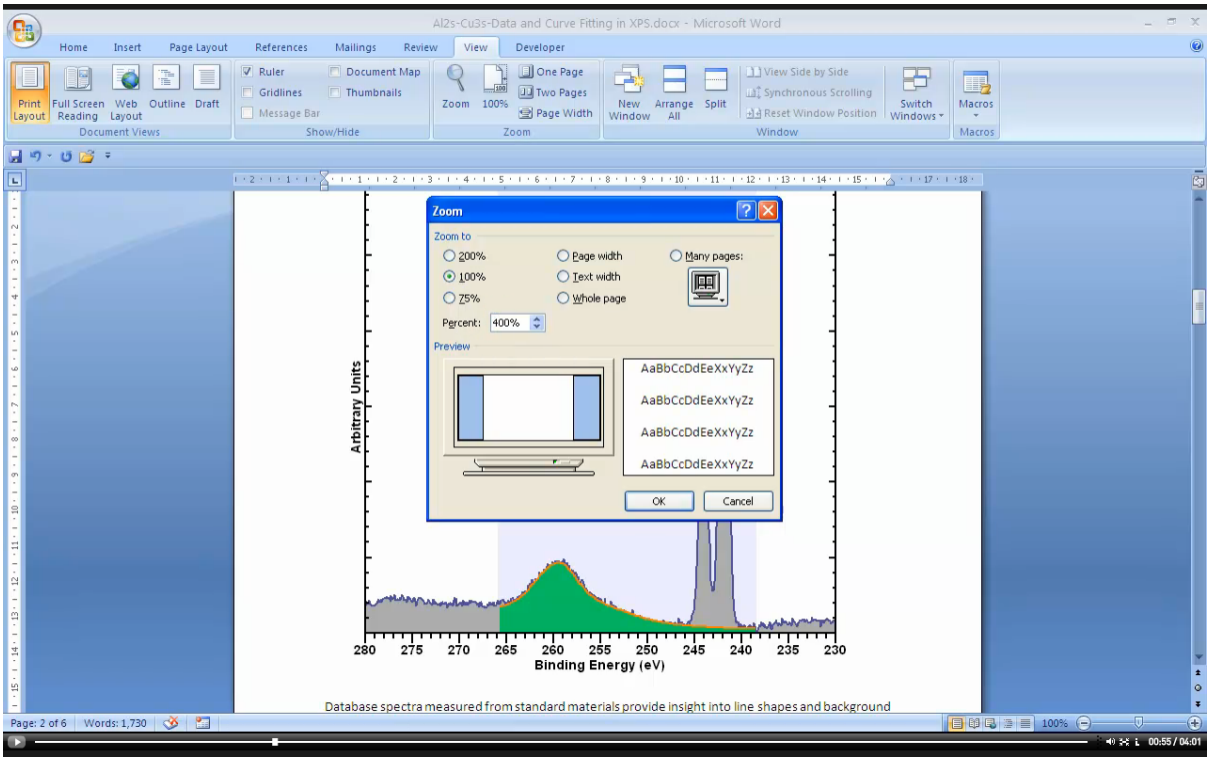

When displayed in Microsoft Word, a bitmap transferred through the clipboard is scaled in size to match page dimensions active in Word. It is not always obvious from Word that a low resolution bitmap is in use. However, to confirm a bitmap is of suitable pixel resolution for printing switching the Zoom state in Word to 400% and reviewing text printed to the bitmap provides an indication that the resolution is correct for printing on high resolution printers. Bitmaps prepared with 100 dpi when viewed at Zoom state of 400% tend to display text with a blurred appearance.

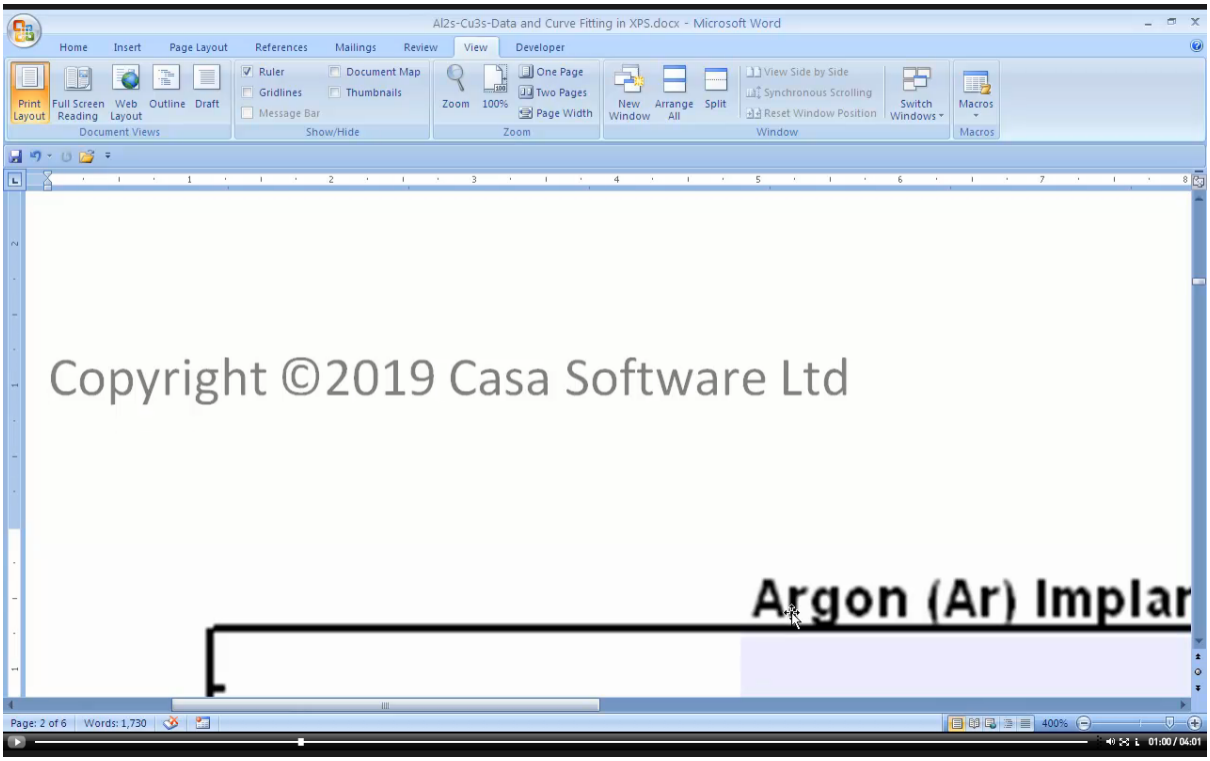

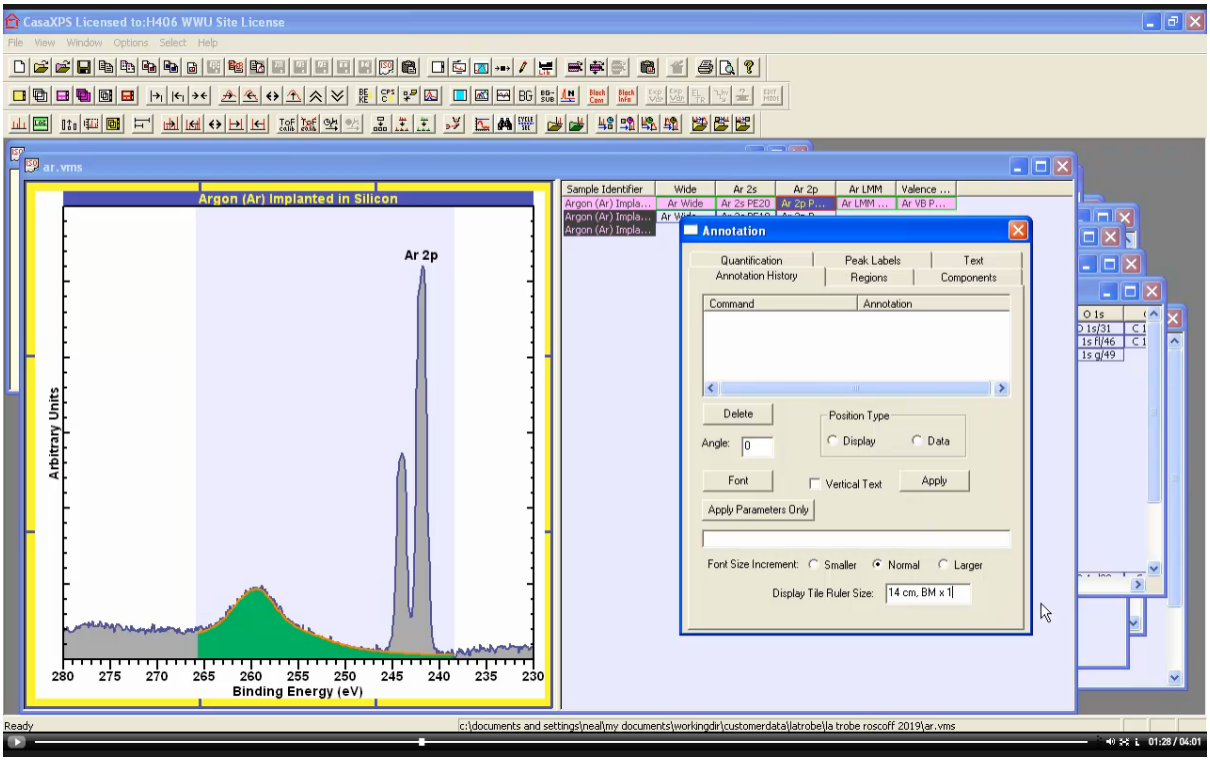

The option used to change the bitmap pixel resolution is on the Annotation dialog window on the Annotation History property page. A scale factor is display in a text-field as well as a dimension for a formatting box size that is displayed whenever the Annotation History property page is top-most on the Annotation dialog window. The text-field displays the active pixel resolution for a bitmap using the format BM x 1, meaning default dpi. Entering BM x 3 and pressing the Enter key results in 300 dpi.

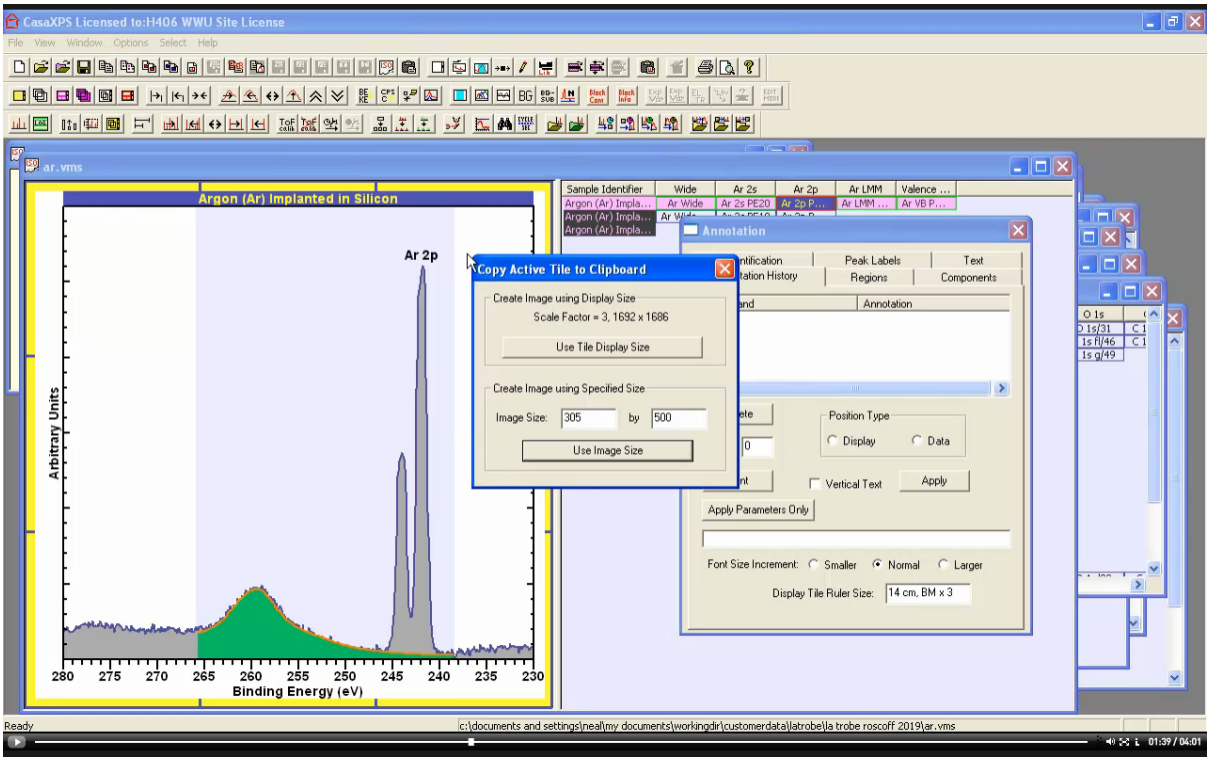

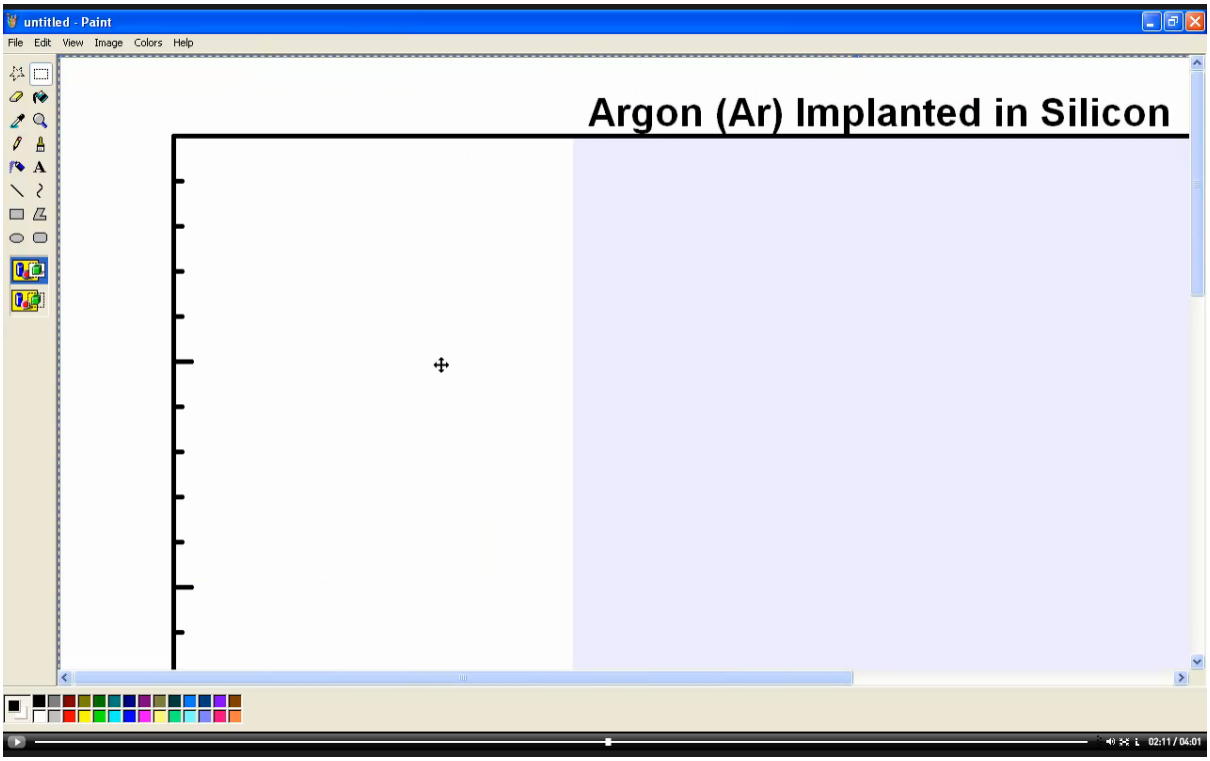

After changing the Annotation History text-field to BM x 3, pressing the Copy toolbar button results in a bitmap of size three times the current display page size and all graphical parameters such as line width and fonts are scaled by a factor of three too. These changes to a bitmap placed on the clipboard can be visualised in Paint and also assessed within Word using a Zoom state of 400%.

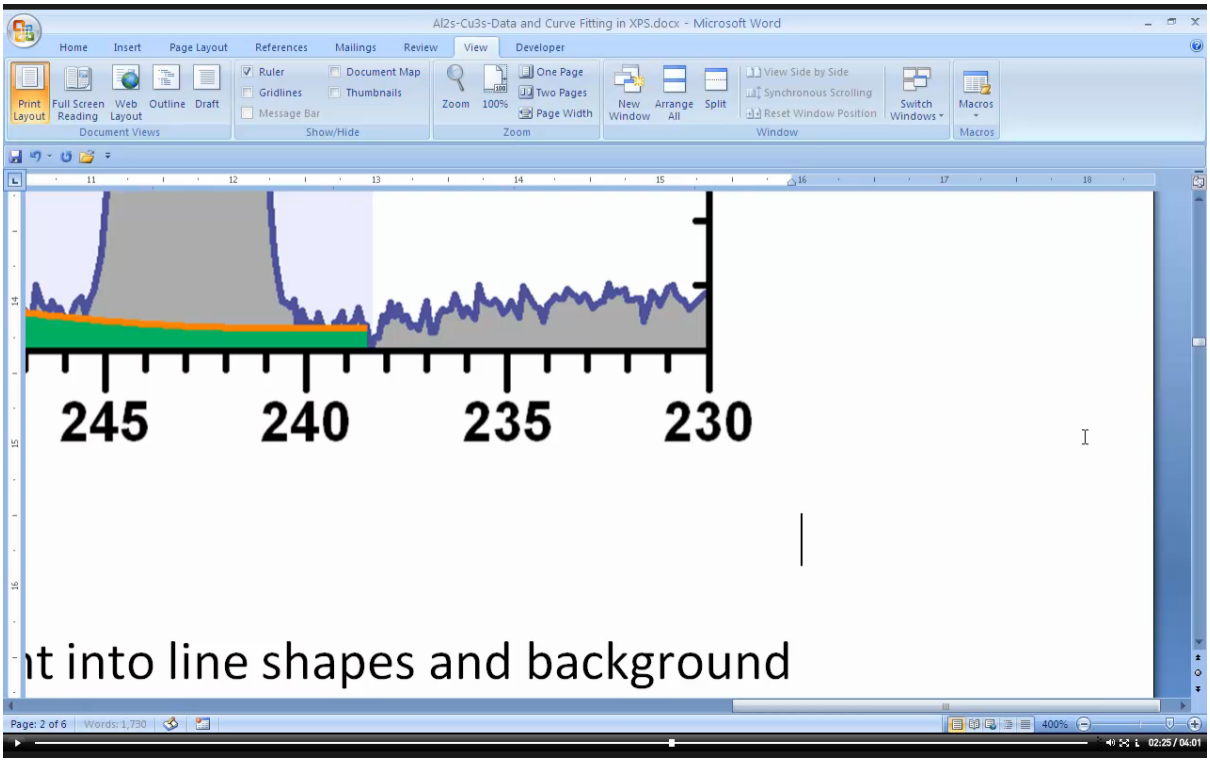

Text when viewed at 400% Zoom in Word now appears crisp in appearance, thus demonstrating 300 dpi pixel resolution was used to prepare a bitmap for export via the Copy button.

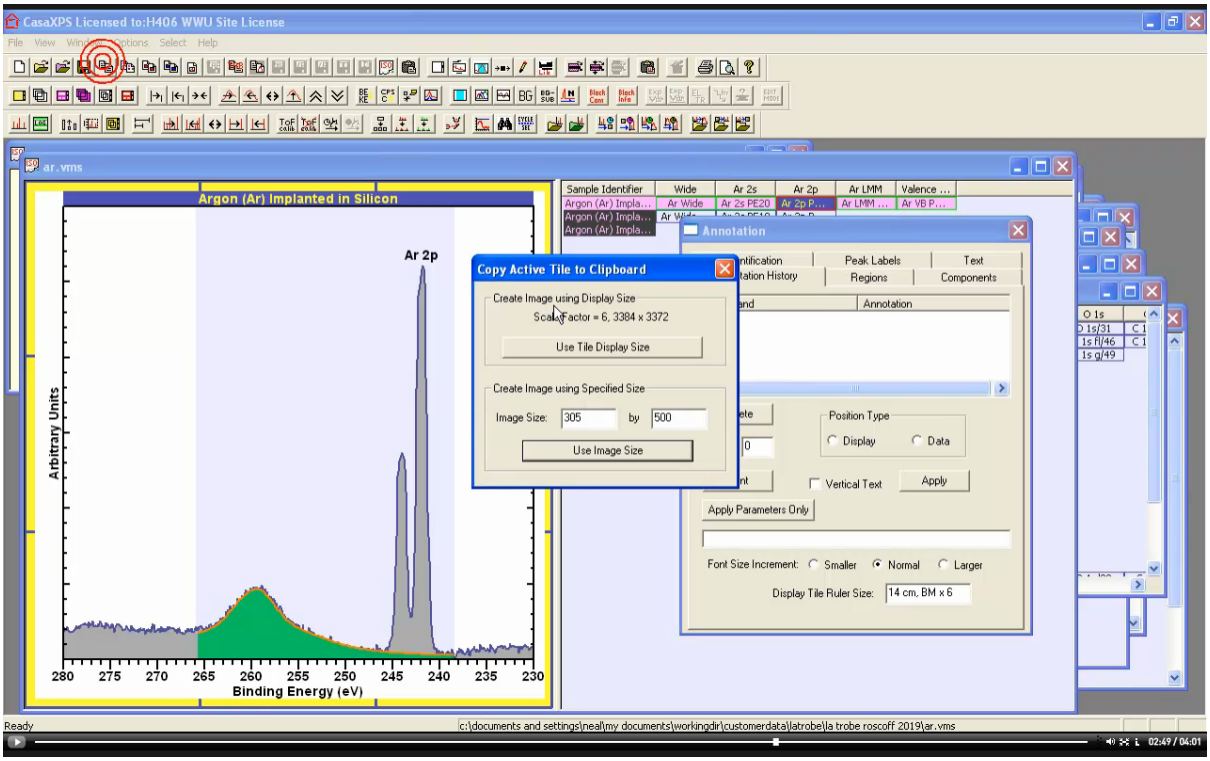

A bitmap with 600 dpi pixel resolution is obtained by entering BM x 6 into the text-field and pressing the Enter key on the keyboard. The size in pixels is displayed on the dialog window invoked by the Copy toolbar button.

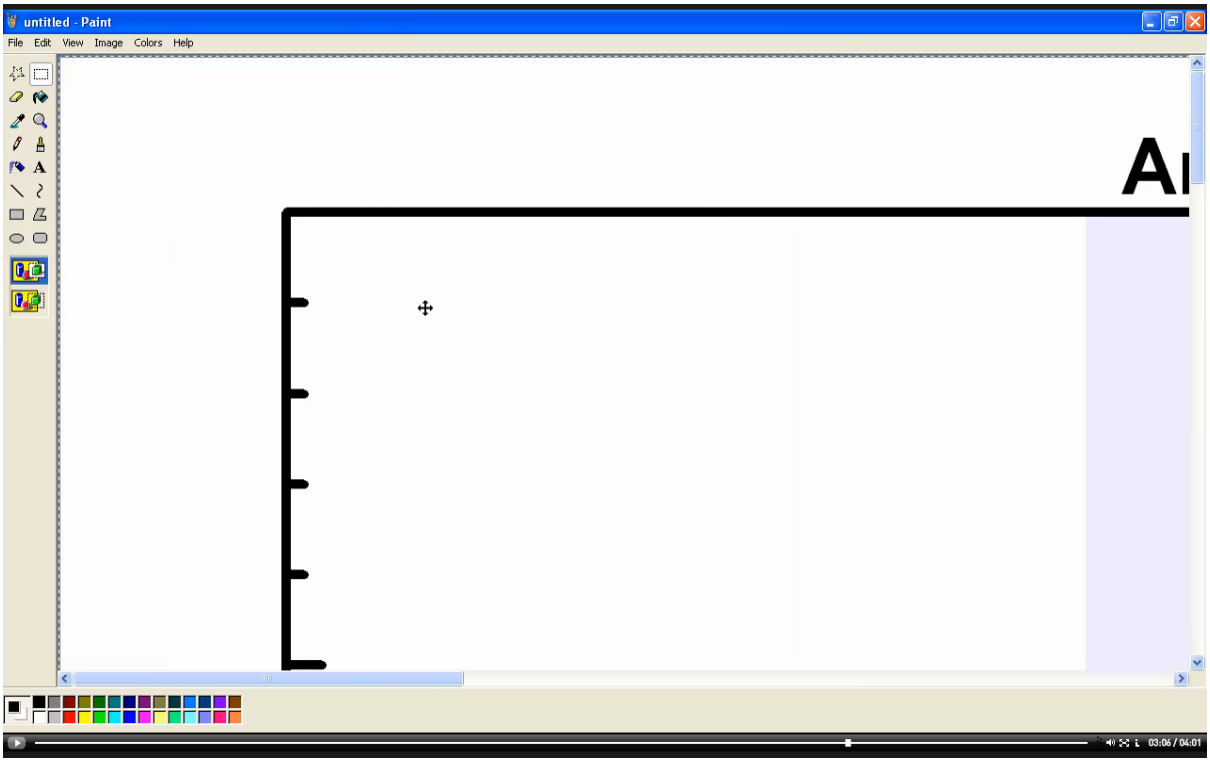

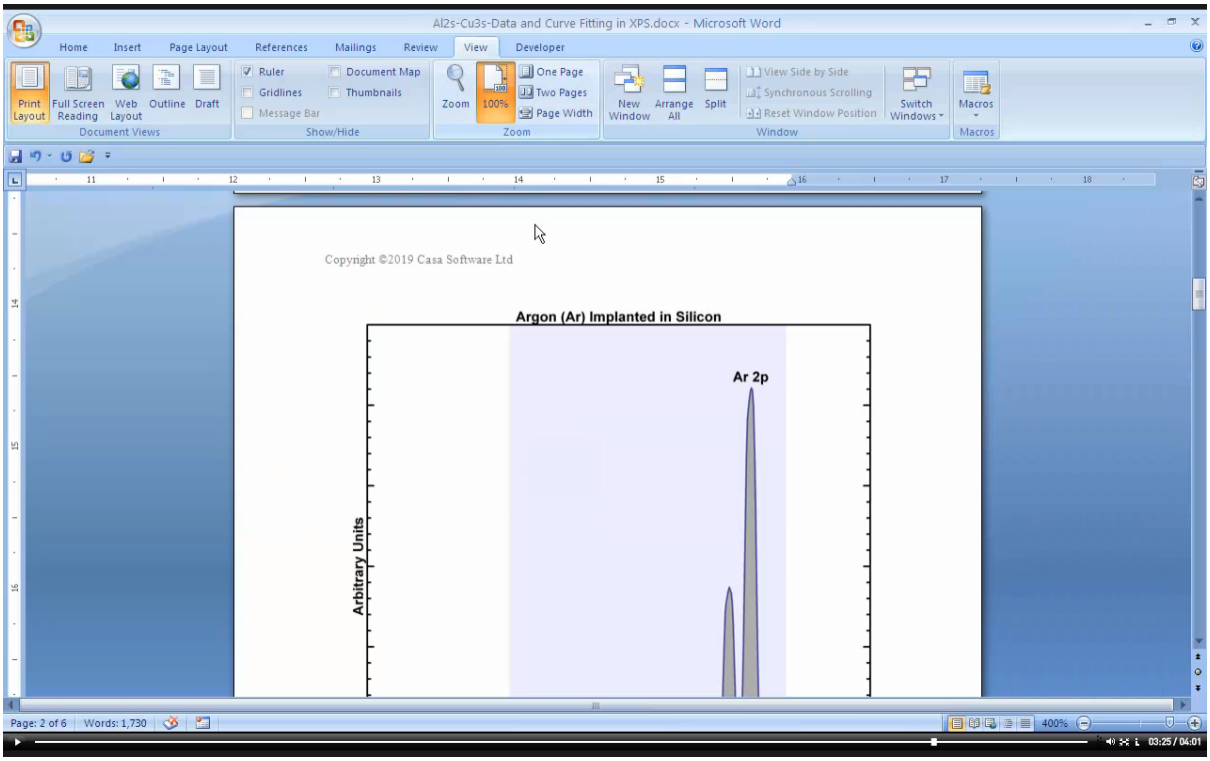

Word documents operating using a Zoom state of 100%, when displaying bitmaps with 600 dpi typically appear similar to bitmaps with pixel resolution of 100 dpi. The difference in terms of display is only important if the Word document is printed on a high resolution device. If bitmaps are prepared with 600 dpi rather than 100 dpi a further consequence in terms of Word documents is an increase in size when measured in bytes.

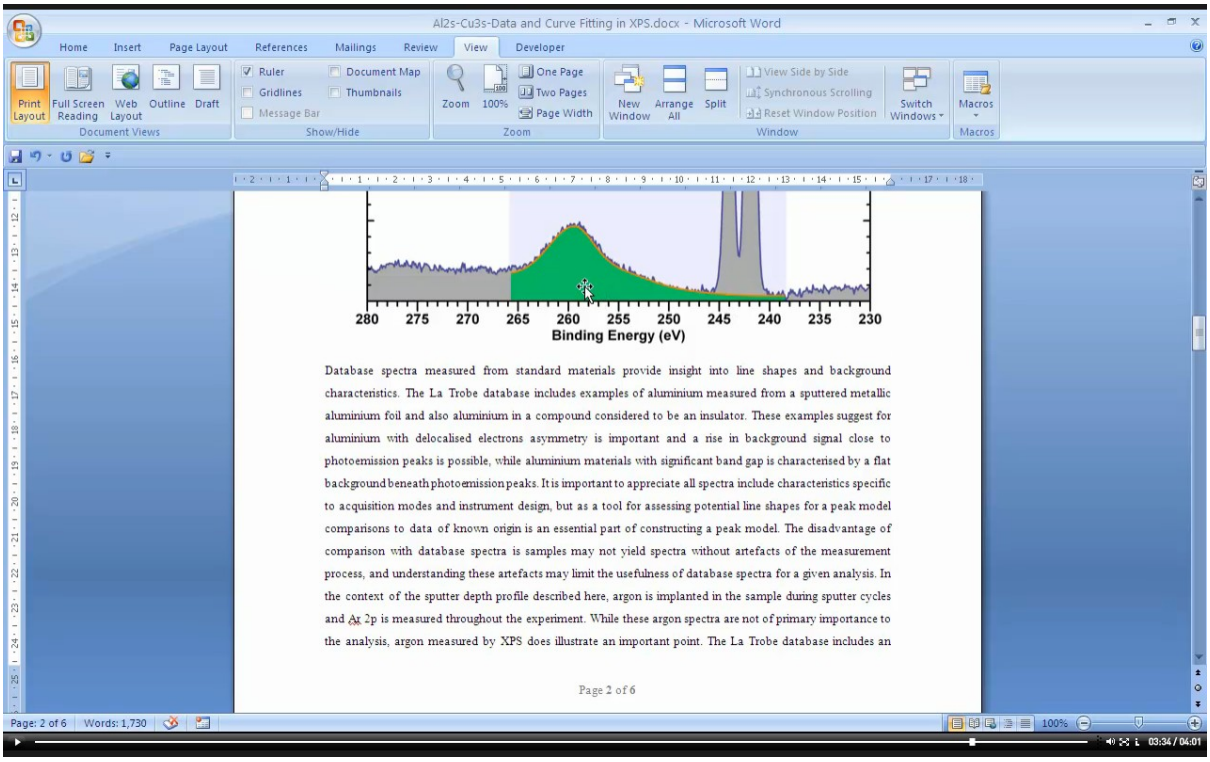

Appendix

Voigt Based Lineshapes

$$Lorentzian: l(x) = \frac{1}{1+4x^2}$$

$$Gaussian: g(x:w) = e^{-4ln2\left(\frac{x}{w}\right)^2}$$

$$Generalised\ Lorentzian: l_g(x:\alpha,\beta) = \begin{cases} [(l(x)]^{\alpha} & x \le 0 \\ [l(x)]^{\beta} & x > 0 \end{cases}$$

$$Lineshape: LA(x:\alpha,\beta,w) = N\int_{-\infty}^{\infty} l_g(\tau:\alpha,\beta)g(x-\tau:w)d\tau$$

$$Abbreviation\ for\ LA\ lineshape: LA(x:\alpha,w) = LA(x:\alpha,\alpha,w)$$

$$Asymmetric\ Lorentzian:\ T(x:\alpha,\mu) = \left[\frac{1}{1+4x^2}\right]^{\alpha} \times \left[\frac{\pi}{2} - \tan^{-1}(2x) + \frac{\pi}{\mu}\right]\cdots \quad \mu > 0\ \&\ \alpha > 0$$

$$Lineshape: TLA(x:\alpha,\mu,w) = N\int_{-\infty}^{\infty} T(\tau:\alpha,\mu)g(x-\tau:w)d\tau$$

Generalised TLA Asymmetric Lineshape:

Rather than using a Lorentzian any lineshape can be used to generalise the TLA to all lineshapes in CasaXPS. The specification for the ST modification is described below in terms of the LA lineshape but the same applies to all lineshapes used to define component peaks in a model.

$$\boldsymbol{A = \int_{-\infty}^{\infty} LA(\varphi:\alpha,\beta,\omega)d\varphi}$$

$$\boldsymbol{ST(\mu)LA(x:\alpha,\beta,\omega) = N \times LA(x:\alpha,\beta,\omega) \times \left[\int_{x}^{\infty} LA(\varphi:\alpha,\beta,\omega)d\varphi + \frac{A}{\mu}\right]\cdots \quad \mu > 0}$$

$$\boldsymbol{ST(\mu,\gamma)LA(x:\alpha,\beta,\omega) = N\int_{-\infty}^{\infty} ST(\mu)LA(\tau:\alpha,\beta,\omega)g(x-\tau:\gamma)d\tau}$$

Pseudo Voigt Lineshapes

Product form of the pseudo Voigt lineshape is formed from a product of a Lorentzian and Gaussian functions where the FWHM for each function varies with the parameter m.

$$GL(x,m) = \frac{1}{(1+4\frac{m}{100}x^2)} \times exp\left(-\left(1-\frac{m}{100}\right)(4ln2)x^2\right)$$

For $0 < m < 1$

$$GL(x,m) = \frac{1}{1+4\left(\frac{x}{f_L}\right)^2} \times exp\left(-(4ln2)\left(\frac{x}{f_G}\right)^2\right)$$

$${f_L}^2 = \frac{1}{\frac{m}{100}} \text{ and } {f_G}^2 = \frac{1}{1-\frac{m}{100}}$$

The sum form for a pseudo Voigt function combines a Lorentzian and a Gaussian of unit FWHM by varying the relative height for these two functions before summation.

$$SGL(x,m) = \frac{m}{100}\frac{1}{(1+4x^2)} + \left(1-\frac{m}{100}\right) exp\,(-(4ln2)x^2)$$

$$SGL(x,m) = H_L\frac{1}{(1+4x^2)} + H_G exp\,(-(4ln2)x^2)$$

$$H_L = \frac{m}{100} \qquad\qquad H_G = 1-\frac{m}{100}$$

Both sum and product forms are computationally expedient tools for creating lineshapes, but do not simulate the response of an analyser as well as the Voigt formalism.

Shirley Background Profile

$$\boldsymbol{SB(0)ST(\mu,\gamma)LA(x:\alpha,\beta,\omega) = \int_x^\infty ST(\mu,\gamma)LA(\varphi:\alpha,\beta,\omega)d\varphi}$$